Design and Modification of Half-Sandwich Ir(III), Rh(III), and Ru(II) Amino Acid Complexes for Application in Asymmetric Transfer Hydrogenation Reactions

David Michael Morris

Dissertation submitted to the faculty of the Virginia Polytechnic Institute and State University in partial fulfillment of the requirements for the degree of

Doctor of Philosophy

In

Chemistry

Joseph S. Merola

Karen J. Brewer

Paul A. Deck

Brian E. Hanson

Blacksburg, VA

Keywords: asymmetric transfer hydrogenation; amino acid; half-sandwich complex; iridium; rhodium; ruthenium; tetramethylcyclopentadiene, arene, solvent effects

Design and Modification of Half-Sandwich Ir(III), Rh(III), and Ru(II) Amino Acid Complexes for Application in Asymmetric Transfer Hydrogenation Reactions

David Michael Morris

Abstract

This dissertation describes the design and synthesis of a series of half-sandwich amino acid complexes of the form [(η^n-ring)M(aa)Cl], ((η^n-ring)M = (η^6-arene)Ru(II), (η^5-Me_4C_5R)Rh(III), (η^5-Me_4C_5R)Ir(III), (aa = α-amino carboxylate), and their utility as asymmetric transfer hydrogenation catalysts of ketones. Variation of the metal center, the η^n-ring, and the aa was used to tune these systems for specific sets of ketones. Upon reaction with homochiral aa's, the ligand environment in all of these complexes is pseudotetrahedral, leading to stereogenic metal ions (S_M, R_M). The addition of another stereogenic center from the amino acid ligand (the carbon, R_C or S_C; aa ≠ glycine) gives rise to two pairs of diastereomeric complexes. The ratio of diastereomers depend on the steric environment produced by the aa ligand, with aa's with larger R groups favoring one configuration at the metal center (R_M or S_M) to a greater degree than amino acids with less bulky R groups.

The modified Cp*^{R} (R = phenyl, benzyl, isopropyl, cyclohexyl, n-octyl, and n-dodecyl) type ligands were synthesized by reaction of 2,3,4,5-tetramethylcyclopent-2-en-1-one with the respective Grignard reagent, followed by elimination of water under acidic conditions to produce the tetramethyl(alky or aryl)cyclopentadienes with yields ranging from 37 -94 %. Reaction of the Cp*^{R} ligands with $IrCl_3$• xH_2O gave the dimer complexes [(Cp*^{R})$IrCl_2]_2$ with yields ranging from 14 to 91%. The metal dimers [(η^n-ring)$MCl_2]_2$ react with 2 equivalents of an amino acid in the presence of base to produce the aforementioned [(η^n-ring)M(aa)Cl] yields ranging from 20 to 90%. These complexes were characterized by nuclear magnetic resonance (NMR) experiments, especially nuclear Overhauser

effect (NOE) studies, as well as single-crystal X-ray diffraction, high-resolution mass spectroscopy (HRMS), powder diffraction, and elemental analysis.

During the course of the work, it was found that all ring containing aa ligands produced the highest enantioselectivities, (ee). This was due to only one diastereomer being active in the reduction of ketones. The (η^5-Me_5C_5)Ir(L-aze)-Cl (aze = azetidine-2-carboxylate) complex was the most selective in the reduction of aliphatic ketones, effecting an ee of 93% for the reduction of pinacolone. The (η^5-Me_5C_5)Ir(L-pip)-Cl (pip = piperidine-2-carboxylate) complex was the most effective for the reduction of highly hindered ketones, producing ee's of 81% for 2,2-dimethyl-1-phenylpropan-1-one. The (η^6-Me_6C_6)Ru(L-pip)Cl complex was most selective in the reduction of acetophenone and its derivatives , producing an 89% ee for acetophenone. The method of chiral induction in the substrate was found to correlate to the chirality of the coordinated N, with N_R producing S products, and N_S producing R products, though this can only be applied to mono-alkylated amino acids, such as L-proline. A mechanistic investigation revealed that the classical concerted mechanism, which involves the transfer of the hydride and proton from catalyst to substrate in a single step was not in effect in the case of these catalysts. Instead, a stepwise mechanism is in play with the rate determining step and enantiodetermining step being the hydride transfer from metal to carbonyl carbon, followed by proton transfer by either solvent or amine proton.

Acknowledgements

First and foremost, I must thank my parent's Jim and Liz Morris. The whole "you didn't build that" pertains here. Without their constant love and support, both emotional and financial, I would not be where I am now. I thank my fiancée Amanda Nelson who has supported/tolerated me through this entire time in graduate school, the good and the bad, and provided much-needed advice in organic chemistry. I cannot imagine life without her. I wish to thank my two best friends Andrew Widmeyer and Scott Forbey, Andrew for always backing whatever I did and offering advice on life, and Scott for his help with graduate school, I never would have made it without you. I would like to thank my instructors at Frostburg State University who introduced me to chemistry, especially Dr. Jerald Simon, who introduced me to inorganic chemistry. I would like to thank my committee members, Prof. Karen Brewer, Prof. Paul Deck, and Prof. Brian Hanson, who challenged my knowledge and forced me to become better. Additionally, I need to thank Dr. Amanda Morris, her assistance and advice to me have helped me immensely in my career here at Virginia Tech. I need to thank William Bebout, Dr. Mehdi Ashraf-Khorassani and Geno Iannaccone, who have analyzed countless samples for me, and took the time to explain so many aspects of their methods to me. I owe a great deal to my fellow graduate students and post-doctoral researchers in the department, past and present. Of these, I must mention Dave Hobart, Dr. Travis White, Dr. Gerald Manbeck, Roberto Padilla, Dr. Rongwei Zhou, Dr. Brandon Thorpe, and Dr. Mike Berg. In addition, I must mention and thank the undergraduate researchers who have worked under me, Chad Bernier, Michael McGeagh, Nicholas Deweerd, and David DePena. Finally, I have to thank my graduate research advisor Prof. Joseph Merola. He took me in, and provided guidance, support, and belief that I could actually do this.

List of Tables

List of Figures

List of Schemes

Abbreviations

ACP = Acetophenone
Ala = Alanine
ATH = Asymmetric transfer hydrogenation
Ar = Aromatic
Arg = Arginine
Asn = Asparagine
Asp = Aspartic Acid
Aze = Azetidine-2-carboxylic acid
Bn = Benzyl
$CDCl_3$ = Chloroform-*d*
Cp* = Pentamethylcyclopentadienyl Ligand
Cy = Cyclohexyl
Cys = Cysteine
DCM = Dichloromethane
DMSO = Dimethylsulfoxide
Et_3N = Triethylamine
FA = Formic acid
F-Pro = 4-Trans-Fluoro-L-Proline
Gln = Glutamine
Glu = Glutamic Acid
Gly = Glycine
H-Pro = 4-Trans-Hydroxy-L-Proline
HCl = Hydrochloric Acid
HCOONa = Sodium Formate
Hex = Hexanes
His = Histidine
KOH = Potassium Hydroxide
Ile = Isoleucine
KIE = Kinetic Isotope Effect
Leu = Leucine
Lys = Lysine
MeOH = Methanol
Met = Methionine
$NaHCO_3$ = Sodium bicarbonate
NaOH = Sodium Hydroxide
Ph = Phenyl
Phe = Phenylalanine
Phengly = Phenylglycine
Pin = Pinacolone
Pip = Piperidine-2-carboxylic acid
Pro = Proline
RBF = Round bottom flask
Ser = Serine
SiO_2 = Silica gel
Thr = Threonine
TOF = Turnover Frequency
TON = Turnover Number

Trp = Tryptophan
Tyr = Tyrosine
Val = Valine

1. Introduction

1.1. Asymmetric transfer hydrogenation reaction of ketones

Transfer hydrogenation and hydrogenation of ketones are the delivery of H_2 across a C=O bond, producing an alcohol. Hydrogenation uses molecular hydrogen to achieve this purpose, while transfer hydrogenation uses any hydrogen source that is not molecular hydrogen. When these processes take place in the presence of a chiral catalyst and a prochiral substrate, they become asymmetric transfer hydrogenation (ATH) and asymmetric hydrogenation (AH), with ATH being the enantioselective version of transfer hydrogenation and AH being the enantioselective version of hydrogenation. The chiral catalyst favors the approach of only one "face" of the substrate, (re or si, figure 1.1). The catalyst offers alternative reaction pathways that favor one diastereomeric transition state over the other. This process is summarized in figure 1.2.

1.1.1. Transfer Hydrogenation vs Hydrogenation

The reduction of prochiral ketones to their respective optically active alcohols is one of the most important chemical transformations used today.[1-3] These chiral alcohols are used as intermediates in pharmaceutical and other fine chemical processes,[4,5] or the alcohol itself is used directly.[6] Chiral alcohols are used in the synthesis of a cholesterol reducing drug (**1**), as well as a potential Alzheimer's drug (**2**). Direct hydrogenation of a prochiral precursor leads to the anti-psychotic BMS (**3**).

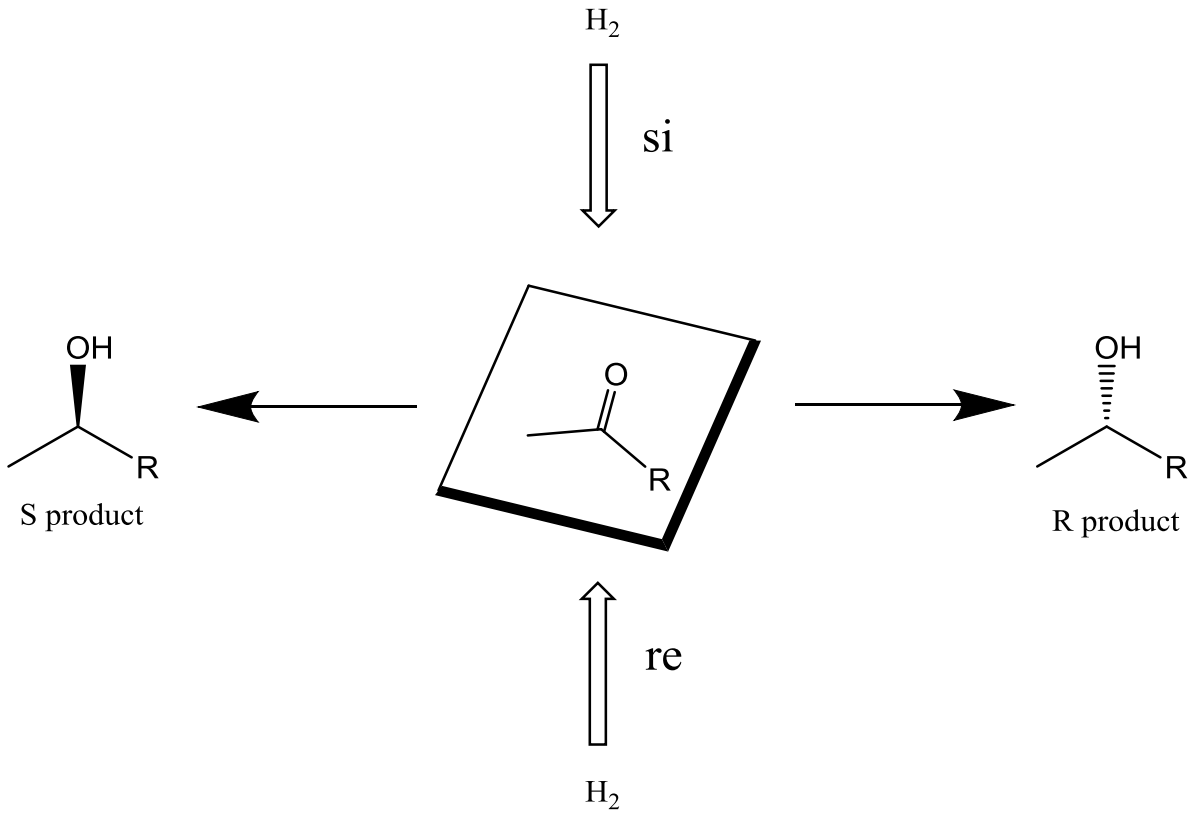

Figure 1.1: Delivery of H_2 across trigonal planar sp^2 – hybridized carbon to create a chiral alcohol product. Assignment of re or si follows Cahn-Ingold-Prelog priorities, with re having decreasing orders in the clockwise direction and si the opposite. The final configuration of the product is dependent on the incoming group.

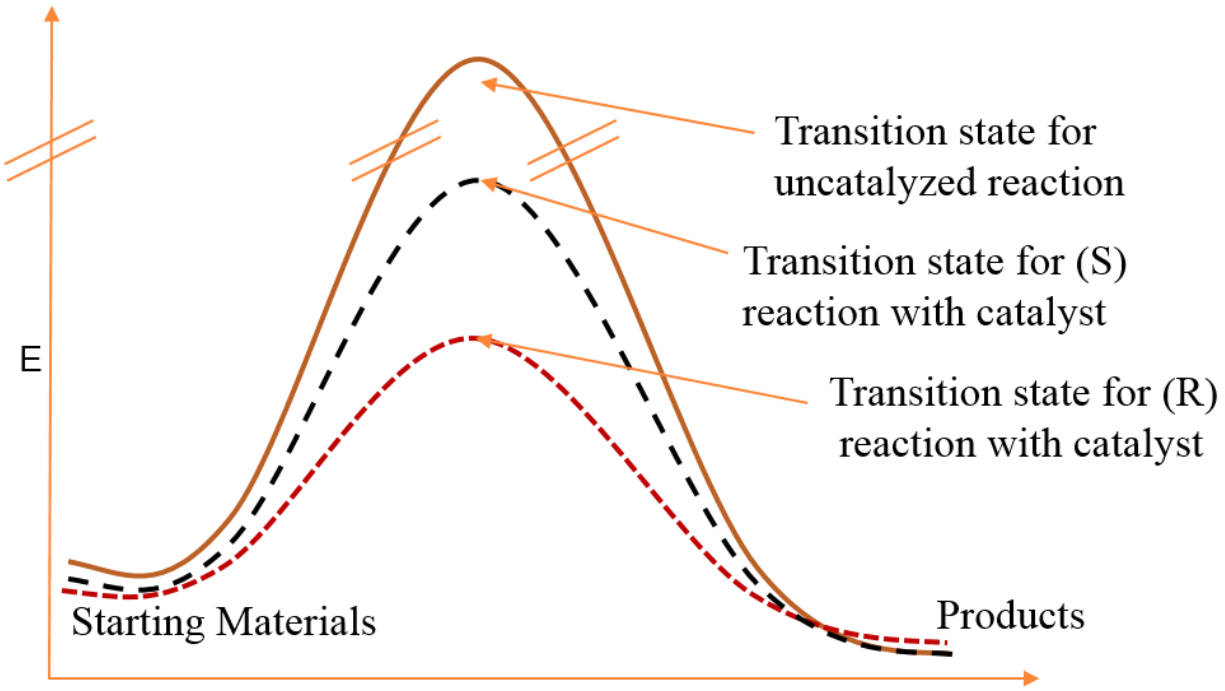

Figure 1.2: Reaction coordinate of an asymmetrically catalyzed reaction. Use of a chiral catalyst favors one diastereomeric transition state, leading to the faster formation of the R product. This results in the major product of the reaction being R.

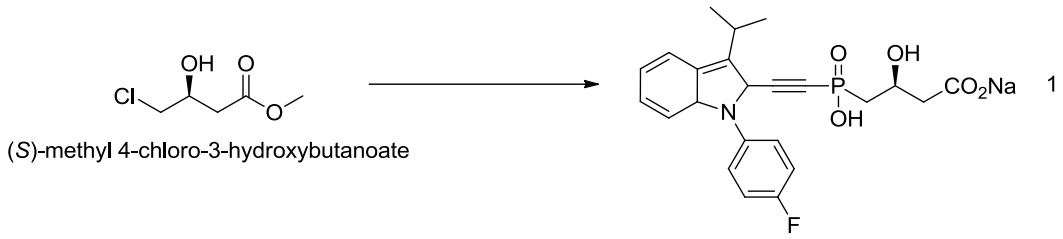

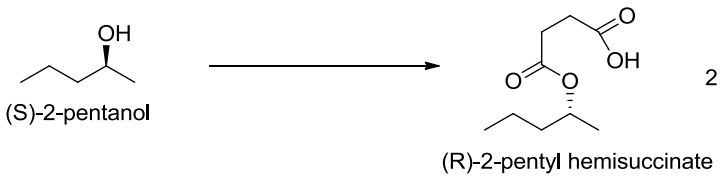

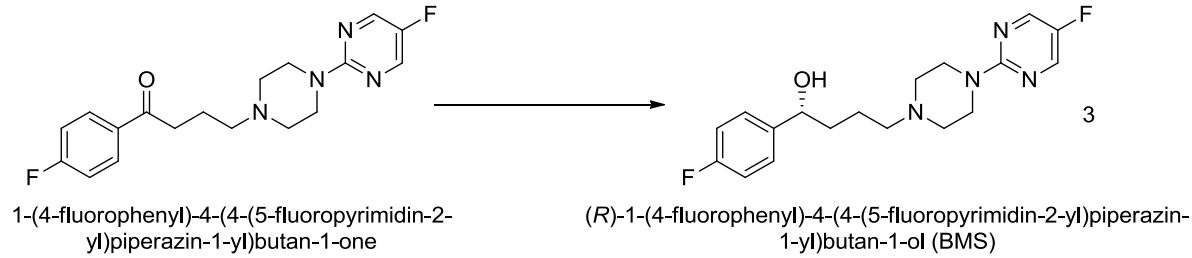

The catalytic reduction of C=O double bonds to their respective alcohols was first discovered by Meerwein, Ponndorf, and Verley in 1925 (MPV reaction). The reaction is highly chemoselective, reducing only aldehydes and ketones but not alkenes or alkynes. The reaction first used an achiral aluminum catalyst, which requires high temperatures and long reaction times and effects no enantioselection. Nguyen and coworkers introduced 1,1'-Bi-2-naphthol (BINOL) to aluminum as a C_2-symmetric ancillary ligand (**4**) to achieve enantioselectivities of a modest degree (80 %ee, 8 examples, 10 mol% catalyst, toluene, T= 298 K).[7] A samarium based system and C_2 tridentate ligand (**5**) converted aryl methyl ketones to secondary alcohols, with conversions exceeding 80% and enantioselectivities of >90% (10 examples, T = 298 K, 5 mol% catalyst, THF, 1-2 h).[8]

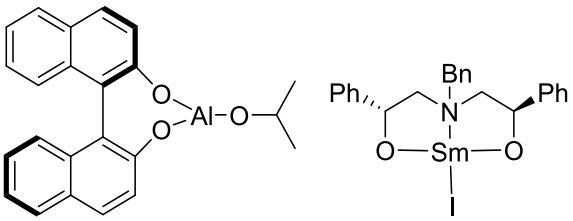

4 **5**

Figure 1.3: Catalysts used in the Evans method and Campbell method of reduction of prochiral ketones. 4 was able to achieve enantioselectivities of a modest degree (80 %ee, 8 examples, 10 mol% catalyst, toluene, T= 298 K). 5 converted aryl methyl ketones to secondary alcohols, with conversions exceeding 80% and enantioselectivities of >90% (10 examples, T = 298 K, 5 mol% catalyst, THF, 1-2 h).

The major breakthrough in asymmetric transfer hydrogenation came from Noyori in 1996, with his now famous mono-tosylated 1,2-diphenylethane-1,2-diamine (DPEN) ligand in combination with a Ru arene. The system of **(S,S)-6** is (see scheme 1.1) capable of reducing a large scope of substrates with high selectivities at low catalyst loadings. Acetophenone is reduced quantitatively to the (S) alcohol with an 98% ee (scheme 1.1).[9] For a more in depth review and substrate scope the reader is directed to the review by Xiao et al.[10]

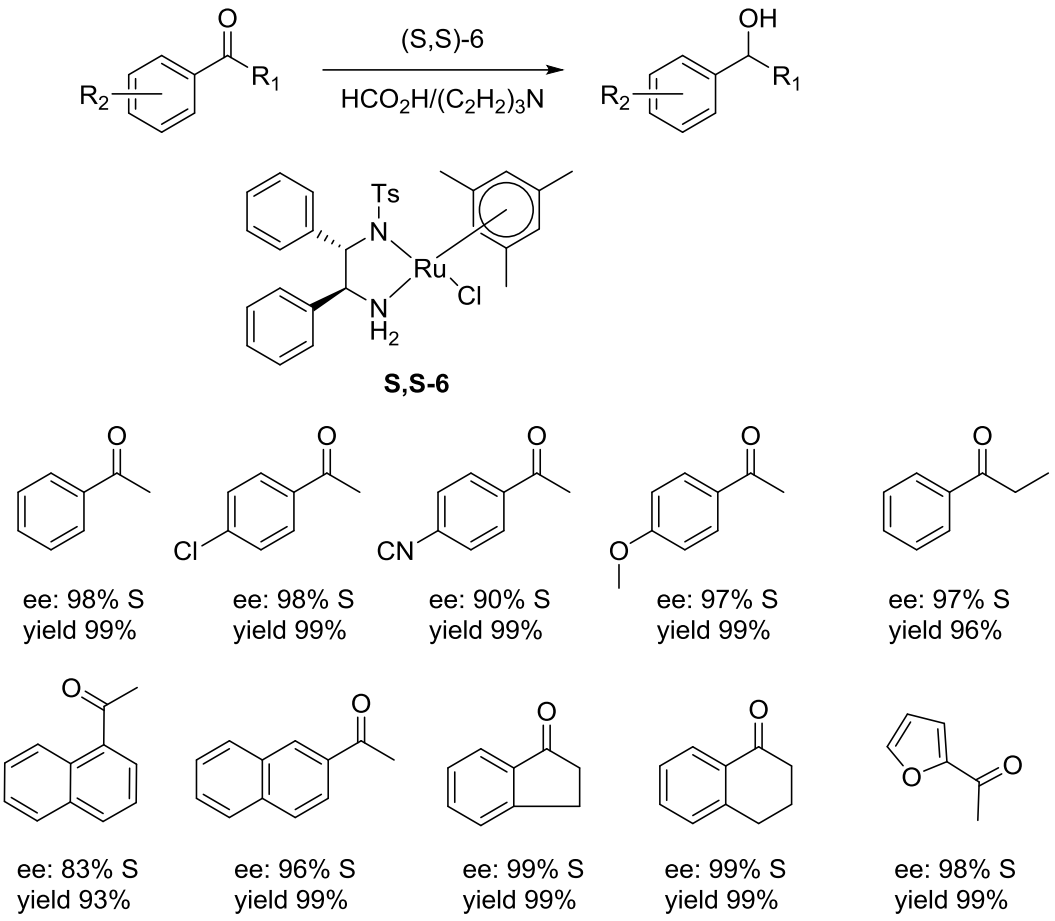

Scheme 1.1: Noyori's catalyst for ATH, showing large substrate scope for aromatic ketones. Reactions took place in formic acid/triethylamine solvent mixture with 1% catalyst loadings.

The original system described by Noyori is highly chemoselective, with olefins, halogens, esters, and nitro groups not reduced under the reaction conditions. Other ligands employed in ATH are chiral amino alcohols such as indanol **(7)**, 2-azanorbornyl alcohol **(8)**,[11] and various forms of 2-amino-1,2-diphenylethanol **(9).**[12] Amino alcohol ligands produce similar selectivities to their diamine counterparts, but the rate is decreased when a formic acid/triethylamine mixture is used as the hydrogen source. This rate effect is reversed when the reaction is performed in 2-propanol. Amino alcohols can have both cis and trans-configured ligands at R_1 and R_2 and achieve high

enantioselectivies (**9a** and **9b**), whereas the monotoslyated diamines require a trans configuration for good selectivity (**9c**). The R_2 center is considered more important for the configuration of the product in the case of amino alcohols but in the case of tosylated diamines the center at R_1 is more important.[13]

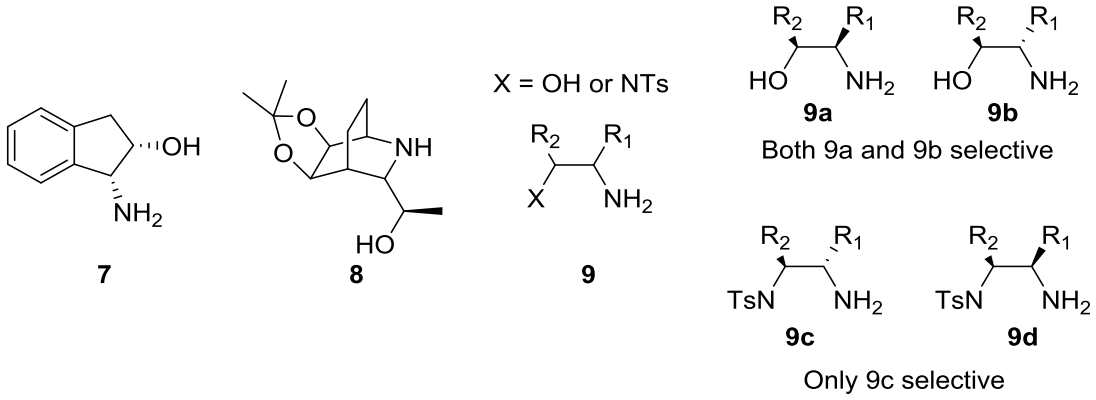

Figure 1.4: Amino alcohol ligands used in ATH. Amino alcohol based systems are generally incompatible with the formic acid/triethylamine based reductions but show a rate enhancement in 2-propanol based reductions. The metals used in conjuctions with these ligands are the same for the related monotosylated diamine ligands, (Ru, Rh, Ir).

In a rare example of improvement upon Noyori's original design, Wills and co-workers[14] employed a tethered Ru(II) complex with an arene ligand that is covalently bound to the amine functionality. When the complex is tethered through the sulfur as in **10**, both reactivity and selectivity were lowered. But the tethered complex (**11**) showed higher reactivity and the catalyst loading could be lowered. Further investigation has shown that the length of the tether can be optimized in the case of **11**. When the tether length is reduced to 2 carbons conversion drops significantly. A length of 5 carbon atoms increases reactivity to beyond that of **11.**[15]

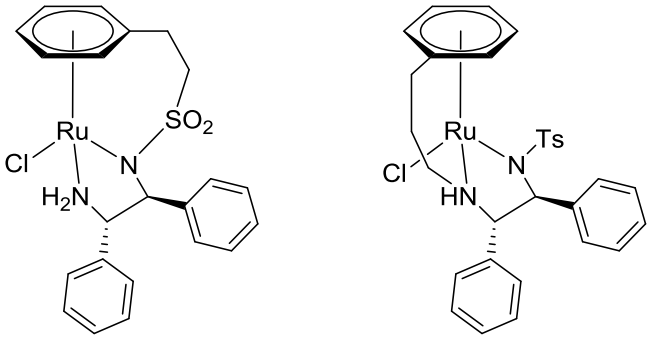

10 **11**

Figure 1.5: Wills' tethered catalyst system. Tethering the ligand through the sulfur (10) reduces reactivity and selectivity compared to an untethered ligand. In the case of the tether forming between the amine and arene, lengthening of the carbon chain increased activity, with 3 carbons (11) showing higher reactivity than 2 carbons (not shown), and a 5 carbon chain showing the highest reactivity, (not shown).

Wills used a similar method with Ir(III) and Rh(III) variants of ATH catalysts.[16] While complications in the synthesis led to inconclusive results for the iridium analog, the rhodium analog again showed increased reactivity compared to the untethered variant.

Ancillary ligand modification (the arene) has also been studied, though this has been limited to the ruthenium arene system due to the availability of the arene precursors. Both arene and pentamethylcyclopentadiene ligands are quite common in asymmetric catalysts due the fact that they will occupy three of the six coordination sites of the metal leaving two sites open for the bidenate ligand and one for the halide. They are also modified with ease or have several variants commercially available. The effects of differing arene ligands on ATH was investigated by Mortreux et al.[17] The results are summarized in scheme 1.2.

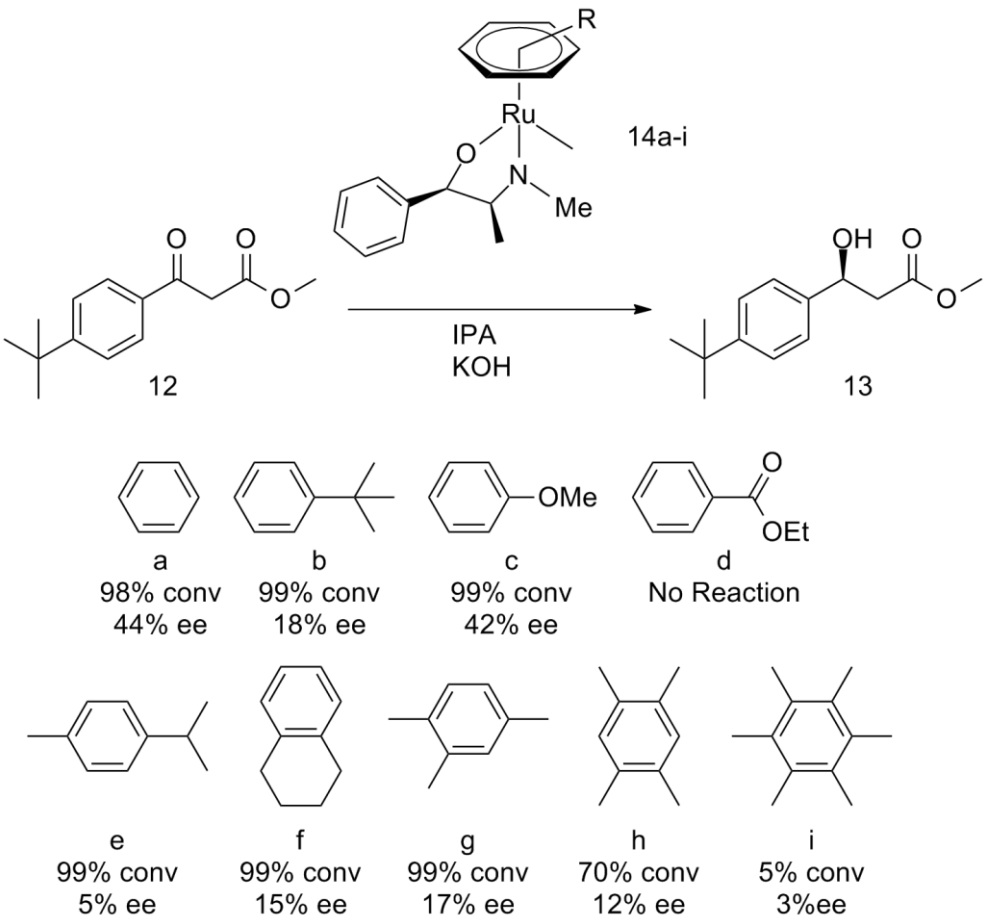

Scheme 1.2: Results of Mortreux study. Little correlation between steric bulk or electronic environment and the effectiveness of the catalyst was found.

Steric effects influence the reactivity as seen with the lower conversions of **14i** and **14h**, with the benzene (**14a**) variant having the greatest reactivity. However, no true correlation can be seen with sterics and selectivity. Additional electronic effects are seen with **14c** and **14d. 14c** showed similar rates of reaction to 1**4a**, whereas the deactivating group of **14d** led to no reaction at all. A different study by Noyori[18] showed that the arene ligand did directly impact the selectivity of the catalyst but not reactivity. Benzene was shown to be least selective (17% ee), followed by $C_6H_3Me_3$ (56% ee), p-cymene (59% ee), and hexamethyl benzene (92% ee), when acetophenone is the substrate and **15** as the ligand.

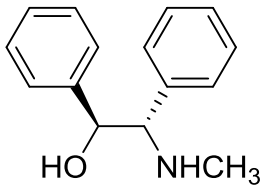

15

Figure 1.6: Amino alcohol ligand used in Noyori's Ru arene study. The steric bulk of the arene used lead to greater selectivity in the reduction of acetophenone. Benzene was shown to be least selective (17% ee), followed by $C_6H_3Me_3$ (56% ee), p-cymene (59% ee), and hexamethyl benzene (92% ee). Reactivity was unaffected by the change in arene ligand.

Noyori's landmark paper used 2-propanol as the hydrogen source with an alkoxide base being necessary to obtain the active hydride catalyst.[19] However, when this system is used the reaction is reversible, which causes both low conversions and lowered selectivities if the reactions are not performed with a low concentration of substrate. An initial solution to this problem was to perform the reaction with low substrate concentrations (0.1 M). A year later this problem was solved by Noyori et al. by using an azeotropic mixture of formic acid and triethylamine. This mixture leads to the formation of CO_2 gas when formic acid is used as the hydrogen source, thus making the overall reaction irreversible. This allows both the yields to be increased and the reaction to be carried out at much higher concentrations (10M) with no adverse effects.[9] The overall simplicity of the organic hydrogen sources mentioned above provide an advantage to using molecular hydrogen such as the elimination of high pressure reaction vessels and gaseous H_2 which is highly flammable.

In the area of asymmetric hydrogenation (AH), where the hydrogen source is molecular hydrogen, Noyori again developed the leading catalyst (scheme 1.3). In the case of AH, a chrial diamine is used in combination with a chiral diphosphine (**16)**.[20] In the presence of base and 2-propanol, this catalyst achieves remarkable activity and selectivity, though it is limited to aromatic ketones like its ATH counterpart.

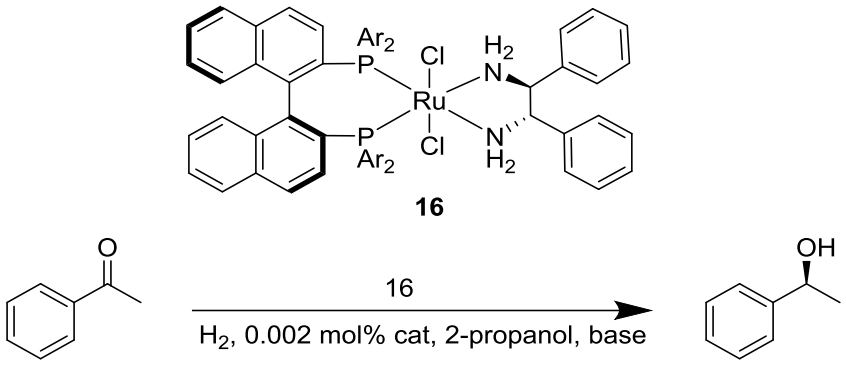

Scheme 1.3: Noyori's asymmetric hydrogenation catalyst system. Extremely low catalyst loadings can be achieved using the ligand combination of a chiral DPEN ligand and chiral diphosphine with a Ru metal center.

Since the initial discovery, attempts to improve Noyori's system have been done through modulation and synthesis of ligand sets. Very few ligand sets improved upon the catalytic activity, and are shown in figure 1.7. Like the original catalyst, these are combinations of chiral diphosphines and 1,2 or 1,4 diamines. The proper combinations lead to excellent reduction of a large number of aromatic ketones, with the combination of **15** and **19** being able to reduce 1-tetranones and analogs with high selectivity. However, there is no universal catalyst for all ketones.[21-24]

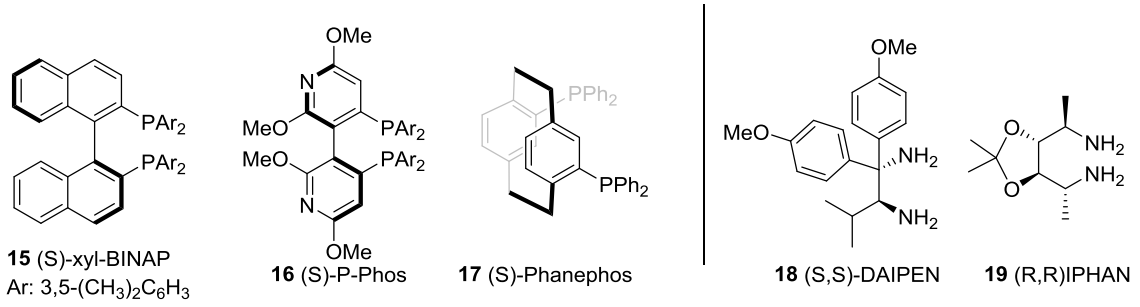

Figure 1.7: Selected diphosphine and diamine ligands used in asymmetric hydrogenation. Ligand combinations of 15 and 19 with Ru produced selectivities and conversions for several cyclic ketones in the range of 98-99% and 97-100% respectively. 16 in combination with a DPEN ligand reduced acetophenone derivatives with full conversions and selectivities ranging from 93-99%. Ligands 17 and 18 show high conversions but reduced selectivity in comparison with the prior combinations.

Table 1.1 provides a summary of the current methods for ATH and AH. For the most part hydrogenations are still the industry standard due to lower catalyst loading, however ATH is also performed on the industrial scale.

Table 1.1: Comparison of ATH and AH methodology

	ATH	**AH**
Selectivity	Aromatic: 95-99%	Aromatic: > 98%
Substrate concentration	Up to 1M	Up to 10M
Reactivity	Slower than AH	Faster than ATH
Solvent	Organics or Water	Organics
Scale of synthesis	Small to Medium	Large Scale
Turn over Number	Up to 10^4	Up to 10^6
Catalyst loading	0.1000 in standard conditions	0.00010 in standard conditions
Hydrogen source	2-propanol, sodium formate	Molecular H_2

1.1.2. Mechanistic Aspects of ATH

Numerous experimental and theoretical studies show that ATH involves a pathway in which one hydrogen is delivered directly from the metal ion (hydride) and the other from an amine ligand (proton). These bifunctional catalysts serve as both base (hydride) and acid (proton), and proceed through an outer sphere mechanism with the substrate binding at the ligands,[25] as opposed to the MPV reaction where the substrate binds to the metal ion. A pericylic transition state with concerted hydride and hydrogen transfer is the rate limiting step, shown in scheme 1.4. The overall mechanism proceeds as follows; In the presence of base, the 18 electron complex (a) eliminates HCl to become the coordinately unstaturated 16 electron complex (b). The 16 electron complex reacts with 2-propanol (c) to form the active hydride species (d) which will then reduce acetopheone to 1-

phenylethanol (e). Both the 16 electron complex (**20**) and the hydride (**21**) of the ruthenium based system have been isolated and characterized by X-ray diffraction, as seen in figure 1.8.[26] The 16 electron intermediate adopts a square planar-like configuration, with a short Ru-N bond length, (1.897), compared to the chloride species, (2.108) , indicating π donation from the nitrogen into the Ru center.

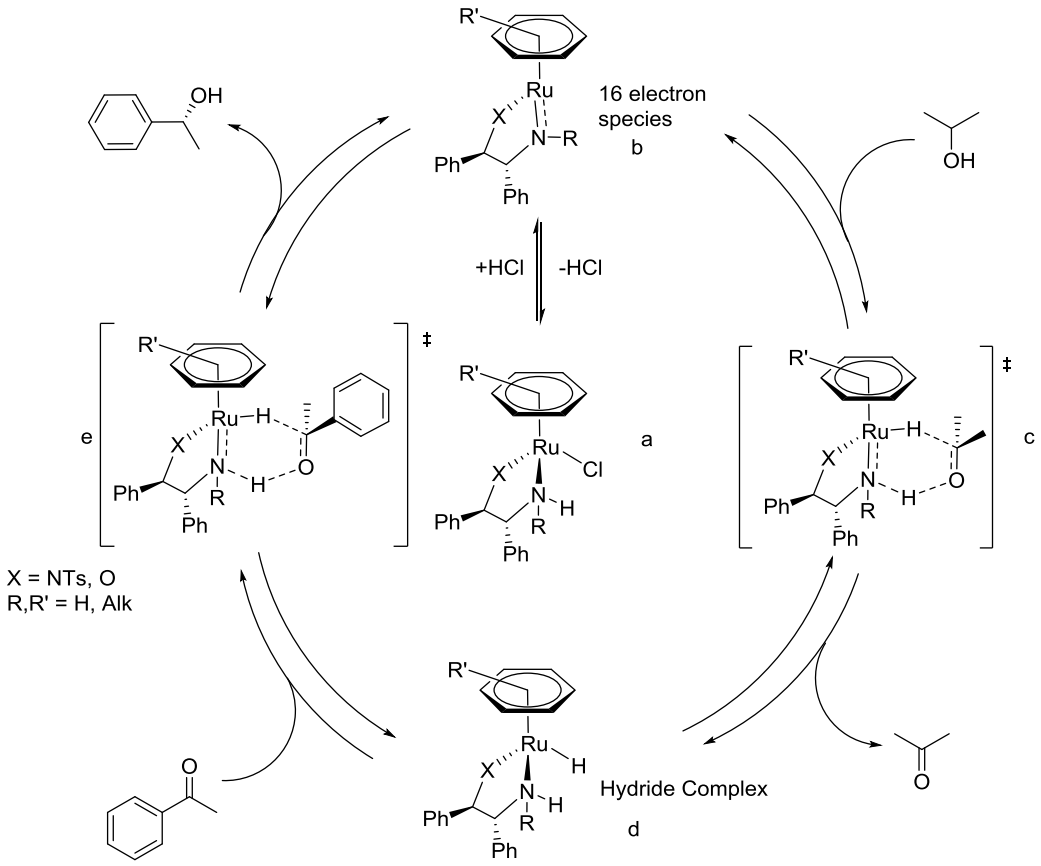

Scheme 1.4: Classical pathway for ATH as described by Noyori.[27] The rate determining step and entantio-determining step is the concerted transfer of the amine proton and hydride to the substrate. This generates the 16 electron species which reforms the active hydride species through oxidation of 2-propanol to acetone.

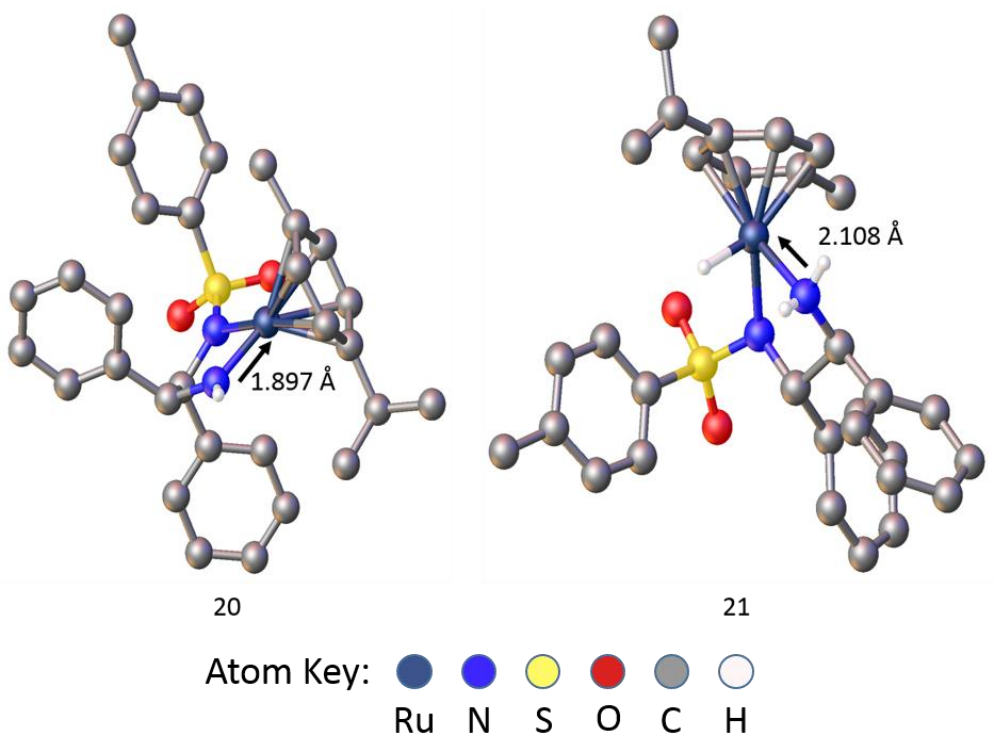

Figure 1.8: Molecular structures of the catalytic intermediates 20 and 21 as observed by single crystal X-ray diffraction. Formal addition of the H_2 to the amido complex 20 affords the amine complex 21. 21 shows a decrease in the formal Ru-N bond order and a lengthening of the Ru-N intramolecular distance.[26]

However, several papers contest the concerted pathway displayed above.[28-30] There is a significant rate enhancement when ATH is performed in water, and using a co-solvent study showed an increase in reaction rate with increasing polarity of co-solvent, (hexane < Et_2O < toluene < CH_2Cl_2 < DMF). The pericylic transistion state cannot account for this rate enhancement, as charge distributions are similar in both the activated complexes and reactants. A dipolar transition state does account for this, having vast differences in charge separation and distribution in the activated complexes versus the reactants. Kinetic isotope effect studies also support a non-concerted pathway (table 2). Little to no KIE is observed (k_H/K_D = 1.06) when [D_7]DMF is the only isotope changed to deuterium, indicating that DMF is acting only as a co-solvent. Changing H_2O to D_2O gives rise to a

slight KIE of 1.68. This experiment is changing the hydrogen transferred from the amine to a deuterium. The large KIE (2.24) observed for the DCOONa labeled study show that transfer of the hydride from the metal center to the substrate is most likely the rate-determining step, since the KIE oberserved here is larger than what was seen in the D_2O experiment (2.24 vs 1.68). Most important is that in a concerted reaction, the product of both the KIE of the hydrogen transfer and the hydride transfer should be equal to the doubly labeled experiment (DCOONa and D_2O KIE, 3.05). However, the product of the two runs is 3.76, larger than the KIE of the doubly labeled experiment (3.05). This gives credible evidence for a step-wise mechanism, with hydride transfer from the metal to substrate being the rate-determining step.

Table 1.2. Kinetic isotope effects of ATH of acp.[28]

Isotope Used	k_H/k_D
HCOONa/H_2O/DMF	1
HCOONa/H_2O/[D_7]DMF	1.06±0.10 ($k_{DMF}/k_{[D7]DMF}$)
HCOONa/D_2O/DMF	1.68±0.10 (k_{RuHNH}/k_{RuHND})
DCOONa/H_2O/DMF	2.24±0.10 (k_{RuHNH}/k_{RuDNH})
DCOONa/D_2O/DMF	3.05±0.50 (k_{RuHNH}/k_{RuDND})
DCOONa/D_2O/[D_7]DMF	3.10±0.50 (k_{RuHNH}/k_{RuDND})

A revised pathway using 2-propanol as solvent and hydrogen source was proposed by Dub and Ikariya and is shown in scheme 1.5. There are two different cycles presented. In each case, the first step is the hydride transfer from the Ru to substrate (a). From here the cycle can go through two difference pathways. The first involves the transfer of the hydrogen from the 2-propoanol (b). From b, the active hydride species is regenerated through beta-hydride elimination of 2-propoanol (e). In the other pathway, the hydrogen is transferred from the amine (c). This is followed by protonation of the 16e species by 2-propoanol (d), which leads to regeneration of the hydride species through step e.

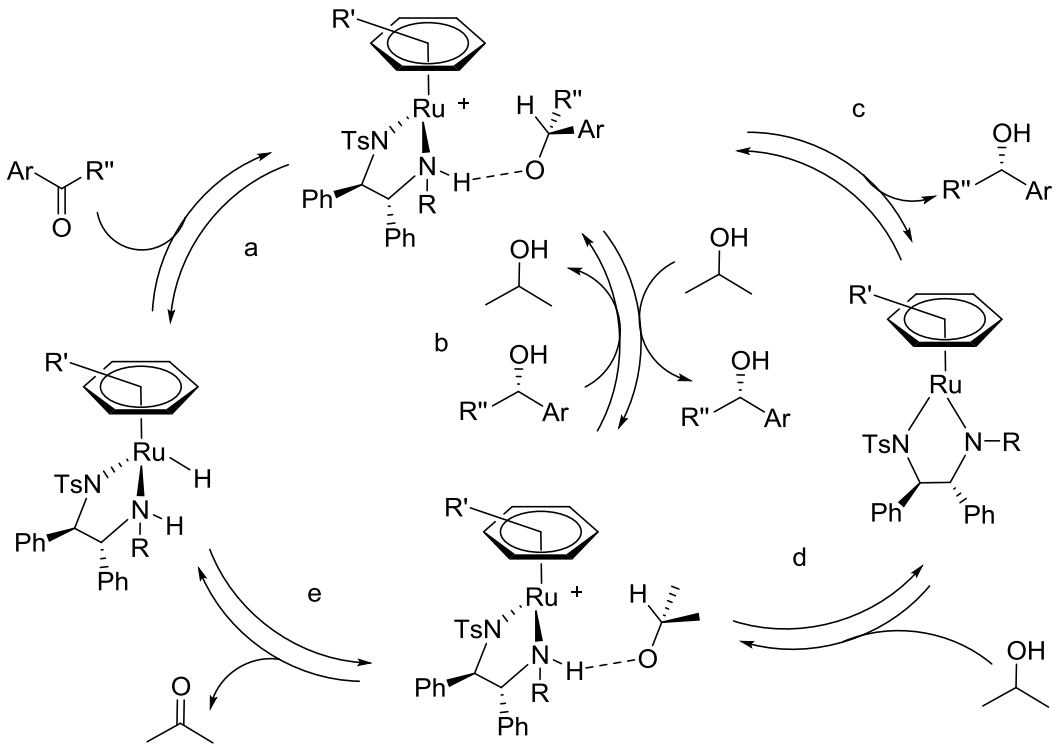

Scheme 1.5: (a) involves the transfer of the hydride from the Ru center to the substrate. (b) is the transfer of the hydrogen from 2-propoanol to substrate. (c) is the transfer of hydrogen from the amine ligand to substrate. (d) is the protonation of the 16e species from 2-propoanol. (e) is the regeneration of the active hydride species through beta-hydride elimination of 2-propoanol.

It is agreed that an NH or NH_2 group is needed in the ligand for high catalytic activity, since similar dialkylated variants show decreased activity or none at all.[25] The hydrogen bond formed between the oxygen of the carbonyl compound and the NH portion facilitates the hydride transfer to the carbon atom. Pavlova and Meijer[30] performed similar calculations using water as the solvent. Their work led to the conclusion that the proton transferred to the substrate is from the water, not the amine. While the NH or NH_2 is not necessary for the for formation of the alcohol product by transferring a hydrogen, the hydrogen bond formed between the amine hydrogen and the carbonyl oxygen lowers the overall energy of the reaction by increasing the partial positive charge on the carbon of the substrate.

Selectivity is influenced by the ligand through several interactions. First, that the DPEN backbone allows the formation of almost exclusively one diastereomer in solution. Second the Tosyl group increases the acidity of this amine so it is unprotonated, leaving only the non-Tosylated amine group capable of interacting with the substrate through hydrogen bonding. This creates only one face of the catalyst with a favorable hydride/hydrogen alignment (figure 1.8, **21**). However, these factors alone do not account for all sources of selectivity. The (CH or CH_3)/π interaction is key in determining the final configuration of the alcohol product, displayed in figure 1.9.[27] The interaction is supported by the final configuration of the product with the Re face of acetophenone being favored due to this electronic interaction. Using para-substituted benzaldehyde-1-d derivatives as a model substrate, it was noted that two factors impact this favorable interaction. The first being the increased acidity on the arene hydrogens when coordinated to the ruthenium with the second being the partial negative charge on the ortho carbon. These electronic effects are supported in a study by Noyori in the reduction of several para-substituted benzaldehyde-1-d derivatives outlined in scheme 1.6.[31] The electron donating groups of methoxy and methyl increase the acceptor character of the aromatic ring whereas electron withdrawing groups such as CF_3 and bromine decrease selectivity. Also included in the study were the reductions of trans-cinnamaldehyde-1-d and dihydrocinnamaldehyde-1-d. The reduction of these substrates under the same conditions as above resulted in nearly racemic products due to lack of CH- π interactions.

An additional factor contributing to selectivity is the destabilization of the transition state of the minor enantiomer by repulsion between the SO_2 group of the tosyl moiety and the π-cloud of the ketone. This factor explains why complexes using the N-sulfonylated DPEN outperform their amino alcohol counterparts.[29]

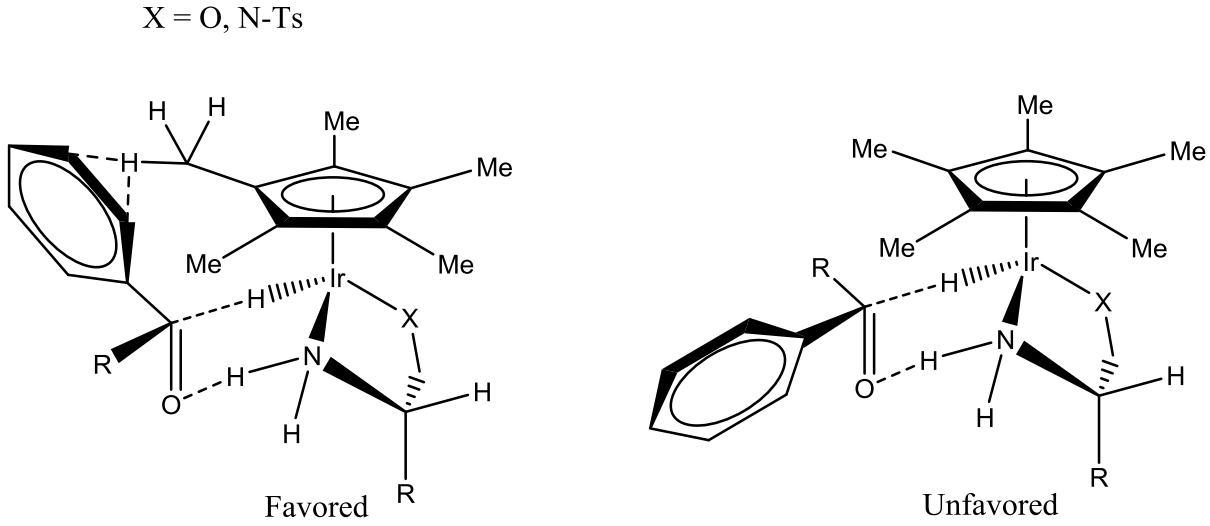

Figure 1.9: Transition state showing CH_3/π interaction. The re face of the acetophenone is favored due to this interaction. The addition of electron withdrawing groups to the para position of the acetophenone reduces this effect, as seen in a loss of selectivity. This is further outlined in scheme 1.6

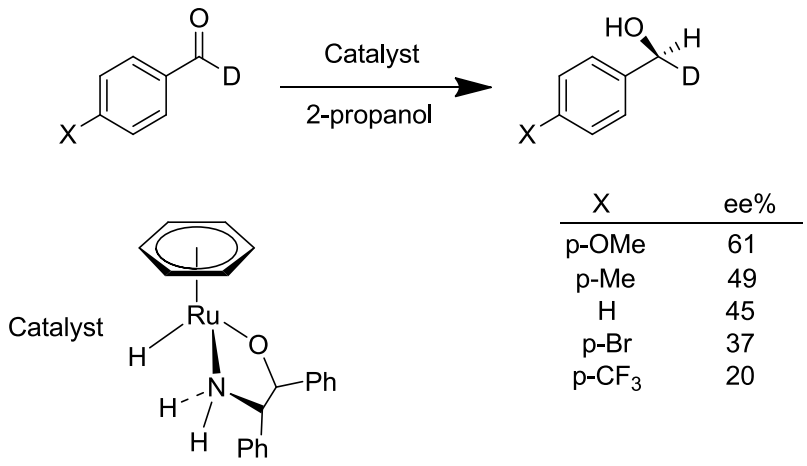

X	ee%
p-OMe	61
p-Me	49
H	45
p-Br	37
p-CF_3	20

Scheme 1.6: Results supporting CH/π interaction, Electron withdrawing groups decrease ee% due to destabilization of the CH/π interaction.

1.1.3. Mechanistic Aspects of AH

The mechanism for AH is very similar to the one for ATH, scheme 1.7. The active hydride complex is formed from loss of chlorine and coordination of hydrogen followed by heterolytic cleavage.[32] As

with the hydride species in ATH, the active hydride in AH was isolated and characterized by X-ray diffraction.

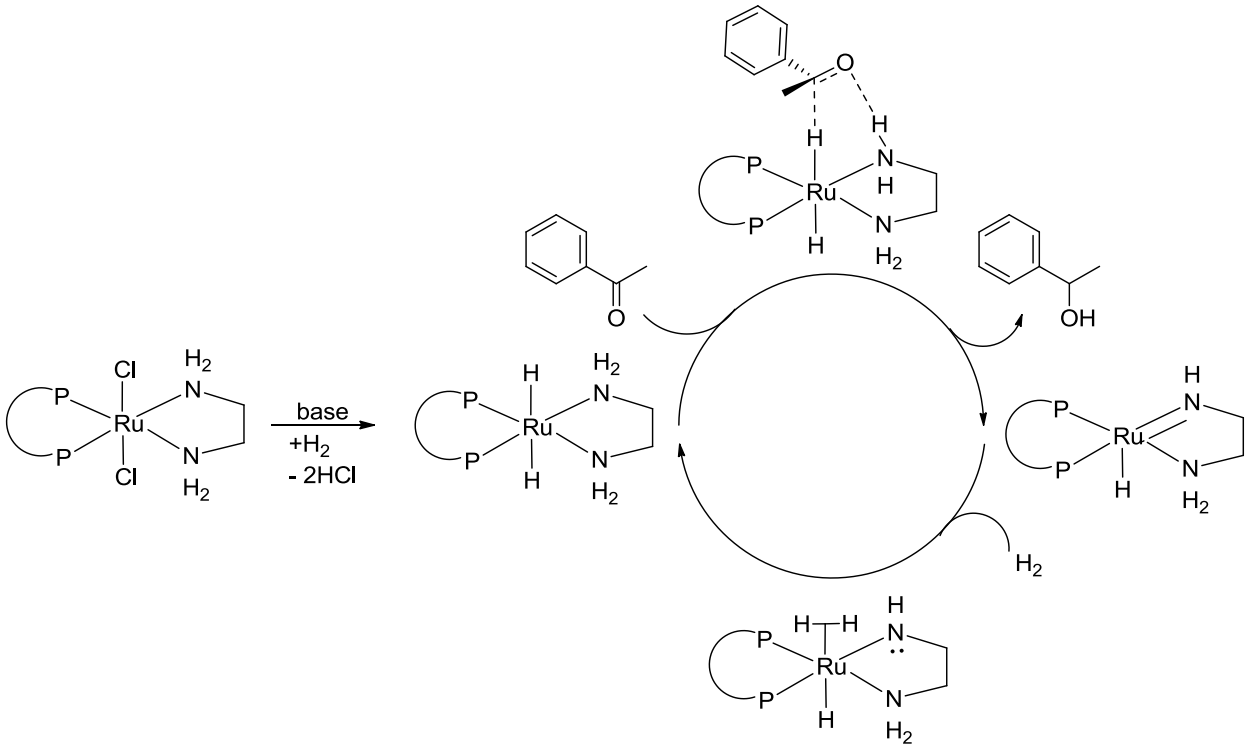

Scheme 1.7: The proposed mechanism for asymmetric hydrogenation.[32] The RDS and EDS are the transfer of the hydride and hydrogen from the catalyst to the substrate. The catalyst is regenerated through binding of hydrogen followed by heterolytic cleavage.

As is the case in ATH, the mechanism proceeds through the outer sphere with at least a part of the action taking place at the ligands. The transition state is a six membered ring, with transfer of the hydride to the carbon and proton transfer to the oxygen occurring in a concerted step. Regeneration of the catalyst is through the cyclic imido intermediate, which reacts with molecular hydrogen.[33] However, recent work by Dub and co-workers has revised several steps in this pathway extensively, but the key hydride transfer from the metal to the substrate remains unchanged.[34] A full discussion of the mechanism is beyond the scope of this work.

Until very recently catalysts for AH could not perform ATH and vice versa, even though the critical hydride transfer step of each mechanism is largely the same. Both metal hydride and precursor are nearly identical,[35] but transfer hydrogenation catalysts would not react with molecular H_2 to form the active hydride species. However, if the AH conditions are switched to acidic instead of the basic, the active catalytic species is generated through the cationic Ru species (scheme 1.8).[36] The generation of the 16e cationic complex is key, with less polar solvents slowing the reaction.[37] Additionally, excess chloride ions will retard the reaction. Xiao has also shown that using water as a media, basic conditions could be used in conjunction with IrCp*diamine complexes for the reduction of simple aldehydes.[38]

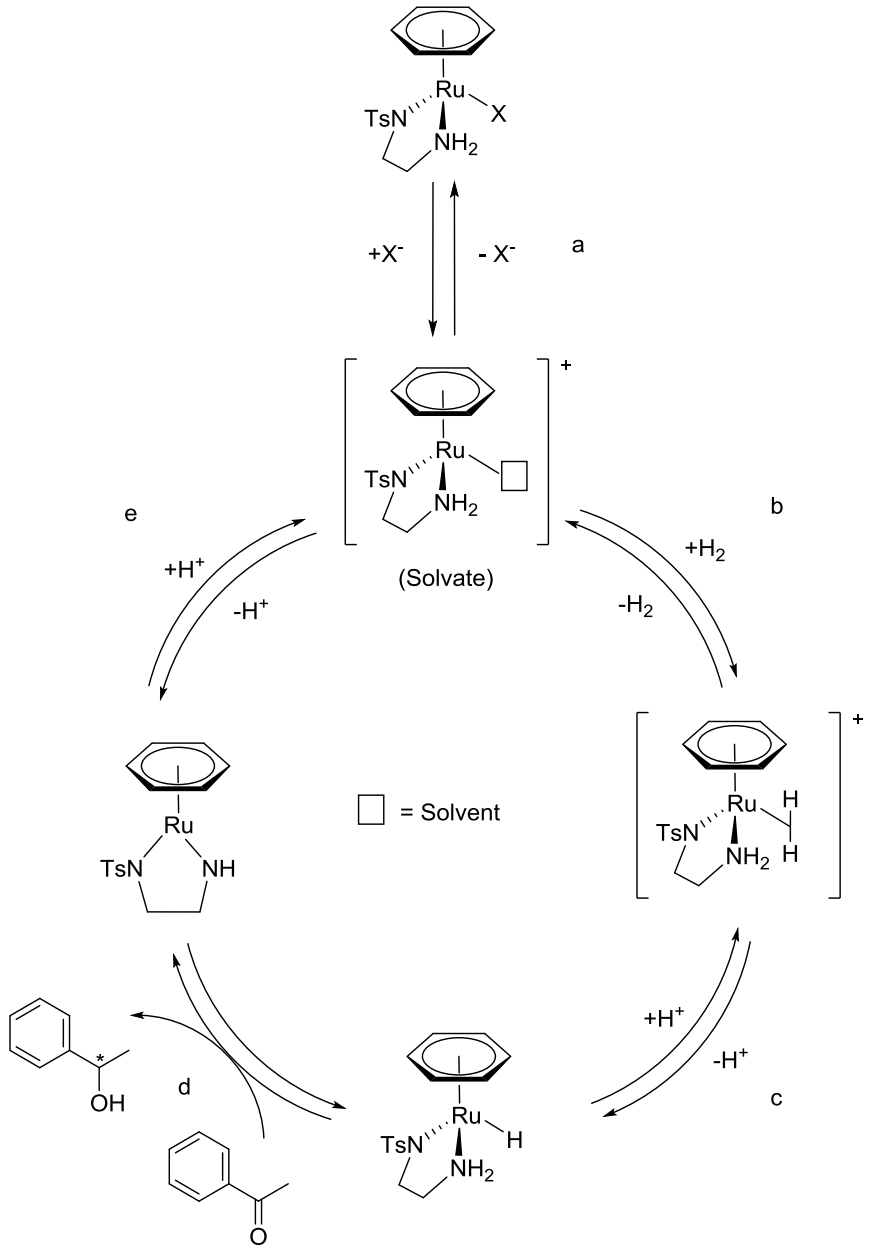

Scheme 1.8: Mechanism for AH using the ATH catalyst. Forming of the 16e$^-$ solvate complex is key to the reaction (a). From here H_2 binds to the open coordination site (b). Deprontation of this η^2-H_2 complex leads to the active hydride species (c), followed by the binding and reduction of acetophenone (d). The 16e$^-$ species is reprotonated through acidic conditions (e).

1.1.4. ATH in Aqueous Media

There has been considerable interest in performing ATH reactions in water in recent years. Water allows for easy separation of products from solvent and allows the use of sodium formate as

the hydrogen source which is readily available and inexpensive. Initial studies focused on biphasic systems incorporating water soluble ligands containing sulfates. Work by Thorpe et al. used ligands **22**, **23**, **24** on ruthenium, iridium, and rhodium based systems to reduce various aromatic ketones in 2-propanol/water in the presence of base.[39,40] While the selectivities were lower than previously reported systems, a rate enhancement was observed for the reactions with an increased water concentration, which at the time was unexplained.

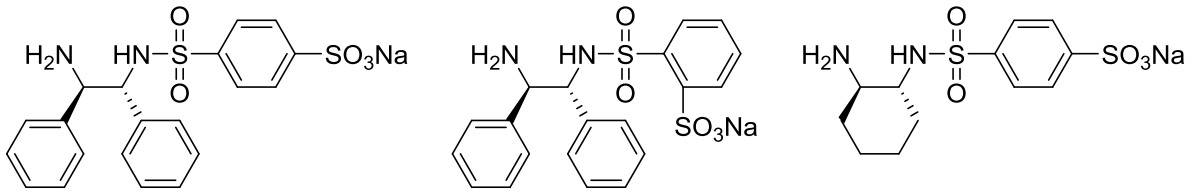

Figure 1.10: Sulfonated ligands used for water-based ATH. Ligands 22 and 23 produced the highest selectivities. 22 and 24 had similar reactivity, with 23 significantly decreasing reactivity. Rh and Ru based systems outperformed the Ir counterparts.

In 2004, Xiao et al. used the previously described Ru-TsDPEN system in water for the reduction of several ketones with sodium formate as hydrogen source.[41] Compared to the TEA/FA mixture there is a significant rate enhancement. In the case of acetophenone there is full conversion in 1 h in water, with the TEA/FA mixture requiring more than 10 h. The reduction was faster for all ketones examined, though selectivities were slightly lower.

The iridium and rhodium based systems also see a significant rate enhancement in water when compared to the 2-propanol based system.[42] Neither the iridium nor rhodium are compatible with TEA/FA mixture unless water was introduced to the system. Table 1.3 summarizes the results of the study. Moreover, the reaction can be carried out under air. In another study, the reaction was performed in DMF with varying levels of water concentrations. Upon increasing the water concentration from 20% to 80% the rate constants increase from $k = 0.05\ min^{-1}$ to $0.18\ min^{-1}$. DFT

calculations reveal a lowering of the activation energy for the hydrogen transfer to acetone when water is included in the reaction pathway.[28]

Table 1.3: Results of solvent variation in ATH systems. A clear rate enhancement is seen in reductions performed in water

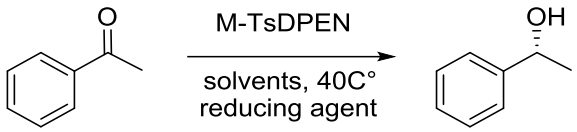

Reductant/ Solvent	**Ru**			**Rh**			**Ir**		
	t (h)	Conv %	%ee	t (h)	Conv %	%ee	t (h)	Conv %	%ee
$HCOONa/H_2O$	1	99	95	0.5	99	97	3	99	93
2-propanol	24	81	89	24	45	89	24	48	87
Azeotrope (FA/TEA)	10	98	97	16	1	-	16	No	-

The mechanism in water is summarized in scheme 1.9. There are several cycles present depending upon pH, but the overall steps remain the same. The catalyst exchanges chloride with water to form a mono-aqua cation. This cation binds formate which undergoes a beta-hydride elimination to create the active hydride species. Following this, the substrate binds to the outer sphere, meaning the metal hydride and the amine hydrogen. The hydride and hydrogen are then transferred, generating the 16e complex found in the 2-propanol based systems. The active hydride species is regenerated with water and formate.

When ATH is performed in water there is an optimal pH window for both selectivity and rate of reaction. The Ru based system performs best at pH = 5-8.[43] Rh and Ir systems have optimal windows of pH from 5.5 to 10.0 and 6.5 to 8.5 respectively. In any case, the decrease in selectivity at lowered pH is attributed to the protonation and subsequent decoordination of the tosylated amine group, allowing for greater steric freedom in the catalytic system. The increased rate of reaction at these pH levels is generally thought to be from greater concentrations of the formate anions in

solution, leading to faster generation of the hydride species. At higher pH the reaction will cease due to high concentrations of hydroxide anion which will bind irreversibly to the open coordination site of the catalyst. As stated before the mechanism is step-wise, with the rate determining step and the enantiodetermining step are the hydride transfer from the metal to the carbon of the substrate. The oxygen is protonated via either water or the amine proton.

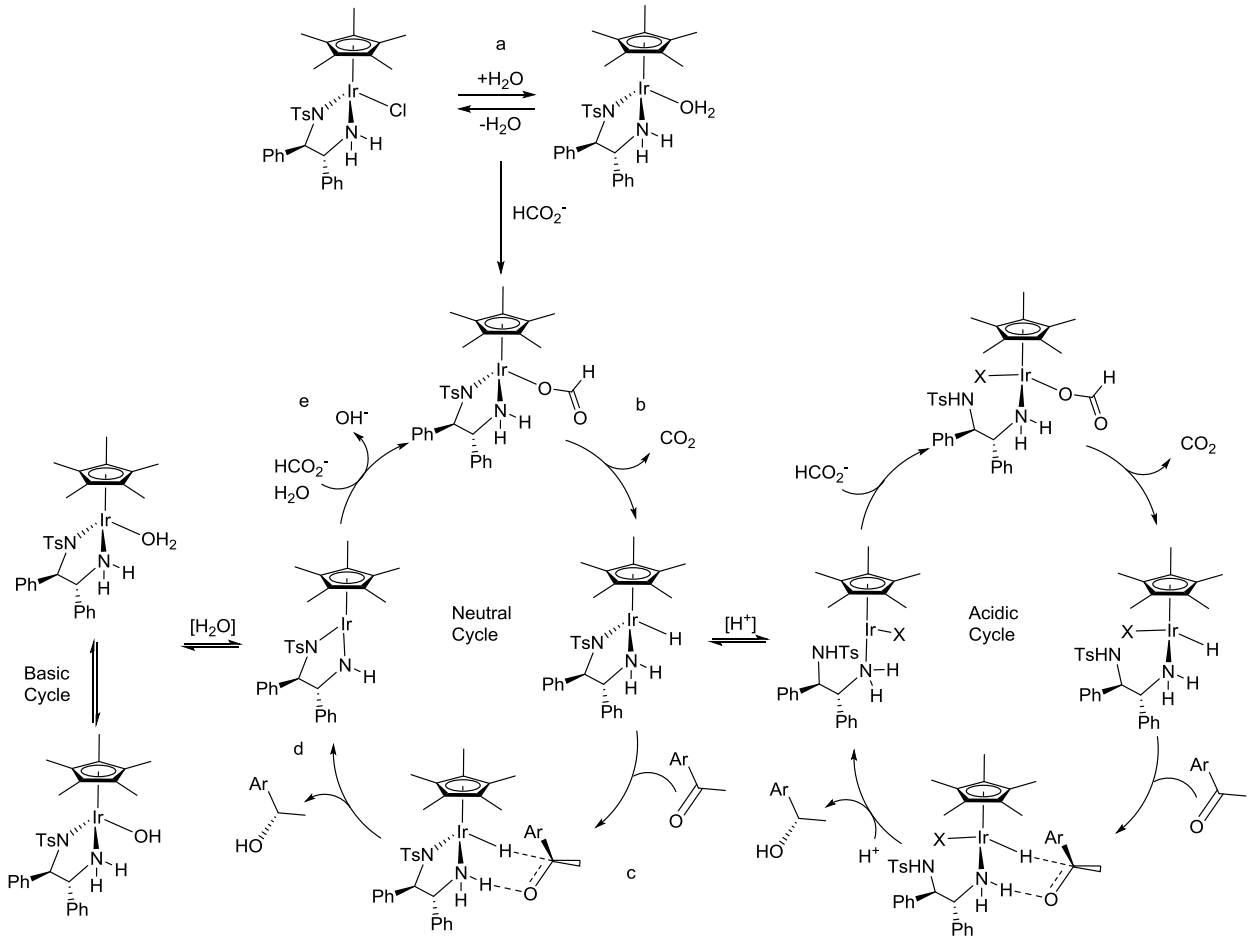

Scheme 1.9: ATH in aqueous media; the different pH cycles are shown.[10] a. Generation of the mono-aqua cation. b. Binding and beta-hydride elimination of formate to produce the active hydride species. c. Binding of the ketone to the metal hydride and amine hydrogen. d. Transfer of the hydride and hydrogen to produce the alcohol product. e. Regeneration of the active catalytic species with water and formate.

1.1.5. Reduction of Aliphatic Substrates

Unlike their aromatic counterparts, asymmetric reduction of aliphatic ketones remains a challenge. The reason for this is the lack of an aromatic portion, which is postulated to be responsible for both reactivity and selectivity as theorized by Noyori's $CH/CH_3 - \pi$ attraction. Until recently, strictly aliphatic substrates were mainly reduced via asymmetric enzymatic reduction.

While not an ATH based process, a borane based system (**25**) described by Corey in 1987 was able to reduce aryl containing ketones with good selectivities (scheme 1.10). The system uses chrial oxazoborolidines derived from amino acids as the catalysts. Several aryl ketones are able to be reduced quickly in high yields (>85 %) and good ee's with 3,3-dimethylbutan-2-one being reduced at 97 %ee. The system had a remarkably high selectivity for 1-cyclohexylethanone, (84 %ee). The reaction proceeds quickly even at low catalytic loadings (5 to 10%) and it generally finished in 2 minutes, though reaction times of 25 minutes were observed. One drawback to this system was that the highest selectivities were obtained at temperatures of -10 °C. The catalyst used acts as both a lewis acid and a lewis base with the boron of the ring fixing the oxygen of the carbonyl bond and the nitrogen adjacent to the boron binding the boronhydride, closing the proximity of the hydride and carbonyl bond as seen in scheme 1.10.[44]

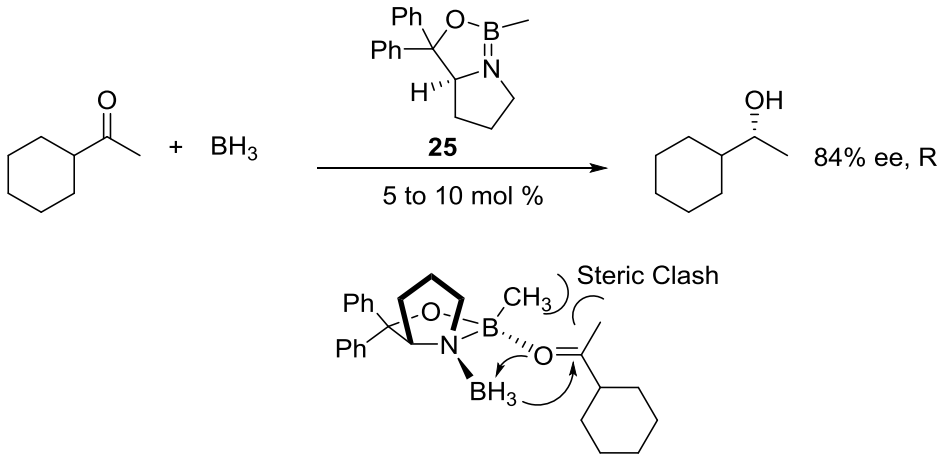

Scheme 1.10: Reduction of 1-cyclohexylethanone via Corey's reagent. A steric clash results in the favorable production of the R enantiomer of 1-cyclohexylethanone. This reagent is only affective for aryl ketones.

A ruthenium based 2,2'-bis(diphenylphosphino)-1,1'-binaphthyl (BINAP) and α-picolylamine catalyst (**26**) designed by Noyori was able to reduce tert-alkyl ketones with high ee's. Unfortunately, other less bulky aliphatic and even aromatic ketones are reduced with poor enantioselectivity, scheme 1.11.[45]

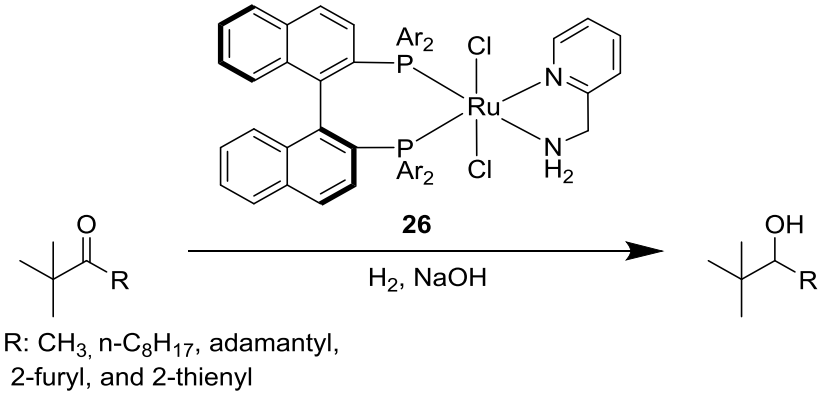

Scheme 1.11: AH of t-butyl containing ketones using 26. Expansion to other aliphatic ketones produced limited selectivity. The mechanism of reduction is the same as described in scheme 1.7.

BINOL derived diphosphonites (**27**) in conjunction with Ru(II) were used in the reduction of several alkyl/alkyl and aryl/alkyl ketones and achieved a remarkable substrate scope (figure 1.11). 1-cyclohexylethanone and 3-methylbutan-2-one were reduced with ee's of 99 % with 2-propanol acting as the hydrogen donor in the presence of base. When more linear substrates are reduced the selectivity begins to erode, 90 % ee for 2-octanone and 82 % for 2-hexanone. The mechanism of chiral induction is not fully understood.[46]

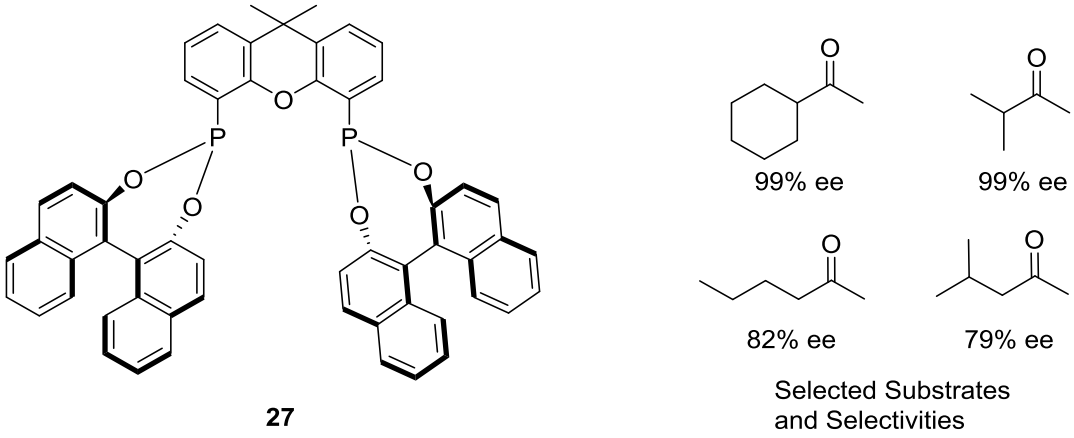

27

Figure 1.11: Diphosphonite ligand used in conjunction with Ru(II) metal for reduction of aliphatic ketones. This catalyst was able to a broad range of aliphatic ketones if the R group had significant steric bulk. Linear substrates were reduced with less selectivity. The mechanism of chiral induction is not fully understood.

In 2008 Schlatter obtained high selectivities (70-93%) for long chain aliphatic substrates by attaching a ruthenium based catalytic system to β-cyclodextrin (**28**).[47] The Ru becomes chiral upon attachment to the secondary face of the cyclodextrin (figure 1.12). This allows the preferential transfer of the hydride to the re-face of the carbonyl group. The reductions were carried out in a DMF/water mixture with sodium formate as the hydrogen source.

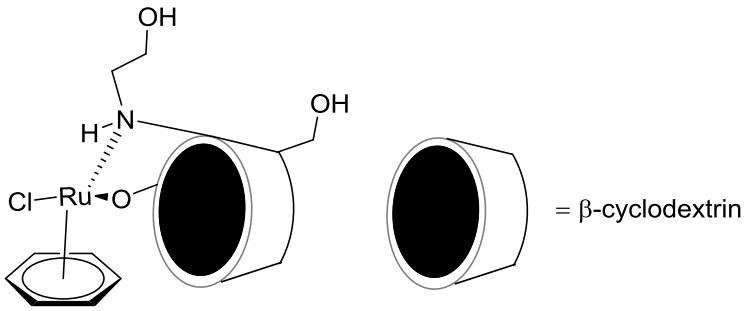

28

Figure 1.12: Chiral ruthenium complex formed through attachment to β-cyclodextrin. This system was able to reduce linear ketones with high selectivity due to a preferential transfer of the hydride to the re-face of the carbonyl group.

A variety of modified L-proline ligands and (1S,2S)-2-amino-2,3-dihydro-1H-inden-1-ol, in combination with $[RuCl_2(p\text{-}MeC_6H_4iPr)]_2$, Figure 1.13, were used in a screening method to find a suitable ligand for the reduction of aliphatic substrates in water.[48] It was found that the ligand used tended to be specific to the substrate with no general ligand found capable of reducing all type of ketones. A general trend was that as the steric bulk of the R group on the ketone was reduced, the ee% would decrease as well. 3,3-dimethylbutan-2-one and 1-adamantyl methyl ketone could both be reduced with 68 % and 82 % ee in 3 h, but linear chain aliphatics could not (4% ee).

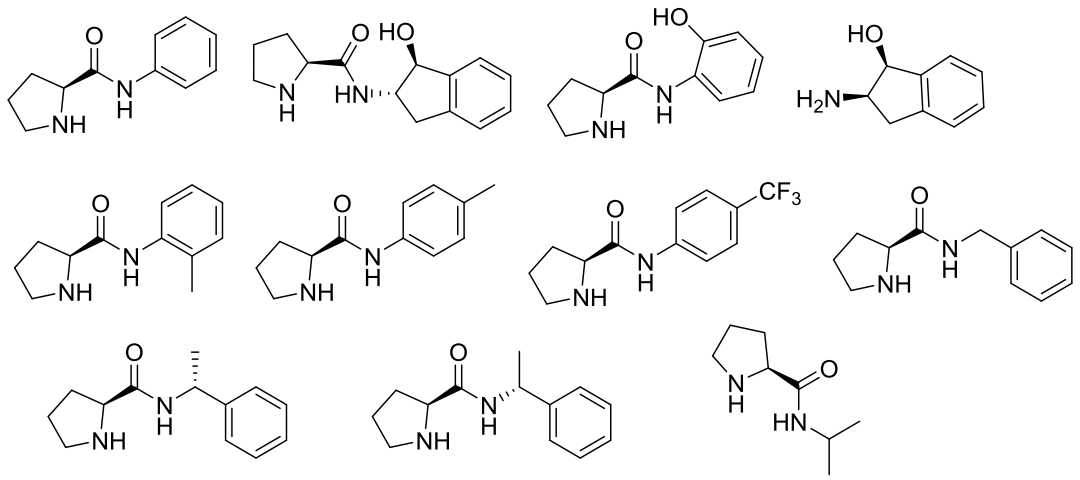

Figure 1.13: Ligands used in high throughput screening against aliphatic substrates.[48] No single ligand was capable of reducing all substrates with high selectivity. Steric bulk was found to impact %ee, with substrates containing larger R groups being reduced with high selectivity.

Recently, modified TsDPEN ligands **29**, **30**, and **31** (figure 1.14) were used with great effectiveness in the reduction of long chain aliphatics of the form $CH_3(CH_2)_{n(3-10)}COCH_3$ by Li et al.[49]

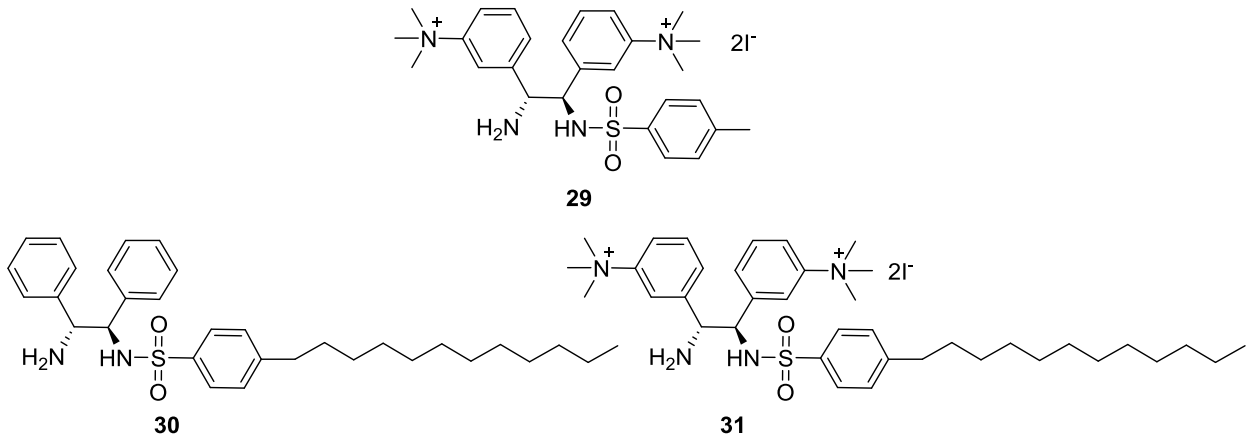

Figure 1.14: Modified TsDPEN ligands used by Li in aliphatic ketone reduction; both the long chain and charged groups are necessary for selectivity.[49] High selectivity is only achieved at low

temperatures (5 to 10 °C). The Rh based catalyst was more reactive and selective than the Ru and Ir based variants.

Each ligand, as well as TsDPEN were used with Rh in the reduction of octan-2-one in the screening process. **31** was found to be the most selective, with conversions of 94% and ee of 84% in neat water at 40°CC. When used with Ru and Ir the conversions and selectivities were 72%, 40% ee, and 98% and 82% ee respectively. The catalyst forms micelles in an aqueous solution with the the long chain pointing inwards. Attraction between the two long chains of the catalyst and substrate effectively hold the substrate in a favorable position while it is reduced, (figure 1.15). There is no such attraction when TsDPEN or 29 is used as a ligand, and enantioselectivities are decreased to 37% and 35% respectively. There is also an erosion of enantioselectivity as temperature increases, with the optimal temperature being 5 to 10 °C.

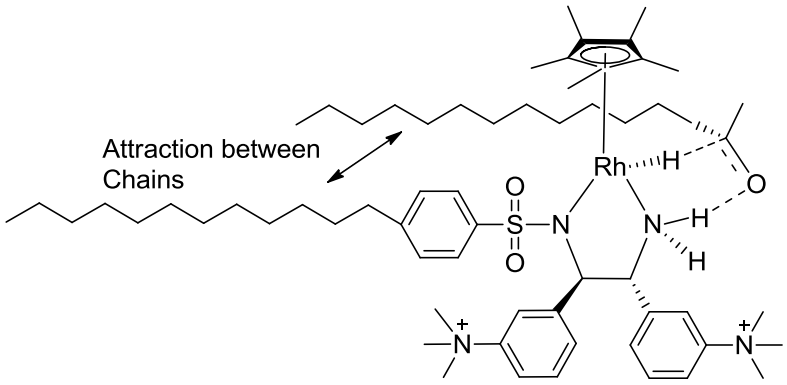

Figure 1.15: Hydrophobic attraction between long aliphatic chains, which is consistent with chirality of product.[49] If ligand 29 is used, no improvement in selectivity is seen. Substrates with shorter chain lengths then 2-octanone are reduce with less selectivity.

1.2. General Chemical Properties of Amino Acids

Alpha amino acids, (aa), are the building blocks of proteins and are differentiated by the R group on the alpha position (figure 1.16). There are 22 amino acids which exist naturally and are

called the standard amino acids, with a great deal many others being made synthetically. The vast variety of aa's lead to a great deal of diversity that they can impart into catalysts when used as ligands.

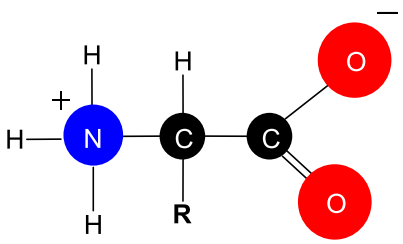

Figure 1.16: General structure of an amino acid in its zwitterionic form. 22 amino acids exist naturally, with extensive lists of synthetic amino acids also being available commercially. Amino acids offer a low cost source of chiral ligands, which have been used quite successfully in asymmetric catalysis.

Additionally amino acids are a low cost "off the shelf" chiral ligand source. L-proline has been used in asymmetric reactions and transformations quite effectively.

1.3. Metal Containing Amino Acid Complexes

1.3.1. Carbonyl Complexes

The first isolated α-amino complex was the Fe carbonyl complex $Fe(Cys)_2(CO)_2$.[50,51] Using IR spectroscopy, the coordination mode was found to be an N,S-chelate with the CO ligands arranged in a cis-orientation. It would later be revealed that Ni/Fe based hydrogenases, **32**, also contain an iron carbonyl complex, (figure 1.17).

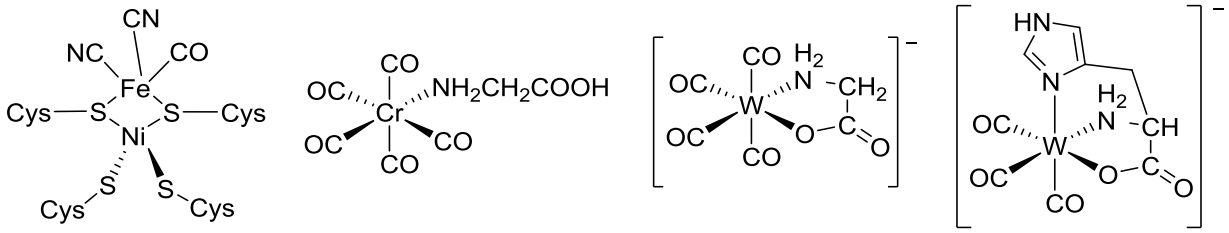

32 **33** **34** **35**

Figure 1.17: Structure of Ni/Fe hydrogenase, as well as general structures of amino acid carbonyl compounds. The complexes can display differing coordination modes dependent upon the amino acid R group. Bidentate coordination through the amine and carboxylate groups is most common (34). If the amino acid contains coordinating side chains, a tridentate coordination mode is seen (35).

$[Cr(CO)_6]$ and $[W(CO)_6]$ react with amino acids under photolytic conditions to produce complexes in which the amino acid is bound through the amine group alone as seen in figure 1.17, complexe **33**.[52] With solvent occupying one coordination site, the W complex $[W(CO_5)(thf)]$ reacts with sodium salts of amine acids to form a bidentate complex coordinated through the N and O, **34**. The glycine complex forms intermolecular hydrogen bonds through the protons of the amine and the oxygen on the carbonyl producing a helical lattice pattern which was eventually found to be a common occurrence of complexes containing amino acid ligands.[53] In the case of coordinating side chains such as cysteine and histidine a tridenate complex is formed, **35**.[54] The chirality of the alpha carbon determines the overall orientation of donor atoms.

Metal carbonyl cluster chemistry gives rise to additional coordination modes. For example when the Os trinucear carbonyl clusters are reacted with an amino acid ester it will lead to thiolate or alkoxide bridged complex or carbonyl hydride complexes, Figure 1.18.[55]

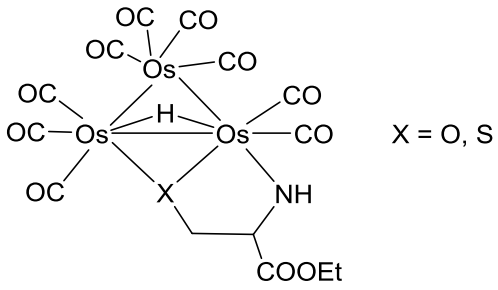

Figure 1.18: Os carbonyl cluster complex of serine and cysteine showing coordination through the R group.[55] The R groups act as bridging ligands in the case of cysteine and serine.

Reaction of phosphine-based carbonyl complexes of Rh, Os, and Ru was a large area of interest due to potential catalytic applications. Complexes of the form $[MHCl(CO)(PPh_3)_3]$[56] and $[MHCl(CO)\text{-}(PMe^tBu_2)_2]$,[57] with the metal being Ru or Os, react with amino acids to generate octahedral hydride complexes like **36,** figure 1.19. If the same reaction is performed in the absence of base evolution of hydrogen gas is observed and a chloride species is observed to produce $[RuCl(NH_2CHRCO_2)CO(PPh_3)]$. Interestingly, the PPh_3 groups adopt a cis configuration. The Ru variant $[Ru(CO)_2(PPh_2)](BF_4)$ retains a carbonyl ligand when undergoing the same reaction to produce **37**. The amino acid is added through oxidative addition to $[Ru(CO)_2(PPh_3)_2]$ to produce a ruthenium complex of the same configuration as **36**, figure 1.19.

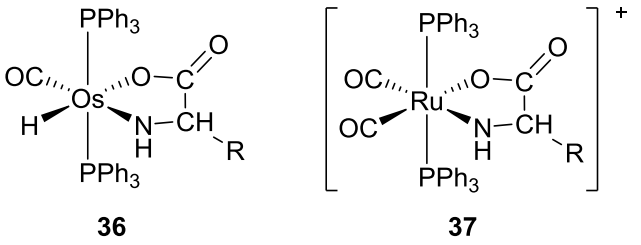

Figure 1.19: Showing osmium and ruthenium based carbonyl complexes. 36 is produced through reaction of [OsHCl(CO)(PPh_3)$_3$] with amino acids in the presence of base. If this same reaction is done in the absence of base 37 is produced.

The d^8 metals of Pt(II) and Rh(I) form square planar carbonyl complexes (**38**, **39**, **40**). When L-alanine and L-phenylalanine react with [Rh(CH_3CN)(CO)(PPh_3)$_2$]BF_4 the phosphine complex **39** forms. These complexes establish a hydrogen bonding network between the amine proton and the carbonyl oxygen of the adjacent complex in the crystal lattice, which has been found to be common in amino acid complexes.[58] The dicarbonyl Rh aziridine complex was prepared through the lithium salt of aziridine-2-carboxylate and $(CO)_2Rh(\mu\text{-}Cl_2)Rh(CO)_2$ and adopts a similar configuration to **38**.[59]

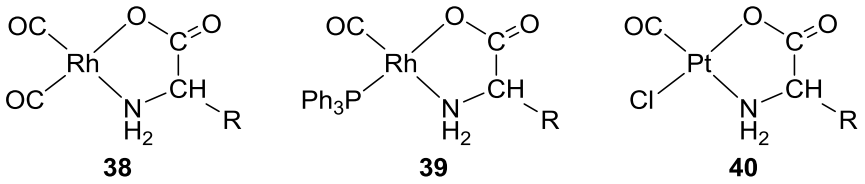

Figure 1.20: Square planar complexes of the Rh(I) and Pt(II).

1.3.2. η^2-Olefin and η^3-ally complexes

The Rh and Ir chlorine bridged 1,5-cyclooctadiene complexes reactions with glycine and proline and produces the N,O chelates common in amino acid chemistry (**41**, **42**). In addition to these Rh and Ir complexes, two octahedral complexes of the form [(diene)Ru($gly)_2$] were described, with

the diene being COD or norbornadiene (**43**).[60] Subsequently, Sheldrick et al. extensively studied the chemistry of $[(diene)RuCl_2]_n$. It was found that if reacted in methanol, an insoluble polymeric structure formed, most likely of the formula $[[(diene)RuCl(NH_2CHRCO_2)]_n]$. If the reaction is performed in water, complexes adopt the configuration of **43** figure 1.21.

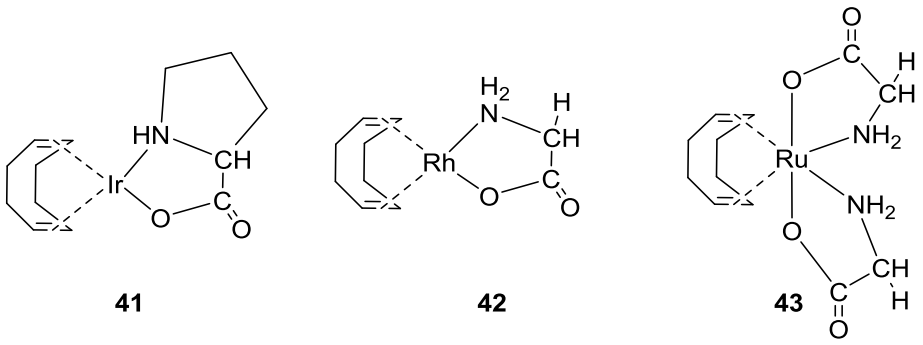

Figure 1.21: Diene complexes of Ir, Rh, and Ru with amino acid ligands. 41 and 42 are formed through the reaction of $[MCl_2COD]_2$ and amino acid in the presence of base. 43 is prepared through the reaction of $[(diene)RuCl_2]_n$ with two equivalents of amino acid in water.

The amino acid carboxylate groups function as bridging groups, with the carbonyl oxygen bonded to the adjacent metal center. This was elucidated through analysis of the IR spectra, and the subsequent crystal structure analysis of the $[(COD)RuCl(D,L\text{-}PheO)]_4$ complexes, shown in figure 1.21.[61] Amino acids containing coordinating side chains form complexes with the amino acid as a tetradentate ligand in the form of S,S,N,O coordination.

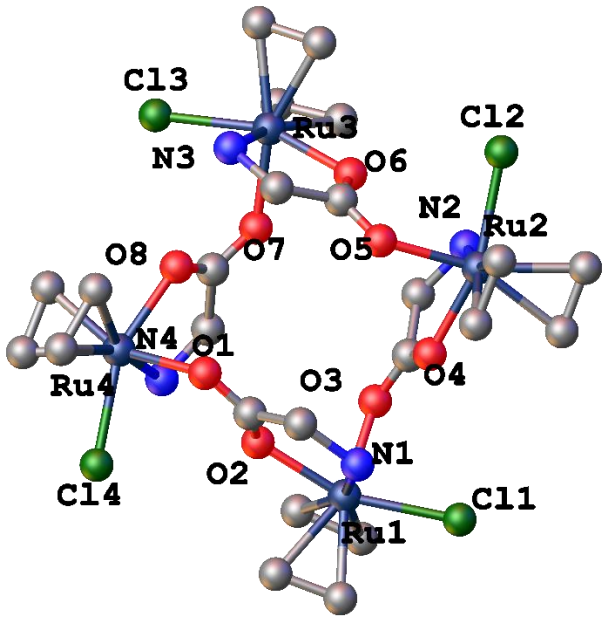

Figure 1.22: Tetramer of [(COD)RuCl(D,L-PheO)]$_4$ with the carboxylate groups serving as bridging ligands, COD and phenyl portions omitted for clarity. Carbons unlabeled.

Platinum complexes [Pt(II)Cl(NH_2CHRCO_2)olefin)] form trans-(N,olefin) and cis-(N,Olefine) structures, both of which are stable isomers. As with other square planar Pt complexes, reaction sequence is crucial to arrive at the desired product. Zeise's salt reacts with amino acids to produce the trans-(N,olefin) isomer.[62] The cis isomer can be made through substitution of the chloride ligand with ethylene and HCl elimination.

1.3.3. Half Sandwich Complexes

The piano stool complexes of arene complexes of Ru and Os, and the η^5-cyclopentadienyl complexes of Rh, Ir, and Ru show very similar structures, and a great many have been synthesized

over the years. The reaction of the appropriate halogen bridged dimer with amino acid will yield diastereomers with differing N,O chelation. A general structure is shown in figure 1.23 with priority rules for assignment.

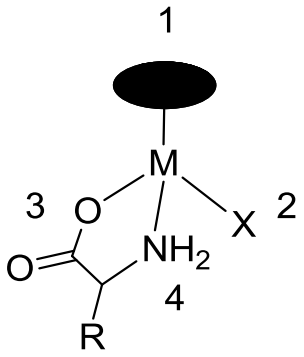

Figure 1.23: General structure of piano stool amino acid complexes. Priority rules are stool, halide, oxygen, and nitrogen.

Amino acids with less sterically bulky side chains result in a diastereomeric ratio of near 1:1, as observed with L-alanine and L-valine. As the R group becomes larger the ratios begin to favor against one diastereomer with L-leucine producing a 20% excess, and L-phenylalaine producing a 50% excess. alkyated nitrogen systems, such as proline form with the highest selectivity, 90%.[63] The similar Ru and Os p-MeC_6H_4iPr based systems produce similar ratios, though in the case of L-alanine and L-valine the compositions are no longer racemic.[64] All complexes undergo epimerization at the metal center in solution, which happens too quickly to be observed on an NMR time scale. One exception is the Os L-pipecolic-2-carboxylate complex, which will epimerize over the course of several days, from a 77/23 molar ratio to 25/75. The complexes exist in the solid state in differing ratios than in solution, as observed from the X-ray crystallography of Cp*Ir(L-pro)Cl where the ratio is 1:1, but quickly changes to the reported 90/10 when dissolved in solution.

When the chloride is removed using an appropriate scavenger such as silver ion followed by isolation and growth of single crystals, X-ray crystallography reveals that these complexes form trimers in the solid state. The carboxylate group functions as a bridge between the complexes, as observed with related cyclooctadiene complexes. These complexes seem to form exclusively as one form of trimer through a chiral self-recognition, meaning the S_C ,S_C ,S_C, S_M, S_M, S_M is formed. The osmium proline trimer is shown in figure 1.24.[64]

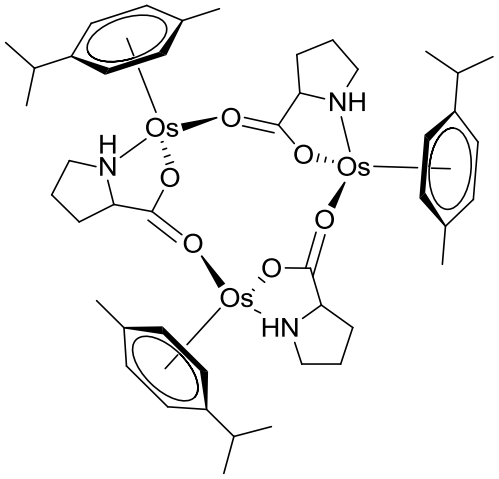

Figure 1.24: Trimer of [(p-MeC_6H_4iPr)Os(L-pro)]$_3$ with bridging carboxylate groups. The trimer forms through chiral self-recognition, which each monomer having the same chirality at the metal, nitrogen and carbon (S_C, S_M, S_N).

In the case of coordinating side chains, the amino acid may function as a tridentate ligand, such as N,O,N in the case of histidine,[65] N,O,O in asparagine and aspartic acid,[66] and N,O,S in methionine.[67] Serine and cysteine apparently lack the chain length to function as tridentate ligands. In the case of amino acid esters, a mono-dentate complex is formed. A summary of binding modes is shown in figure 1.25.

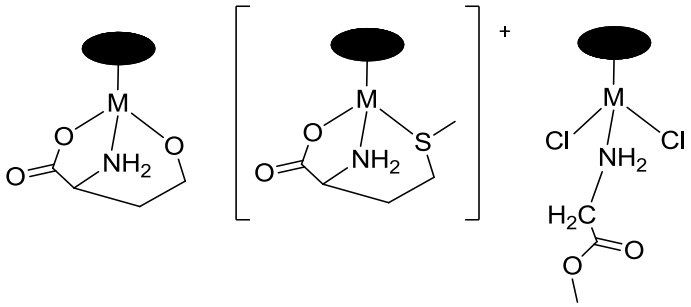

Figure 1.25: Common coordination modes of amino acids and amino acid esters. Amino acids with coordinating sides chains function as tridentate chelates. Amino acid esters act as monodentate ligands, bonding only through the amine functionality.

1.3.4. Other complexes:

Chris Roy of the Merola group synthesized a several of iridium complexes of the form [Ir(aa)(H)(PMe_3)$_3$Cl.[68] The complex [Ir(COD)(PMe_3)$_3$Cl oxidatively adds amino acids to produce the octahedral complexes shown in figure 1.26. The L-valine complex adopts a meridional arrangement as seen in **44**, figure 1.26. This arrangement was assigned through the coupling pattern of the hydride resonance. The complexes themselves are not inert, as less sterically demanding amino acids can replace ones already coordinated to the iridium center. Glycine will fully replace L-valine if excess is reacted with the L-valine complex. Like other amino acid complexes, an extended hydrogen bonding network is observed in the crystal lattice.

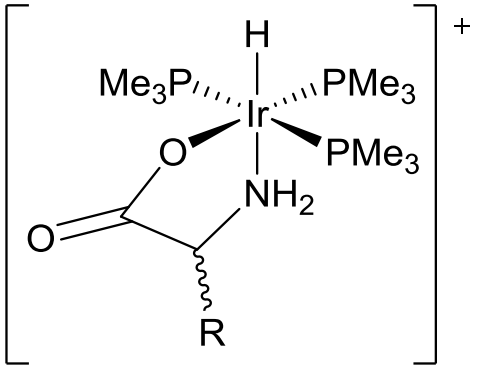

44

Figure 1.26: General structure of mer-[Ir(aa)(H)(PMe_3)$_3$]$^+$ complex. 44 is formed through the oxidative addition of an amino acid to [Ir(COD)(PMe_3)$_3$Cl]. Smaller amino acids are capable of displacing larger amino acids which are already coordinated.

Sheldrick and Exner investigated the reaction of $RuCl_2(PPh_3)_2$ with several α-amino acids. Reaction of the respective amino acid with $RuCl_2(PPh_3)_2$ in refluxing methanol in presence of sodium bicarbonate results in the formation of an octahedral complex of the form $Ru(aa)_2(PPh_3)_2$ **45**, with the general structure shown in figure 1.27.[69] As in the case of the half-sandwich complexes, the amino acid forms a bidentate chelate through the amino and carboxylate groups with amine is trans to the carboxyl oxygen. A Schiff base complex is formed when the reaction is performed in acetone with either glycine or L-alanine. The glycine complex forms with the phosphines trans to one another, **46**, with the L-alanine complex forming with the phosphines trans to the amine nitrogens, **47**.

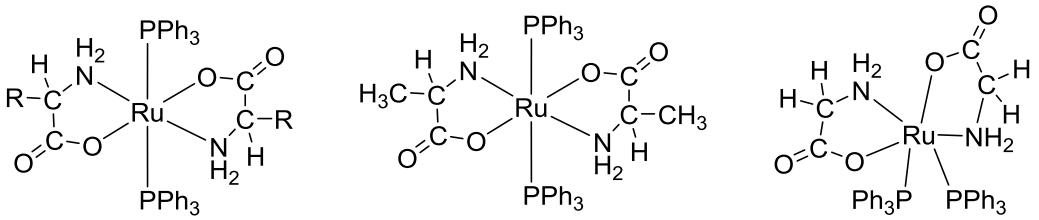

Figure 1.27: General structure of $Ru(aa)_2(PPh_3)_2$, $Ru(L\text{-alanine})_2(PPh_3)_2$, and $Ru(glycine)_2(PPh_3)_2$, with phospines cis, and trans to one another respectively. These complexes are formed through the reaction of $RuCl_2(PPh_3)_2$ with two equivalents of amino acid in the presence of base.

Meggers et al. used proline as a chiral reagent to synthesize optically pure ruthenium polypyridyl complexes. Starting from racemic $[Ru(pp)(pp')Cl_2]$ complexes, subsequent chelation of L or D proline and heating results in the kinetic resolution of an enantiomerically enriched product. In the case of L-proline Λ products are formed with D forming Δ, both in an enantiomeric ratio (er) of 99:1. These proline containing intermediates can be reacted further to produce pure Ru(pp)(pp')(pp'') products.[70] The final ruthenium polypyridyl complexes do racemize under visible light in solution, with a racemic mixture being produced after approximately 50 h.

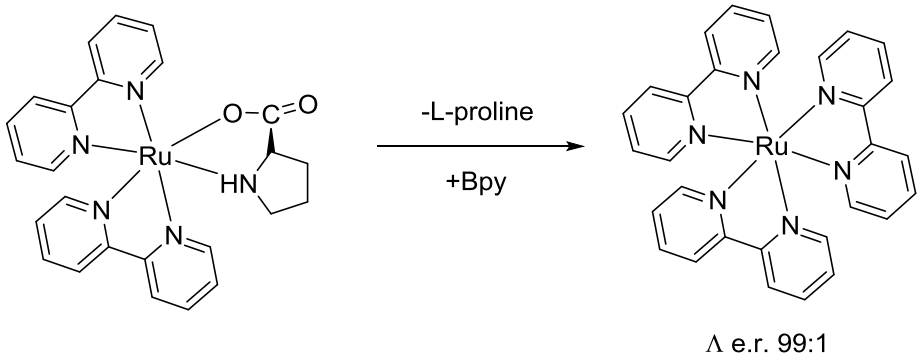

Figure 1.28: Asymmetric synthesis of $Ru(bpy)_3$ using L-proline as a chiral scaffold. The final product (Δ or Λ) can be controlled using either L or D proline. This chiral template reaction can be applied to other polypyridyl complexes and can even produce optically pure mixed species Ru(pp)(pp')(pp'').

Sandwich complexes of the form $[(Cp)Ru(\eta^6\text{-aa})]^+$ were synthesized in the pursuit of selectively labeling peptides with organometallic compounds. Under visible light, the complex $[Ru(C_{10}H_8)(Cp)]^+$ undergoes exchange with other arene ligands to form the complex $[Ru(\eta^6\text{-arene})(Cp)]^+$.[71] In the case of amino acids L-phenylalanine, L-tyrosine, L-tryptophan, D-phenylglycine, and L-threo-3-phenylserine, the corresponding π complex is formed (scheme 1.12). The reaction is carried out in water at room temperature, and can proceed with high selectivity in the presence of other amino acids. Sulfur containing amino acids will hinder the reaction due to coordination of the sulfur atom to the ruthenium.

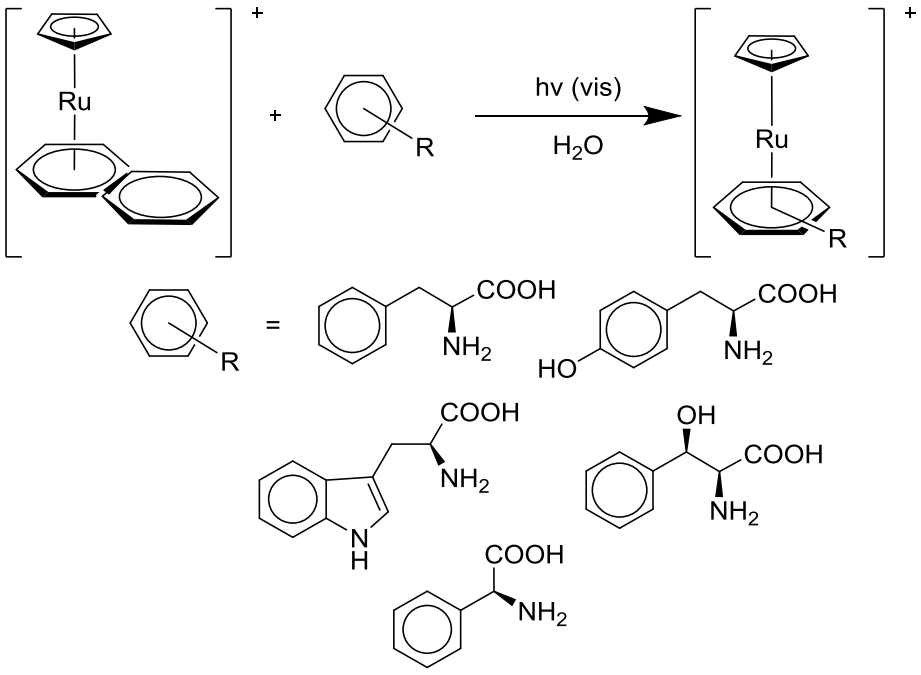

Scheme 1.12: Synthesis of Ru sandwich complexes. Amino acids containing aromatic rings were able to displace the napthyl ring system of the Ru sandwich complex when irradiated with visible light

A large number of palladium methionine complexes were synthesized by Charnova et al.[72] Depending on the reaction conditions used, the complexes had a large variety of formulas, though the

methionine was generally coordinated through the nitrogen and sulfur portions, as determined through the IR spectrum. The $[Pd(MetH)_2Cl_2]$ variant has an IR spectrum which exhibits both ionized and un-ionized carboxyl groups. The bis methinone complex $[Pd(Met)_2]$ contains an uncoordinated carboxyl group in the ionized form. A polymeric complex is formed between the molecules of $[Pd(Met)(H_2O)]Cl$. The methionine is tridentate, with the choride acting as a counterion. Lastly, the $[Pd(NH_3)_2(MetH)_2]Cl$ complex contains methionines bound solely through the sulfur group, with the remaining portion of the amino acid existing unbound in the zwitterionic state.

The tetraaceto Rh(II) ion will react with sulfur containing amino acids to form a square planar monomeric Rh(II) complex with the amino acid coordinated through the N and S.[73] These $[Rh(L)_2]$ complexes have been isolated with cysteine and penicillamine as ligands and are one of the few mononuclear Rh(II) complexes isolated.

1.4. Concept and design of catalysts

The modular design and function for the system is shown in scheme 1.14. Using a three point modulation system, the catalyst can be tailored for specific substrate reductions. This is required since no single ATH catalyst has been shown to reduce differing groups of substrates effectively. Generally catalysts are only effective at selectively reducing aromatic ketones, aliphatic ketones, or high hindered ketones, with no universal catalyst existing.

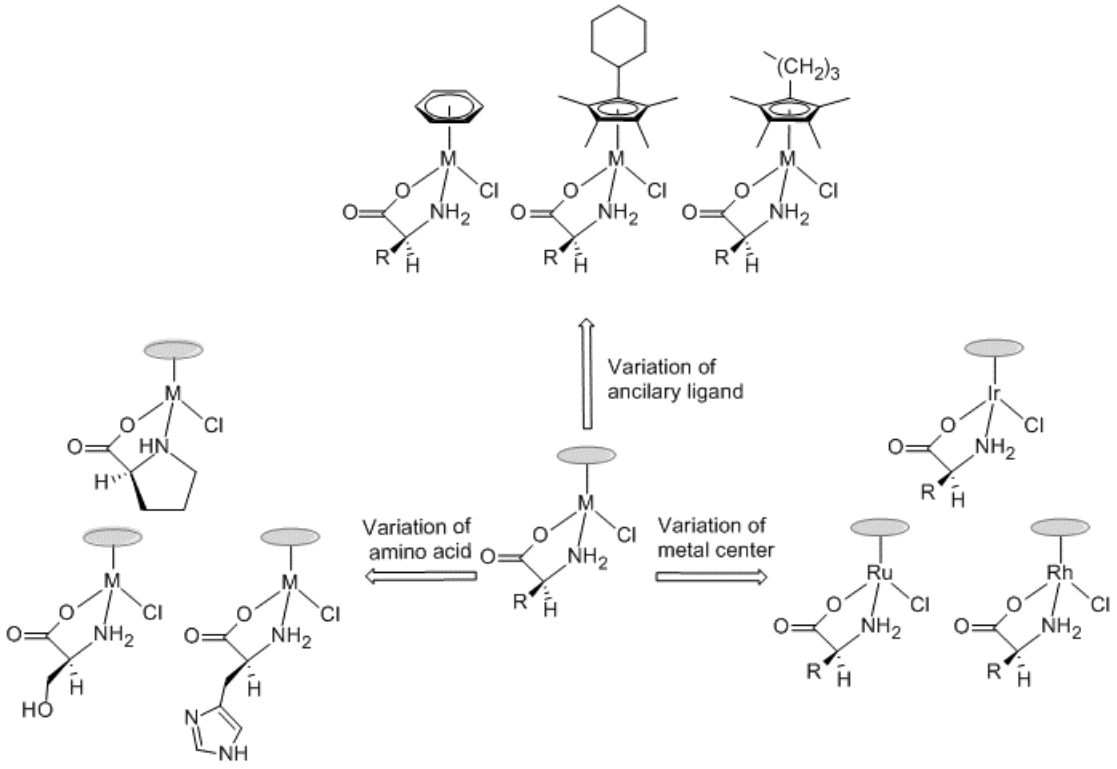

Scheme 1.14: Modular design of catalyst systems, showing variation of ancillary ligand, metal center and amino acid ligand.

Ru, Rh, and Ir were selected to act as the metal center due to their well documented ability to act as ATH and AH catalysts. There are few examples of other metals which exhibit the robustness of these systems. All are compatible with 2-propanol, formic acid/triethylamine/ and formate as hydrogen donors. This becomes important since the ATH of aliphatic ketones is not well understood, and solvents effects on selectivity could play a crucial role. In addition, Ru, Rh, and Ir have a well explored chemistry with amino acids as ligands.

Modification to the ancillary ligand allows for an increase in steric bulk at the active site of the catalyst and permits tailoring of solubility properties. Aromatic ketones are reduced selectively through the electronic $CH_3 - \pi$ interaction. This interaction is lacking for aliphatic ketones and requires a different catalyst design. Modification to the Cp* functionality allows for another method

of substrate-catalyst interaction. One method is increased steric bulk, as mentioned previously, which would have an unfavorable interaction with large R groups of unsymmetrical prochiral ketones. The second method would be an electronic interaction mimicking the $CH_3 - \pi$ interaction. The use of a long chain aliphatic group provides such an interaction, as Deng and co-workers have shown.[49] Cp* type ligands were chosen due to the ligands well defined organometallic chemistry. Cp* is less easily displaced than Cp due to being more electron rich. η^6-arene ligands were chosen due to the commercial availability of several precursors, and their similarly well defined organometallic chemistry with Ru complexes.

Lastly, variation of the amino acid ligand will provide insight into the mechanism of selectivity for these catalysts. Amino acids serve as abundant and cost-effective chiral ligands, while maintaining all of the functionality of the DPEN and amino alcohol ligands used by Noyori and Wills respectively. Additionally, their inorganic and organometallic chemistry is well studied, as shown from the array of complexes in the previous sections. Since these complexes will be used as asymmetric catalysts, knowing the coordination environment, as well as solution stability is required, and vastly developed chemistry of amino acid ligands assists in this. Amino acids will act as bidentate chelates, like the amino alcohol and DPEN ligands. Additionally, the overall charge and oxidation state of the half-sandwich complexes will be maintained, as amino acids, amino alcohols and tosylated diamines all have a negative charge when bound to the metal, since they become carboxylates, alkoxides, and amine anions. They also provide a good method of screening; by simply switching amino acids the reaction can be tailored to a different substrate. Enantioswitchability becomes simplified by changing the amino acid from L to D. The ease of changing the configuration of the final alcohol is crucial if the product is to be used in a higher level synthesis. This modular nature will allow for the development of a structure function relationship between classes of aliphatic

ketones and their most effective catalyst. This would then allow a catalyst specific reduction of ketones.

1.5. Project Description

The reduction of aromatic ketones to their chiral alcohols via AH and ATH is well understood, the currently available catalytic systems described previously has little room for improvement in the area of selectivity, substrate scope, and reactivity. Cost is the area were systems could be improved, either through use of an "off the shelf" chiral ligand, such as amino acids, or through the use of an earth abundant transition metal. Aliphatic ketone reduction, on the other hand, has a great deal of room for improvement. While the mechanism is the same, the substrate scope is extremely limited and generally only one type of catalyst can reduce one "class" of aliphatic substrates selectivity. The aim of this work is to, through systematic variation of components, develop new catalysts for asymmetric reduction of aliphatic and aromatic ketones, as well as obtain a fundamental understanding of how this variation will affect the properties of said catalysts.

2. Iridium Cp* Amino Acid Complexes

2.1. Synthesis of Iridium Cp* Amino Acid Complexes and Chemical Properties

The reaction of $[IrCp^*Cl_2]_2$[83] with two equivalents of an α-amino acid in the presence of base leads to the formation of the (Cp*)Ir(aa)Cl complexes (Equation 2.1). The orange suspension will become a clear yellow solution over the course of 15 to 60 min, in the presence of slight heat. The solvent is removed by reduced pressure, and the crude product is dissolved in DCM and filtered to remove any unreacted amino acid and base. The complexes can be recrystallized from DCM and diethyl ether/hexanes to yield the desired product as a yellow powder.

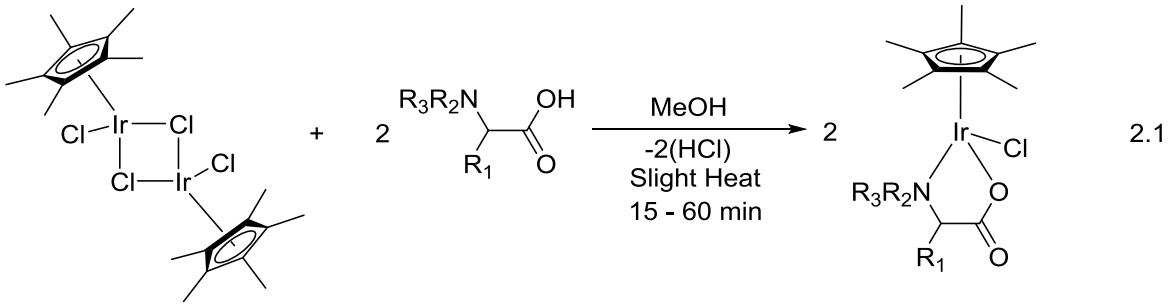

2.1

These complexes adopt a piano-stool configuration, with the amino acid forming a bidentate chelate with the amino and carboxylate groups, similar to reported amino-alcohol and diamine ligands, and as outlined in prior work by others. The iridium center becomes a stereogenic center upon chelation, and leads to the formation of two diastereomers, of the form Ir_SC_S, Ir_RC_S, if homochiral amino acid(s) are used. Glycine produces two entantiomers, with the metal center being R or S. In the case of N-alkylated nitrogens such as proline, the nitrogen will also become a chiral site, raising the possibility of four diastereomeric products. However, only two diastereomers are ever observed in either the solid state or solution state for these complexes, with the chirality of the nitrogen being preserved between the two different diastereomers and the metal being the only change in chirality (R or S). For example, (Cp*)Ir(L-pro)Cl displays two diastereomers of the form

$S_{Ir}S_CS_N$ and $R_{Ir}S_CS_N$. A diastereomer with R_N is not observed. The (Cp*)Ir(N-Me-gly)Cl complex presents a case where there is no chiral carbon, yet still produces two diastereomers due to both the Ir and nitrogen being chiral.

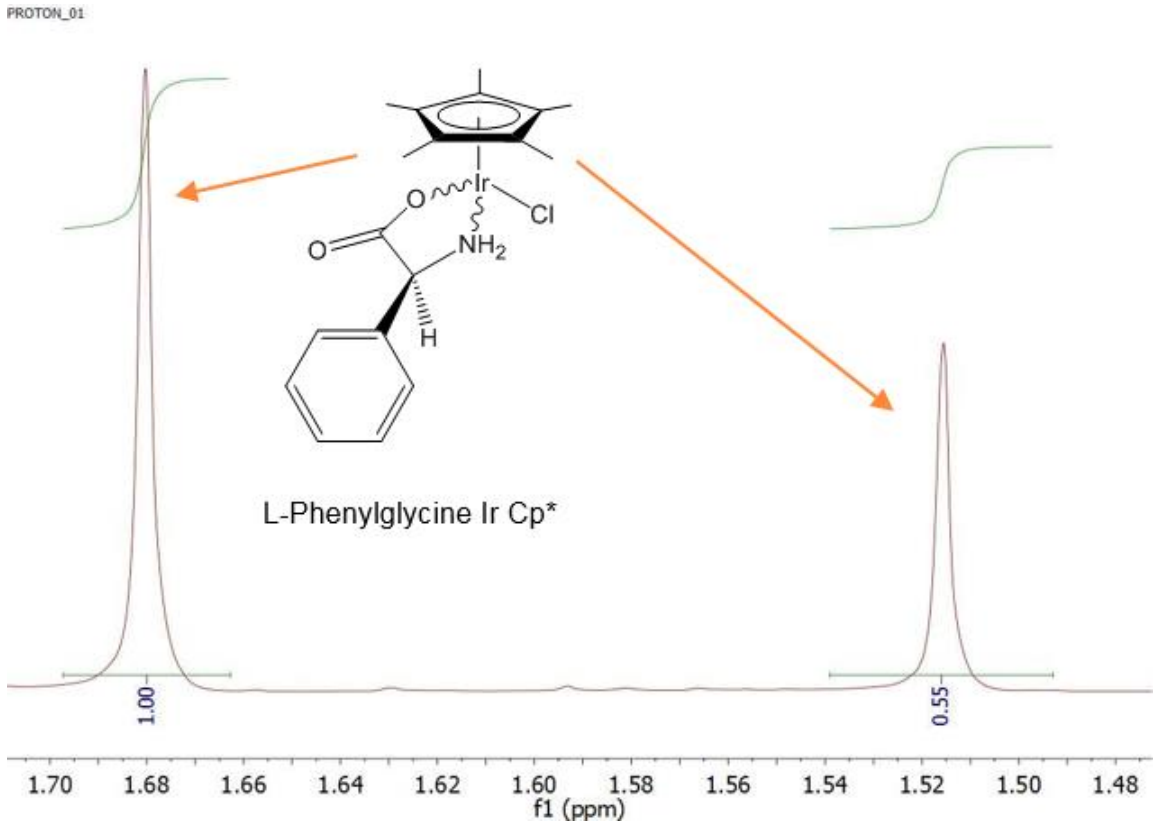

Figure 2.1. ^{1}H NMR of the Cp* region of (Cp*)Ir(L-phengly)Cl. The diastereomeric ratios are determined through the integration of Cp* Methyls. Ratios are from the integration of the major component (S_{Ir}) divided by the total integration of both components.

The ratio of diastereomers is dependent on the R group of the amino acid, with larger side chains leading to higher selectivity in formation. For example, the alanine complex produces a near racemic mixture, (56/44), whereas the larger group of phenylalanine produces a 70/30 ratio of diastereomers. The mixture of diastereomers is best determined through integration and comparison of the Cp* methyl portion in the ^{1}H NMR, as displayed in figure 2.1. Cyclic amino acids such as proline form diastereomers with much higher selectivity, (92/8). However, addition of an electron

withdrawing group, such as fluorine or a hydroxyl reduces this ratio significantly, with trans-4-fluoro-L-proline and tran-4-hydroxy-L-proline producing ratios of 70/30 and 73/27 respectively. Interestingly, N-methly proline produces only one diastereomer, as observed via NMR spectroscopy. For example, (Cp*)Ir(N-methly-D-pro)Cl forms only as the $R_{Ir}R_{C}R_{N}$ isomer, which was confirmed through X-ray diffraction and NMR spectroscopy. Complexes with coordinating side chains show two different results. The (Cp*)Ir(L-his)Cl shows only one diastereomer in solution, whereas the (Cp*)Ir(L-met)Cl shows two distinct Cp* peaks. These ratios are in good agreement with what has been reported in the literature.[65,84-87] A summary of ratios and yields is displayed in table 2.1.

Table 2.1. Summary of molar ratios of amino acid complexes.
Ratios are based upon Cp* integration in the ^{1}H NMR spectrum.

Amino Acid	Ratio of Diastereomers (S/R) at metal center	Yield %
L-alanine	56/44[a]	88
L-asparginine	84/16	84
L-aspartic Acid	51/49	86
glycine	na	80
N-methyl-glycine	72/28[b]	73
N,N-dimethyl-glycine	na	71
L-glutamic acid	na	81
L-histidine	na	52
D-histidine	na	41
L-isoleucine	50/50	58
L-leucine	nd[c]	59
L-methionine	61/39	93
L-phenylalanine	69/31	88
D-phenylalanine*	70/30	88
L-phenylglycine	42/58	82
N-methyl-L-phenylglycine	63/47	97
L-proline	92/8	89
D-proline*	92/8	87
hydroxy-L-Pro	73/27	89
fluoro-L-pro	70/30	73
N-methyl-D-pro	na	72
L-serine	62/38	86
L-threonine	68/32	76
L-valine	53/47[d]	80
L-azetidine	93/7	94
L-pipcolinic	74/26	94

[a]:Determined through integration of R group. [b]:Determined through integration of N-CH_3.
[c]:Significant overlap of NMR signals prevents determination. [d]:Determined through integration of R group. na = not applicable. * = Ratios of S_{Ir}/R_{Ir} are reversed.

The solvent used for the NMR spectra affects the observed ratios. In the case of the (Cp*)Ir(L-pro)Cl complex, the ratio of 92/8 is observed in $CDCl_3$. In D-acetone, this ratio falls to 86/14, with the same major and minor peaks based upon chemical shift. A plot of solvent polarity

index vs diastereomeric ratio shows a correlation between decreasing ratio and higher polarity index, with the exception being methanol, most likely due to its protic nature. In D_2O only one diastereomer appears in solution, though is it possible that labile chloride is rapidly exchanging with water. Others have proposed that these complexes form trimers in water from subsequent chloride elimination, and hence only appear as one diastereomer in D_2O, though work with the Ru variants rules this unlikely (chapter 4). Additionally, formation of the hydride complexes (chapter 6) requires an open coordination site, which the trimer complexes lack. These ratios for (Cp*)Ir(L-pro)Cl are displayed in table 2.2

Table 2.2: Diastereomeric ratios in relation to solvent polarity index

Ratio	Polarity Index	Solvent
93	3.1	CD_2Cl_2
92	4.1	$CDCl_3$
86	5.1	acetone
78	5.1	methanol
85	5.8	acetonitrile
80	7.2	DMSO

Temperature appears to affect the ratio of diastereomers to a degree. The (Cp*)Ir(L-phengly)Cl complex, which displays only one diastereomer in the solid state, forms both diastereomers in a near equal mixture in CD_2Cl_2, (51%). If the solution is cooled to 0 °C the ratio will change to 56%. At -25 °C the ratio is 61%. These changes are shown in figure 2.2. Warming of the solution returns the diastereomers to 56% and 51% at 0 °C and room temperature (RT), respectively. This means that the system is under thermodynamic control, but no direct chemical evidence for the exact process is observable on the NMR timescale. The (Cp*)Ir(L-pro)Cl complex does not show any observable differences when cooled to 0 °C and 25 °C, with the diastereomeric ratios remaining 93/7.

Similarly, (Cp*)Ir(L-phengly)Cl produces 65/35 mixture in DMSO at RT, but at 70 °C the ratio changes to 51/49. Interestingly, heating both the (Cp*)Ir(L-pro)Cl and (Cp*)Ir(N-Me-L-pro)Cl to 80 °C produces no observable difference in the ^{1}H NMR spectrum with the ratio of diastereomers remaining 80/20 and 100 respectively.

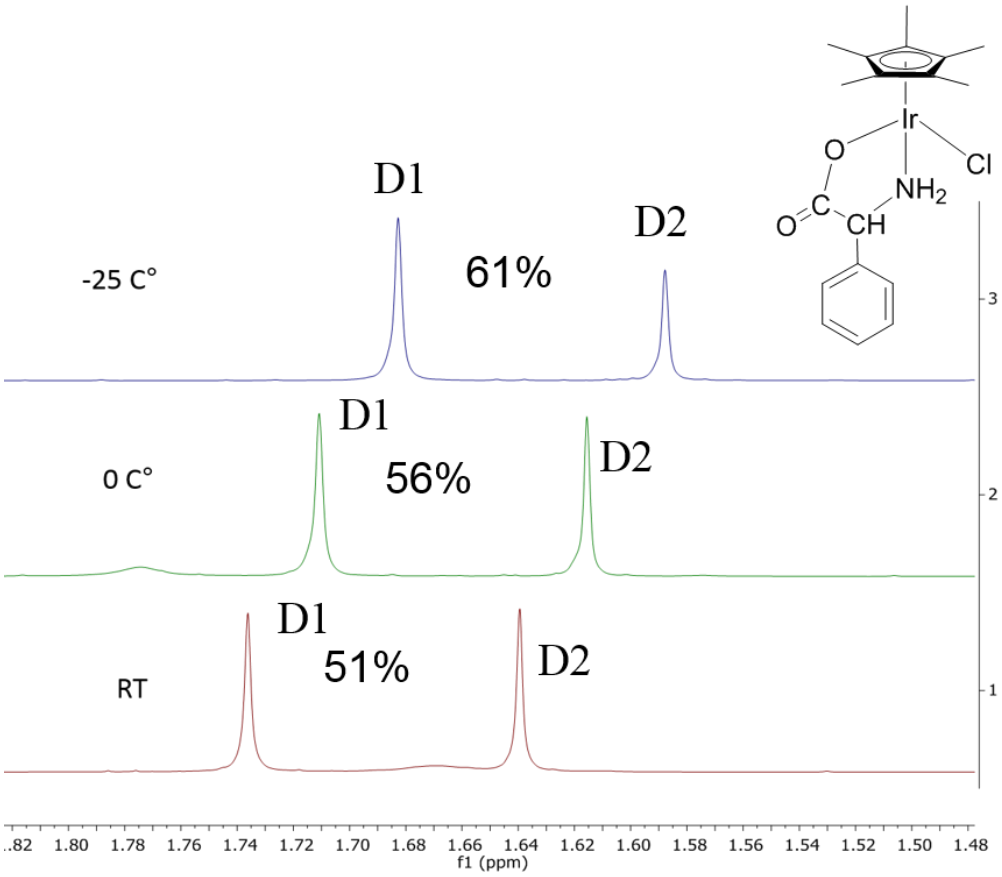

Figure 2.2: Variable temperature ^{1}H NMR spectrum showing change in the ratios of the (Cp*)Ir(L-phengly)Cl diastereomers. D1 and D2 refer to the major and minor product respectively.

The ratios in solution do not correspond to the solid state, as observed by X-ray diffraction. The proline based complex crystalized as a 50/50 mixture of diastereomers in the asymmetric unit, but as stated before, when put into solution, the complex epimerizes at the metal center to produce primarily one diastereomer. A comparison of a ^{1}H NMR spectra of bulk powder sample in $CDCl_3$ to

the ^{1}H NMR spectra of a single crystal dissolved in $CDCl_3$ shows that the composition is identical upon epimerization (figure 2.3).

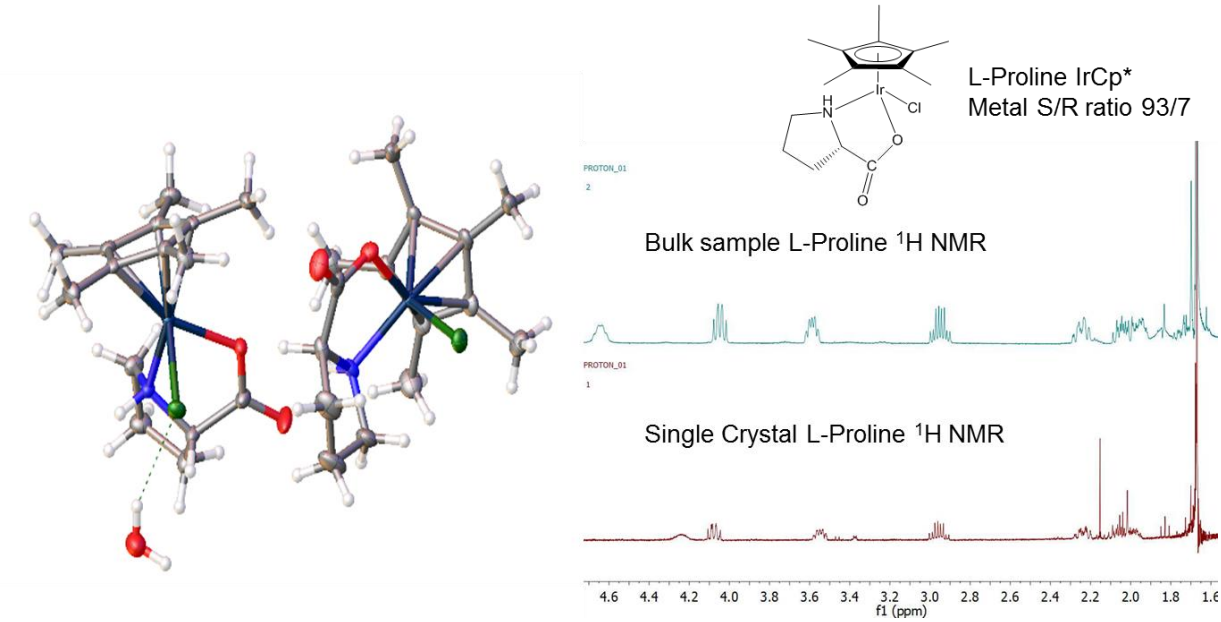

Figure 2.3: Crystal structure showing 50/50 mixture of (Cp*)Ir(L-pro)Cl complex in the solid state and comparison of ^{1}H NMR spectra of a single crystal to the bulk sample in solution. The complex undergoes rapid epimerization at the metal center upon entering solution, going from a 50/50 mixture to a 93/7 mixture of diastereomers.

The process of epimerization is extremely fast at room temperature, with the 50/50 mixture of the L-proline complex achieving the 92/8 ratio over the course of seconds in $CDCl_3$. Once this ratio is reached it remains unchanged for days. It is proposed that the mechanism of epimerization requires the amine protons, and an intermolecular hydrogen bonding network, hence why the methylated proline complex remains unchanged through transition from solid to liquid. Section 2.3 expands upon the mechanism of epimerization

However, the observed ratios in the single crystal and bulk powder sample do match. The calculated powder pattern from the single crystal X-ray diffraction of (Cp*)Ir(D-phe)Cl match the powder pattern obtained for the bulk sample, as shown in figure 2.4, meaning that like the single

crystal, both diastereomers exist in a 50/50 ratio in the isolated powder. The same is true for (Cp*)Ir(N-Me-L-phengly)Cl, which comprises only one diastereomer in both the single crystal and the bulk powder, but upon solvation quickly epimerizes to the ratio of 63/47. Most interesting is that [(Cp*)Ir(L-met)]Cl complex, which exists as a tridentate complex in the single crystal and solid state, clearly shows two diastereomers in solution, meaning that one of the groups is dissociating in solution.

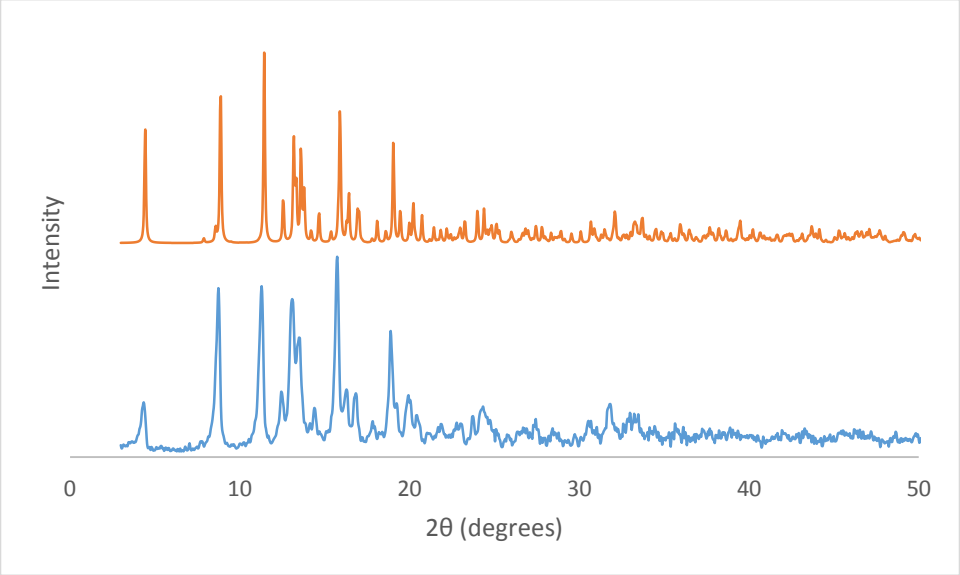

Figure 2.4. Calculated powder pattern (orange) vs powder pattern (blue) of bulk sample for (Cp*)Ir(D-Phe)Cl. The single crystal and powder sample consist of the same distribution of diastereomers.

2.2. Mechanism of Epimerization at the Metal Center:

There are several potential mechanisms for epimerization. Decoordination of chloride from these complexes would provide an open site allowing the ligand to shift to the opposite position. Following re-coordination of the chloride, the chirality at the metal center would be inverted. This mechanism does not account for the fact that the N-methyl variants only form one diastereomer. Additionally, Oro and coworkers have shown that if chloride is replaced with 3,3-dimethylbut-1-yn-1-ide the non-methylated complexes will still form diastereomers.[88] Elimination of HCl from

nitrogen and iridium from these complexes would form a coordinately unsaturated complex, allowing chirality at the metal center to change from R to S in a similar manner to decoordination of chloride. Subsequent addition of HCl would then lock the chirality of the metal center to what is observed in the NMR spectra. The N,N-dimethyl and N-methyl-cyclic variants lack the acidic proton necessary for this mechanism to occur, which may explain why only one diastereomer is found in the NMR spectra of these complexes.

2.3. Crystal structures:

Single crystal X-ray diffraction allowed for the assignment of the absolute chirality at the Ir center and chiral N center. Additionally, analysis of the coordination sphere of the complexes provided evidence as to how chirality is set for the final product in the ATH reaction, as well as why certain catalysts produced higher selectivities. Single crystals of complexes formed from glycine, L-phenylglycine, N-methyl-L-phenylglycine, L-phenylalanine, D-phenylalanine, L-valine, L-serine, L-proline, trans-4-fluoro-L-proline, N-methyl-D-proline, L-azetidine-2-carboxylic acid, L-pipecolic acid, L-hisidine, and L-methionine were obtained from slow diffusion of ether or hexanes into dichloromethane.

2.3.1. Ring Containing Systems

Table 2.3 displays the selected bond lengths and angles of the ring containing Cp*Ir(aa)Cl complexes. Of the ring based systems, only the (Cp*)Ir(L-pro)Cl structure co-crystallized with both diastereomers in the lattice. Analysis of the crystal structures shows an average Ir-Cl bond length of 2.4215 Å. The lengthening of Ir-Cl bond (2.4185(7) to 2.4260(6) Å) observed for the major diastereomer of (Cp*)Ir(L-pro)Cl is due to the hydrogen bond formed between the water molecule and chlorine in the lattice (figure 2.5).

Table 2.3: Selected Bond Lengths (Å) and Angles (deg) for Ring Based (Cp*)Ir(aa)Cl

Measurement	L-proline Major Dia	L-proline Minor Dia	N-methyl-D-proline	F-pro	L-Aze	L-Pip
Cl-Ir	2.4260(6)	2.4185(7)	2.413(2)	2.4314(6)	2.416(1)	2.424(1)
N-Ir	2.140(2)	2.135(3)	2.147(5)	2.151(2)	2.097(5)	2.132(4)
O-Ir	2.086(2)	2.090(2)	2.076(4)	2.103(2)	2.119(4)	2.101(3)
G-Ir	1.766	1.761	1.765	1.767	1.769	1.772
Cl-Ir-N	85.34(6)	87.87(7)	87.7(1)	84.18(6)	83.3(1)	86.0(1)
Cl-Ir-O	86.38(5)	82.53(6)	85.0(1)	86.27(5)	84.1(1)	88.15(8)
N-Ir-O	77.23(8)	79.31(9)	76.5(2)	77.74(7)	77.7(2)	77.1(1)
Cl-Ir-G	125.69	127.62	124.83	127.3	126.61	125.89
N-Ir-G	136.16	131.99	135.89	134.16	133.85	134.8
O-Ir-G	128.44	129.95	129.18	129.4	132.47	128.09

G represents the centroid of the Cp* ligand

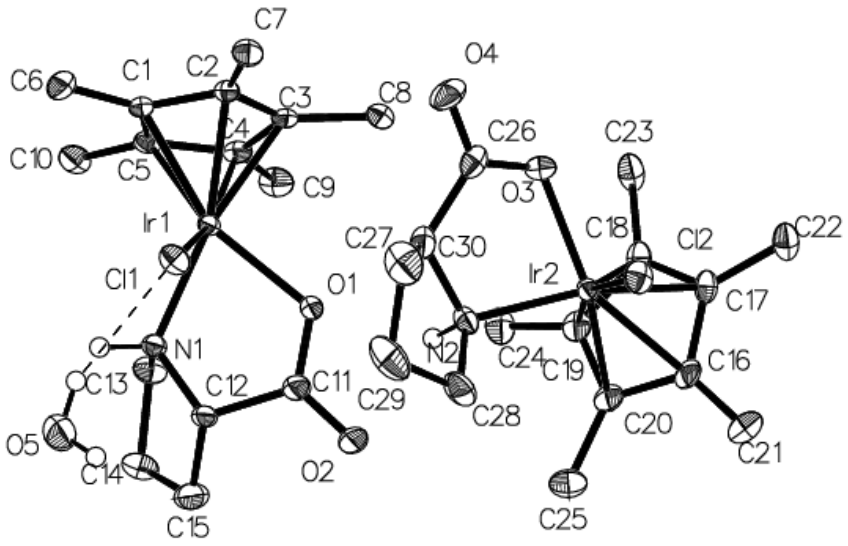

Figure 2.5: ORTEP of (Cp*)Ir(L-pro)Cl complex showing hydrogen bond between chloride and hydrogen of water. All hydrogens not involved in H-bonding omitted for clarity. Ellipsoids shown at 50%.

The minor diastereomer lacks this interaction, and has a bond length very close to the (Cp*)Ir(D-N-Me-pro)Cl and (Cp*)Ir(L-azetidine-2-carboxylic-acid)Cl structures. The (Cp*)Ir(L-trans-4-fluoro-pro)Cl structure has the longest bond of 2.4314(6) Å, potentially due to electron

withdrawing fluorinated ligand, weakening the Ir-Cl bond. The Ir-N bond lengths average 2.1337 Å, with very little difference between the structures. Of these, the L-aze structure has a shortened bond, 2.097(5) Å, due to the ring strain imparted by the 4 remembered ring of the azetidine. The centroid-Ir bond lengths do not vary significantly. These structures are displayed in figure 2.6

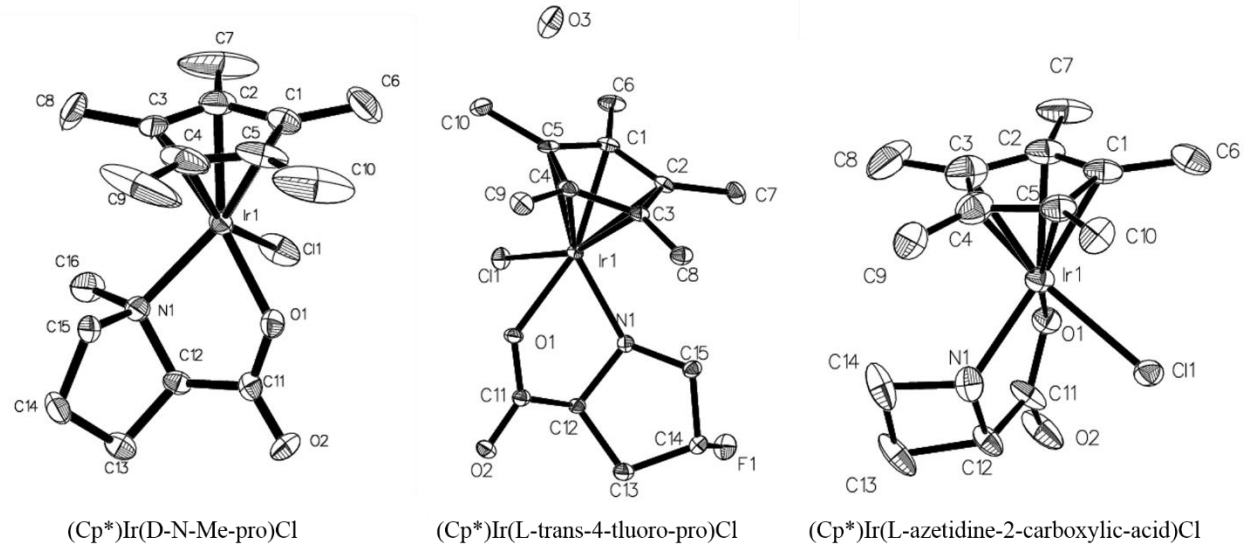

(Cp*)Ir(D-N-Me-pro)Cl (Cp*)Ir(L-trans-4-tluoro-pro)Cl (Cp*)Ir(L-azetidine-2-carboxylic-acid)Cl

Figure 2.6: ORTEP plots for (Cp*)Ir(D-N-Me-pro)Cl, (Cp*)Ir(L-trans-4-fluoro-pro)Cl, and (Cp*)Ir(L-azetidine-2-carboxylic-acid)Cl. Hydrogens omitted for clarity. Ellipsoids shown at 50%.

An intermolecular hydrogen bonding network is observed for each structure, except (Cp*)Ir(D-N-Me-pro)Cl (figure 2.7). In the case of the (Cp*)Ir(L-pro)Cl structure, the observed bonding network is formed through the chlorine, amine proton, and carbonyl oxygens of the two diastereomers, down a 2_1 screw axis. While the water molecule is hydrogen bonded to the chlorine of the minor diastereomer, it is not involved in the larger network formed by the complexes themselves. The (Cp*)Ir(L-trans-4-fluoro-pro)Cl complex, which also co-crystallizes with water, forms a network directly through the individual water molecules. This water molecule forms hydrogen bonds to the amine proton and carbonyl oxygen of symmetry related molecules. However, in the structures

lacking a water molecule, the network still persists, being formed through the amine proton and carbonyl oxygen. No interaction is observed with the chlorine atom, unlike the L-proline structure. These networks are displayed in figure (2.7).

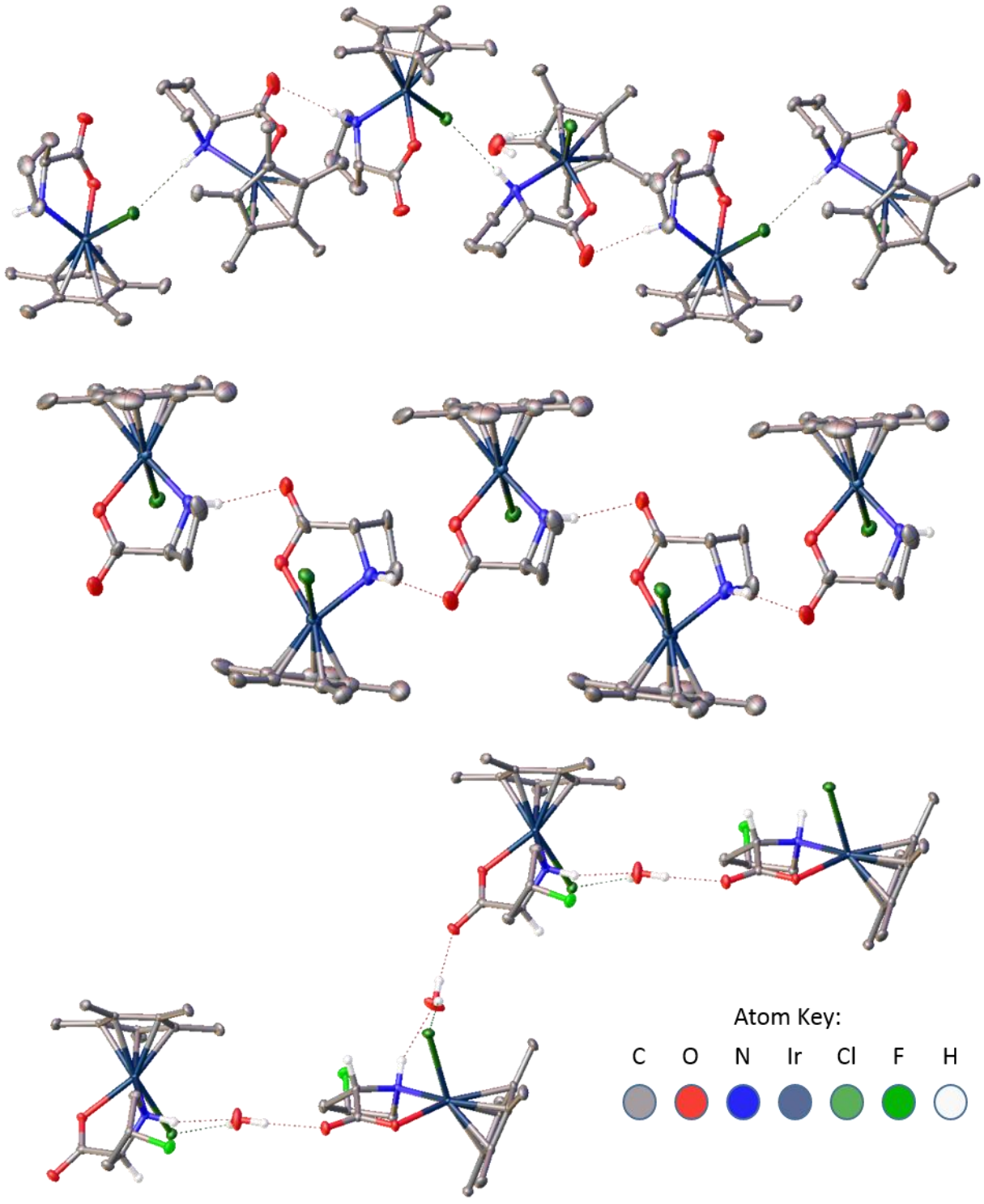

Figure 2.7: The Three Different Types of Intermolecular Hydrogen Bonding Networks. From top to bottom, (Cp*)Ir(L-pro)Cl, (Cp*)Ir(L-azetidine-2-carboxylic-acid)Cl, and (Cp*)Ir(L-trans-4-fluoro-pro)Cl

2.3.2. Structures of Non-ring Containing Amino Acid Complexes

The two enantiomers of (Cp*)Ir(L-gly)Cl possess very similar bond lengths and angles, as expected. The only significant difference is the length of the Ir-N bond, which is lengthened in the R_{Ir} enantiomer. The hydrogen bond formed between the chloride and one of the amine protons is most likely the cause of this lengthening Ir-N bond. Extension of the unit cell shows a hydrogen bonding network between the chloride and amine protons and the carbonyl oxygen to the next amine proton (figure 2.8). The (Cp*)Ir(L-ser)Cl complex displays similar bond lengths and angles to the achiral glycine complex. The only key difference is that the chloride is no longer involved in the extended hydrogen bonding network. Both amine protons are involved in this extended network, with one bound to the oxygen of an adjacent carbonyl oxygen and the other to the oxygen of the R group (figure 2.8).

Table 2.4: Selected Bond Lengths (Å) and Angles (deg) of Non-ring Containing (Cp*)Ir(aa)Cl complexes

Measurement	Gly 1	Gly 2	L-ser	L-Phengly	N-methyl-L-phengly
Cl-Ir	2.4120(7)	2.4147(7)	2.397(1)	2.4095(8)	2.4117(7)
N-Ir	2.131(2)	2.117(2)	2.124(3)	2.126(2)	2.134(2)
O-Ir	2.101(2)	2.101(2)	2.112(3)	2.091(2)	2.119(2)
G-Ir	1.755	1.75	1.75	1.76	1.765
Cl-Ir-N	85.08(7)	83.73(7)	82.65(8)	82.63(6)	88.00(6)
Cl-Ir-O	85.20(6)	86.78(6)	85.28(7)	86.15(6)	86.76(5)
N-Ir-O	78.31(9)	78.45(9)	77.2(1)	78.92(8)	76.04(8)
Cl-Ir-G	126.92	126.03	129.14	126.26	126.24
N-Ir-G	134.87	134.42	133.94	133.76	132.49
O-Ir-G	128.68	129.99	129.79	131.23	130.25

G represents the centroid of the Cp* ligand

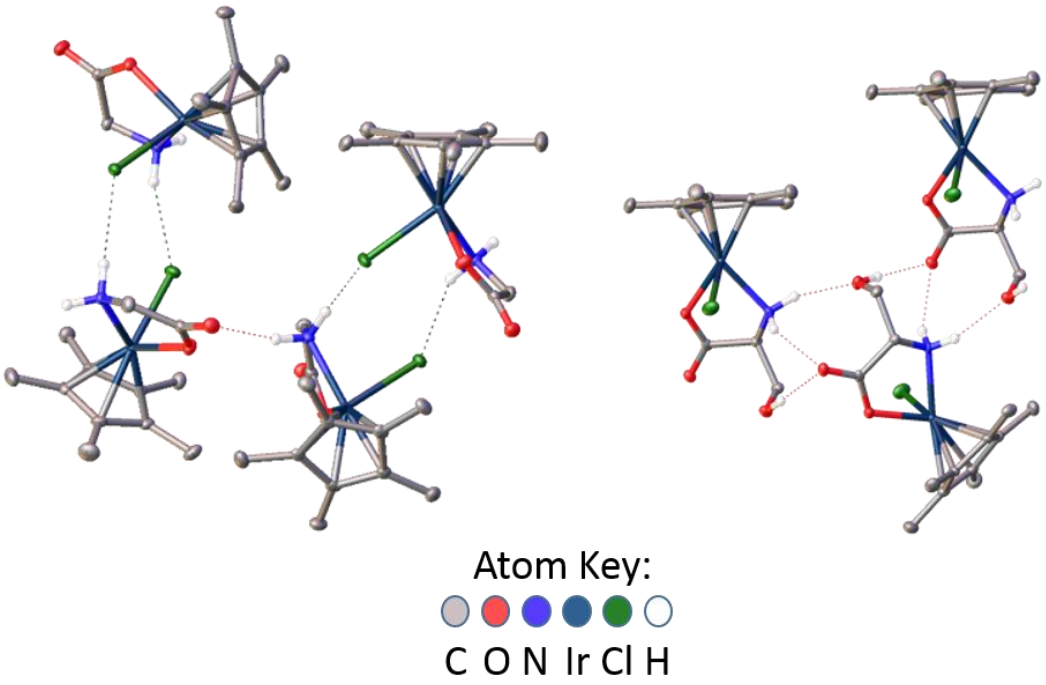

Figure 2.8: Hydrogen Bonding Network Formed by (Cp*)Ir(L-gly)Cl (left) and (Cp*)Ir(L-ser)Cl (right). The hydrogen bond between the chloride and amine in the (Cp*)Ir(L-gly)Cl structure results in a lengthening of the Ir-N bond.

The 5-membered ring formed between the amino acid and Ir of (Cp*)Ir(N-Me-L-phengly)Cl is puckered compared to the non-methylated variant. This is due to the steric strain between the amino-methyl and the Cp* ring and chloride. When viewed down the N-Ir bond, the (Cp*Ir(N-Me-L-phengly)Cl complex adopts a gauche configuration to alleviate this strain, with the (Cp*)Ir(L-phengly)Cl having an eclipsed configuration. This is shown in the large Cl-Ir-N bond angle for the methylated complex, as well as the lengthened Ir-N bond. Figure 2.9 displays the plots for of the complexes in table 2.4.

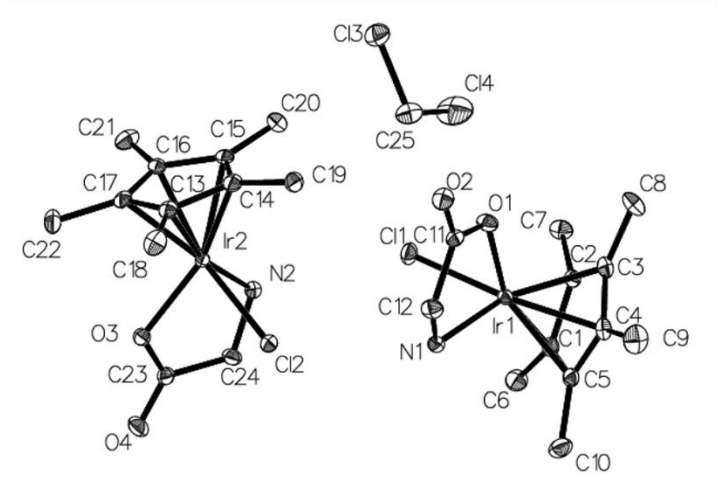

(Cp*)Ir(L-gly)Cl

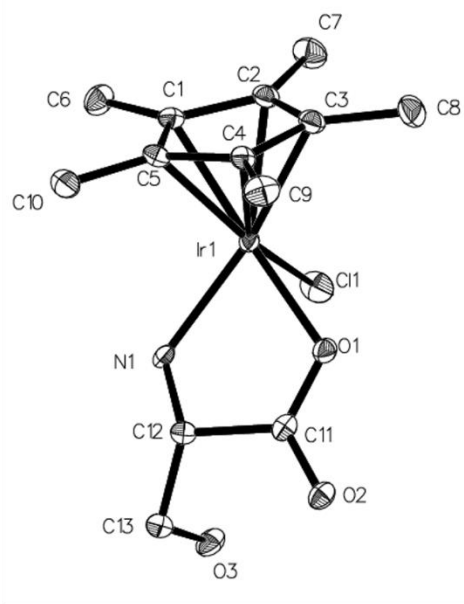

(Cp*)Ir(L-ser)Cl

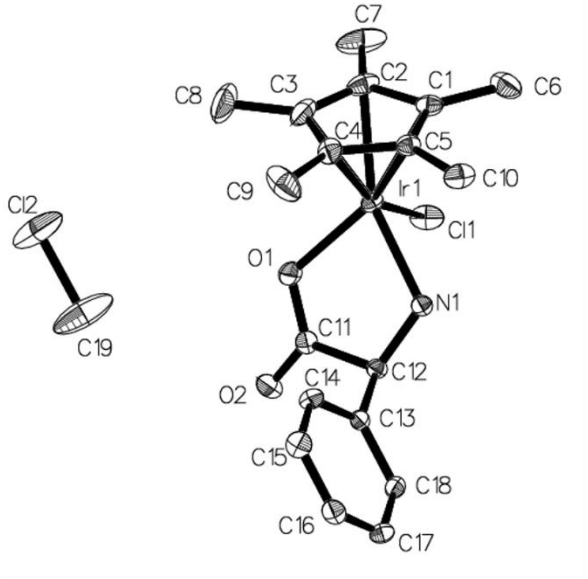

(Cp*)Ir(L-phengly)Cl

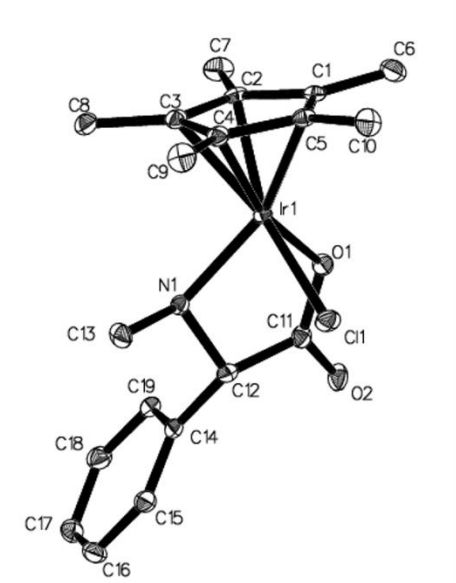

(Cp*)Ir(N-Me-L-phengly)Cl

Figure 2.9:Plots for (Cp*)Ir(L-gly)Cl, (Cp*)Ir(L-ser)Cl, (Cp*)Ir(L-phengly)Cl, and (Cp*)Ir(N-Me-L-phengly)Cl. Hydrogens omitted for clarity. Ellipsoids shown at 50%. Refer to text for explicit descriptions of structures.

Table 2.5: Selected Bond Lengths (Å) and Angles (deg) of Non-ring Containing (Cp*)Ir(aa)Cl complexes

Measurement	L-val major	L-val Minor	L-phe major	L-phe minor	D-phe major	D-phe minor
Cl-Ir	2.410(1)	2.414(1)	2.406(1)	2.401(1)	2.406(1)	2.404(1)
N-Ir	2.134(3)	2.129(4)	2.132(3)	2.101(3)	2.136(2)	2.110(3)
O-Ir	2.105(3)	2.093(3)	2.098(3)	2.119(3)	2.103(2)	2.125(3)
G-Ir	1.763	1.757	1.757	1.754	1.762	1.753
Cl-Ir-N	83.3(1)	83.6(1)	84.8(1)	82.3(1)	84.90(7)	82.43(9)
Cl-Ir-O	86.70(8)	86.42(8)	85.84(9)	86.12(9)	85.93(7)	86.05(7)
N-Ir-O	76.9(1)	78.0(1)	78.4(1)	77.1(1)	78.5(1)	77.1(1)
Cl-Ir-G	127.71	126.92	129.59	127.36	129.7	127.46
N-Ir-G	135.7	134.40	132.49	133.75	132.27	133.54
O-Ir-G	128.21	129.67	127.96	131.55	127.81	131.66

G represents the centroid of the Cp* ligand

The (Cp*)Ir(L-val)Cl diastereomers display very similar bond lengths and angles, most likely due to the low steric strain of the R group. This decreased steric strain also results in the low selectivity of one diastereomer over the other in solution, (53/47). Both phenylalanine based complexes display significant differences in Ir-N and Ir-O bond lengths between the two diastereomers. Examination of the structures show that the minor diastereomer has a puckered ring system formed by the chelated amino acid and the Ir, leading to the shortening and lengthening of the Ir-N and Ir-O bonds respectively. The D-phenylalanine complex displays nearly identical measurements as the L variant, which is to be expected. Figure 2.10 displays these structures.

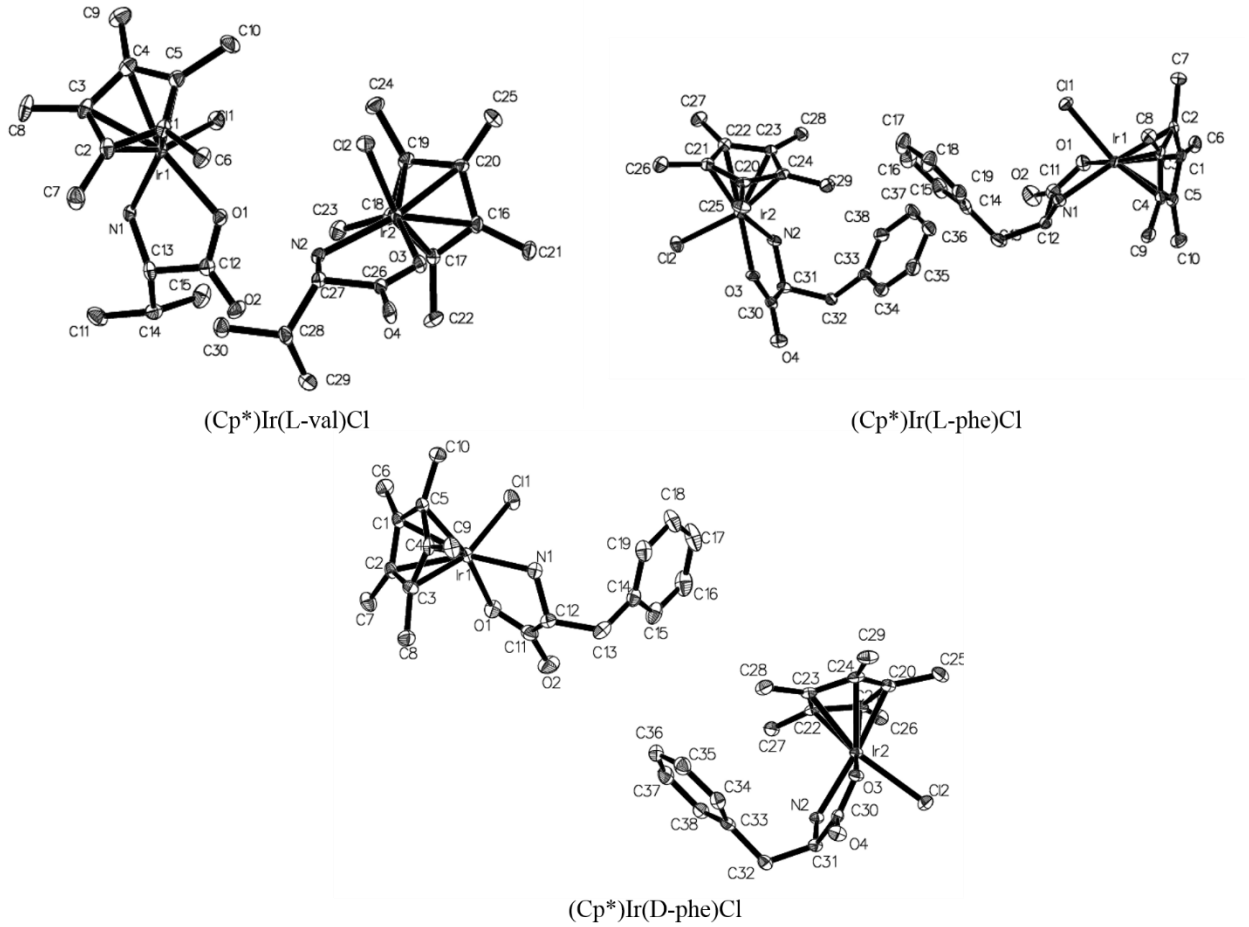

Figure 2.10: ORTEP Plots for (Cp*)Ir(L-val)Cl, (Cp*)Ir(L-phe)Cl, and (Cp*)Ir(D-phe)Cl. Hydrogens omitted for clarity. Ellipsoids shown at 50%. Little difference in bond lengths and angles are seen in the (Cp*)Ir(L-val)Cl complex, due to the low steric strain of the R group. The larger R group of phenylalanine causes the two diastereomers to adopt differing bond lengths and angles. Refer to table 2.5 for specific measurements.

2.3.3. Structures of Complexes with Amino Acids Containing Coordinating Side Chains.

The (Cp*)Ir(L-his)Cl complex presents an interesting case where the amino acid coordinates exclusively through the side chain and amine group, in both solid state and solution. The carboxylic acid presents in the deprotonated form, with both C-O bonds being of similar lengths of 1.244(4) and 1.254(3) Å. The Ir-N(amine) bond length is significantly longer than the other complexes (2.151(3)), most likely due to the short Ir-N(imidazole) bond length, (2.081(2)) in comparison to Ir-O bond

lengths. The elongation of the Ir-G bond (1.781) occurs due to the amino acid ligand presenting significantly "flatter" than other amino acid ligands due to the aromatic nature of the imidazole ring (Figure 2.11). The normally straight Cp*methyl groups are slightly displaced due to this interaction. The (Cp*)Ir(L-met)Cl complex presents as the amino acid acting as a tridentate ligand with the sulfur displacing the chloride, which then acts as a counter ion. The complex presents with shortened and nearly identical bond lengths of Ir-N and Ir-O to accommodate the 6 membered ring formed using the sulfur containing R group, (Figure 2.11). The bond lengths and angles are summarized in table 2.6.

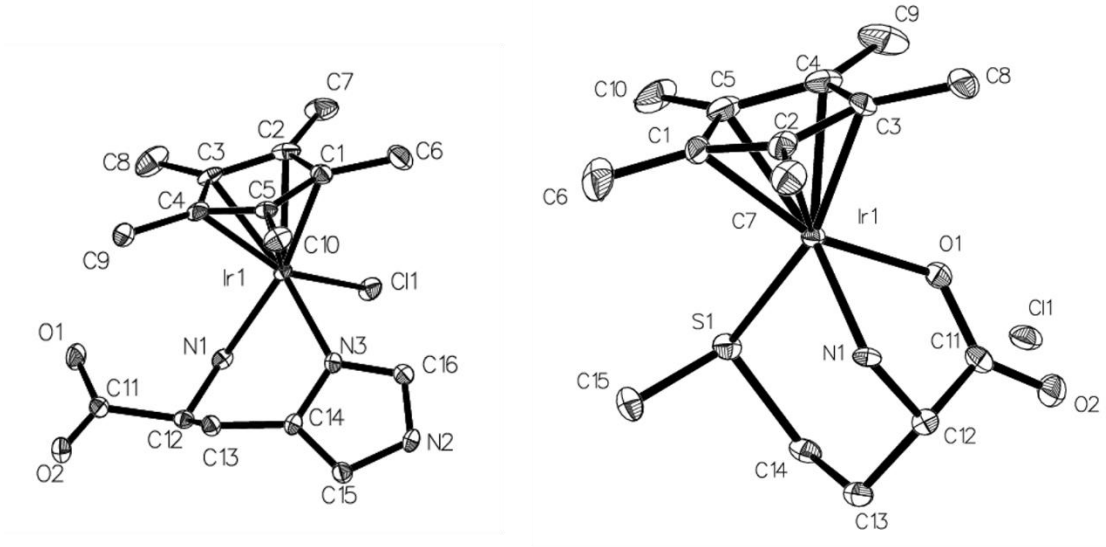

(Cp*))Ir(L-his)Cl **(Cp*))Ir(L-met)Cl**

Figure 2.11: Plots of (Cp*)Ir(L-his)Cl (left) and (Cp*)Ir(L-met)Cl. Hydrogens omitted for clarity. Ellipsoids shown at 50%. (Cp*)Ir(L-his)Cl shows the L-his ligand coordinated in a bidentate fashion through the amine and imidazole ring system. (Cp*)Ir(L-met)Cl has L-met acting at a tridentate ligand, displacing the chloride, which acts as a counter ion.

Table 2.6: Bond Lengths and Angles for (Cp*)Ir(L-his)Cl and (Cp*)Ir(L-met)Cl

Measurement	L-His	L-Met
Cl-Ir	2.4007(8)	
N-Ir	2.151(3)	2.099(2)
N(imidazole)-Ir	2.081(2)	
O-Ir		2.099(3)
S-Ir		2.365(1)
G-Ir	1.781	1.774
Cl-Ir-N	83.77(7)	
S-Ir-N		88.86(8)
Cl-Ir-N(imidazole)	86.87(7)	
S-Ir-O		86.36(8)
N-Ir-N(imidazole)	81.60(9)	
N-Ir-O		77.6(1)
Cl-Ir-G	125.44	
O-Ir-G		127.54
N-Ir-G	133.28	130.82
N(imidazole)-Ir-G	129.43	
S-Ir-G		128.77

2.4. Solution State Configuration and Identification

2.4.1. Nuclear Overhauser Effect (NOE) Experiments

The configuration of the complexes in the solid state can be correlated to the solution state through the use of 1-D NOE experiments. NOE spectroscopy measures the change in the intensity of an NMR resonance when the transitions of another one are perturbed. This is achieved through saturation of a selected resonance, followed by the elimination of the population differences across a transition, while observing the signals of others. NOE is normally only capable of seeing these interactions at distances of 3 Å or less. Figure 2.12 display several 1D ^{1}H NOE spectra for Cp*Ir(L-aze)Cl. The blue spectrum is the irradiation of one of the protons of the N-CH_2 at 3.8 ppm and the enhancement of the Cp* methyls at 1.7 ppm. The green spectrum is the irradiation of the other N-CH_2 proton at 4.2 ppm and the enhancement of the Cp* methyls at 1.7 ppm. Irradiation of the alpha proton at 4.5 shows no enhancement of the Cp* methyls.

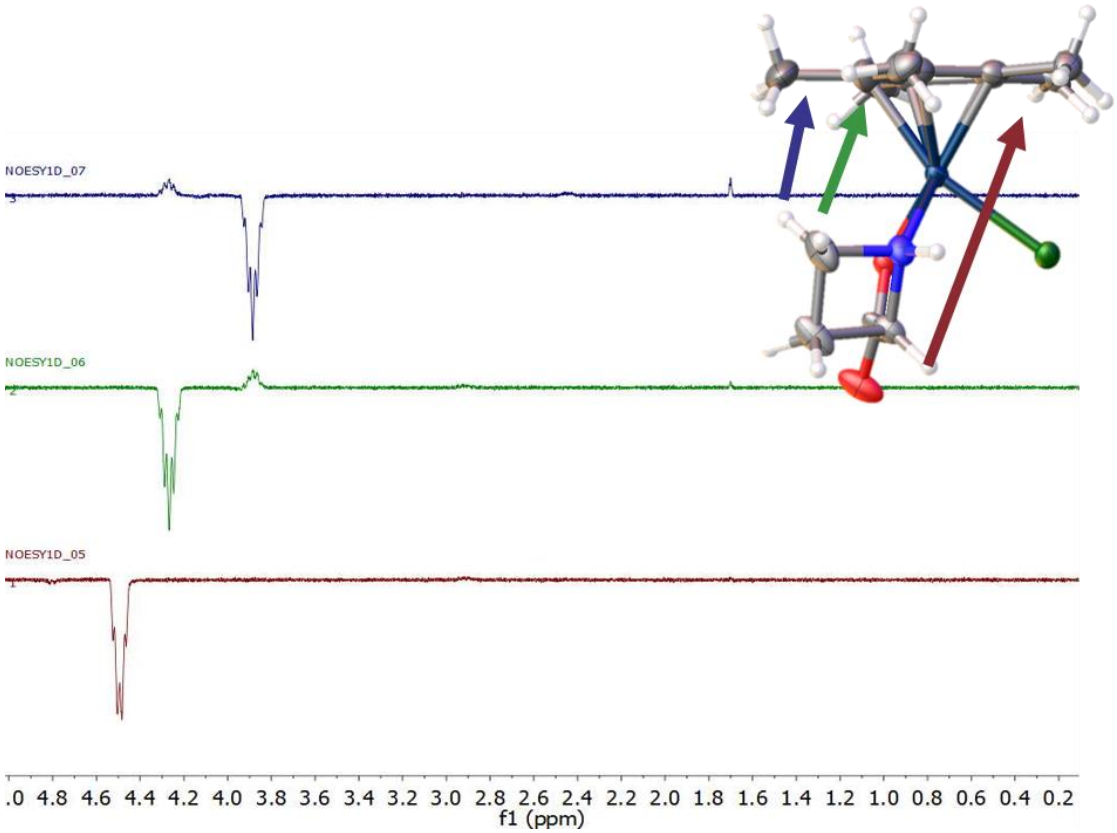

Figure 2.12: 1D ^{1}H NOE spectra of Cp*Ir(L-aze)Cl. The blue spectra is the irradiation of a N-CH_2 proton and the enhancement of the Cp* methyls. The green spectra is the irradiation of the other N-CH_2 proton and enhancement of the Cp* methyls. Irradiation of the alpha proton (red) displays no enhancement.

In the case of the (Cp*)Ir(L-phe)Cl complex (figure 2.13), selective irradiation of the Cp* resonance of the major component results in the enhancement of the aromatic protons of the side chain, indicating that the major component is of the configuration $S_{Ir}S_C$. This same irradiation for the minor component results in no such enhancement, indicating that the minor component consists of the R group pointing down and away from the Cp* moiety,. The configurations of (Cp*))Ir(L-ser)Cl, (Cp*))Ir(L-val)Cl, and (Cp*))Ir(L-ile)Cl are established through similar experiments, with irradiation of the side chain producing enhancement of the Cp* moiety and vice versa. The minor components lack this interaction.

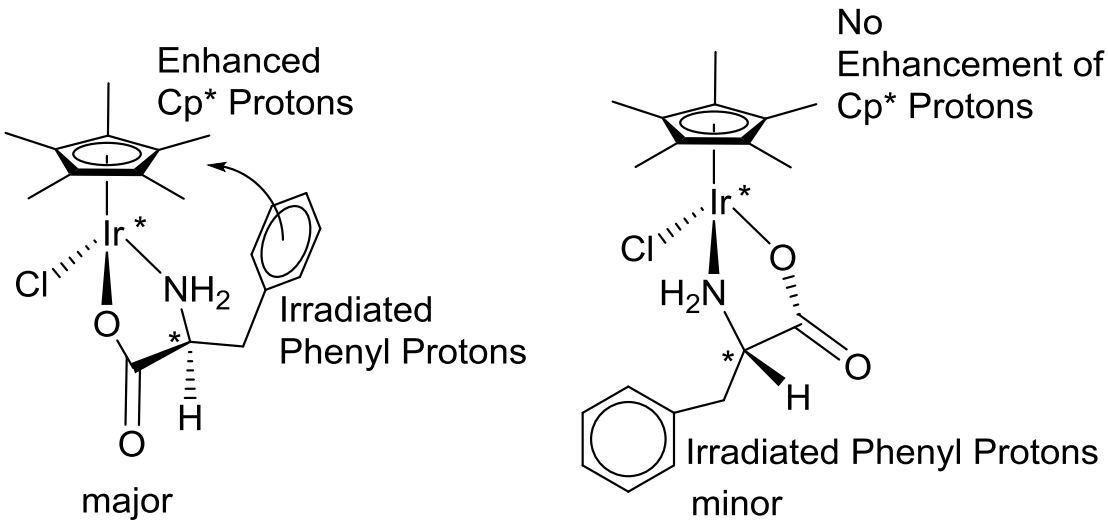

Figure 2.13: NOE of complexes (Cp*)Ir(L-phe)Cl showing through space interactions between the phenyl protons and the Cp* methyls. Only one configuration shows this enhancement. The major component is S at the metal center, with the minor being R.

The (Cp*)Ir(L-pip)Cl complex's major component in solution has the configuration of $S_{Ir}S_{C}R_{N}$. Irradiation of the amine proton of the major component results in the enhancement of the Cp* methyls, which can only result in from the previously stated configuration. The minor component lacks this interaction, but shows a clear enhancement of the Cp* methyls if the alpha proton is selectively irradiated, resulting from the configuration of $R_{Ir}S_{C}R_{N}$. These interactions are displayed in figure 2.14.

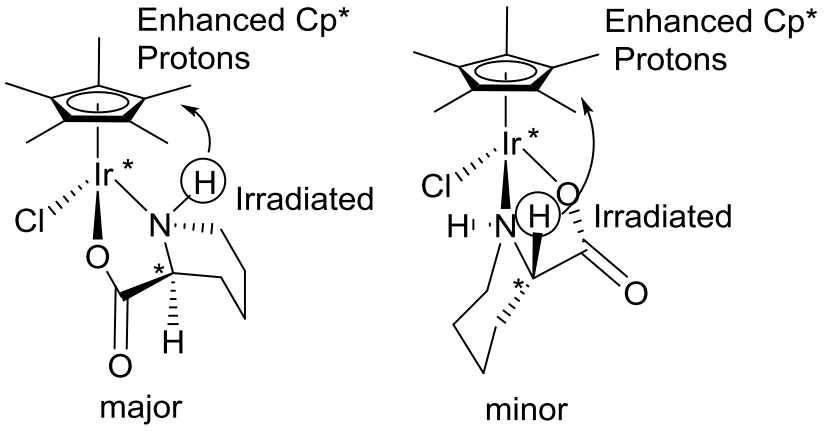

Figure 2.14 NOE of (Cp*)Ir(L-Piperdine-2-carboxylic-acid)Cl complex. The irradiation of the amine proton (Circled) in the major component produces an enhancement of the Cp* methyls. Irradiation of the alpha proton (Circled) produces a similar enhancement in the minor component.

The smaller ring systems of both (Cp*)Ir(L-pro)Cl and (Cp*)Ir(L-azetidine-2-carboxylate)Cl exhibit the opposite chirality at nitrogen once chelated to the metal center due to steric constraints. The chirality of the nitrogen and the alpha carbon are the same, both S, in the case of L amino acids. The major configuration places the N-CH_2 group of the ring in close proximity to the Cp* methyls, resulting in an NOE enhancement. The minor configuration of $R_{Ir}S_CS_N$ shows an interaction between the alpha proton and amine proton, (figure 2.15). The other proline based complexes adopt the same major and minor configurations as the non-modified variants.

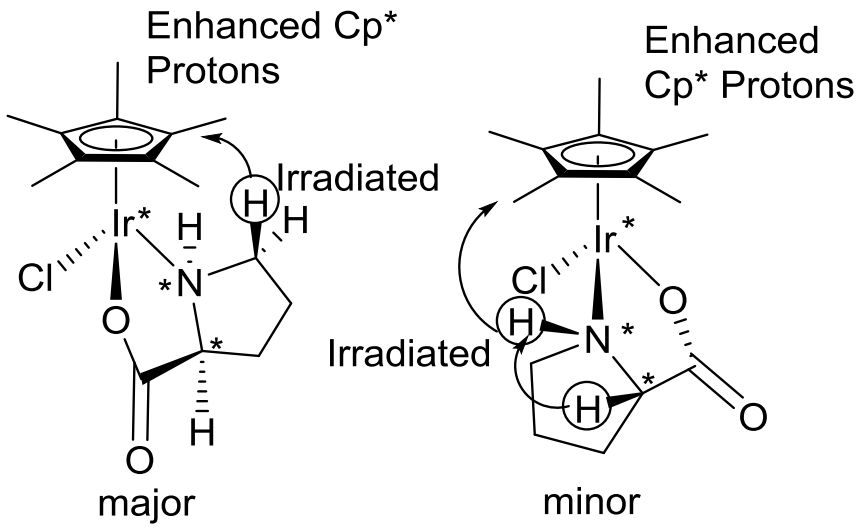

Figure 2.15: NOE of complex (Cp*)Ir(L-pro)Cl. The major component showing enhancement of the Cp* methyls upon irradiation of N-CH_2 group (Circled). The minor component showing enhancement of Cp* methyls upon irradiation of the amine proton (Circled).

2.4.2. Assignment of NMR spectra

In addition to NOE experiments to ascertain the configuration in solution, 2D techniques such as gradient correlation spectroscopy (gCOSY) allowed for the assignment of the complex splitting patterns that arise from the amino acid's coordination to the metal center. gCOSY allows for the identification of spins that are coupled to one another through bonds. This aids in the assignment of signals when the diastereomers appear in near 50/50 mixtures and simple integration is not enough for assignment. The protons of the amine become diastereotopic due to the nitrogen being 4 coordinate. (Cp*)Ir(*N*-Me-L-phengly)Cl presents a case where the amine protons of each diastereomer overlap in the proton spectra. However, gCOSY clearly shows that amine protons at δ 4.53 ppm coupled to both alpha protons at δ 4.33 ppm and δ 3.93 ppm of the minor and major diastereomers respectively (figure 2.16). Both the methyl and the alpha proton are only coupled to the amine proton, with J's of 6.0 Hz and 11.4 Hz respectively. Other ^{1}H NMR spectra of other complexes were assigned using similar techniques.

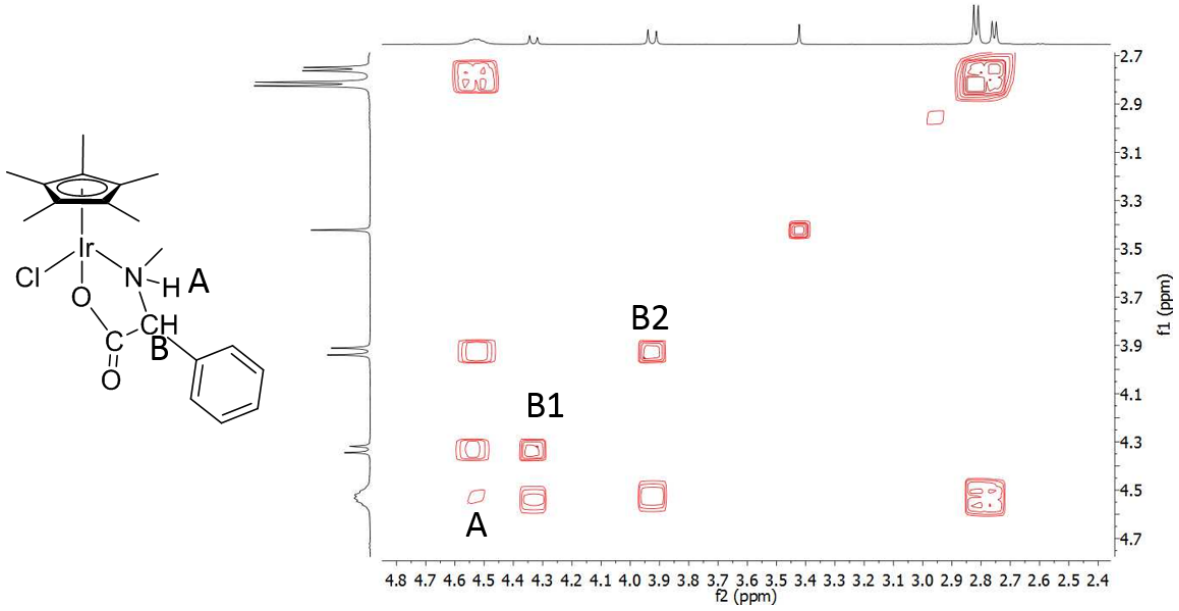

Figure 2.16: gCOSY of (Cp*)Ir(N-Me-L-phengly)Cl, showing coupling of the alpha protons and amine protons. A1 Refers to the overlapping amine protons of the diastereomers, B1 is the alpha proton of the minor component, and B2 is the alpha proton of the major component.

2.5. Chloride Abstractions

If the neutral chloride complexes are reacted with a suitable chloride scavenger such as $AgBF_4$ or $AgPF_6$, the complexes form aggregates. In the case of chiral complexes, a trimer of the form $[(Cp^*)Ir(aa)_3]X_3$, with X being a non-coordinating counter-ion, is produced. These trimers form through chiral self-recognition, in that each component is the same diastereomer. For example, the L-pro based timer forms exclusively from the $R_{Ir}S_CS_N$ diastereomers (figure 2.17). All reported structures of trimers using chiral amino acids have formed with only one diastereomer in the lattice.[89-91] It must be noted that the ^1H NMR spectra of the trimers are identical to their chloride variants. This is most likely due to the trimers disassociating upon entering solution.

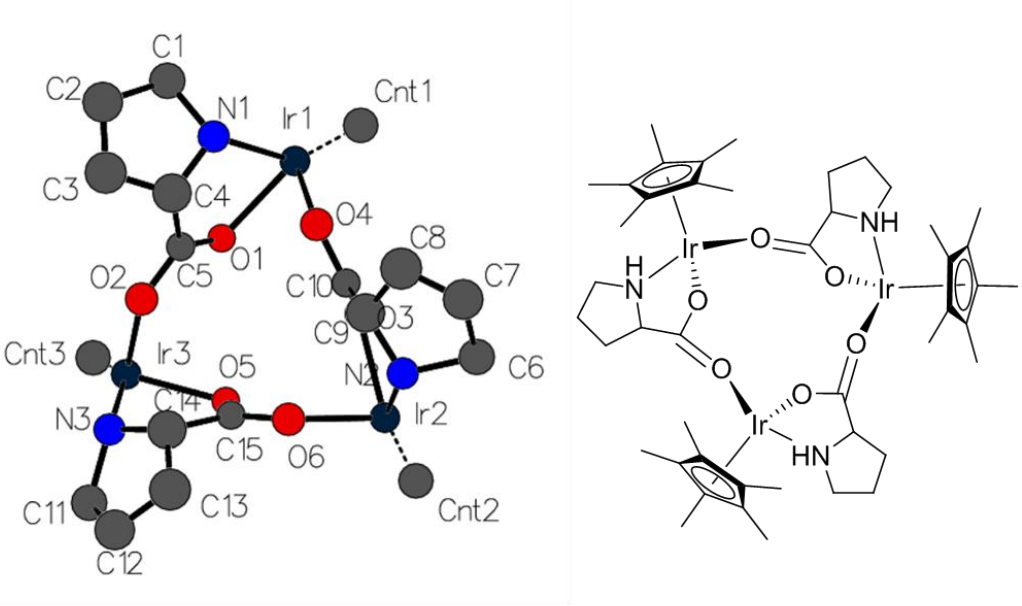

Figure 2.17: Trimer complex of $[(Cp^*)Ir(L\text{-}pro)_3][PF_6]_3$ with a representative diagram on the right. Cp* rings, hydrogens, and PF_6 ions omitted for clarity . This trimer forms through chiral self-recognition, with each monomer being of the form $R_{Ir}S_CS_N$.

In the case of the achiral glycine, an octamer is formed through semi alternating chiral units of the form $R_{Ir}R_{Ir}S_{Ir}S_{Ir}R_{Ir}R_{Ir}S_{Ir}S_{Ir.}$ The asymmetric unit contains only half of the structure, with the octamer completed through a C2 rotation. The Ir-O bond strengths differ slightly, even between entantiomers of the same configuration. Units 1 and 4, both R_{Ir} have Ir-O bond lengths of 2.134(6) and 2.126(5) Å. Similarly units 2 and 3 have lengths of 2.140(6) Å and 2.119(4) Å. The differences in bond lengths and angles are brought on by the constraints imparted by the ring system formed by the complex and are summarized in table 2.6. It should be noted that a trimer of the glycine complex has been isolated that only consists of the R_{Ir} enantiomer.[92] The octamer is displayed in figure 2.18.

Table 2.6: Selected Bond Lengths (Å) and Angels (deg) of the Octamer of Glycine

	1[a]	2[a]	3[a]	4[a]
Ir-O(Cord)	2.134(6)	2.140(6)	2.119(4)	2.126(5)
Ir-O(Bridge)	2.138(5)	2.122(5)	2.134(5)	2.119(5)
Ir-N1	2.140(5)	2.146(7)	2.148(8)	2.130(7)
Ir-G[b]	1.751	1.768	1.759	1.761
O(Cord)-Ir-O(Bridge)	79.0(2)	78.0(2)	78.0(2)	77.9(2)
O(Cord)-Ir-N	77.5(2)	76.9(2)	77.6(2)	77.1(2)
O(Bridge)-Ir-N	84.8(2)	81.7(2)	84.4(2)	81.1(2)
G-Ir-O(Cord)	131.66	131.09	132.02	129.94
G-Ir-O(Bridge)	130.14	133.62	132.2	133.43
G-Ir-N	130.14	133.54	131.81	135.05

[a] The columns represent the bonds and angles for each independent moiety, the numbering refers the Iridium atom in figure 2.17. [b] G represents the centroid of the Cp*

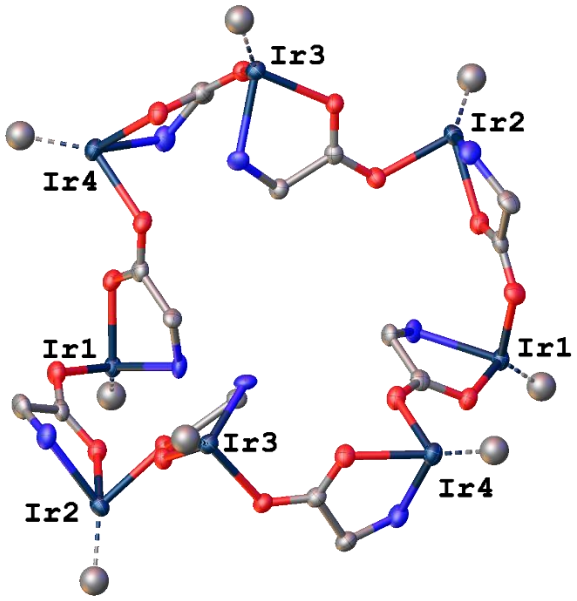

Figure 2.18: Octamer complex [(Cp*)Ir(gly)$_8$][PF$_6$]$_8$. Cp* rings, hydrogens, and PF$_6$ ions omitted for clarity. The ocotmer consists of semi-alternating enantiomers of the (Cp*)Ir(gly) monomer, with the overall configuration being $R_{Ir}R_{Ir}S_{Ir}S_{Ir}R_{Ir}R_{Ir}S_{Ir}S_{Ir}$.

2.6. Summary of Iridium Cp* Amino Acid Complexes

Cp*Ir(aa)Cl complexes are synthesized by reaction of the [(Cp*)IrCl$_2$]$_2$ dimer with two equivalents of amino acid and base in methanol. All are isolated as yellow powders and in yields ranging from 52 to 94%. The iridium becomes a stereogenic site upon coordination of the amino

acid, when treated as a pseudo tetrahedral center. If L-amino acids are used, the complexes form diastereomers of the form $R_{Ir}S_C$ and $S_{Ir}S_C$, with the major isomer being S at the metal center. Absolute configurations were assigned through a combination of single X-ray diffraction and 1D ^{1}H NOE techniques. The complexes epimerize at the Ir center when dissolved in solution, forming diastereomeric ratios which are dependent on the amino acid R group. Cyclic amino acids favor one diastereomer over the other to a greater degree than non-cyclic amino acid, with Cp*Ir(L-pro)Cl having a ratio of 93/7 and Cp*Ir(L-ala)Cl having a ratio of 56/44, most likely due to steric constraints. Chloride abstraction yields polymeric structures, which have been previously reported. The glycine based complex forms an octamer, $[(Cp^*)Ir(gly)_8][PF_6]_8$, with semi-alternating chirality at the metal center.

3. Modified Iridium Cp*R Amino Acid Complexes

This chapter concerns the synthesis and characterization of the modified (Cp*R)Ir(aa)Cl complexes. These complexes have a similar configuration to the related (Cp*)Ir(aa)Cl complexes. Absolute configurations at the metal center, coordinated amine, and chiral carbon were confirmed with single X-ray diffraction. The solid state configurations were correlated to the configurations in solution using NOE techniques.

3.1. Synthesis of modified Cp*R ligands and dimers

The Cp*R variants were synthesized via reaction of 1.25 to 1.50 molar equivalents of a Grignard reagent and 2,3,4,5-tetramethylcyclopent-2-enone in anhydrous THF. This reaction results in an alcohol product, and water is then eliminated to form the respective diene using HCl (equation 3.1).

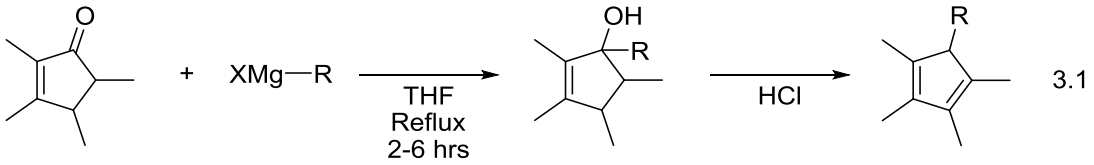

3.1

Purification of the final Cp*R variant is carried out with column chromatography on silica gel using hexanes as the eluent. This was followed by removal of solvent through reduced pressure to obtain the products as clear to yellow liquids. Purity was confirmed by liquid chromatography in comibation with mass spectrometry. Yields ranged from fair to excellent, with the product being a combination of several isomers. Yields are summarized in table 3.1. These dienes have the potential to polymerize when stored for long periods of time and are best used right away. The ^{1}H NMR spectra of the pentasubstituted dienes are fairly complex due to signal overlap of the multiple isomers, Figure 3.1.

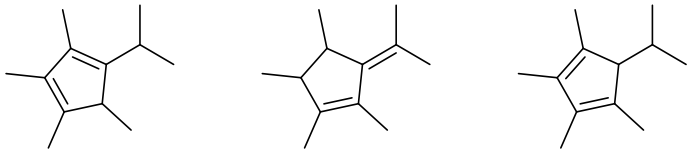

Figure 3.1: Potential isomers of Cp*^{iPr} precursor ligands formed through the elimination of the alcohol precursor. The second isomer is incapable of acting as the anionic ligand.

Table 3.1: Percent Yields of Cyclopentadienyl Ligands

R group	% Yield
Phenyl (ph)	69
Benzyl (bn)	94
Isopropyl (iPr)	37
Cyclohexyl (cy)	41
n-octyl	71

The reaction of the dienes with $IrCl_3 \bullet xH_2O$ using the method established by White, yields orange crystalline powders, with no physical differences from the $[IrCp^*Cl_2]_2$ dimer.[83] In the case of the $[(Cp^{*ph})IrCl_2]_2$ complex, it was found that synthesis via microwave reaction could vastly improve the yield when compared to conventional heating methods (30% yield to 69% yield).

The ^1H NMR pattern becomes simplified on complexation as the diene mixture forms a single respective anion. Unlike the $[IrCp^*Cl_2]_2$ which exhibits a lone singlet, these modified dimers display two singlets due to the methyl groups not being chemically equivalent. The ^1H NMR spectra of the $[(Cp^{*iPr})IrCl_2]_2$ complex is displayed in figure 3.2. Yields for the dimer complexes are summarized in table 3.2.

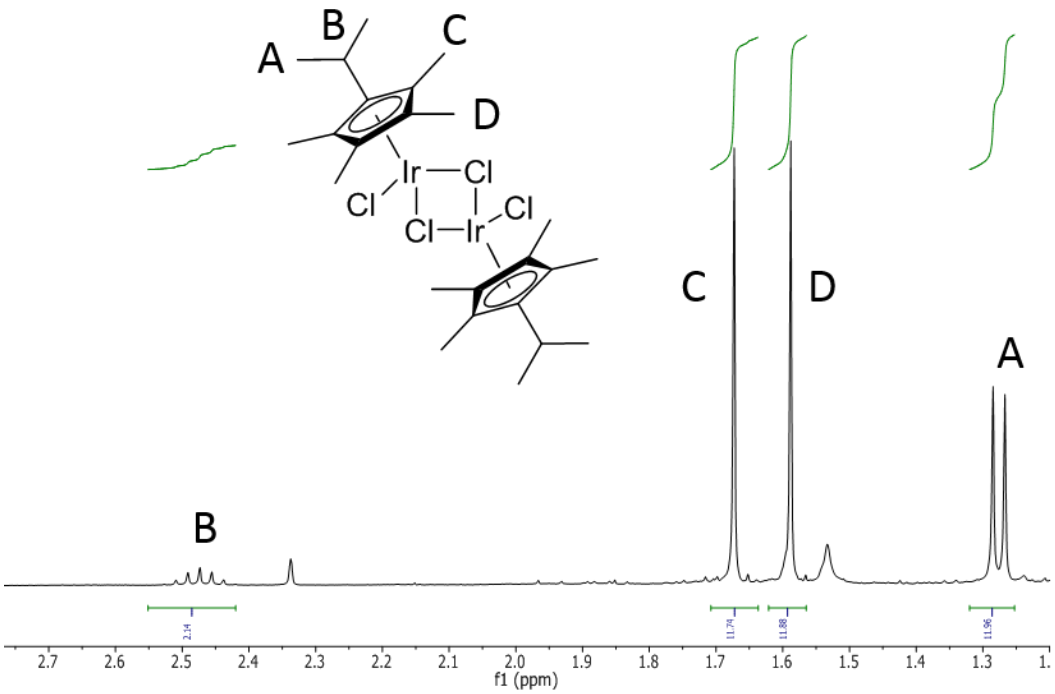

Figure 3.2: ^{1}H NMR spectrum of $[(Cp^{*iPr})IrCl_2]_2$. Cp^{*R} methyls are not equivalent due to addition of the R group.

Table 3.2: Yields of isolated Cp^{*R} dimers

Cp^{*R}	Yield%
(Cp^{*ph})*	60
(Cp^{*bn})	40
(Cp^{*iPr})	57
(Cp^{*cy})	49
$(Cp^{*\text{-n-Propyl}})$	91
$(Cp^{*\text{n-Octyl}})$	59
$(Cp^{*\text{n-Dodecyl}})$	14

*yield obtained through microwave heating, conventional methods produced 30% yield

3.2. Crystal Structures of Dimers:

Single crystals of $[(Cp^{*bn})IrCl_2]_2$, $[(Cp^{*iPr})IrCl_2]_2$, $[(Cp^{*cy})IrCl_2]_2$, $[(Cp^{*\text{n-propyl}})IrCl_2]_2$, and $[(Cp^{*\text{n-octyl}})IrCl_2]_2$ were grown by slow evaporation of methanol solutions. The structures of $[(Cp^{*bn})IrCl_2]_2$,

$[(Cp^{*iPr})IrCl_2]_2$, $[(Cp^{*n\text{-}propyl})IrCl_2]_2$, and $[(Cp^{*cy})IrCl_2]_2$ have an inversion center which generates the total dimer structure, figures 3.3, 3.4, and 3.5.

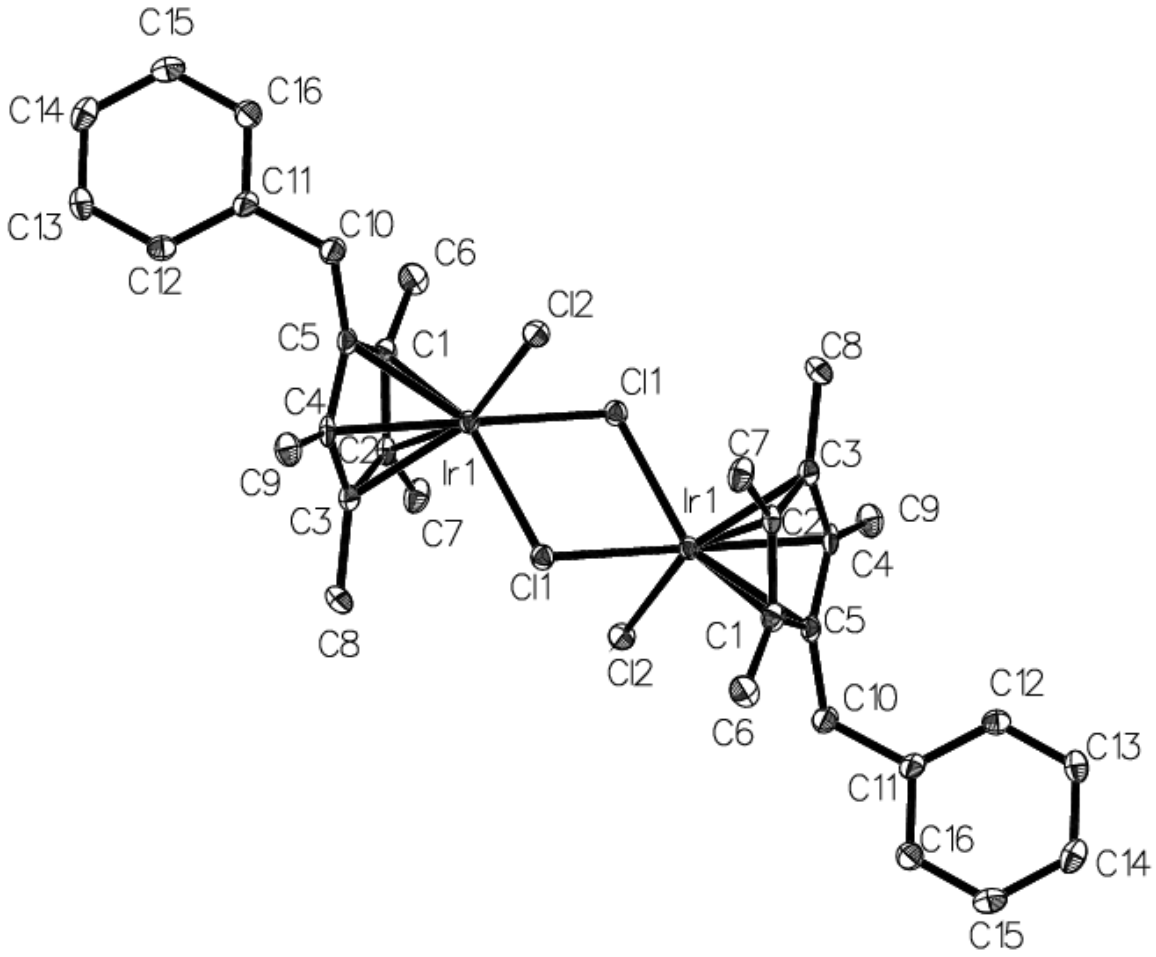

Figure 3.3: ORTEP Plot of $[(Cp^{*bn})IrCl_2]_2$. Hydrogens omitted for clarity. Ellipsoids shown at 50%. Refer to table 3.3 for discussion of bond lengths.

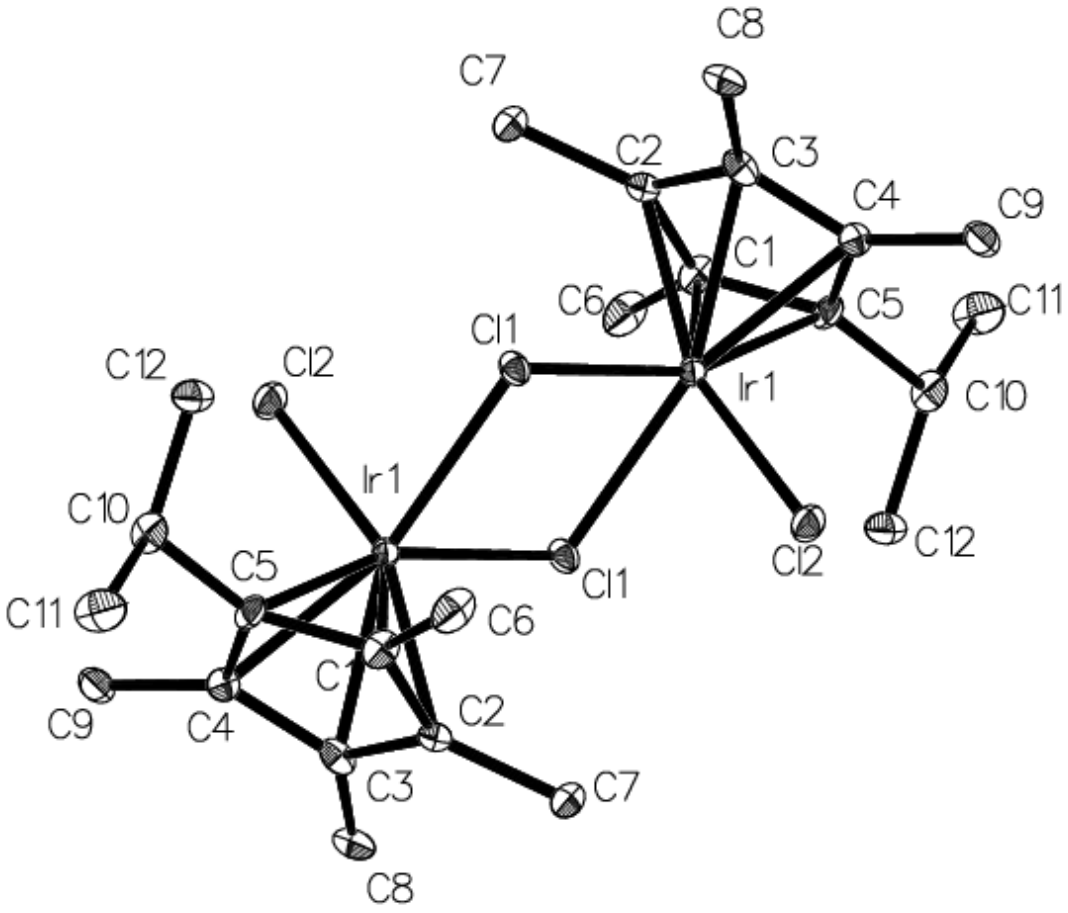

Figure 3.4: ORTEP Plot of $[(Cp^{*iPr})IrCl_2]_2$. Hydrogens omitted for clarity. Ellipsoids shown at 50%. Refer to table 3.3 for discussion of bond lengths.

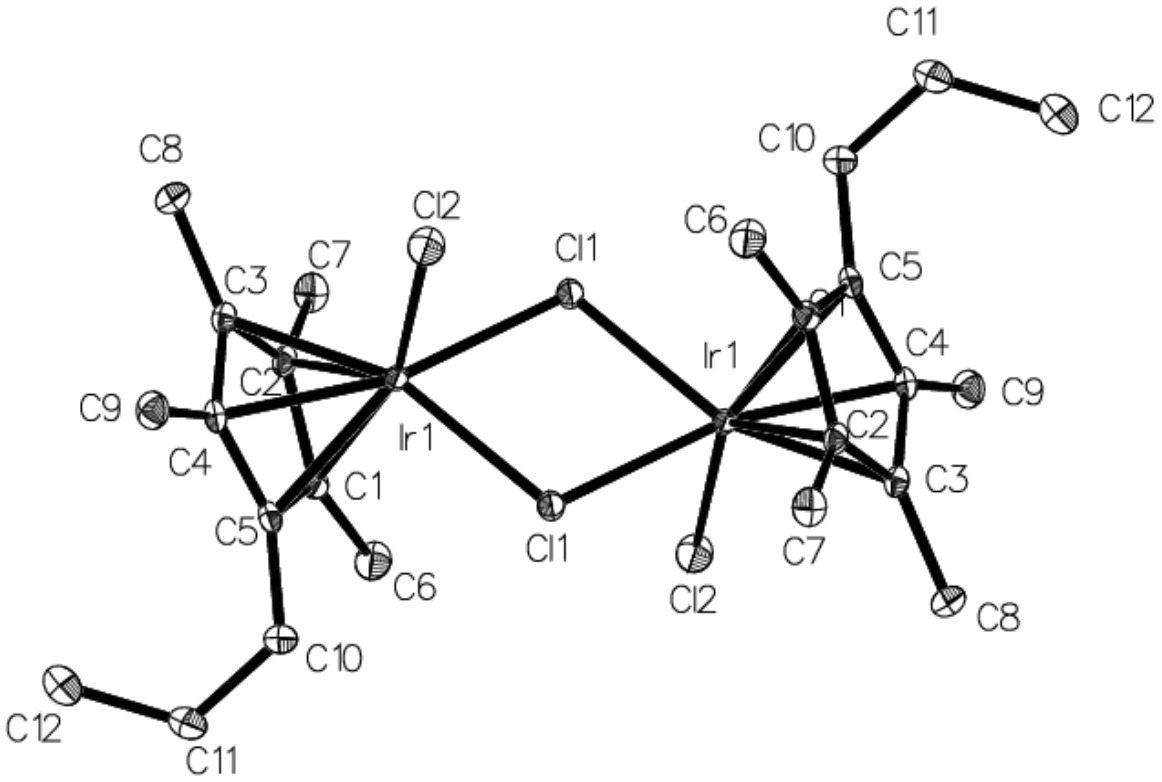

Figure 3.5: ORETP Plot of $[(Cp^{*n\text{-}propyl})IrCl_2]_2$. Hydrogens atoms omitted for clarity. Ellipsoids shown at 50%. Refer to table 3.3 for discussion of bond lengths.

The bond lengths are summarized in table 3.3. Analysis of the bond lengths of the bridging chloride reveals no direct correlation between the Cp^{*R} and the Ir-Cl bond length. The $[(Cp^{*n\text{-}octyl})IrCl_2]_2$ structure lacks an inversion center. In addition, the $[(Cp^{*n\text{-}octyl})IrCl_2]_2$ crystal undergoes a phase transition at approximately 240 K, with the crystals "shattering". Due to this phase change data collection was performed at room temperature and the structure is highly disordered.

The $[(Cp^{*ph})IrCl_2]_2$ structure was reported by Sadler et al. and displays π-π stacking between the centroids of the phenyl systems (3.956 Å).[93] The related $[(Cp^{*Bn})IrCl_2]_2$ complex lacks these interactions, due to the benzyl group being less rigid than the phenyl ring. Additionally, the $[(Cp^{*Cy})IrCl_2]_2$ structure shows two different chair configurations when the disorder is appropriately modeled (figure 3.6).

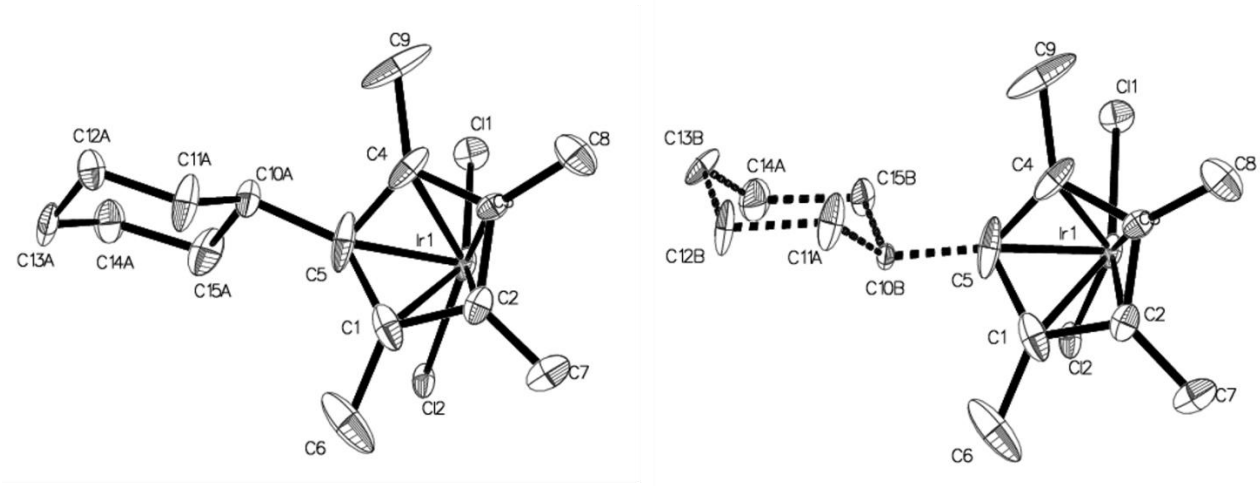

Figure 3.6: ORTEP Plot of the $[(Cp^{*cy})IrCl_2]_2$ showing the two differing chair configurations. Hydrogens omitted for clarity. Ellipsoids shown at 50%. Refer to table 3.3 for discussion of bond lengths.

Table 3.3: Comparison of Bond lengths (Å) of modified dimer complexes

	Cp^{*R}			
Measurement	$Cp^{*n\text{-propyl}}$	Cp^{*iPr}	Cp^{*Bn}	Cp^{*Cy}
Ir-G	1.754	1.759	1.753	1.751
Ir-Cl	2.3925(7)	2.392(2)	2.3914(7)	2.383(1)
Ir-Cl(bridging)	2.4486(6)	2.444(1)	2.4549(7)	2.439(1)

G represents the centroid of the Cp^{*R}

3.3. Synthesis and characterization of $Cp^{*R}Ir(aa)Cl$ complexes

The amino acid complexes of the form $(Cp^{*R})Ir(aa)Cl$, with R = phenyl, benzyl, iso-propyl, n-propyl, cylcohexyl, n-octyl, and n-dodecyl were synthesized in a similar fashion to their (Cp*)Ir(aa)Cl counterparts, equation 3.2.

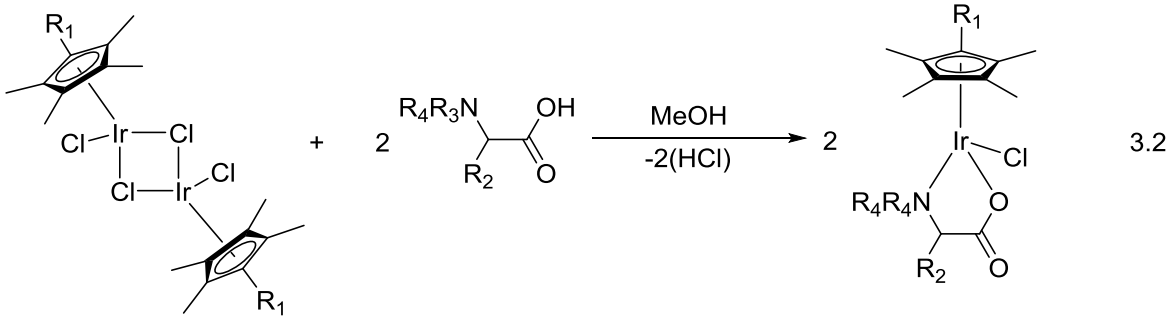

3.2

All complexes adopt the same three-legged piano stool (half-sandwich) configuration, as expected. These complexes also form diastereomers that differ at the metal center, like the unmodified complexes, which are distinguishable by both ^{1}H and ^{13}C NMR spectroscopy. Yields and ratios are summarized in table 3.4.

Due to the R group on the Cp* moiety, the methyl groups are not chemically equivalent. This leads to a more complex pattern in both the ^{1}H and ^{13}C NMR. The methyl groups can appear as a broad overlapping singlet, with integration of 12 protons, to completely distinct individual singlets integrating for 3 protons, and patterns in-between these two extremes. The R group of the amino acid has a greater effect on the degree of splitting of the Cp methyls than the R group of Cp^{*R} portion, with similar patterns presented by complexes using the same amino acid ligand but differing Cp^{*R}.

Table 3.4: Yields and ratios of the major isomers of (Cp^{*R})Ir(aa)Cl complexes. All amino acids are L unless otherwise stated

Cp^{*ph}			Cp^{*bn}		
aa	Yield %	Ratio S_{Ir}/R_{Ir}	aa	Yield%	Ratio S_{Ir}/R_{Ir}
Ala	52	54	Phe	93	69
Phengly	43	68	Pro	77	85
Phe	94	55	Aze	83	88
Pro	94	89	Pip	98	69
Pip	94	69			
Cp^{*iPr}			Cp^{*cy}		
aa	Yield %	Ratio S_{Ir}/R_{Ir}	aa	Yield %	Ratio S_{Ir}/R_{Ir}
Gly	88	na	Gly	59	na
N,N-dimeth-Gly	74	100	Ala	80	56
Ala	68	50	Phe	85	68
Phe	82	71	Phengly	80	58
Pro	71	83	Pro	69	88
$Cp^{*n\text{-}dodecyl}$			$Cp^{*n\text{-}octyl}$		
aa	Yield %	Ratio S_{Ir}/R_{Ir}	aa	Yield	Ratio S_{Ir}/R_{Ir}
Phe	94	70	Gly	79	na
Phengly	85	62	Ala	83	51
Pro	69	91	Aze	88	86
D-Pro*	20	91	Phengly	94	56
			Pro	64	90

$Cp^{*n\text{-}propyl}$		
aa	Yield %	Ratio
Ala	50	55
Phengly	85	62
Aze	42	83
Pro	79	91

*Ratio of S_{Ir}/R_{Ir} are reversed. na = not applicable due to formation of enantiomers

The diastereomeric ratios of these (Cp^{*R})Ir(aa)Cl complexes are similar to their (Cp*)Ir(aa)Cl counterparts, with the ring based systems such as L-proline and L-azetidine-2-carboxylic acid again having the highest selectivity, with smaller R groups such as L-alanine having the least. The Cp^{*R} variant has little effect on these ratios because the largest R groups are rotated away from the bulkiest portion of the amino acid, as observed in the crystal structures. These ratios

are unchanged over time as observed by NMR spectroscopy. The major and minor configurations of these complexes, (S_C, S_{Ir}) or (S_C, R_{Ir}) in the case of non-alkylated amine ligands, or ($R_{Ir}R_CS_N$, $S_{Ir}R_CS_N$) for alkylated amine ligands, are the same as those reported for the (Cp*)Ir(aa)Cl complexes, as determined through NOE experiments. Similar irradiation methods used for the unmodified complexes produce the same enhancements for their Cp^{*R} counterparts. For example, the (Cp^{*ph})Ir(L-pip)Cl displays the same interactions as the (Cp*)Ir(L-pip)Cl variant, Figure 3.7. NOE experiments showed that the major component has an interaction between the amine proton and the Cp^{*R} methyls, while the minor component displays interactions between the alpha carbon proton and the Cp^{*R} methyls.

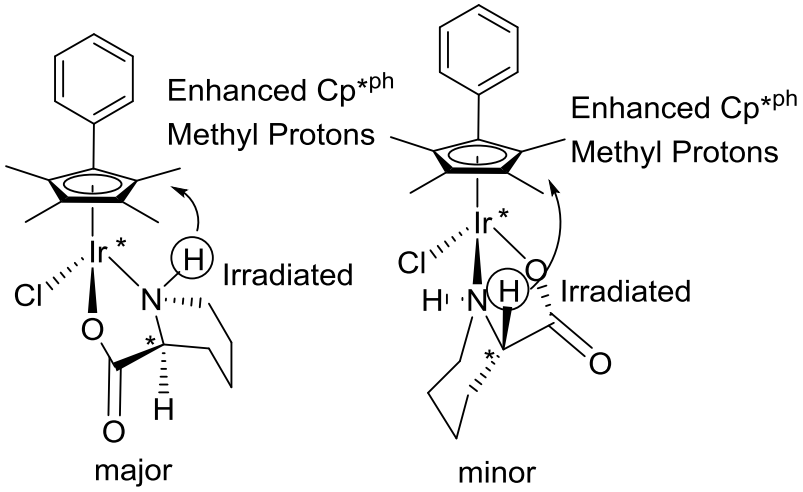

Figure 3.7: NOE effects on (Cp^{*ph})Ir(L-pip)Cl, showing the same enhancements as the unmodified (Cp*)Ir(aa)Cl complexes. The irradiation of the amine proton (Circled) in the major component produces an enhancement of the Cp^{*ph} methyls. Irradiation of the alpha proton (Circled) produces a similar enhancement in the minor component.

The R groups of these modified Cp* type ligands can be under significant steric hindrance when amino acids with larger side chains are used as ligands. This is observable in the ^{1}H NMR spectrum, most specifically for the iPr complexes due the simple pattern produced by the Cp^{*iPr}. The ^{1}H NMR of the (Cp^{*iPr})Ir(L-phe)Cl complex displays characteristics of restricted rotation of the iPr

portion of the molecule (figure 3.8). Both the major isomer and minor isomer lack a doublet for the iPr, instead showing what resembles a doublet of doublets. This is in contrast to $[(Cp^{*iPr})IrCl_2]$ ^1H NMR spectra (figure 3.2) which shows a doublet for the iPr portion of the complex, indicating free rotation of the iPr group.

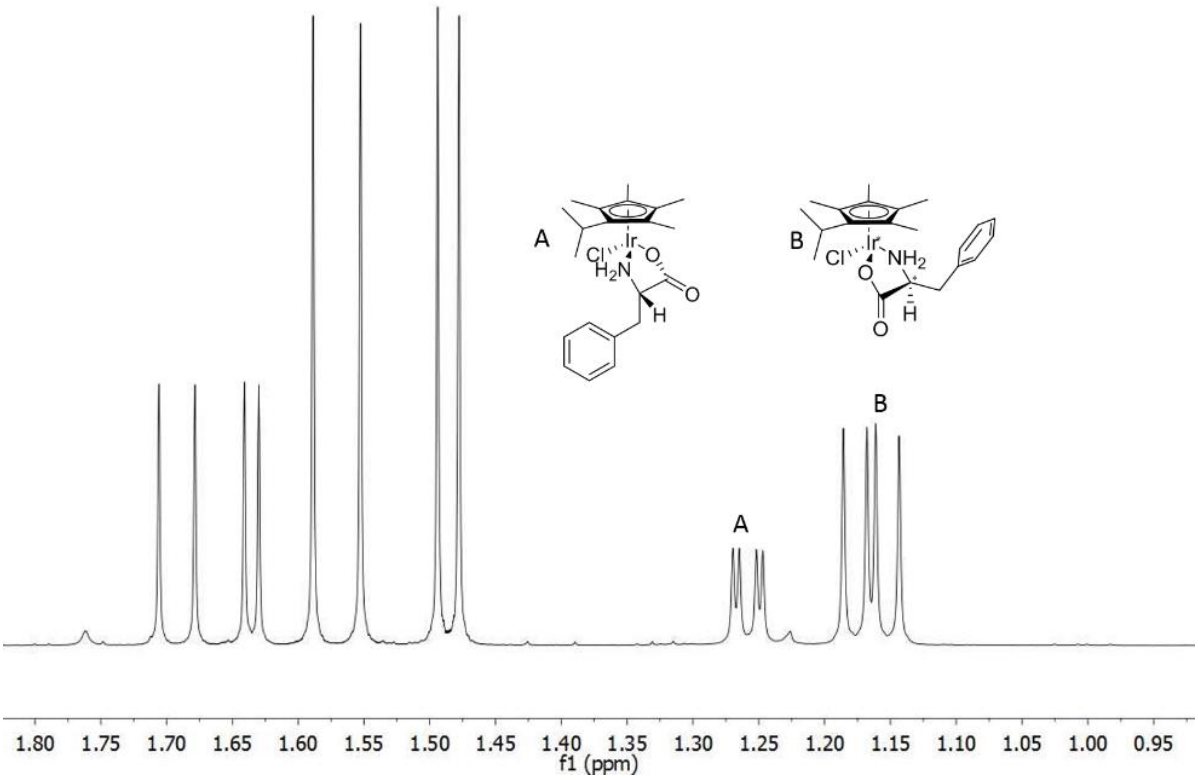

Figure 3.8: ^1H NMR spectrum of the Cp* region of (Cp^{*iPr})Ir(L-phe)Cl. Hindered rotation of the isopropyl portion of the Cp^{*iPr} results in splitting pattern differences between the isopropyl groups of the diastereomers of complex (Cp^{*iPr})Ir(L-phe)Cl. Refer to appendix for NMR spectra for the related (Cp^{*iPr})Ir(aa)Cl complexes.

The two differing configurations produce different overlapping doublet patterns. The L-alanine produces a single doublet in the same range as the (Cp^{*iPr})Ir(L-phe)Cl iPr group (1.15 -1.28 ppm), similar to the $[(Cp^{*iPr})IrCl_2]_2$ complex, with the doublets of the Cp^{*iPr} being isochromatic. The

L-phenylglycine complex produces a pair of overlapping doublets, but with similar coupling constants. These spectra can be found in Figures A24 –A32. Interestingly, none of these complexes exhibit an NOE enhancement between the Cp*^{R} and the amino acid ligand, despite most Cp*^{R} groups having protons within the <3 Å range of protons on the amino acid ligand, considered to be the maximum range of NOE interactions. The enhancements seen for the Cp*Ir(aa)Cl were only on the order of 2 – 5% enhancement, and it is possible that decreasing the number of irradiated protons further diminished this enhancement to the point that is not observable.

3.3.1. Crystals Structures of Cp*^{R}Ir(aa)Cl complexes:

The R groups of the Cp*^{R} moiety are forced away from the sterically demanding amino acid and chloride ligands, as observed in the crystal structures. In the case of complexes formed from Cp*^{ph}, Cp*^{iPr}, and Cp*$^{n\text{-propyl}}$ the R group of the Cp* moiety is forced in-between the chlorine and the nitrogen to relieve their steric interaction. Complexes formed from the Cp*^{bn} ligand adopt a configuration similar to the Cp* complexes, with the benzyl portion having freedom of rotation placing the phenyl group in an anti position with respect to the metal. Comparison of the bond lengths and angles of the L-proline complexes shows a significant lengthening of the Ir-Cl bond in the case of (Cp*^{ph})Ir(L-pro)Cl compared to (Cp*^{bn})Ir(L-pro)Cl, (Cp*^{iPr})Ir(L-pro)Cl, and (Cp*$^{n\text{-propyl}}$)Ir(L-pro)Cl. Distances from the centroid to the iridium are nearly identical, with complex (Cp*^{ph})Ir(L-pro)Cl being shorter by 0.01 angstroms. Complex (Cp*^{bn})Ir(L-pro)Cl, (Cp*^{iPr})Ir(L-pro)Cl, and (Cp*$^{n\text{-propyl}}$)Ir(L-pro)Cl are nearly identical to the unmodified complex, which has a distance of 1.766 Å. Ir-N bonds are also nearly identical between (Cp*^{ph})Ir(L-pro)Cl, (Cp*^{bn})Ir(L-pro)Cl, (Cp*^{iPr})Ir(L-pro)Cl, and (Cp*$^{n\text{-propyl}}$)Ir(L-pro)Cl, but shorter than the unmodified complex (2.140 Å). Ir-O bond lengths are similar between the (Cp*^{ph})Ir(L-pro)Cl, (Cp*^{bn})Ir(L-pro)Cl, and (Cp*$^{n\text{-propyl}}$)Ir(L-pro)Cl complexes but the (Cp*^{iPr})Ir(L-pro)Cl has a lengthening of more than 0.3 angstroms. All Ir-O bonds in these complexes are significantly longer than the Cp* complex (2.086

Å). This is most likely due to the increased steric bulk of the Cp*^{R} moiety. Bond lengths and angles are summarized in table 3.5.

Table 3.5: Selected bond lengths and angles of complexes (Cp*^{ph})Ir(L-pro)Cl, (Cp*^{bn})Ir(L-pro)Cl, (Cp*^{iPr})Ir(L-pro)Cl and (Cp*$^{n\text{-propyl}}$)Ir(L-pro)Cl.

Cp^{R}	**Cp*^{ph}**	**Cp*^{bn}**	**Cp*^{iPr}**	**Cp*$^{n\text{-propyl}}$**
Ir-Cl	2.434(4)	2.3999(7)	2.416(1)	2.4197(6)
Ir-O	2.12(1)	2.111(2)	2.155(3)	2.100(2)
Ir-N	2.12(1)	2.127(2)	2.129(3)	2.127(2)
Ir-G	1.755	1.767	1.76	1.760
C5-C10	1.50(2)	1.490(5)	1.513(6)	1.496(3)
Cl-Ir-O	86.9(3)	86.92(7)	86.14(8)	87.28(5)
Cl-Ir-N	83.4(3)	84.35(7)	86.34(9)	84.19(5)
O-Ir-N	78.4(4)	77.44(9)	76.5(1)	77.38(7)
Cl-Ir-G	125.03	127.08	125.75	125.85
O-Ir-G	129.91	126.91	129.58	129.34
N-Ir-G	135.72	136.38	134.95	135.34

G refers to the centroid of the Cp*^{R}Ir(aa)Cl complexes

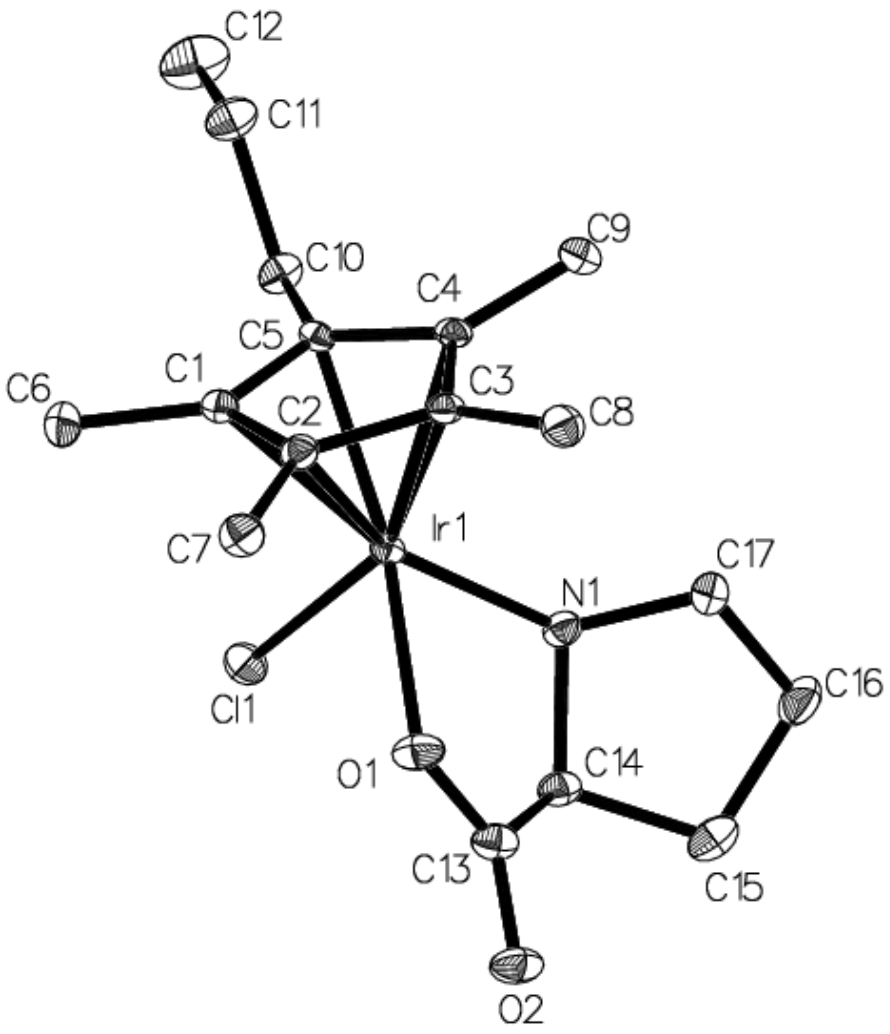

Figure 3.9: Crystal structure of (Cp*$^{n\text{-propyl}}$)Ir(L-pro)Cl. All hydrogen atoms are omitted for clarity. Ellipsoids shown at 50%. Refer to table 3.5 for bond lengths and angles.

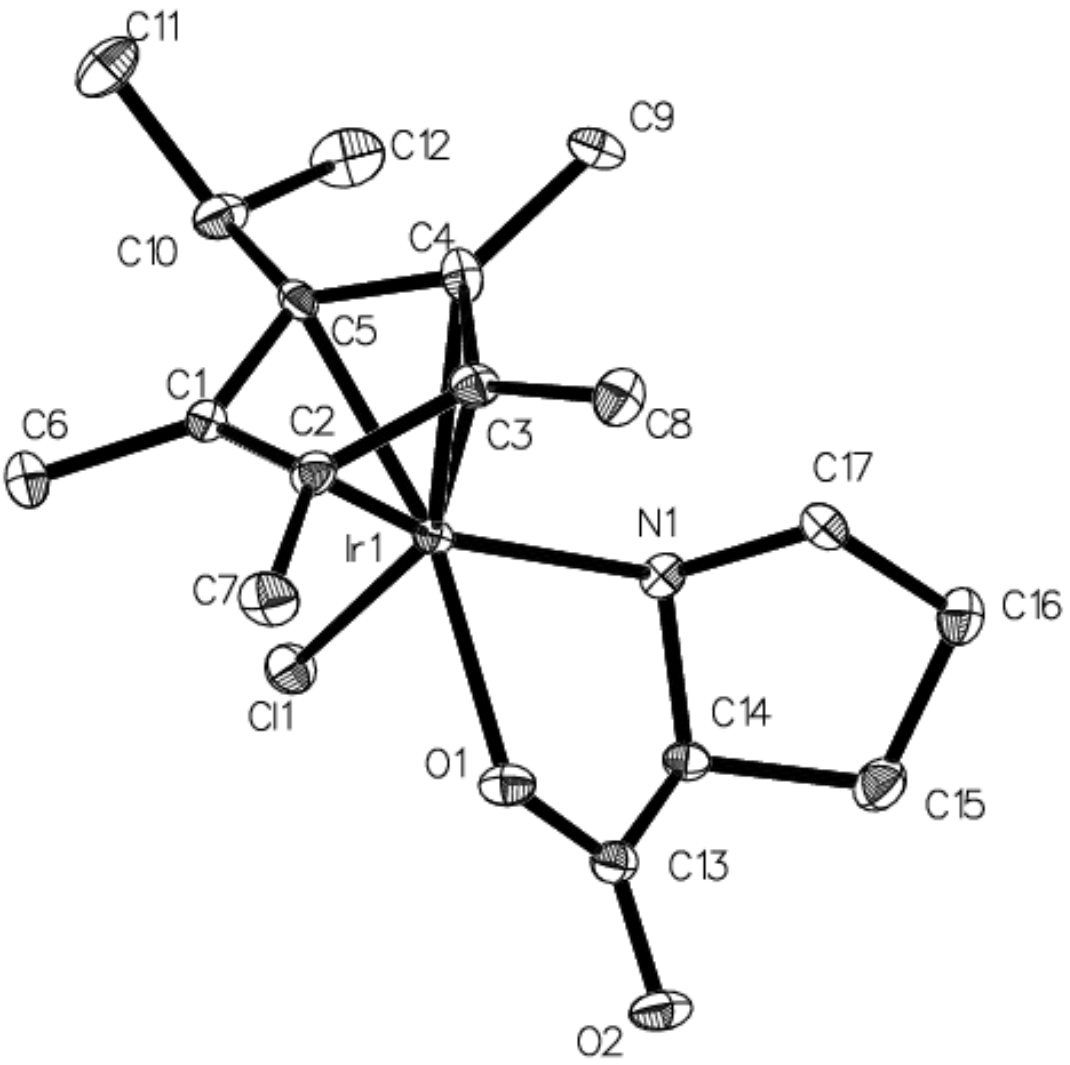

Figure 3.10: Crystal structure of (Cp*^{iPr})Ir(L-pro)Cl. All hydrogen atoms are omitted for clarity. Ellipsoids shown at 50%. Refer to table 3.5 for bond lengths and angles.

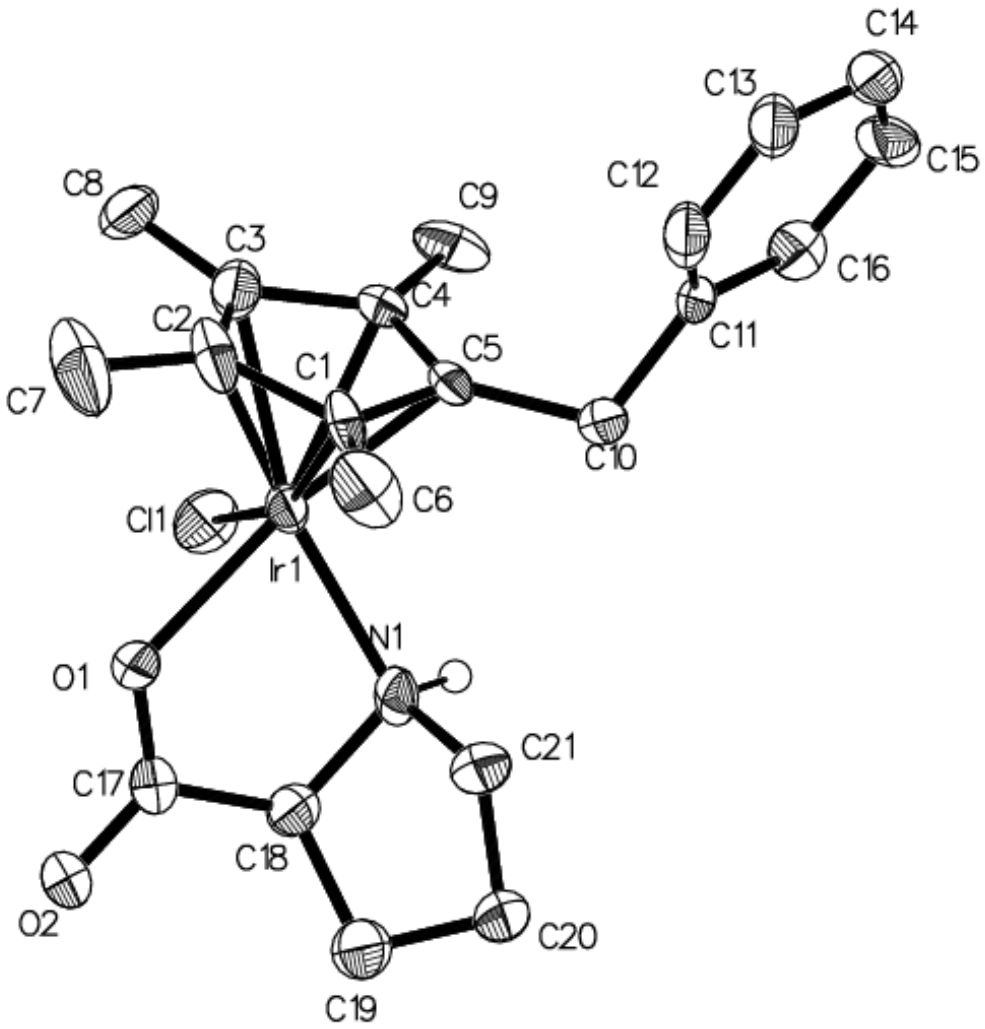

Figure 3.11: Crystal structure of (Cp*^{bn})Ir(L-pro)Cl. All hydrogen atoms except the amine hydrogen are omitted. Ellipsoids shown at 50%. Refer to table 3.5 for bond lengths and angles.

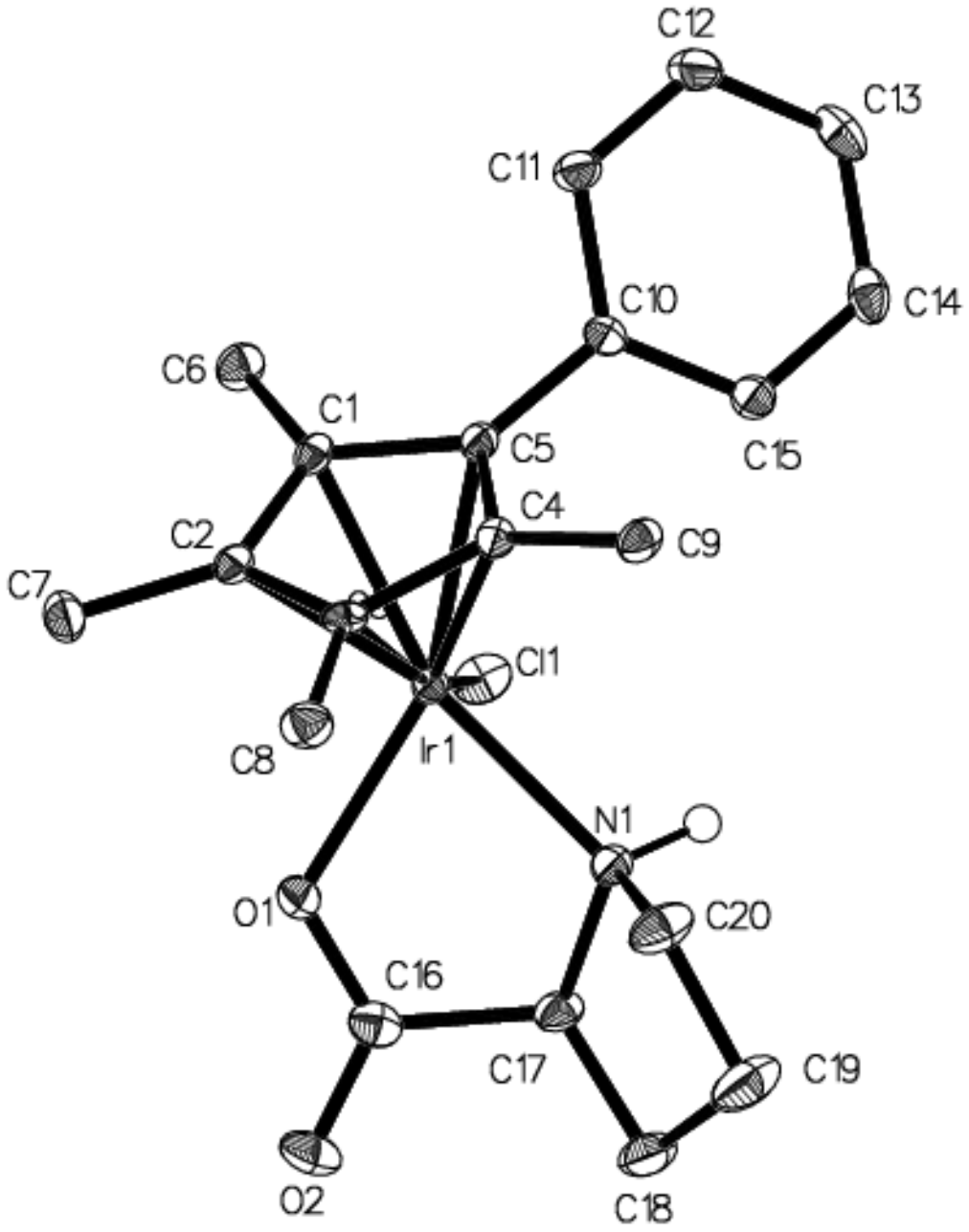

Figure 3.12: Crystal structure of (Cp*^{ph})Ir(L-pro)Cl. All hydrogen atoms except the amine hydrogen are omitted. Ellipsoids shown at 50%. Refer to table 3.5 for bond lengths and angles.

Unlike the crystal structures obtained of (Cp*)Ir(L-pro)-Cl only one diastereomer (the $S_{Ir}S_{C}S_{N}$; major component in solution) is present in the lattice for the related (Cp*^{ph})Ir(L-pro)Cl, (Cp*^{bn})Ir(L-pro)Cl, (Cp*^{iPr})Ir(L-pro)Cl, (Cp*$^{n\text{-}propyl}$)Ir(L-pro)Cl. These structures also lack the water molecule which co-crystallized in the (Cp*)Ir(L-pro)-Cl structure. However, an inter-molecular hydrogen bonding network still persists, formed through the amino proton and the carbonyl oxygen of a symmetry related complex in the lattice. The network is also found in the related complexes of (Cp*^{bn})Ir(L-aze)Cl and (Cp*^{bn})Ir(L-pip)Cl. The hydrogen bond length varies slightly between the 6 complexes, with the L-proline based complexes having the shortest lengths of 2.050 Å, 2.027 Å, 1.935 Å, and 2.028 Å for (Cp*^{ph})Ir(L-pro)Cl, (Cp*^{bn})Ir(L-pro)Cl, (Cp*^{iPr})Ir(L-pro)Cl, and (Cp*$^{n\text{-}propyl}$)Ir(L-pro)Cl respectively. The (Cp*^{bn})Ir(L-aze)Cl and (Cp*^{bn})Ir(L-pip)Cl have longer bonds of 2.166 Å and 2.139 Å respectively. In the case of the L-proline complexes, the lengthening of the hydrogen bond is correlated to the size of the Cp*^{R} group and packing in the lattice.

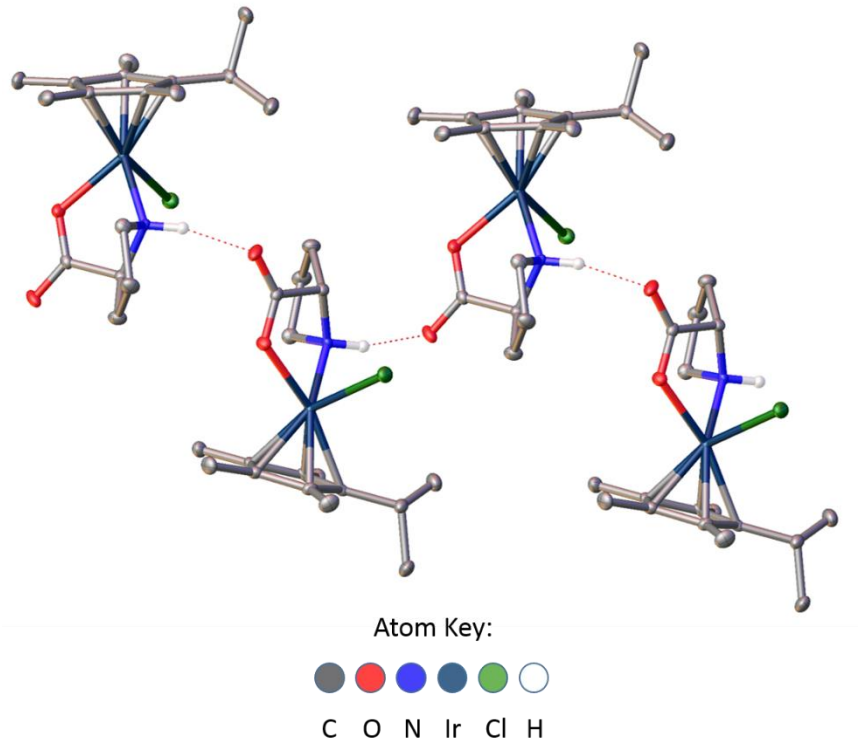

Figure 3.13: Intermolecular hydrogen bonding network formed between (Cp*^{iPr})Ir(L-pro)Cl. The network is formed through the amine proton and carbonyl oxygen of the adjacent molecule.

3.3.2. Solution state behavior:

Similar to the Cp*Ir(aa)Cl complexes, the complexes epimerize in solution, producing the two diastereomers. The rate of epimerization is fast; equilibration occurs nearly instantaneously at room temperature. These ratios remain unchanged over time.

While the Cp*Ir amino acid complexes were highly soluble in water due to chloride dissociation and formation of a mono-aqua cation, the increased hydrophobicity of the R group lessens water solubility. The general trend is Cp*$^{n\text{-propyl}}$ = Cp*^{iPr} > Cp^{*ph} > Cp*^{bn} > Cp^{cy} > Cp*$^{n\text{-octyl}}$ ≈ Cp*$^{n\text{-dodecyl}}$. The long chain aliphatic variants are insoluble in water, but potentially form micelle like mixtures. Chloride disassociation is still occurring however, as these complexes are active for ATH, which requires an open coordination site for hydride formation.

3.4. Summary of Modified Iridium Cp^{*R} Amino Acid Complexes

Modified HCp^{*R} ligands were synthesized by reaction of 2,3,4,5-tetramethylcyclopent-2-en-1-one with its respective Grignard reagent, followed by elimination of water. Several isomers are produced, presenting complex NMR spectra. Reaction of these HCp^{*R} complexes with $IrCl_3 \bullet xH_2O$ produces the respective dimer $[(Cp^{*R})IrCl_2]$ in good yields, 40 to 91%). The complex NMR patterns observed for the HCp^{*R} become simplified due to the ligand becoming its anion Cp^{*R} upon coordination to the metal center. When these dimers are reacted with two equivalents of amino acid, the $Cp^{*R}Ir(aa)Cl$ complexes are produced. Yields were generally good. The complexes displayed similar characteristics to the Cp*Ir(aa)Cl complexes. Overall configurations (S/R) at the Ir, N, and C were the same as the Cp*Ir(aa)Cl complexes. Diastereomeric ratios were also very similar, meaning that the amino acid ligand is primarily responsible for the observed ratios in solution.

4. Synthesis and Characterization of (η^6-arene)Ru(aa)Cl complexes

This chapter details the synthesis and characterization of (arene)Ru(aa)Cl complexes. There is slight variation in diastereomeric ratios when the arene ligand varies from p-MeC_6H_4iPr, mesitylene, and hexamethylbenzene (HMB). Overall configurations were established through NOE techniques and are the same as those found for related Cp*Ir variants. In addition, these (arene)Ru(aa)Cl complexes form stable aqua adducts which are observable by NMR spectroscopy.

4.1. Synthesis of Dimers:

Reactions of the respective cyclohexadiene with $RuCl_3$ hydrate in ethanol yields dimer complexes $[(arene)RuCl_2]_2$ with arene = p-MeC_6H_4iPr or mesitylene (equation 4.1). $[(C_6Me_6)RuCl_2]_2$ is synthesized through reaction of $[(p\text{-}MeC_6H_4iPr)RuCl_2]_2$ with excess HMB in a 180 °C melt in a closed pressure tube to induce a ligand substitution, followed by column chromatography.

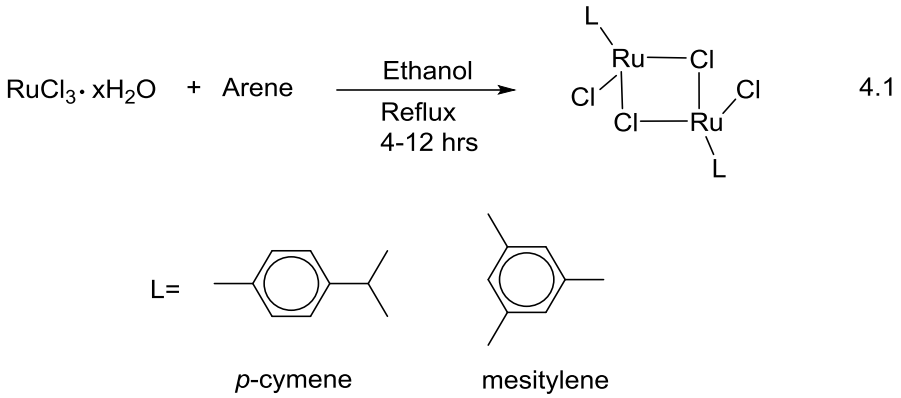

4.1

4.2. (arene)Ru(aa)Cl complexes

(Arene)Ru(aa)Cl complexes were synthesized in a similar manner to the Ir and Rh analogues, with slight variations in reaction time and heating depending upon the amino acid used. Yields and

diastereomeric ratios are summarized in table 4.1. The ratios were determined from the integration of the methyl singlets of the p-MeC_6H_4iPr, C_6Me_6, and $C_6H_3Me_3$ in the ^1H NMR, similar to our analysis of the Cp* based complexes.

Table 4.1: Yields and Diastereomeric Ratios at Ru(S/R) center for (arene)Ru(aa)Cl complexes

p-MeC_6H_4iPr	Yield %	Ratio % S_{Ru}/R_{Ru}
L-Phengly	56	74
L-Phe	91	60
L-Pro	91	89
L-Pip	70	63
C_6Me_6	Yield %	Ratio % S_{Ru}/R_{Ru}
L-Phengly	88	56
L-Phe	86	75
L-Pro	74	93
L-Pip	80	78
$C_6H_3Me_3$	Yield %	Ratio % S_{Ru}/R_{Ru}
L-Pro	82.	92
L-Pip	85	92

As with the iridium based complexes, these form diastereomers with ratios dependent upon the amino acid ligand. There is significant variation between diastereomeric ratios of these Ru based complexes depending upon the arene moiety. While the ring based prolinate complexes retain a high selectivity for all arenes, the L-piperidine-2-carboxylate complexes vary greatly, with the $C_6H_3Me_3$ complex having a selectivity of 92. This ratio lowers for the hexamethylbenzene and p-MeC_6H_4iPr variants, (78 % and 63 % respectively). This high level of preference for one diastereomer over the other is only observed for the ($C_6H_3Me_3$)Ru(L-pip)Cl complex, though the exact reason is not known. The (C_6Me_6)Ru(L-pip)Cl will epimerize at the metal center over time, changing the distribution of diastereomers over the course of 48 h, with the ratios reversing to 78/22 and 25/75. Similarly, the (p-MeC_6H_4iPr)Ru(L-pip)Cl forms exclusively one diastereomer when kept in solution for a prolonged period of time (24h), with only one set of signals observable in the ^1H NMR spectrum.

Comparison to the IrCp*(aa)Cl complexes of the same ligand, shows that the (C_6Me_6)Ru(aa)Cl complexes have similar selectivities with L-phengly, L-phe, L-pro, and L- pip complexes. This is most likely due to the similar steric constraints imparted by the Cp* and hexamethyl moieties. The L-phengly and L-phe complexes switch selectivities between the hexamethyl and p-MeC_6H_4iPr variants. The steric bulk of the 2-propyl group disfavors the formation of the major configuration of the L-phe complex, which is with the benzyl group facing "up" toward the arene portion of the molecule, similar to the Ir variant, (Figure 4.1). This causes the ratio of the (p-MeC_6H_4iPr)Ru(L-phen)Cl to be closer to a 50/50 mixture (60/40), with neither diastereomer favored over the other. By contrast, the Cp*Ir(L-phe)Cl complex forms in a ratio of 70/30, due to the reduced steric strain of the Cp* vs the p-MeC_6H_4iPr of the (p-MeC_6H_4iPr)Ru(L-phen)Cl. This is observable in the NMR spectra with the *i*Pr methyls producing different overlapping doublet patterns due to restricted rotation depending upon the bulk of the amino. This restricted rotation is observed for other p-MeC_6H_4iPr complexes as well, similar to the Cp*^{iPr} complexes presented in the previous chapter.

The configurations at the metal center in solution are measured with NOE NMR experiments. While the ratios between diastereomers vary among the differing arene groups, the major and minor configurations remain the same, and are the same for those established with the Ir complexes. However, in the case of the L- pip complexes, the major and minor configurations appear to be different from those established with Ir complexes depending on the time (10 min in solution vs ≥ 2h) of the NOE experiment, due to the slow epimerization at the metal center. For example, in the case of (p-MeC_6H_4iPr)Ru(L-pip)Cl, the major configuration at the time (2 h in solution) of the NOE experiment is $R_{Ru}S_CR_N$, as irradiation of the amino acid α-proton results in the enhancement of the methyl of the arene ring. This is the opposite of the Ir based complexes, as well as to the related Os complexes reported by Carmona.[64] This interaction is displayed in figure 4.2.

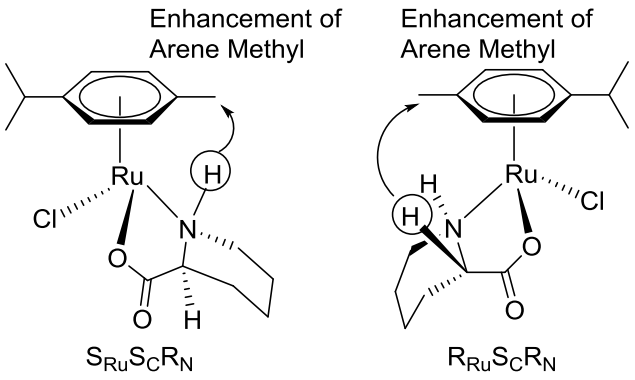

Figure 4.2: NOE irradiation of selected protons (circled) and the enhancement of the arene methyls for the diastereomers of the (p-MeC$_6$H$_4$iPr)Ru(L-pip)Cl. The major component is S at the Ru center.

If the NMR experiment is performed in D_2O, the aqua species becomes visible in the ^1H spectrum. In the case of (p-MeC$_6$H$_4$iPr)Ru(L-phen)Cl four different signals appear, both with diastereomeric ratios similar to what is found in $CDCl_3$. Addition of NaCl to the sample causes these new peaks to diminish in intensity. The loss of the aqua species is also seen in the reduction of the number of septets from the C**H**-CH_3 proton, which returns to just a pair of septets with the addition of NaCl. A comparison of the spectra in $CDCl_3$, D_2O, and D_2O with NaCl is displayed in figure 4.3. The (p-MeC$_6$H$_4$iPr)Ru(L-phengly)Cl and (p-MeC$_6$H$_4$iPr)Ru(L-pro)Cl display identical behavior in D_2O. This is unique to the Ru based complexes, which appear to form a much more stable aqua complex than the related Ir and Rh based complexes. The Ir variants generally display very poor spectra in D_2O, with the Cp* methyls overlapping completely. The IrCp*(L-pro)Cl complex is one exception and displays a clean NMR spectra in D_2O. However, only one set of signals is seen in both ^1H and ^{13}C, with no visible distinction between aqua or chloride complexes.

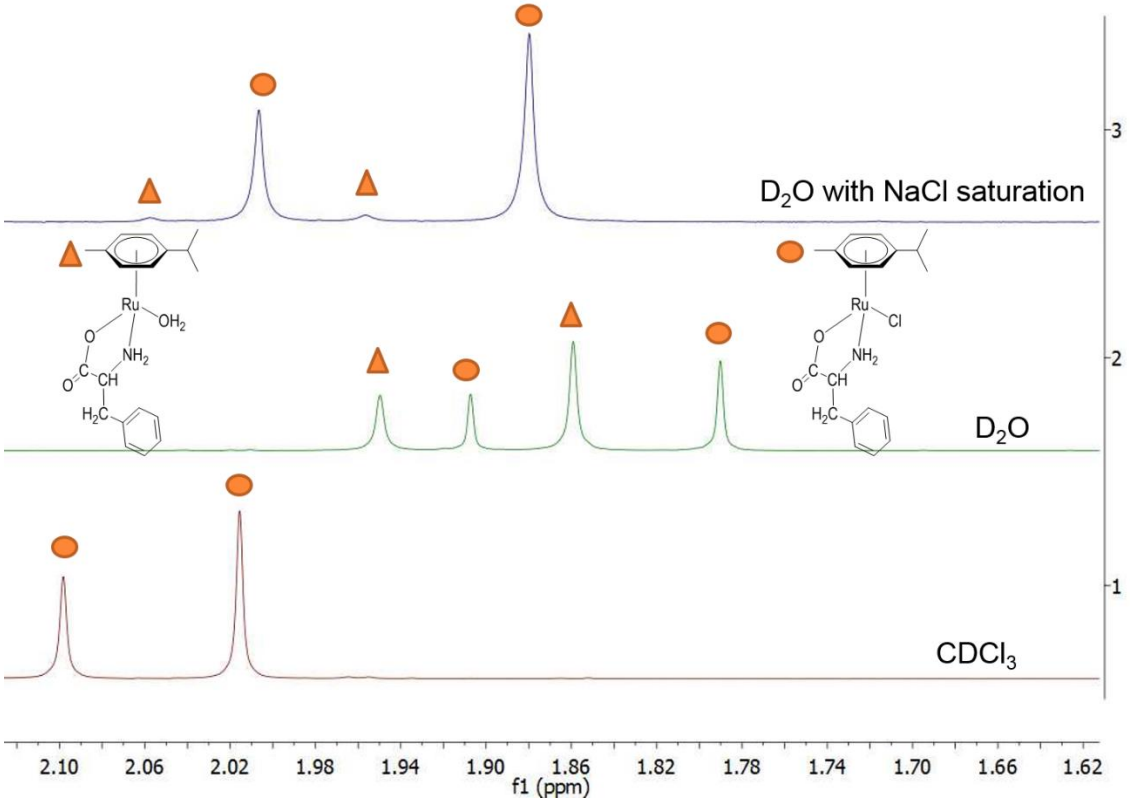

Figure 4.3: ^{1}H NMR spectra of (p-MeC$_6$H$_4$iPr)Ru(L-phen)Cl in CDCl$_3$ (1), D$_2$O (2), and D$_2$O with NaCl (3). The equilibrium between the aqua and chloride species can be shift through addition of NaCl.

4.3. Crystal structure of ($C_6H_3Me_3$)Ru(L-pip)Cl:

Single crystals of the ($C_6H_3Me_3$)Ru(L-pip)Cl were grown by slow diffusion of hexanes into dichloromethane. Comparison of the bond lengths and angles of the Ir and Ru L-pip complexes show very little difference in the two structures, only the M-N bond and the M-centroid bond vary to any significance, meaning the two complexes are nearly iso-structural around the ligand and metal center, table 4.2. A hydrogen bonding network similar to that formed between the amine hydrogen and the carbonyl oxygen in the related Ir structures is present in the ($C_6H_3Me_3$)Ru(L-pip)Cl structure. This network forms a helical lattice down a 2_1 screw axis similar to the other complexes. The structure for ($C_6H_3Me_3$)Ru(L-pip)Cl is displayed in figure 4.4.

Table 4.2: Comparison of Bond Lengths (Å) and Angles (deg) of ($C_6H_3Me_3$)Ru(L-pip)Cl and (Cp*)Ir(L-pip)Cl

Measurement	L-pip Ru Mes	L-pip Ir Cp*
Cl-Ir	2.4231(6)	2.424(1)
N-Ir	2.122(2)	2.132(4)
O-Ir	2.097(1)	2.101(3)
G-Ir	1.668 Å	1.772
Cl-Ir-N	85.60(4)	86.0(1)
Cl-Ir-O	88.85(4)	88.15(8)
N-Ir-O	76.78(6)	77.1(1)
Cl-Ir-G	128.53	125.89
N-Ir-G	132.03	134.8
O-Ir-G	127.91	128.09

G = centroid of Cp* or $C_6H_3Me_3$

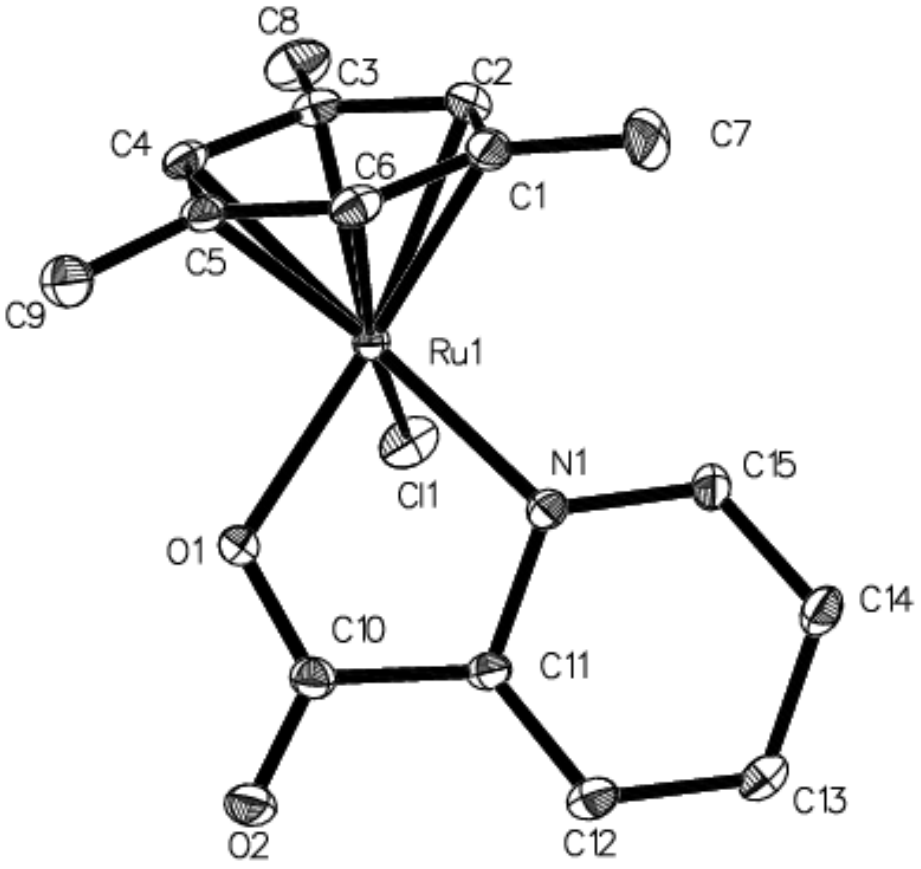

Figure 4.4: ORTEP Plot of ($C_6H_3Me_3$)Ru(L-pip)Cl. Hydrogen atoms omitted for clarity. Ellipsoids shown at 50%. Refer to table 4.2 for a description of bond lengths and angles.

4.4. Summary of (η^6-arene)Ru(aa)Cl complexes

(η^6-arene)Ru(aa)Cl complexes where synthesized by the reaction of two equivalents of amino acid with the respective [((η^6-arene)$RuCl_2$] dimer. Yields ranged from moderate to excellent, with all complexes forming orange solids. Like the Cp*Ir(aa)Cl complexes, the (η^6-arene)Ru(aa)Cl complexes form diastereomers, with the Ru center acting as a stereogenic site. Ratios of these diastereomers were similar to those found for the Cp*Ir(aa)Cl complexes. Cyclic amino acids, such as L-pro, were more selective for one diastereomers than non-cyclic amino acids. Overall configurations of the Ru center and N were the same as what was observed for the Cp*Ir(aa)Cl complexes, with all major configurations being S at the metal center when L-amino acids are used. Unlike the Cp*Ir(L-pip)Cl variant, the (η^6-arene)Ru(L-pip)Cl complexes are unstable in solution, with the ratios changing over time (2 h) from what is observed when the complexes are initially dissolved in solution. The (η^6-arene)Ru(aa)Cl form stable mono-aqua cations, which can be observed in the ^{1}H NMR spectra. The exchange of Cl with D_2O is in equilibrium, and addition of NaCl causes the D_2O species to diminish.

5. Cp* Rhodium Amino Acid Complexes

This chapter describes the synthesis and characterization of Cp*Rh(aa)Cl complexes. Overall, the complexes display nearly identical characteristics to the Cp*Ir(aa)Cl complexes. The Cp*Rh(aa)Cl were synthesized in good yields and characterized by NMR spectroscopy, HRMS, single X-ray diffraction and elemental analysis.

5.1. Synthesis and characterization of Cp*Rh(aa)Cl complexes

(Cp*)Rh(aa)Cl complexes were synthesized by reaction of $[(Cp^*)RhCl_2]_2$ complex with 2 equivalents of amino acid in the presence of base ($NaHCO_3$, KOH), similar to the previous syntheses for (Cp*)Ir(aa)Cl complexes. A summary of the ratios and yields are shown in table 5.1. The ratios formed by the Rh variants are close to those of the Ir complexes, though the L-pip complex has a ratio smaller by about 10 percent than its Ir counterpart. The major and minor configurations are identical to their Ir and Ru counterparts, as seen from NOE experiments.

Table 5.1: Isolated Yields and Diastereomeric Ratios at Rh center (S/R) of (Cp*)Rh(aa)Cl complexes

Amino Acid	Yield %	Ratio % S_{Rh}/R_{Rh}
L-Phengly	86	65
L-Phe	67	72
L-Pro	90	91
L-Pip	88	64

5.2. Crystal Structure of (Cp*)Rh(L-phe)Cl

Single crystals of the (Cp*)Rh(L-phe)Cl complex were grown by slow diffusion of hexanes into dichloromethane. Like the Ir complex, the major isomer places the R group of the amino acid up towards the Cp* ring, with the minor isomer arranging the R group down and away from the Cp* portion (see figure 2.12). There is small but significant variation between the two structures. The most pronounced is the shortened Rh-N bond in the minor isomer and the smaller angle between the

Cl-Rh-N. The Rh structure matches well with the Ir, with the diastereomers being nearly iso-structural. Bond lengths and angles are summarized in table 5.2. The structure for (Cp*)Rh(L-phe)Cl is shown in figure 5.1.

Table 5.2: Bond Lengths (Å) and Angles (deg) of (Cp*)Rh(L-phe)Cl

Measurement	Rh L-phe Major	Rh L-phe Minor
Cl-Rh	2.4232(8)	2.4093(8)
N-Rh	2.135(2)	2.092(2)
O-Rh	2.102(2)	2.116(2)
G-Rh	1.759	1.755
Cl-Rh-N	87.49(7)	84.03(7)
Cl-Rh-O	88.44(6)	89.24(6)
N-Rh-O	79.15(8)	77.96(9)
Cl-Rh-G	128.38	126.05
N-Rh-G	130.76	132.45
O-Rh-G	126.66	130.33

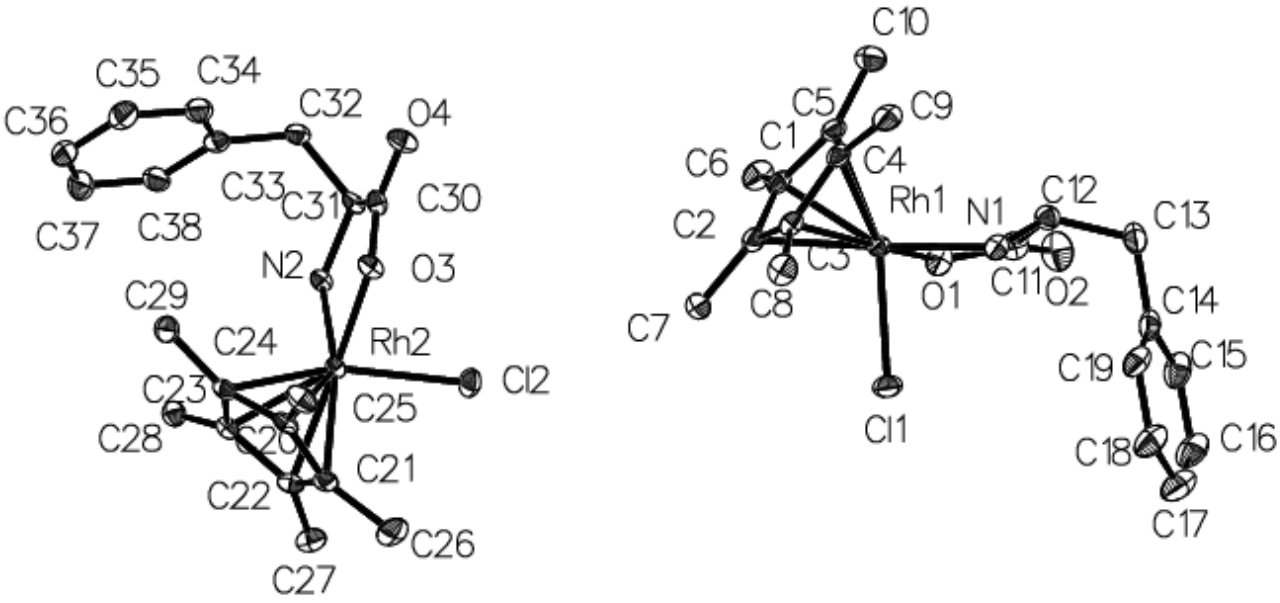

Figure 5.1: ORTEP Plot of (Cp*)Rh(L-phe)Cl. Hydrogen atoms omitted for clarity. Ellipsoids shown at 50%. Refer to table 5.1 for a description of bond lengths and angles.

5.3. Summary of Cp* Rhodium Amino Acid Complexes

Complexes of the form Cp*Rh(aa)Cl were synthesized by the reaction of the [(Cp*)$RhCl_2$] dimer with two equivalents of amino acid and in good yields (65 – 91%). The ratios of diastereomers is nearly identical to the Cp*Ir(aa)Cl complexes, which is unsurprising due to Rh and Ir being in the same group. Overall configuration (S/R) at the Rh center, C, and N were the same as those observed for the Ir and Ru variants, as established through 1D NOE experiments and X-ray diffraction.

6. Asymmetric Transfer Hydrogenation of Ketones

For the asymmetric transfer hydrogenation of ketones to take place, the catalysts used require several features. One, a chiral ligand must be employed. Two, this ligand must possess an amine functionality. Three, the formation of a metal-hydride must take place. Amino acid ligands satisfy requirements 1 and 2, all the while being low cost off the shelf ligands. When dissolved in water the complexes form mono-aqua cations through displacement of the chloride ligand by water. Addition of sodium formate leads to the formation of the active metal-hydride species through binding of formate followed by beta-hydride elimination of CO_2 (scheme 6.1).

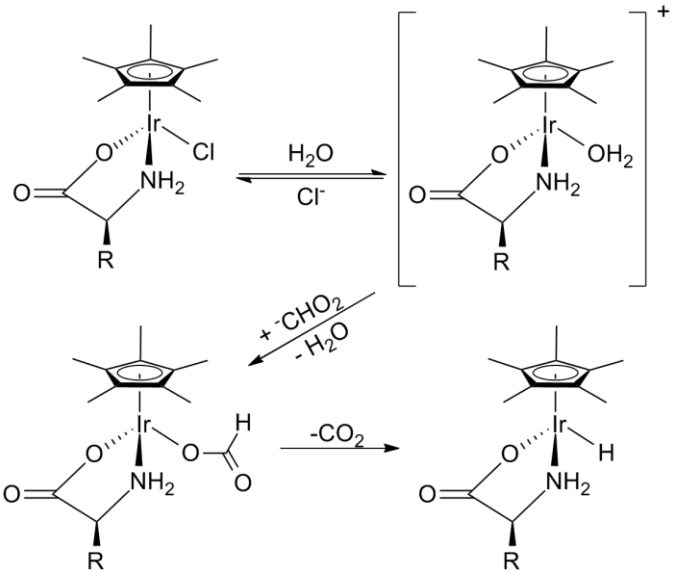

Scheme 6.1: Chloride dissociation and formation of Ir hydride via beta hydride elimination from formate. Hydride peaks appear at --7.84 and -8.53 ppm over the course of 20 min in the ^{1}H NMR spectra.

Upon the addition of 5 equivalents of sodium formate to any amino acid complex, the pale yellow solution will become a dark red color with evolution of CO_2. The hydride peaks appear over the course of 20 minutes in D_2O, as observed with ^{1}H NMR. In the case of the (Cp*)Ir(L-pro)Cl the signals appears at -7.84 and -8.53 ppm, (figure 6.1).

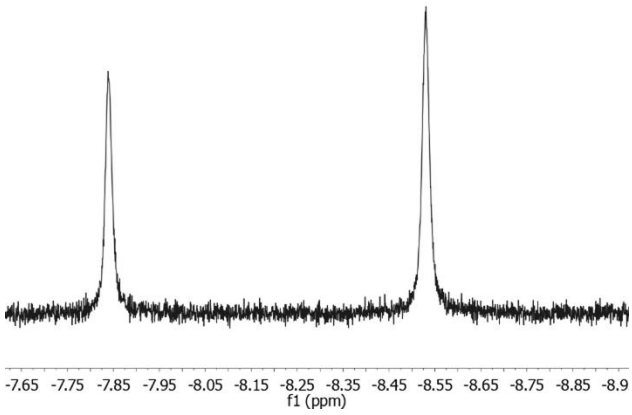

Figure 6.1: ^{1}H NMR spectrum of the hydride region of (Cp*)Ir(L-pro)H. The ratios of the hydride species differ from the parent chloride complex.

Their respective Cp* peaks appear at δ 1.66 and 1.68 ppm. Interestingly, the diastereomeric ratios of the hydride complexes do not match those of the chloride complexes, and are closer to a racemic mixture (53/47). The corresponding Cp* peaks have a similar ratio (57/43). This trend occurs with **(**Cp*)Ir(4-trans-fluoro-L-proline)Cl and (Cp*)Ir(L-aze)Cl as well, with hydride ratios of 63/47 and 54/46 respectively. Deuterium exchange causes the hydride peaks to diminish in intensity over time and it is possible that this exchange is more rapid for one diastereomer than another, resulting in the different ratios between chloride and hydride complexes. In addition, the difference in ratios could be do to the hydride being only a sigma donor, while chloride can act as a pi donor. This electronic change could affect the diastereomeric ratio.

6.1. Initial Catalytic Studies:

Catalytic activity for ATH was initially monitored by ^{1}H NMR spectroscopy. (Cp*)M(L-phe)Cl, (M = Ir, Rh), acetophenone and sodium formate, were combined in an NMR tube with D_2O as the solvent. In this initial reaction the substrate/catalyst/formate, (S/C/F), ratios were 80/1/500. The reaction was monitored over the course of several h by integration and comparison of the methyl singlet of acetophenone at δ 2.47 ppm and the appearance of the doublet of 1-phenylethanol at δ 1.27

ppm (figure 6.2). The Ir based reaction reaches 50 percent conversion at 190 minutes. At 360 minutes, the Rh based reaction has reached less than 5 percent conversion under the same conditions.

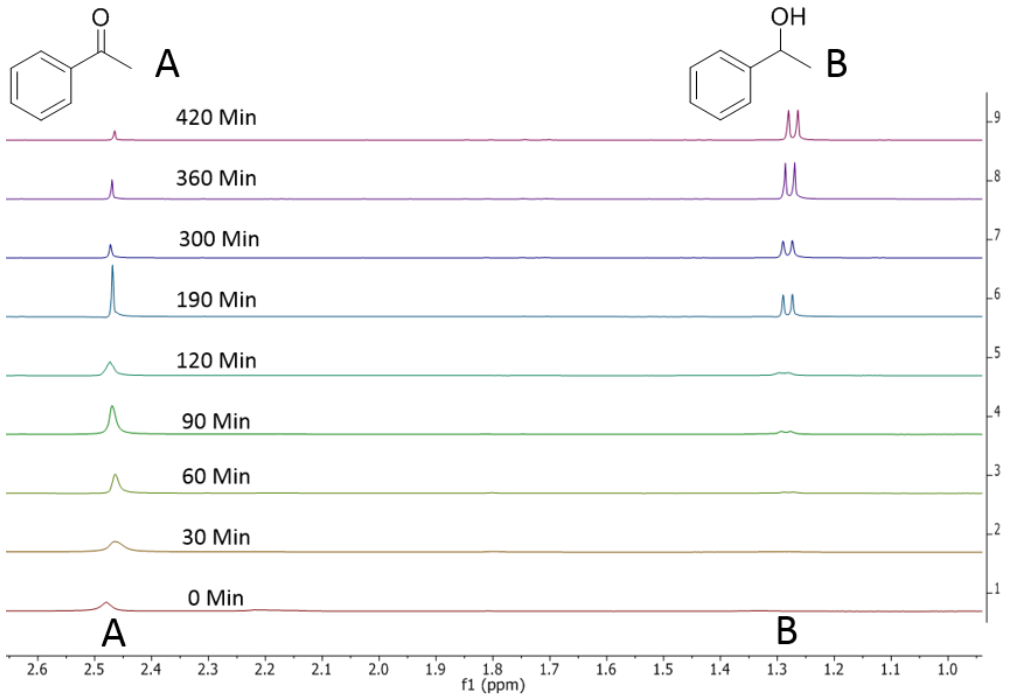

Figure 6.2: Monitoring of the reduction of acetophenone by ^{1}H NMR spectroscopy. The reaction was performed with a S/C/F of 80/1/500 at room temperature. Conversions were monitored by the appearance of the doublet at δ 1.27 ppm

Upon seeing this positive result, several (Cp*)Ir(aa)Cl complexes were tested for ATH. The reactions were carried out at room temperature with S/C/F ratios of 100/1/500 in 2 mL of water and open to air (scheme 6.2).

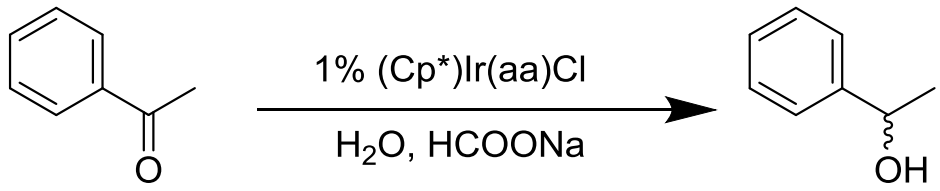

Scheme 6.2: The reduction of acetophenone by (Cp*)Ir(aa)Cl complexes in water using sodium formate (HCOONa) as the hydrogen donor. S/C/F are 100/1/500 unless otherwise stated.

Analysis of the products via chiral GC/MS initially revealed disappointing results. The vast majority of amino acids produced racemic or near racemic mixtures of 1-phenylethan-1-ol. The alkylated D-proline catalyst, despite having no donor proton, did convert the ketone to the alcohol product, which conflicted with the accepted concerted mechanism presented by Noyori where the amine proton is donated to the carbonyl oxygen. This unexpected result is explored further in 6.6.1. The ring based systems of L-pro and L-pip had limited selectivity of 20% ee and 26% ee respectively. The N-methyl-D-pro produced a racemic mixture of products, implying that the amine proton, while not necessary for conversion, is required to impart selectivity, most likely through hydrogen bonding to the carbonyl oxygen. Of the non-ring based systems, only L-phengly and L-phe had any selectivity, though very low. The study did show that L/D amino acids produced the opposite configuration of the alcohol product, at approximately the same selectivity. More interestingly, the configuration of the product (R/S at chiral carbon) using L-pip was the opposite of the L-pro based reaction despite both amino acid ligands having S chirality at the alpha carbon. The exact cause was not known at the time and is described in section 6.5. Initial catalytic results are displayed in table 6.1.

Table 6.1: Initial catalytic results of the reduction of acetophenone to 1-phenylethanol

Entry	Complex	t(h)	Conv[b] (%)	ee[c] (%)	Conf.[d]
1[a]	(Cp*)Ir(L-pip)Cl	36	99	26	S
2[a]	(Cp*)Ir(L-pro)Cl	36	88	20	R
3[a]	(Cp*)Ir(4-trans-F-L-pro)Cl	36	48	20	R
4[a]	(Cp*)Ir(L-phe)Cl	36	91	5	S
5[a]	(Cp*)Ir(D-pro)Cl	36	52	20	S
6[a]	(Cp*)Ir(N-methyl-gly)Cl	36	84	0	race
7[a]	(Cp*)Ir(N-methyl-D-Pro)Cl	36	10	0	race
8[a]	(Cp*)Ir(L-phengly)Cl	36	24	7	R

[a] Reaction conditions: substrate/catalyst/formate (S/C/F) 100/1/500, in 2 mL of water. [b] Determined by gas chromatography. [c] Determined by gas chromatography using a CP- ChiralSil – Dex CB 25 x 0.25 column. [d] Determined by optical rotation and comparison to literature values

These same conditions were used in the reduction of pinacolone, an aliphatic substrate. The initial results of this reaction were more positive, producing selectivities as high as 77% when L or D proline were used. The proline variant trans-4-fluoro-L-proline produced a slightly higher selectivity, (82%), though at reduced activity. The hydroxyl group in 4-trans-hydroxy-L-proline ligand had no impact on selectivity, but did reduce activity in a manner similar to the fluorinated version. The smaller ring system of L-aze had an impressive selectivity of 92%. Again, the majority of non-ring based amino acids were not significantly selective. The configurations of the products are the opposite of those observed for the reduction of acetophenone. The fully methylated variants of (Cp*)Ir(N-methyl-D-pro)Cl and (Cp*)Ir(N,N-dimethyl-gly)Cl produce no detectable product; however this result is most likely due to the severely reduced rate of reaction observed for pinacolone. The results of the study are summarized in table 6.2.

Table 6.2: Reduction of pinacolone using (Cp*)Ir(aa)Cl in water.

Entry	Complex	T (h)	Conv[b]%	ee[c] %	Conf.[d]
1 [a]	**(Cp*)Ir(L-pip)Cl**	**48**	**91**	**45**	**R**
2 [a]	**(Cp*)Ir(L-pro)Cl**	**48**	**43**	**77**	**S**
3 [a]	**(Cp*)Ir(4-trans-F-L-pro)Cl**	**48**	**40**	**82**	**S**
4 [a]	**(Cp*)Ir(4-trans-OH-L-pro)Cl**	**48**	**26**	**77**	**S**
5 [a]	**(Cp*)Ir(L-aze)Cl**	**48**	**30**	**92**	**S**
6 [a]	**(Cp*)Ir(L-phe)Cl**	**48**	**10**	**12**	**R**
7 [a]	**(Cp*)Ir(N-methyl-L-phenyl-gly)Cl**	**48**	**4**	**29**	**S**
8 [a]	**(Cp*)Ir(D-pro)Cl**	**24**	**33**	**77**	**R**
9 [a]	**(Cp*)Ir(N-methyl-D-pro)Cl**	**24**	**0**	**na**	**na**
10 [a]	**(Cp*)Ir(N,N-dimethyl-gly)Cl**	**24**	**0**	**na**	**na**

[a] Reaction conditions: substrate/catalyst/formate (S/C/F) 100/1/500, in 2 mL of water. [b] Determined by gas chromatography. [c] Determined by gas chromatography using a CP- ChiralSil – Dex CB 25 x 0.25 column. [d] Determined by optical rotation and comparison to literature values

The substrate 2,2-dimethyl-1-phenylpropan-1-one, which features the functionalities of acetophenone and pinacolone, was reduced using the same conditions as above. Unlike acetophenone, selectivities were quite good. Only ligands that showed selectivity for acetophenone and pinacolone were used in this reduction. The (Cp*)Ir(L-pip)Cl was the most selective and most active, with a conversion of 90% and enantiomeric excess of 81%. More constrained ring systems lowered the ee, with L-pro and L-aze systems producing nearly identical ee of 60%. The configuration of the products is the same as 1-phenylethan-1-ol as determined through comparison to GC retention times with pure R or S products, indicating that the transition state is one with the aromatic ring system "up" next to the Cp* moiety. These results are summarized in table 6.3.

Table 6.3: Reduction of 2,2-dimethyl-1-phenylpropan-1-one by (Cp*)Ir(aa)Cl in water

Entry	Complex	T (h)	Conv[b]%	Ee[c] %	Conf.[d]
1 [a]	**(Cp*)Ir(L-pip)Cl**	**52**	**90**	**81**	**S**
2 [a]	**(Cp*)Ir(L-pro)Cl**	**56**	**30**	**60**	**R**
3 [a]	**(Cp*)Ir(L-aze)Cl**	**56**	**30**	**61**	**R**
4 [a]	**(Cp*)Ir(N-methyl-L-phenyl-gly)Cl**	**48**	**3**	**52**	**S**

[a] Reaction conditions: substrate/catalyst/formate (S/C/F) 100/1/500, in 2 mL of water. [b] Determined by gas chromatography. [c] Determined by gas chromatography using a CP- ChiralSil – Dex CB 25 x 0.25 column. [d] Comparison to literature retention times

6.2. Role of the mono-alkylated amine in selectivity:

Analysis of the crystal structures reveals why the ring-containing and mono-alkylated amino acids display greater selectivity. The formation of diastereomers is problematic for the asymmetric reduction of pro-chiral substrates. The transition state formed with one diastereomer will be the opposite of the other, leading to reduced selectivity ((Cp*)Ir(L-val)Cl in figure 6.3). The DPEN ligands employed by others form one diastereomer nearly exclusively to eliminate this problem. The ring-based systems effectively prevent this by rendering one diastereomer inactive ((Cp*)Ir(L-pro)Cl in figure 6.3). A comparison of the torsional angle between the H-N-Ir-Cl bond as well as the

distance between the amine proton and chloride displays this, since these angles and distances would be similar to what is found in the active hydride complex (table 6.4). The high torsional angle and large distance between the active amine proton and chloride show that the R configuration of (Cp*)Ir(L-pro)Cl would not be active in ATH, unlike the (Cp*)Ir(D-phe)Cl complex, whose distances and angles are similar.

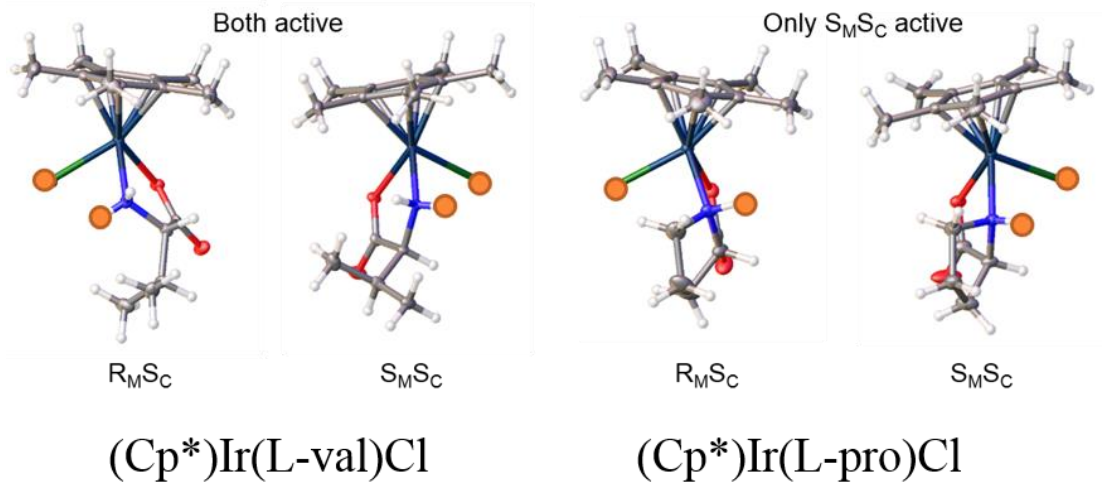

Figure 6.3: Comparison of the structures of (Cp*)Ir(L-val)Cl and (Cp*)Ir(L-pro)Cl showing the active and inactive diastereomers. Complexes with the chloride and hydride (highlighted in orange) on the same face of the catalyst are active for ATH. Both R_MS_C and S_MS_C are active for (Cp*)Ir(L-val)Cl, while only S_MS_C is active for (Cp*)Ir(L-pro)Cl.

Table 6.4: H-N-Ir-Cl Torsional angles and Hydrogen – Chloride distances of selected complexes

Complex	Configuration at metal and C	H-N-Ir-Cl Torsional Angle (°)	H-Cl Distance (Å)
(Cp*)Ir(L-val)Cl	**$R_{Ir}S_C$**	**-11.50**	**2.654**
	$S_{Ir}S_C$	**49.70**	**2.913**
(Cp*)Ir(L-pro)Cl	**$S_{Ir}S_C$**	**55.13**	**3.029**
	$R_{Ir}S_C$	**170.46**	**4.027**
(Cp*)Ir(L-aze)Cl	**$S_{Ir}S_C$**	**58.59**	**2.989**
(Cp*)Ir(4-trans-F-L-pro)Cl	**$S_{Ir}S_C$**	**49.39**	**2.936**

6.3. Optimization of catalytic conditions:

6.3.1. Solvent:

Certain subsets of ketones could only be reduced selectively in specific solvents. Acetophenone and para-substituted derivatives had a severe drop off in selectivity if the reduction was performed in water with formate as hydrogen donor. However, the rate of reduction is higher in water. 2-Propanol with base, (NaOH, $NaHCO_3$, $NaHCO_2$), was found to increase selectivity in all cases. Different sources of base had little impact on selectivity, but did drastically affect the rate of reduction, with NaOH effecting the greatest rate of reduction. Using (p-MeC_6H_4iPr)Ru(L-pip)Cl, reduction of acetophenone was carried out using 2 equivalents of NaOH, $NaHCO_3$ or $NaHCO_2$ in 2-propanol. The reaction using NaOH reached 92 % conversion at 3 h, with the $NaHCO_3$ and $NaHCO_2$ reaching similar conversions at 26 h and 56 h respectively. The differences in rate can be attributed to the slower rate of hydride formation. Weaker bases such as $NaHCO_3$ have more difficulty in facilitating the oxidation of 2-propanol to acetone by the metal center through a β-hydride elimination. This slows initial formation of the active hydride species. The loadings for 2-propanol based reactions were substrate/catalyst/base (S/C/B) 100/1/2 in subsequent reactions.

Any amount of NaOH above 2 equivalents decreases the rate of reduction, with 3 and 4 equivalents reaching 33 and 25 % conversion while a reaction using 2 molar equivalents reaches 91 % conversion on the same time scale (16 h), using (Cp*)Rh(L-pip)Cl. These results indicate that hydroxide may act as a poison to the catalyst. The metal hydroxide species have been shown to slow and poision ATH catalysts in aqueous conditions (Scheme 1.9).

Aliphatic substrates such as pinacolone had both rate of reduction and selectivity eroded if the reduction was performed in 2-propanol with NaOH. Reduction of pinacolone via the (Cp*)Ir(L-aze)Cl complex in 2-propanol results in only 25 % conversion and a near racemic mixture at 50 h.

The L-pip and L-pro also show reduced selectivity under these same conditions. The degradation of selectivity for aliphatic substrates in 2-propanol is not fully understood.

Similarly, the substrate 2,2-dimethyl-1-phenylpropan-1-one is reduced most selectively in aqueous media with formate acting as the hydrogen source (scheme 6.3). Interestingly, the observed decrease in selectivity when the reaction was performed in 2-propanol was not as substantial when compared to pinacolone, with the selectivity dropping to 52% ee. If the substrate is changed to 2-methyl-1-phenylpropan-1-one, the ee will drop to 55% using aqueous conditions. Propiophenone produces an ee of 5% in aqueous conditions, even lower than that of acetophenone. If these optimized conditions for acetophenone are used the ee increases to 50%. If the reduction of 2,2-dimethyl-1-phenylpropan-1-one is performed in THF using 5 equivalents of formic acid/triethylamine (FA/TEA) mixture as the hydrogen source and Cp*Ir(L-pip)Cl as the catalyst, the selectivity is 54%, nearly the same as when using 2-propanol as solvent and hydrogen source. Conversion in this reaction reached only 30 percent on the same time scale (36 h) as the reaction in 2-propanol. The FA/TEA mixture acts as similar hydrogen donor to formate, meaning that the changes in selectivity are most likely due to a change in solvent, not hydrogen source.

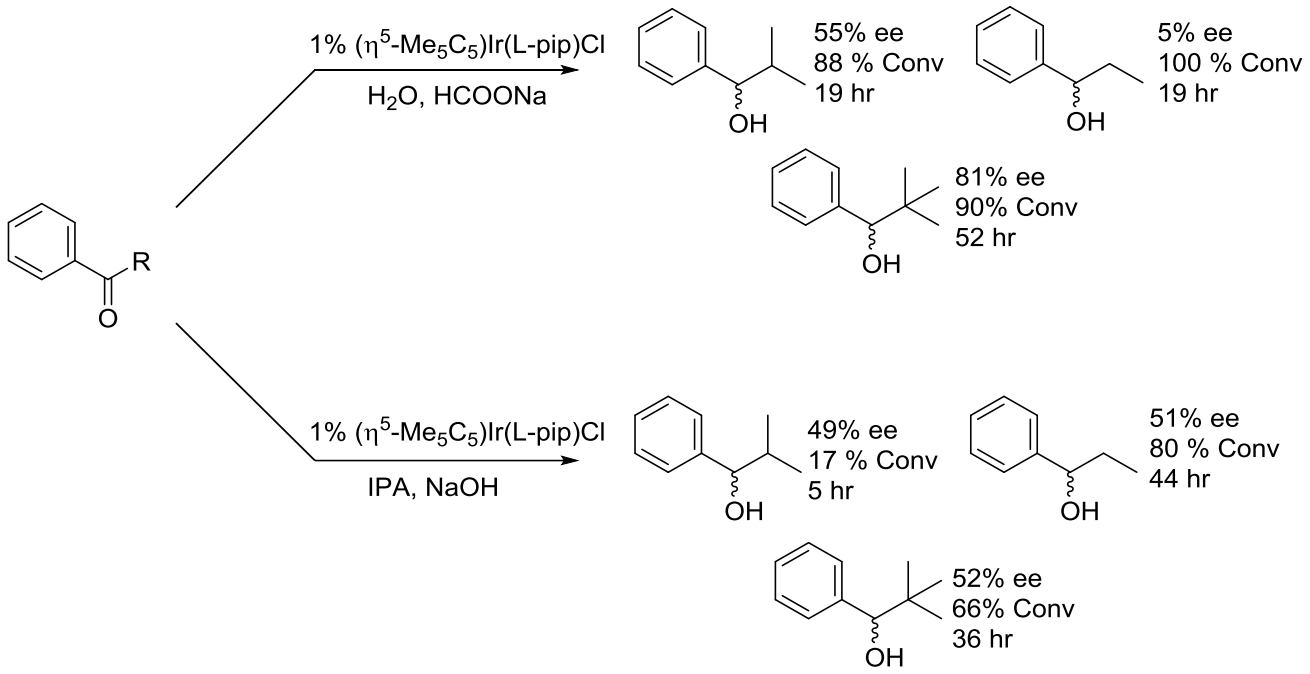

Scheme 6.3: Summary of solvent effects upon decreasing steric constraints of R groups for aromatic substrates. Highly hindered ketones are best reduced, in both selectivity and conversions in water. The smaller substrate of propiophenone is best reduced using a 2-propanol solvent system.

A direct comparison of the reduction of pinacolone with (Cp*)Ir(L-pip)Cl in water vs. 2-propanol reveals drastic differences (figure 6.4). Both reactions were performed in 2mL of solvent (H_2O or 2-propanol) at 40°C with a S/C/F or S/C/B loading of 100/1/500 or 100/1/2. Initial turnover frequencies (TOF) for the aqueous reaction were 19.8, 15.8, and 13.9 mols product/(mols catalyst*h), with the reaction in 2-propanol having TOFs of 3.8, 2.7, and 3.1 mols product/(mols catalyst*h). This rate enhancement has been shown for acetophenone as well by Xiao et al.[28] Several publications have reported theoretical models suggesting that water is lowering the energy of the transition state by forming a hydrogen-bonding network to the substrate during the rate-determining step of hydride transfer.[30] The only exception to this rate enhancement are reactions using the Ru based catalysts. The (p-MeC_6H_4iPr)Ru(L-pip)Cl catalyst shows decreased activity in water. As shown in chapter 3,

Ru based complexes seem to form more stable aqua intermediates, which potentially leads to a decreased rate of reaction in aqueous media.

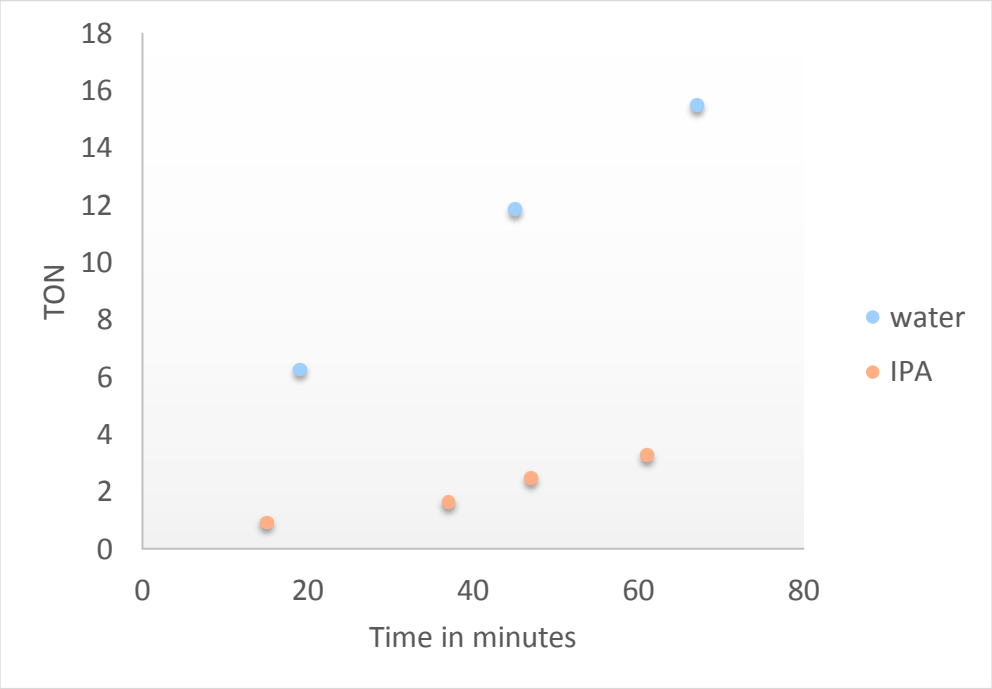

Figure 6.4: Rate comparison of the reduction of acetophenone by (Cp*)Ir(L-pip)Cl in water and 2-propanol. reactions were performed in 2mL of solvent (H_2O or 2-propanol) at 40°C with a S/C/F or S/C/B loading of 100/1/500 or 100/1/2. A significant rate enhancement is observed for the aqueous based reaction, with an intial TOF of 19.8 vs the 3.8 mols product/(mols catalyst*h) in the 2-propanol based reaction.

A further study was done by spiking the reduction of pinacolone by (Cp*)Ir(L-pro)Cl in water with DMF to see if lowering the overall concentration of water would affect the rate of reduction (Figure 6.5). A severe impact on rate was observed when the concentration of water was lowered to 95%. This effect continues until 90% water, where it begins to level out, with 80% water having a similar rate of reduction. Xiao has also observed such effects when using the Ru based Ts-DPEN ligand system for the reduction of acetophenone.[28] However, it is possible that the DMF is poisoning the catalyst.

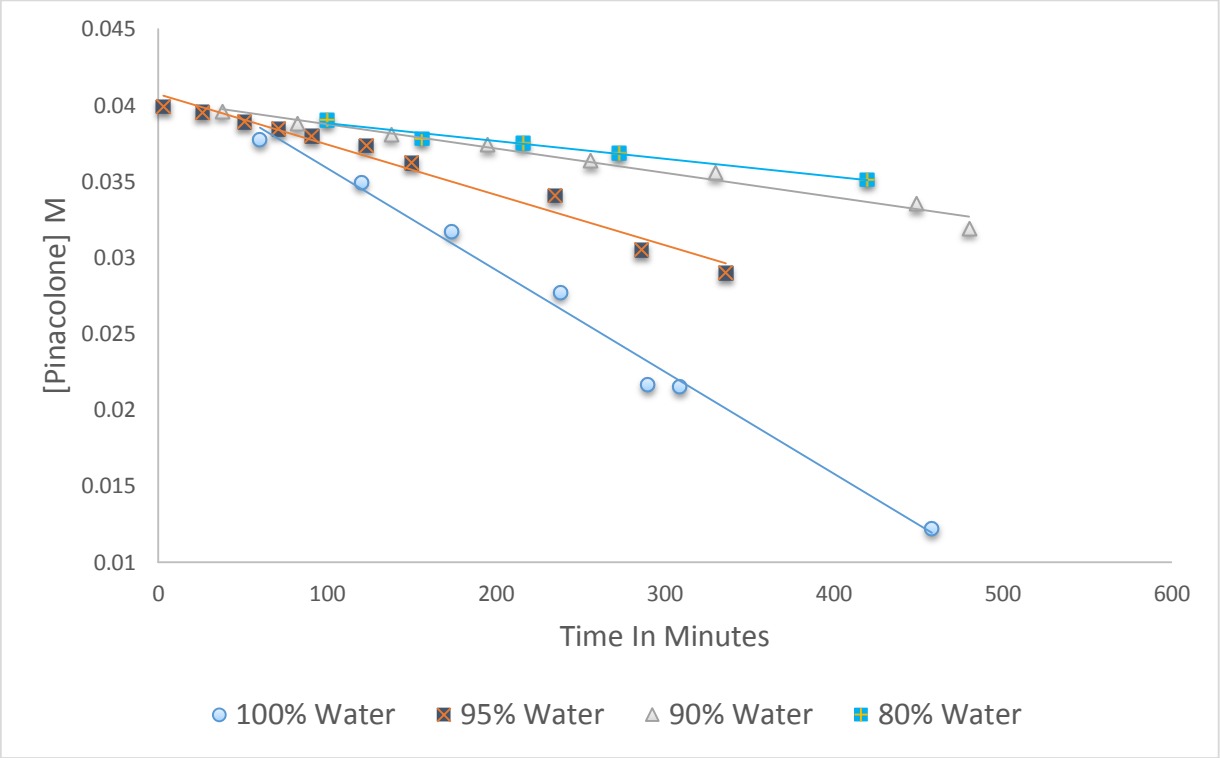

Figure 6.5: Rate of reaction with differing concentrations of water. Decreasing water concentration severely erodes rate of reaction. Decreases in rate begin to level at concentrations below 80%.

6.3.2. pH effects

In the case of the water as solvent, pH affects the rate of reduction. Using differing ratios of formic acid and triethyl amine and monitored using a pH probe, the initial pH was adjusted from 3.44 to 5.3 for the reduction of pinacolone using (Cp*)Ir(L-aze)Cl as the catalyst (figure 6.6). The greatest rate is found to be in the range of 5.3 pH. Increasing the pH past 5.30 results in a decrease in reactivity. Figure 6.7 displays the initial turnover frequency plotted against initial pH. The loss of reactivity at lowered pH can be attributed to the lowered rate of hydride formation due to the formic acid existing predominately in its protonated form (pKa 3.75). Higher pH leads to an overabundance of hydroxide ions in solution, potentially poisoning the catalysts, similar to what is observed in reactions in 2-propanol with higher concentrations of NaOH. Unlike what has been observed for the

related Ts-DPEN ligands, there is no loss of selectivity at lowered pH. It was found that the tosylated amine group becomes protonated under acidic conditions, leading to reduced steric hindrance in the catalyst. The amino acid ligands do not undergo such a change, accounting for the retained selectivity (scheme 1.9).

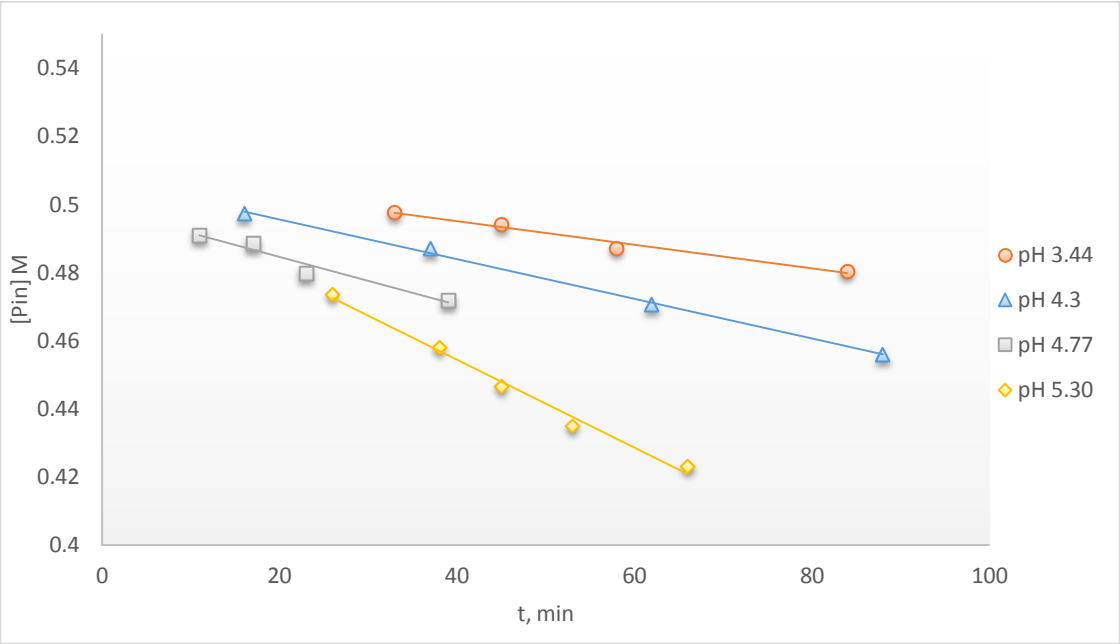

Figure 6.6: Rate of conversion of pinacolone using (Cp*)Ir(L-aze)Cl as catalyst. Initial pH was adjusted through differing ratios of formic acid and triethylamine. 0.1 mL portions were removed over time followed by a micro workup. Rates were determined by GC.

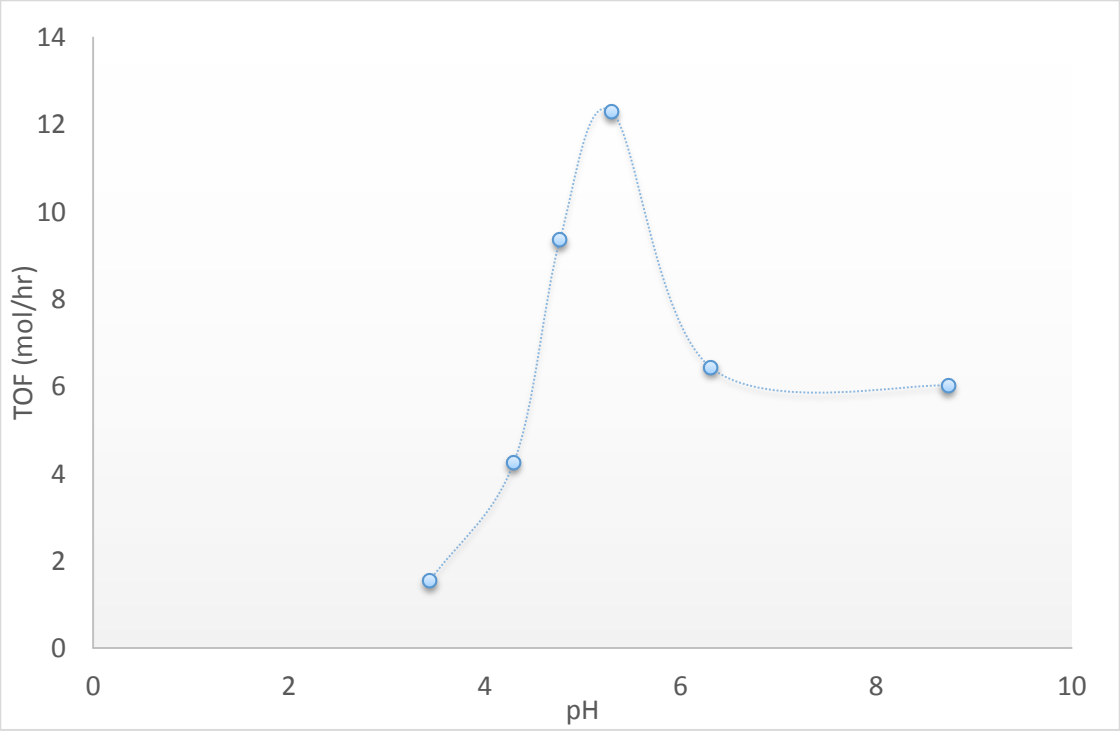

Figure 6.7: Initial TOF vs pH. Optimum TOF is observed at the slightly acidic pH of 5.3. pH lower than 5.3 prevents formation of the active hydride species, limiting rate of reduction. pH above 5.3 results in catalyst poisoning through coordination of hydroxide.

6.3.3. Temperature:

A plot of ee% against temperature (figure 6.7) for the reduction of acetophenone using (Me_6C_6)Ru(L-pip)Cl in 2-propanol displays a loss of 10% ee from 25 °C (89 ee%) to 80 °C (79 ee%). Conversions over this range of temperatures were all over 90%, with the reaction reaching completion at 2 h 15 minutes at 40 °C and less than 30 minutes at 80 °C. The linearity of figure 6.7 indicates that the reaction proceeds with ideal-temperature effects over the temperature ranges tested.

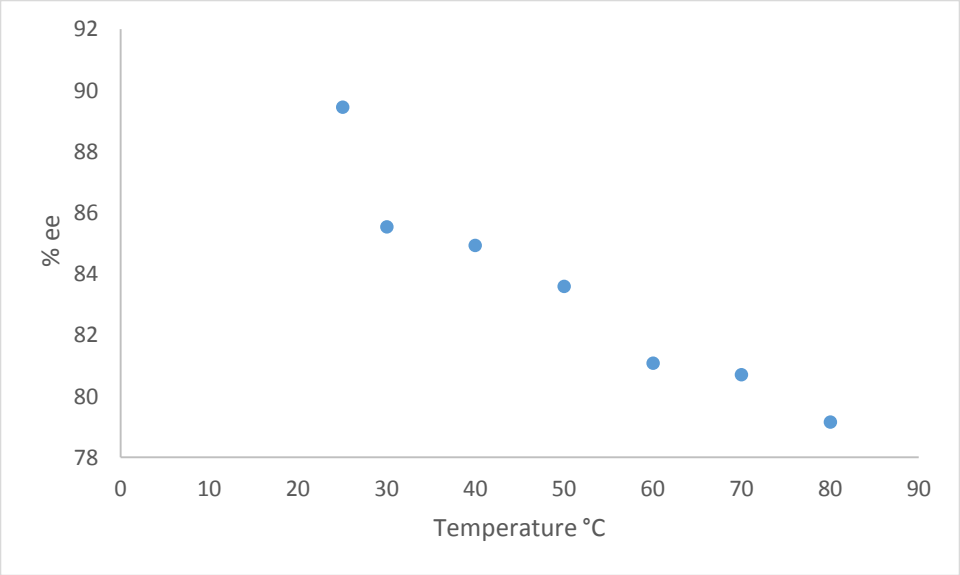

Figure 6.8: Temperature vs ee% of the reduction of acetophenone using optimized conditions. The reaction displays near ideal temperature effects, as seen from the linearity of the plot. Because conversions were all above 90% at any given temperature, the reaction is best performed below 40 °C for the greatest selectivity.

The reduction of pinacolone proceeds with ideal temperature effects as well. The loss of selectivity is not as pronounced as with acetophenone, decreasing from 93% to 87% over the same temperature range. However, conversions begin to erode at temperatures above 40 °C (figure 6.10). The increased volatility of pinacolone (boiling point 103 °C) in comparison to acetophenone (boiling point 202 °C) is most likely the cause, with the substrate existing in the vapor phase above the reaction media. This decreased conversion at higher temperatures is even more substantial for substrates such as butan-2-one, which has an even lower boiling point (80 °C). Due to this loss of conversion and reduction in selectivity, the reduction of aliphatic ketones was performed at 40 °C or below.

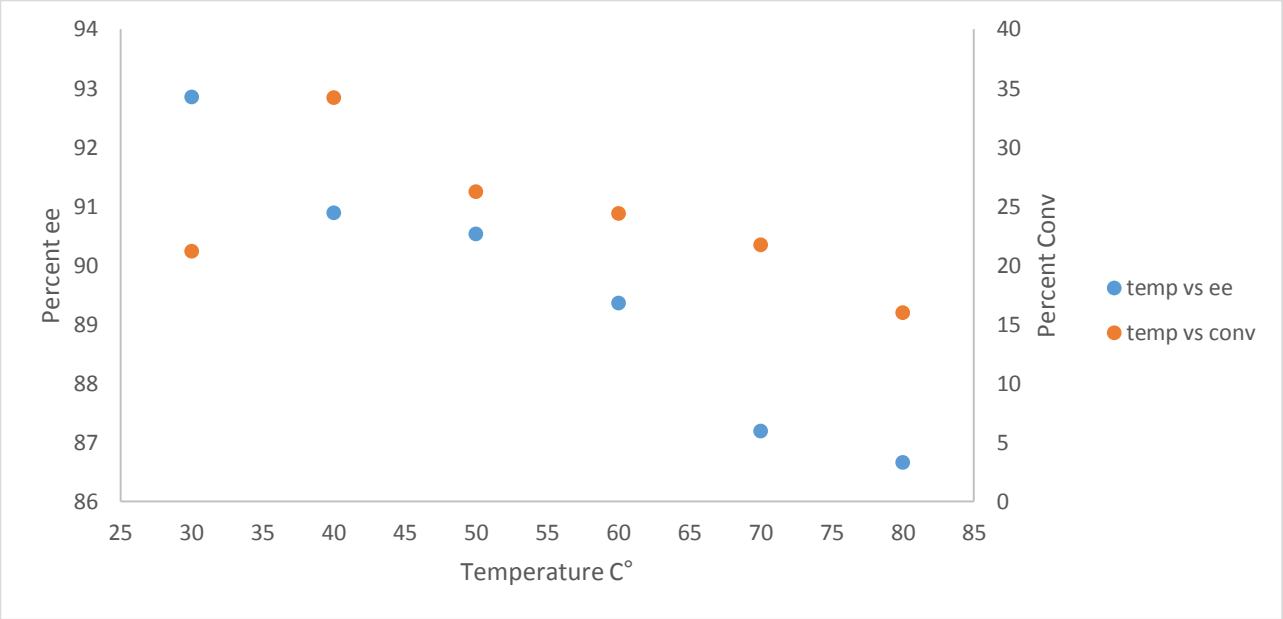

Figure 6.9: Temperature vs ee and temperature vs conversion of pinacolone in water using (Cp*)Ir(L-aze)Cl as catalyst. S/C/F ratios were 100/1/500. The relationship between temperature and ee is near ideal behavior. Decreasing conversion at increased temperatures is most likely due to the volatility of the substrate.

6.3.4. Variation of the Metal Center/Ligand/Pi-Ligand:

With the optimum ligands found to be L-pipecolic, L-proline, and L-azetidine variants, several studies were performed to find the optimum metal center. In the case of purely aliphatic ketones such as pinacolone, iridium outperforms rhodium and ruthenium in selectivity using the optimized conditions of water and formate. For example, the (Cp*)Ir(L-aze)Cl complex achieves an ee of 92%, with the (Cp*)Rh(L-aze)Cl variant having an ee of 86%. The conversions were similar on a 48 h time scale, with the Ir complex reaching 30% and the Rh complex reaching 32%. The ruthenium complexes (p-MeC_6H_4iPr)Ru(L-pro)Cl and ($Me_3C_6H_3$)Ru(L-pro)Cl achieve conversions and selectivities of 45% and 49% and 34% and 60% respectively, whereas the (Cp*)Ir(L-pro)Cl reaches 43% conversion and 77% ee.

While the loss of selectivity in the iso-structural Rh complex is difficult to explain, both Ru variants have reduced steric bulk in the "stool" portion of the complex, when compared to the Cp* variants. The loss of this bulk is most likely the cause of decreased selectivity. The greater selectivity for the mesitylene based complex in comparison to the p-MeC_6H_4iPr complex supports this and supports the proposed transition state (figure 6.9).

This trend is reversed in the case of acetophenone, with the Ru based systems outperforming Rh and Ir based counterparts in both rate of reduction and selectivity under the optimized conditions for acetophenone. Of the Ru catalysts, the (Me_6C_6)Ru(L-pip)Cl is the most selective, with an ee of 89% and conversions reaching 99%. The L-pip ligand is generally the most active and selective, in any combination of metal and seat, however the one exception appears with the p-MeC_6H_4iPr Ru complexes. In this case the L-pro variant is more selective than the L-pip, with ee's of 80% and 71% respectively.

6.4. Mechanism of chiral induction:

The chirality of product is established during transfer of the hydride to the carbonyl carbon. Changing the same amino acid from D to L causes the configuration of the alcohol product to change as well, with D-proline and L-proline will producing the opposite enantiomers. Switching from L to D-pro changes the configuration at each stereogenic site, ($S_{Ir}S_CS_N$ to $R_{Ir}R_CR_N$), which explains the change in product confirmation. However, there is no direct correlation between using D or L amino acid and the final configuration of the product, when the amino acids contain differing R groups. The (Cp*)Ir(L-pip)Cl catalyst produced the R configuration of pinacolone while (Cp*)Ir(L-pro)Cl produced the S, even though both free ligands have the same configuration at the alpha carbon (S) and the same configuration at the iridium center (S). Analysis of the crystal structures of the ring-based systems reveals that the configuration of the chelated nitrogen of the active catalysis correlates to the configuration of the alcohol product. The (Cp*)Ir(L-pip)Cl has a configuration of $S_{Ir}S_CR_N$

leading to a S product in the case of acetophenone. (Cp*)Ir(L-pro)Cl has a configuration of $S_{Ir}S_CS_N$ and produces the R product (figure 6.10).

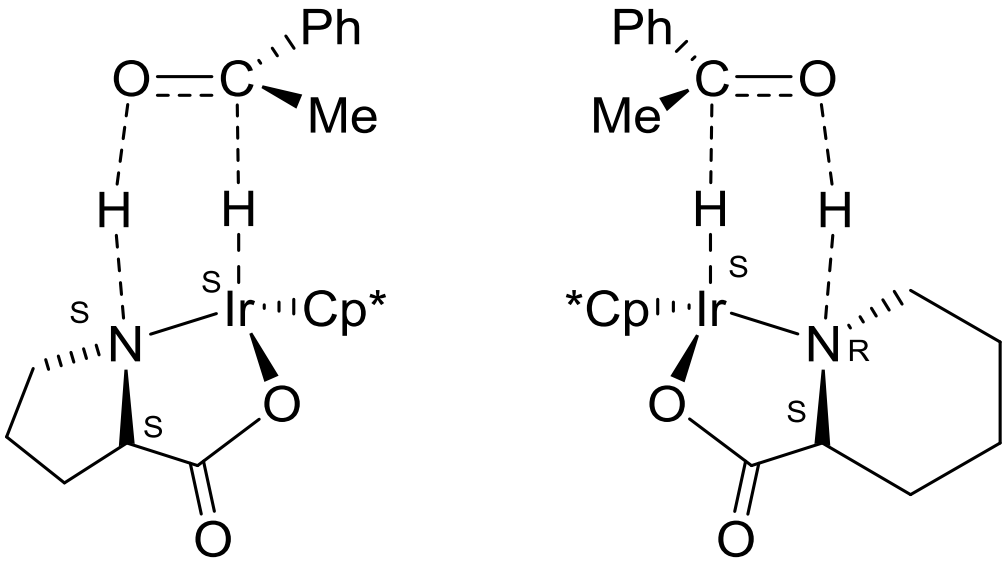

Figure 6.10: Transition states for acetophenone showing differing chirality of the nitrogen leads to differing configurations of products. The nitrogen of the Cp*Ir(L-pro)H complex is S, leading to an R product, while Cp*Ir(L-pip)H has a nitrogen of R, leading to an S product.

The Ir D-pro variant has a configuration of $R_{Ir}R_CR_N$, which produces the R product like the L-pip variant. It is important to show that the configuration at the iridium center is R with D-pro, and S with L-pip, yet both produce the same configurations of products due to the nitrogen having the same configuration. This same trend applies to pinacolone, though due to the change in group priority around the chiral carbon, R_N produces an R product and S_N produces an S product.

The reduction of the aromatic ketones is assisted by the CH-π interaction, outlined previously by Noyori and others, and the configurations obtained for products using our systems agree with this interaction.[10,27] However, pinacolone and related aliphatic substrates lack this interaction. The transition state of aliphatic and aromatic substrates are similar (figure 6.11), both substrates are reduced by transfer of a hydride and proton across the C=O bond. Because of this, it is hypothesized

that the steric clash between the t-butyl group of the pinacolone substrate and the ring portion of the catalysts is the reason for the observed selectivity.

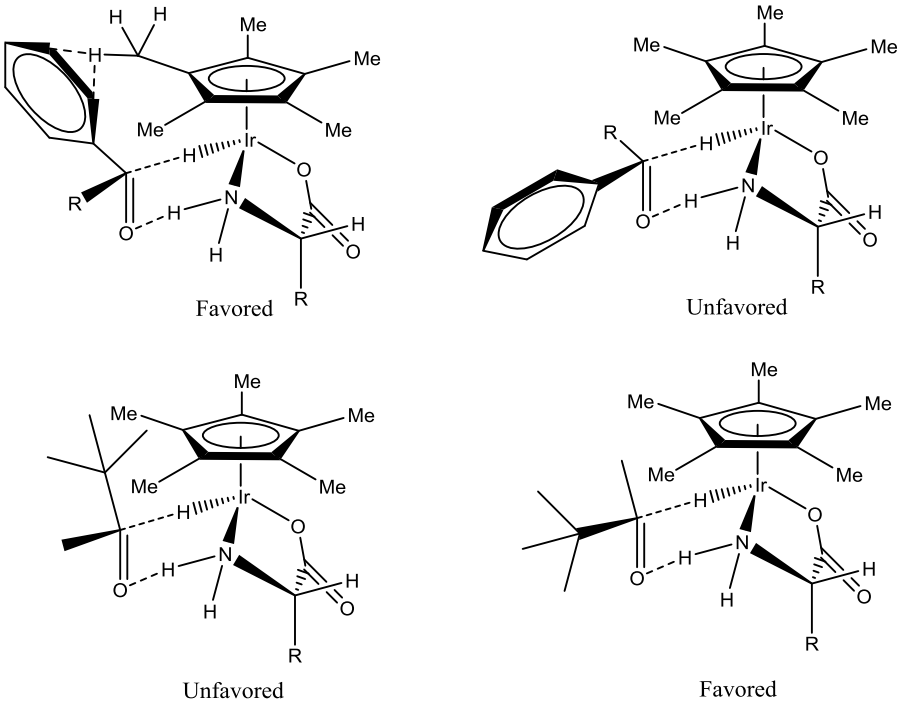

Figure 6.11: Transition states of both aromatic and aliphatic-based substrates. Aromatic substrates are stabilized via the CH_3-π interaction, with the phenyl ring facing up. The aliphatic substrates have a transition state that is destabilized by a steric clash between the R group of the substrate and the Cp* portion of the catalyst.

This steric interaction is supported by the observation that selectivity increases as the ligands are changed from the less strained L-pip to the highly strained L-aze. Additionally, as substrates with smaller R groups are reduced, the ee% decreases. Using 3-methylbutan-2-one and butan-2-one as substrates and (Cp*)Ir(L-aze)Cl as the catalyst, the selectivity decreases from 60% to 49% respectively (table 6.5). The overall trends for conversions and selectivities established with pinacolone are maintained.

Table 6.5: Reduction[a] of 3-methylbutan-2-one and butan-2-one by selected Ir catalysts.

Entry	Complex	Ketone	T (h)	Conv %[b]	ee %[c]	Conf.[d]
1	(Cp*)Ir(L-pro)Cl	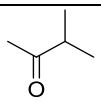	48	91	62	S
2	(Cp*)Ir(N-Me-L-phengly)Cl		48	40	48	R
3	(Cp*)Ir(L-aze)Cl		48	84	60	S
4	(Cp*)Ir(L-pip)Cl		48	91	38	R
5	(Cp*)Ir(L-pro)Cl	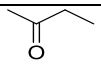	48	96	36	S
6	(Cp*)Ir(N-Me-L-phengly)Cl		48	53	36	R
7	(Cp*)Ir(L-aze)Cl		48	76	49	S
8	(Cp*)Ir(L-pip)Cl		48	>99	27	R

[a] Reaction conditions: substrate/catalyst/formate (S/C/F) 100/1/500, in 2 mL of water. [b] Determined by gas chromatography. [c] Determined by gas chromatography using a CP- ChiralSil – Dex CB 25 x 0.25 column. [d] Comparison to literature retention times

6.5. Reductions using Iridium Cp^{*R} Amino Acid Complexes:

Unfortunately, no modified complex vastly improved selectivity. These results are summarized in table 6.6. Since steric interactions are the key feature in the reduction of aliphatic ketones, it was thought that increasing the steric bulk around the Cp* portion of the catalyst would increase selectivity. Comparison of modified Ir L-proline complexes shows that increase of steric bulk of the π ligand is not directly correlated to increased selectivity. (Cp^{*ph})Ir(L-pro)Cl decreases both selectivity and reactivity. The large bulk of the phenyl group is most likely interfering with substrate binding to the hydride and amine hydrogen, reducing the rate of reaction. Monitoring the rate of reduction over time shows that the iPr complex has the fastest rate of reduction, followed by the cyclohexyl, then benzyl. The rate of reduction when using (Cp^{*ph})Ir(L-pro)Cl was too slow to be measured on a similar time scale. Similarly, the iso-propyl, cyclohexyl, and n-propyl groups decrease selectivity slightly, but retain similar reactivity compared to the unmodified complex. Both the benzyl and n-octyl derivatives increase selectivity slightly, with similar reactivity. Use of the modified pentamethylcylcopentadienes in conjunction with L-aze had little effect on selectivity, producing ee's of 90-94 percent, similar to unmodified (Cp*)Ir(L-aze)Cl.

Table 6.6: Asymmetric transfer hydrogenation of pinacolone using (Cp*R)Ir(L-pro)Cl Catalytics[a]

Entry	Complex	T (h)	Conv %[b]	ee%[c]	Configuration.[d]
1	(Cp*^{ph})Ir(L-pro)Cl	48	16	68	S
2	(Cp*^{bn})Ir(L-pro)Cl	50	41	80	S
3	(Cp*^{iPr})Ir(L-pro)Cl	44	60	74	S
4[b]	(Cp*^{cy})Ir(L-pro)Cl	44	36	74	S
5	(Cp*$^{n\text{-}propyl}$)Ir(L-pro)Cl	68	48	74	S
6	(Cp*$^{n\text{-}octyl}$)Ir(L-pro)Cl	48	30	80	S

[a] Reaction conditions: substrate/catalyst/formate (S/C/F) 100/1/500, in 2 mL of water. [b] Determined by gas chromatography. [c] Determined by gas chromatography using a CP- ChiralSil – Dex CB 25 x 0.25 column. [d] Comparison to literature retention times

The modified complexes did highly impact the reduction of long chain aliphatics such as 2-heptanone and 2-octanone (table 6.7). It was proposed that the addition of a long chain aliphatic group to the Cp portion of the catalyst would stabilize long chain aliphatic substrates. When the octyl and dodecyl Cp^R variants of iridium L-proline tested, the ee fell from 34% using the non-modified complex to 29% and 26% for the octyl and dodecyl respectively. The (Cp*$^{n\text{-}dodecyl}$)Ir(D-pro)Cl complex produced an ee of 23% of the opposite enantiomer. To gain further understanding into the exact cause of the loss of selectivity, the (Cp*)Ir(L-phengly)Cl and (Cp*$^{n\text{-}dodecyl}$)Ir(L-phengly)Cl were tested in the reduction of 2-octanone, since the former produces a near racemic mixture of 5% ee. The dodecyl variant does increase the selectivity by nearly 30 percent, with an ee of 35%.. The configuration of the products obtained are the same as those found for the reduction of pinacolone.

Table 6.7: Reduction of 2-octanone using modified and non-modified Ir complexes[a]

Entry	Complex	T(h)	Conv%[b]	ee%[c]	Conf.[d]
1	(Cp*)Ir(L-pro)Cl	42	57	34	S
2	(Cp*$^{n\text{-octyl}}$)Ir(L-pro)Cl	42	25	29	S
3	(Cp*$^{n\text{-dodecyl}}$)Ir(L-pro)Cl	91	36	26	S
4	(Cp*$^{n\text{-dodecyl}}$)Ir(D-pro)Cl	72	20	23	R
5	(Cp*)Ir(L-phenylglycine)Cl	48	15	5	R
6	(Cp*$^{n\text{-dodecyl}}$)Ir(L-phenylglycine)Cl	48	30	35	R
7	(Cp*)Ir(L-aze)Cl	96	40	52	S
8	(Cp*$^{n\text{-octyl}}$)Ir(L-aze)Cl	96	55	43	S

[a] Reaction conditions: substrate/catalyst/formate (S/C/F) 100/1/500, in 2 mL of water. [b] Determined by gas chromatography. [c] Determined by gas chromatography using a CP- ChiralSil – Dex CB 25 x 0.25 column. [d] Comparison to literature retention times

The change in selectivity from 34% to 26% when comparing (Cp*)Ir(L-pro)Cl to (Cp*$^{n\text{-dodecyl}}$)Ir(L-pro)Cl can be explained through a hydrophobic interaction between the Cp moiety and the tail of the substrate. This interaction is overriding the steric interaction seen with proline based ligands. The increasing loss of ee% as the chain increases displays this. The selectivity instilled upon the phenylglycine complex provides further evidence of this interaction, (figure 6.12). The (Cp*)Ir(L-phengly)Cl complex produces a near racemic mixture (5%), while (Cp*$^{n\text{-dodecyl}}$)Ir(L-phengly)Cl has an increased selectivity (35%) due to the hydrophobic stabilization formed between the R group of the Cp*^{R} moiety and the long chain of the 2-octanone. While this interaction is speculative, it resembles what is proposed by Li and coworkers.[49] Further reactions are needed, using substrates of varying length, as well as Cp*^{R} groups with varying chain length such as pentyl, hexyl and septyl.

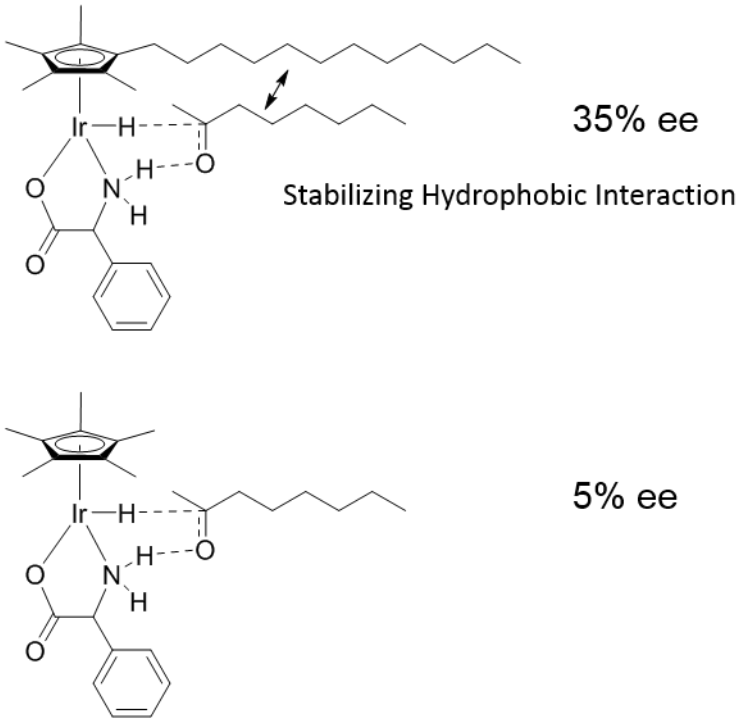

Figure 6.12: Hydrophobic interaction between Cp^R moiety and 2-octanone. The long chain of the $Cp^{*dodecyl}Ir(L\text{-phengly})H$ stabilizes 2-octanone, leading to an increase in selectivity. Table 6.7 displays further interactions and ee's.

6.6. Mechanism of reduction

6.6.1. Frustration study

The generally accepted mechanism for ATH is that presented by Noyori, involving a pericyclic six-membered transition state.[27] The hydride is delivered from the metal-hydride to the carbon, and the proton is delivered to the oxygen from the amine proton in single a concerted step. However, the drastic solvents effects witnessed upon changing from 2-propanol to water do not support this mechanism. Pericyclic reactions occur when the charge distributions in the activated complexes and the reactants are very similar.[94] The changes in rate and selectivity in solvents of differing polarity attest to a dipolar transition state, where the activated complexes differ considerably in charge separation from the initial reactants. Evidence suggests that the proton source can be either the amine proton or solvent itself. A catalyst lacking amine protons such as (Cp*)Ir(N,N-Me_2-gly)Cl would

ensure that the only source of hydrogens transferred to the substrate would be from the solvent. An NMR study using (Cp*)Ir(N,N-Me_2-gly)Cl with 2 equivalents of acetophenone and sodium formate still yielded product, though at a much lower rate, with very little conversion being achieved at 1 h. The only proton source in this reaction is water or formic acid. Similarly, the (Cp*)Ir(N-Me-D-pro)Cl complex converts acetophenone to product, but no selectivity. This loss of selectivity shows the amine proton's importance. While the proton transfer from the amine to the oxygen is not the entantio-determining step, this acidic proton creates a bond to the oxygen during the reaction, effectively holding the substrate in place while the chirality is set from the hydride transfer. The loss in rate of reaction does lead to the conclusion that the amine proton appears to stabilize the transition state, but the amine proton is not required for the reaction to proceed.

6.6.2. Kinetic Isotope Effect Studies

Kinetic isotope effect studies were carried out for the reduction of acetophenone in water using **(**Cp*)Ir(L-aze)Cl as the catalyst and sodium formate as the hydrogen source and H_2O acting as the proton source. Table 6.8 presents the rate constants for the ATH of acetophenone using DCOONa and/or D_2O.

Table 6.8: Kinetic isotope effects of ATH of acetophenone[a]

Isotope Used	Rate[b]	k_H/k_D
$HCOONa/H_2O$	1.93×10^{-2}	1 (k_{IrHNH})
$HCOONa/D_2O$	1.29×10^{-2}	1.5 ± 0.03 (k_{IrHNH}/k_{IrHND})
$DCOONa/H_2O$	9.63×10^{-3}	2.0 ± 0.04 (k_{IrHNH}/k_{IrDNH})
$DCOONa/D_2O$	9.27×10^{-3}	2.1 ± 0.05 (k_{IrHNH}/k_{IrDND})

a: Conditions: S/C/F 100/1/500 in 2 mL of solvent at 40 °C.

b: determined from the initial reaction rates

The $HCOONa/D_2O$ displays a KIE that can barely be considered a primary isotope effect (1.5), indicating that proton transfer is not the rate-limiting step, which agrees with previous studies. The result of the $DCOONa/H_2O$ and the $DCOONa/D_2O$ being nearly identical (k_H/k_D = 2.0 and 2.1

respectively) indicates that the rate-determining step is the hydride transfer to the carbon of acetophenone. These results also indicate that the mechanism of ATH for this system is indeed step-wise, not concerted, because the products of the rates ($k_H/k_D = 3.0$) of the individual isotope studies do not equal the rate of the doubly labeled study ($k_H/k_D = 2.1$). In the doubly labeled experiment, only the deuterium from the formate is causing an isotope effect at all, as observed from rate of the doubled labeled experiment being nearly equal to the deuterated formate experiment. A previous study by Xiao did not produce such a drastic difference in rates, but our data clearly shows that the mechanism for ATH in our system is step-wise, with the rate determining step being hydride transfer. Deuterium scrambling, which can cause issues in D_2O based reactions, can be dismissed based on the ^1H NMR of the isolated products (Figure 6.13). In the case of the HCOONa/D_2O product, there is no D-H coupling observed, only a doublet, as in a normal product. The DCOONa/H_2O product lacks the quartet from the now chiral C-H group and displays distinct D - H coupling.

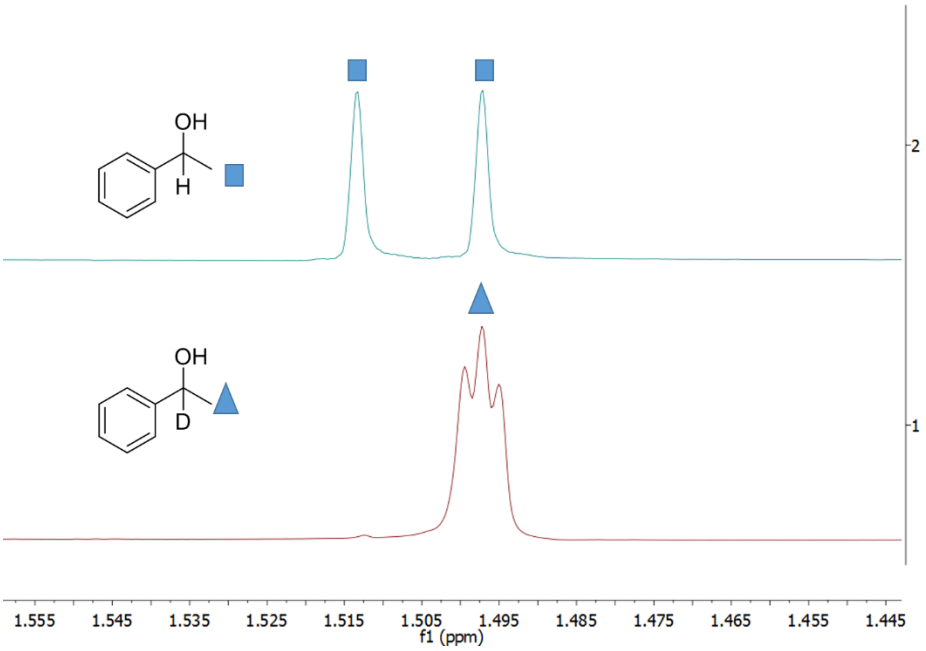

Figure 6.13: ^1H NMR spectra of the products of the HCOONa/D_2O KIE experiment (top) and the DCOONa/H_2O experiment (bottom). The is no evidence of deuterium scrambling between the deuteride and deuterium in either experiment, as seen by the coupling patterns of each 1-phenylethanol methyl group.

6.7. Revised Mechanism

The results of the solvent effects, frustration studies, and the KIE studies, combined with the theoretical studies of others[29,30,34] have allowed the classical mechanism in water to be revised (Scheme 6.4). The mechanism begins with the formation of a mono-aqua cation from the chloride containing complex. Formate can also bind in place of either the water or chloride, which then undergoes a β-hydride elimination to generate the active metal-hydride species and CO_2 as a side product. The ketone substrate then bonds to both the hydride (M-H) and hydrogen (N-H) of the catalyst. The rate determining step and enantio-determining step is the transfer of the hydride to the carbon of the ketone, as shown through the KIE studies. From here two pathways diverge. The classic pathway is the transfer of the amine proton to the oxygen of the substrate. This generates the unsaturated metal complex, which has been dubbed the "16 electron species", though analysis of the crystal structure of the related Ru-DPEN complexes shows that the N-Ru bond is shorter,[26] and more double bond in nature. This complex accepts a proton from the surrounding water to begin the cycle over again. The frustration study shows that an additional pathway is the transfer of a proton from water to an alkoxide intermediate, which is held in place the a hydrogen bonding network formed by solvent molecules and the amine proton. The cation formed from this process can immediately begin the cycle again through binding and β-hydride elimination of formate.

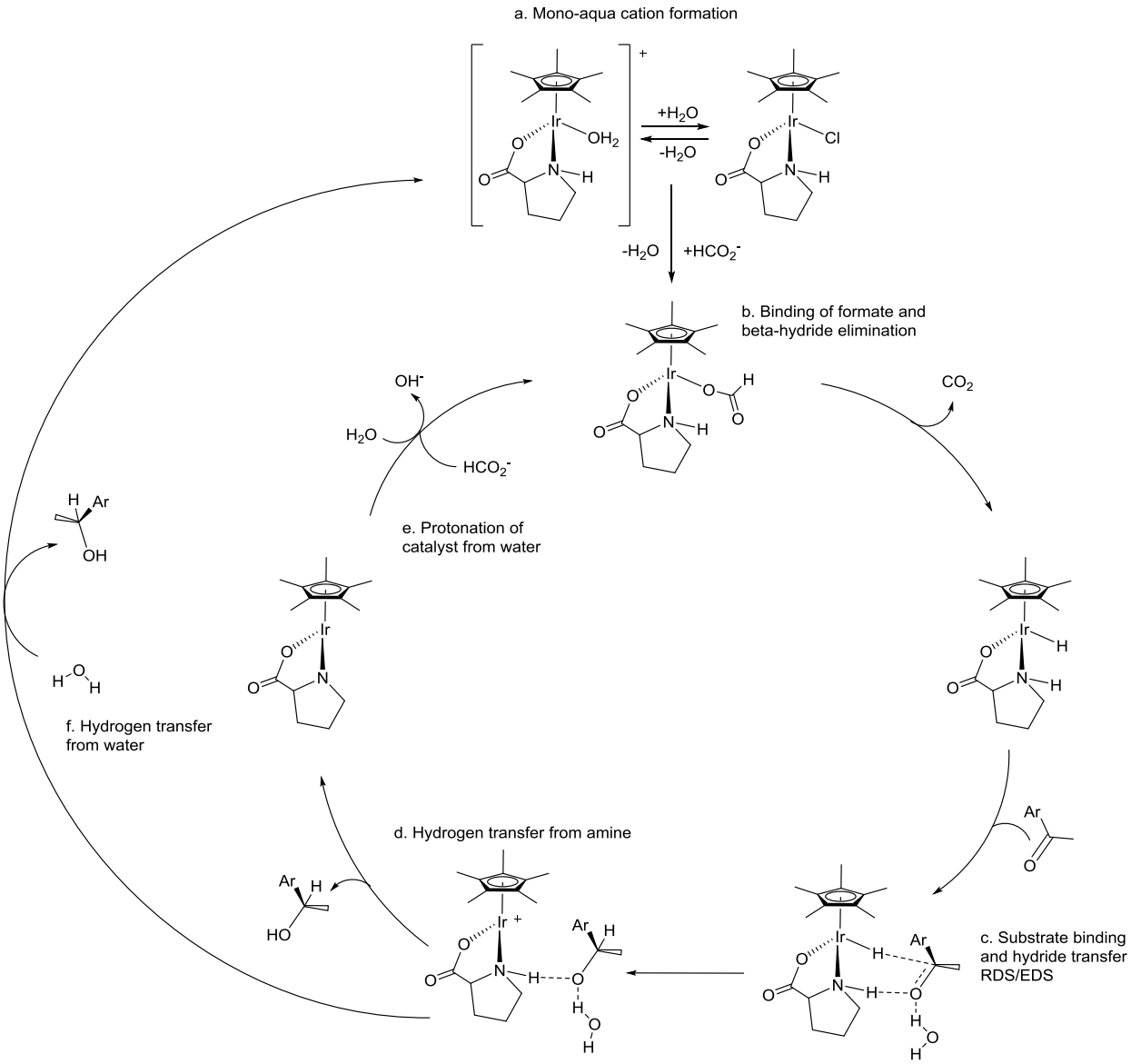

Scheme 6.4: Mechanism of ATH in aqueous media using (Cp*)Ir(L-pro)Cl. a. Mono-aqua cation formation from chloride complex. b. Binding and beta-hydride elimination of formate. c. Binding of substrate and hydride transfer (RDS/EDS). d. Hydrogen transfer to substrate from amine. e. Protonation of catalyst from water. f. Hydrogen transfer from water.

6.8. Substrate Scope

The (Me_6C_6)Ru(L-pip)Cl complex was used in an expanded substrate scope of acetophenone derivatives (Figure 6.14). Addition of electron withdrawing groups F, CF_3, and Cl reduced the ee% significantly, with conversions being effected to a smaller degree. Loss of selectivity can be attributed to a reduction in the CH_3/π interaction. Additionally, amino acids lack the tosyl group which promotes the newly discovered SO_2/π repulsion. A similar loss of activity is seen in amino alcohol based Ru catalysts though in the case of the (Me_6C_6)Ru(L-pip)Cl the loss in selectivity is not as drastic.

Reduction of acetophenone like ketones with modification at the methyl displayed drop offs in selectivity as the size of the R group decreased. All displayed the best selectivity and reactivity in water with **(**Cp*)Ir(L-pip)Cl as catalyst. Even the highly hindered ketone benzophenone could be reduced under these conditions, despite being an insoluble solid.

Aliphatic ketones, which could only be made selective through steric constraints, also saw a drop off in selectivity with the reduction in size of the R group, as shown before. The long chain aliphatics 2-heptanone and 2-octanone were both reduced at similar selectivity, with the result being less selective than 3,3-dimethylbutan-2-one. Results for the reductions of all substrates are shown in figure 6.14.

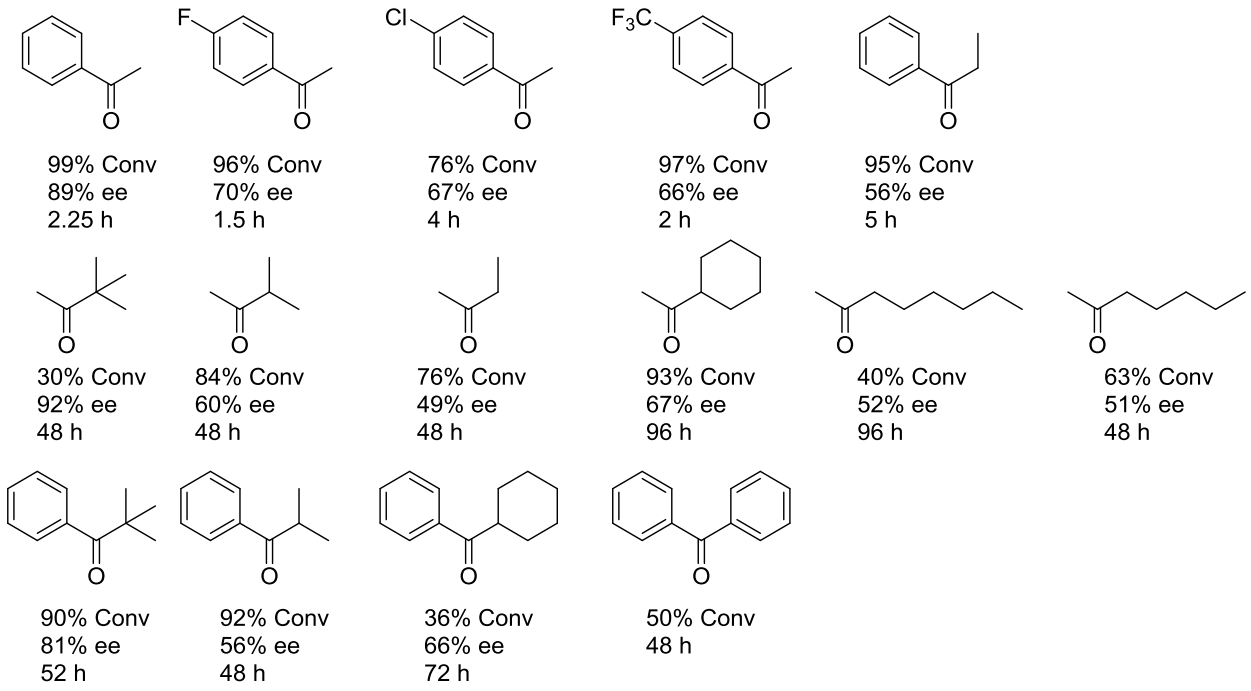

Figure 6.14: Substrate scope of ATH of ketones by half sandwich amino acid complexes. Acetophenone and its derivatives (top row) are best reduced by (Me_6C_6)Ru(L-pip)Cl. Cp*Ir(L-aze)Cl is most selective in the reduction of aliphatic substrates (middle row). Highly hindered ketones (bottom row) are best reduced by Cp*Ir(L-pip)Cl.

6.9. Summary of Asymmetric Transfer Hydrogenation of Ketones

The amino acid complexes were effective ATH catalysts for a range of ketones. Ring based systems were the most selective, with L-pip, L-pro, and L-aze producing the highest selectivities for any given set of ketones. This is due to only one diastereomer being active in the reduction of ketones. Ru based systems were the most selective and most reactive for the reduction of acetophenone and para substituted derivatives. More specifically, (C_6Me_6)Ru(L-pip)Cl had near full conversion and 89% ee at 2.5 hours when the reaction was performed in 2-propanol. Cp*Ir(L-pip)Cl was the most effective in the reduction of highly hindered ketones, when the reaction is performed in water with formate being the hydrogen source. Cp*Ir(L-aze)Cl was the most effective in the

reduction of aliphatic ketones, producing a 92% ee for 3,3-dimethylbutan-2-one, but only 30% conversion at 48h.

Chirality of the alcohol product can be correlated to the chirality of the coordinated nitrogen in the case of mono-alkylated amino acids. An S nitrogen leads to an R product and a R nitrogen leads to an R product, if acetophenone is the substrate. In addition to this, the $CH/CH_3 - \pi$ interaction described by Noyori is most likely responsible for the selectivity observed in the aromatic products. Configurations of the products are consistent with this transition state. Aliphatic substrates have selectivity instilled through steric interactions between the R group of the substrate and the ancillary ligand. The loss of selectivity as the steric bulk of the substrate's bulk decreases is consistent with this conclusion.

The mechanism of reduction is similar to what has been reported in the literature. The active hydride species is formed through binding of formate and beta-hydride elimination of CO_2. The substrate then binds to the metal hydride and amine hydrogen. Hydride transfer is the RDS and EDS, as shown through KIE experiments. The hydrogen can be transferred from either the amine or the solvent itself, as fully alkylated ligands still produce product, but has a much lower rate. The amine hydrogen is required for selectivity, as removal results in a racemic product. This is due to a hydrogen bonding interaction between the amine hydrogen and the carbonyl oxygen, effectively holding the substrate in place while the hydride is transferred. In addition, the reduced rate of reduction when fully alkylated amines are used as ligands is also due to loss of this hydrogen bonding interaction.

7. Conclusions

A range of half sandwich amino acid complexes of the form (η^n-ring)M(aa)Cl was synthesized, characterized, studied to explore fundamental properties and their potential as ATH catalysts for ketones. Tetramethylcyclopentadienyl ligands of the type Cp*^{R} were synthesized by reaction of 2,3,4,5-tetramethylcyclopent-2-en-1-one with the respective Grignard reagent. The alcohol product eliminated water to produce the Cp*^{R} products in yields ranging from 37 to 94%. The Cp*^{R} compounds are isolated as a mixture of isomers, rendering characterization by NMR spectroscopy complicated. The Cp*^{R} were reacted with $IrCl_3 \bullet xH_2O$ to produce the dimer complexes [(Cp*^{R})$IrCl_2$] in yields ranging from 14% to 91%. It was found that microwave heating could improve yields as well as reduce reaction times from 48 h to 1 h. The complicated ^{1}H NMR patterns were simplified when the Cp*^{R} became its respective anion. The amino acid complexes themselves were produced through reaction of the respective dimer [(η^n-ring)MCl_2] with the amino acid ligand in presence of base in a 1:2 ratio in methanol. The complexes could be purified by extraction with DCM followed by filtering the solution. Complexes were then recrystallized with DCM and diethyl ether or hexanes. The (Cp*)Ir(aa)Cl complexes were isolated as yellow powders with yields ranging from 41 to 96%. (Cp*^{R})Ir(aa)Cl complexes were synthesized and isolated through a similar process with yields ranging from 42 to 94%. (Cp*^{R})Ir(aa)Cl groups containing cyclohexyl, n-octyl, and n-dodecyl groups were isolated as gels, and were soluble in solvents ranging from DCM to hexane. Other R groups were isolated as yellow powders. (η^6-arene)Ru(aa)Cl were synthesized using the same methods as the (Cp*)Ir(aa)Cl complexes to give orange powders with yields ranging from 56 to 91%. (Cp*)Rh(aa)Cl complexes were synthesized in the same fashion as the (Cp*)Ir(aa)Cl complexes to give red/orange powders in yields of 65 to 91%. This work represents the first study of (Cp*^{R})Ir(aa)Cl complexes structure, solution and solid state properties, and catalytic capability for ATH.

Coordination of an amino acid produces a chiral metal complex. In the case of amino acids lacking inherent chirality, two enantiomers form. When a homochiral amino acid is used two diastereomers form (R_MS_C, S_MS_C, in the case of most L-amino acids). Amino acids with alkylated amino groups display three stereocenters, with the potential of up to four diastereomers, however only two are witnessed, with the chirality of the nitrogen is potentially preserved. The diastereomers form through epimerization at the metal center, which is nearly instantaneous at room temperature. These diastereomers adopt differing ratios in solution that are dependent upon the R group of the amino acid, with more sterically hindering side chains leading to high selectivity. In the case of some complexes, the ratios can be shifted through changing the solvent temperature, with colder temperatures returning ratios closer to what is observed in the solid state, and higher temperatures pushing the solution state ratio to equilibrium. Upon returning to room temperature the ratios return to the resting state. All complexes with a fully alkylated amine formed only one diastereomer.

Crystal structures of these complexes showed that either one or both diastereomers could appear in the solid state, with no correlation for this observation found between ligand, metal, or ancillary ligand. These structures allowed for the absolute assignment of chirality at the stereogenic centers of the metal, carbon, and nitrogen. The case of the ring based amino acids of Pro, Aze, and Pip, it was found that the chirality of the nitrogen was preserved. The smaller ring systems of Aze and Pro instilled the same chirality between the α-carbon and the nitrogen, (S_CS_N), whereas Pip instilled the opposite, forming a chair conformation similar to cyclohexane (S_CR_N). Nearly all of the complexes form hydrogen bonding networks through their carbonyl oxygens and amine protons, normally taking up a helical structure down a 2_1 screw axis. X-ray powder diffraction showed that the bulk material has the same ratios as the single crystal structures, reinforcing that fact that epimerization occurs nearly instantly upon the complexes entering solution. The configurations of the solid state could be correlated to those in solution through NOE experiments, with the findings

indicating that while the ratios of diastereomers change upon entering solution, their configurations do not.

Abstraction of the chloride ligand leads to oligomer structures formed through a bond from the metal center to the neighboring monomer's carbonyl oxygen. The most common form is a trimer complex, with several being reported by groups other than ourselves. These trimers form with chiral self-recognition, meaning they consist of only one diastereomer. An octomer forms in the case of **[**$((Cp^*)Ir(gly))_8][PF_6]_8$, unlike the trimer variants, both entantiomers are present in the structure, with chirality at the metal center altering every other monomer. These polymeric forms may only exist in the solid state, with ^1H and ^{13}C NMR spectra looking identical to the chloride species from which they are derived.

Modified pentamethylcyclopentadienyl ligands (Cp^{*R}), with R being phenyl, benzyl, iso-propyl, n-propyl, cylcohexyl, n-octyl, and n-dodecyl, were synthesized by the reaction of 2,3,4,5-tetramethylcyclopent-2-enone with the respective Grignard reagent, followed by elimination of the alcohol with HCl. These ligands lead to their respective dimers using the same synthesis as the $(IrCp^*Cl_2)_2$ dimer. The amino acid complexes derived from these dimers displayed diastereomeric ratios similar to their unmodified variants, showing that the amino acid ligand is more responsible for changing the steric environment than the Cp^R moiety, even in the case of sterically demanding groups such as phenyl. A combination of NOE experiments and single X-ray diffraction showed that these complexes adopt the same configurations in both solid and liquid states as the un-modified complexes.

Ruthenium complexes of the form (arene)Ru(aa)Cl were synthesized in a fashion similar to the Ir variants. These complexes adopt the same pianostool configuration as the Ir complexes, with the diastereomeric ratios being similar to the Ir complex with the same aa ligand. The mesitylene and hexamethyl benzene complexes adopted ratios closest to that of the (Cp*)Ir(aa)Cl complexes, most

likely due to the similar steric constraints imparted by their respective ancillary ligands. The configurations of the complexes were the same as those of the Ir variants, at least initially. The (arene)Ru(L-pip)Cl complexes epimerize in solution, with the initial ratios changing over the course of 24 to 48 h. Additionally, the mono-aqua cation variants of the complexes were clearly visible in the ^{1}H NMR spectrum, possibly due to a slower exchange rate of the chloride ligand and H_2O. Addition of NaCl forces this equilibrium to the chloride containing complex, as show from the disappearance of the aqua complex NMR shifts. The related (Cp*)Rh(aa)Cl complexes were nearly identical to the (Cp*)Ir(aa)Cl, with the complexes being isostructural.

The metal complexes form hydrides in the presence of formate or 2-propanol, which leads to the bi-functional catalyst required for ATH of ketones. All of the tested (η^n-ring)M(aa)Cl are active for the ATH of ketones, both aliphatic and aromatic. Ring containing amino acids produced the highest selectivity for both aliphatic and aromatic substrates, with L-aze and L-pip performing the best for aliphatic and aromatic substrates respectively. The diastereomers formed with ring containing systems produce only one active hydride complex, as seen from Cl-H distances and Cl-M-N-H torsional angles, leading to their higher selectivity. Changing the amino acid from L to D did switch the chirality of the alcohol product due to changing the chirality of the amine nitrogen. When D-pro is coordinated the nitrogen is R, leading to an S product, while L-pro has the opposite chirality at the nitrogen and produces the opposite product. This was also seen when L-pip and L-aze are compared, which have differing chirality at the coordinated nitrogen and metal center, leading to a preferred face of the substrate binding to the catalyst.

Drastic solvent effects were observed for subsets of ketones, with acetophenone and para substituted derivatives achieving the high selectivity using 2-propanol with NaOH as base. If the same reduction is performed in water, the selectivity erodes. Interestingly as the methyl portion is substituted for more sterically hindering groups the selectivity in water increases substantially. All

aliphatic ketones are best reduced using aqueous media. While selectivities varied between solvents, rate of reaction was increased when performed in aqueous solvent, which has been seen for other systems. This leads to the conclusion that water is involved in the RDS of hydride transfer. Spiking studies and co-solvent studies support this, with rates of reaction decreasing with increasing amounts of DMF as co-solvent, and rates of reduction decreasing as the polarity of co-solvent decreased. While the increase in rate of reduction is understood, the decrease or increase in selectivity is not fully understood.

Iridium based complexes out-performed all other metal complexes in the reduction of aliphatic ketones and highly hindered aromatic ketones. Ruthenium based complexes were able to reduce acp variants most selectively, with the hexamethyl benzene variants performing the best. The modified (Cp^{*R})Ir(aa)Cl complexes did not overly improve the selectivity in regards to the reduction of aliphatic ketones, with the selectivity of modified (Cp^{*R})Ir(L-aze)Cl complexes, (the most selective ligand), all falling within the range of 90-94% with 3,3-dimethylbutan-2-one as the substrate. However, the long chain variants did impact selectivity of long chain aliphatic substrates due to a hydrophobic interaction, with the addition of an n-dodecyl chain increasing selectivity (Cp)Ir(L-phengly)Cl from 5% to 35% in the case of ($Cp^{*n\text{-}dodecyl}$)Ir(L-phengly)Cl.

The solvent effects, frustration studies, and KIE effects have led to a revised mechanism in aqueous media. The increase in rate of reduction supports several previous studies that show that water assists in the RDS of the reaction. The frustration studies, using fully methylated amino acids, which still reduce acetophenone led to the conclusion that the proton of the alcohol product can be delivered from either solvent or the amine proton. Lastly, the KIE study definitely supports a step-wise mechanism, with hydride transfer being the rate-limiting step, with the doubly labeled rate being the same as the hydride labeled rate of reduction.

In summary, this work has shown that a modular catalyst design is valid for the reduction of different classes of ketones. Tailoring of the metal, amino acid, and ancillary ligand allowed for moderate to high selectivity in aromatics, highly hindered, and aliphatic ketones, with the latter two groups still presenting a challenge to more ligand set more complex than amino acids. This method has also assisted in the development of a revised mechanism of ketone reduction, as well as origin of chirality, and involvement of ancillary ligand.

8. Experimental

8.1. Materials and Instruments

8.1.1. Materials and Methods

All materials for synthesis, purification, characterization, and catalytic reduction of ketones were used as received unless otherwise stated. $RuCl_3 \cdot 3H_2O$, $RhCl_3 \cdot 3H_2O$, $IrCl_3 \cdot xH_2O$ were purchased from Pressure Chemical, Pittsburgh, PA 15201. Sodium formate, pinacolone, L-alanine, L-valine, D-valine, L-leucine, L-isoleucine, D-phenylalanine, L-proline, D-proline, D-N-methyl-proline, L-hydroxyproline, N-methyl-L-phenylglycine, and L-serine, benzyl magnesium chlorine, 1,2,3,4,5-pentamethylcyclopenta-1,3-diene, and 2,3,4,5-tetramethylcyclopent-2-en-1-one were purchased from Alfa Aesar, Ward Hill, MA 01835. Reagent grade solvents and L-pipecolic aicd, L-phenylglycine, L-phenylalanine, L-histidine, D-histidine, L-glutamic acid, L-cysteine, L-threonine, dodecylmagnesium bromine, octylmagnesium bromide, cyclohexylmagnesium bromine, phenylmagnesium chloride, and isopropylmagnesium bromide were purchased from Sigma-Aldrich, St. Louis, MO 63103. Glycine was purchased from Qiagen Sciences, Germantown, MD 20874. *N*,*N*-dimethylglycine was purchased from Spectrum Chemical, Gardena, CA 90248. Dueterated solvents for NMR spectroscopy were obtained from Cambridge Isotope Laboratories, Tewksbury, MA 01876. L-azetidine-2-carboxylic acid and L-trans-4-fluoro-proline were purchased from Indofine Chemical, Hillsborough, NJ 08844. Elemental analyses were performed by Atlantic Microlabs, Norcross, GA. ^{1}H NMR spectra were collected on a Varian MR-400 NMR spectrometer. Optical rotation data were collected on a Jasco P-2000 polarimeter using a 10 cm cell.

8.1.2. Gas Chromatography:

GC chromatograms were collected on a Hewlett Packard 5890 equipped with a CP- ChiralSil – Dex CB, 25 m x 0.25 column for enantiomeric excess analysis and percent conversions. Reactions were monitored on a ZB – 5, 15 m x 0.25 column. Inlet Temperature was 240 °C and detector temperature was 250 °C. See specific substrates/products for column temperatures.

8.1.3. High Resolution Mass Spectrometry

Mass spectrometry was performed by William Bebout of the Virginia Tech Chemistry Department Analytical Service laboratory in Blacksburg, VA. Positive ion electrospray ionization mass spectra ((+)ESI-MS)122 were collected using an Agilent Technologies 6220 Accurate-Mass time-of-flight (TOF) LC–MS with a dual ESI source. The sample was dissolved in HPLC grade solvent and injected through a preloading capillary at 1.2 kV with a flow rate of 0.4 mL/min. N2 gas was used as the inert nebulizing gas at a pressure of 60 psig. The charging voltage was set to 2000 V, the fragmentor voltage set to 125 V, and the skimmer voltage set to 65 V.

8.1.4. Single X-ray Crystal Collection and Data Analysis:

X-ray crystallographic data were collected at 100 K on an Oxford Diffraction Gemini diffractometer with an EOS CCD detector and Mo Kα radiation. Crystals were coated in Paratone® oil and mounted on a fiber. Data collection and data reduction were performed using Agilent's CrysAlisPro software.[95] Structure solution and refinement were performed with ShelXS and SHELXL,[96] and Olex2 was used for graphical representation of the data.[97]

8.2. Synthesis

The following synthetic procedures were conducted in air unless otherwise stated

8.2.1. Synthesis of [(Cp*)Ir(aa)Cl] complexes

8.2.1.1. Synthesis of $[IrCp^*Cl_2]_2$

The iridium dimer precursor was synthesized by a previously reported method.[83] $IrCl_3 \cdot 3H_2O$ (2.0 g, 5.7 mmol) was combined with HCp* (1.16 g, 8.51 mmol), in a 250-mL Schlenk flask with 100mL of methanol and refluxed for 48 h. Upon cooling to 0 °C, an orange powder appeared in solution. This

powder was collected by vacuum filtration and washed with cold methanol and ether to yield 1.41 g. A second crop of crystals were collected after removing solvent to half volume and overnight refrigeration, (0.494 g), with a combined yield of 1.91 g, 2.34 mmol (84.4 %).

^{1}H NMR (400 MHz, Chloroform-*d*) δ 1.59 (s, 15H, Cp*Me)

8.2.1.2. General Procedure for Synthesis of (Cp*)Ir(aa)Cl

A RBF was charged with appropriate amounts of $[IrCp^*Cl_2]_2$, amino acid, base (KOH or $NaHCO_3$), and MeOH. With magnetic stirring, the initial orange solution changed to yellow over the course of 30 min to 2 h depending on the amino acid used. The solvent was removed via reduced pressure. The complex was extracted with 3x10 mL of DCM and filtered to remove excess amino acid and base. The complexes were recrystallized by first dissolving the complexes in minimal DCM, followed by slow addition of and ether or hexanes to produce a yellow powder. The complexes were then collected on a frit as yellow crystalline powders.

8.2.1.3. Synthesis of (Cp*)Ir(L-ala)Cl (**1a**)

Following the general procedure: $[IrCp^*Cl_2]_2$ (0.150 g, 0.189 mmol), L-alanine (0.0689 g , 0.773 mmol), and KOH (0.0430g 0.766 mmol) were reacted in methanol (50 mL) to give **1a** (0.1498 g, 0.3322 mmol, 88%), (56/45 mol ratio of diastereomers): Major Isomer: ^{1}H NMR (400 MHz, $CDCl_3$) δ 6.91 (m, 1H, NH*H*), 3.63 (m, 1H, N*H*H), 3.49 (m, 1H, CHCOO), 1.69 (s, 15, Cp*Me), 1.43 (d, *J* = 6.9 Hz, 3H, CH_3). ^{13}C NMR (101 MHz, $CDCl_3$) δ 183.4 (COO), 84.2 (Cp*), 53.0 (Cα), 21.3 (CH_3), 9.2 (Cp*Me). Minor Isomer: ^{1}H NMR (400 MHz, $CDCl_3$) δ 5.32 (m, 1H NH*H*), 4.37 (m, 1H N*H*H), 3.65 (m, 1H CHOO), 1.69 (s, 15H Cp*Me), 1.39 (d, J = 6.9 Hz, 3H CH_3). ^{13}C NMR (101 MHz, $CDCl_3$) δ 185.4 (COO), 84.1 (Cp*), 52.0 (Cα), 19.3 (CH_3), 9.2 (Cp*Me).

HRMS/ESI+ (*m/z*): [M+Na]+ calcd for $C_{13}H_{20}[^{193}Ir]NNaO_2$ 438.1015, Found 438.0992

Anal. Calcd for $C_{13}H_{21}ClIrNO_2$: C, 34.62; H; 4.69, Found: C, 34.57; H, 4.65

8.2.1.4. Synthesis of (Cp*)Ir(L-asn)Cl (**1b**)

Following the general procedure: $[IrCp^*Cl_2]_2$ (0.100 g, 0.126 mmol), L-asparginine (0.0348 g (0.2635 mmol), and KOH (0.0148g 0.2635 mmol) were reacted in methanol (50 mL) to give **1b** (0.105 g, 0.212 mmol 84%), (mol ratio of diastereomers 84/16): Major Isomer: ^{1}H NMR (400 MHz, CD_3OD) δ 6.10 (s br, 1H NH*H*), 5.55 (s br, 1H N*H*H), 4.20 (m, 1H CHOO), 2.72 (dd, J = 18.2, 5.0 Hz, 1H C*H*H), 2.53 (dd, J = 18.2, 2.5 Hz, 1H CH*H*), 1.71 (s, 15H Cp*Me).^{13}C NMR (101 MHz, $CDCl_3$) δ 185.3 (COO) , 171.6 (CNO), 83.5 Cp*, 55.4 CH, 29.6 CH_2 , 8.7 (Cp*Me). Minor Isomer: ^{1}H NMR (400 MHz, CD_3OD) δ 3.65 (m, 1H CHOO), 2.85 – 2.77 (m, C*H*H), 1.69 (s, 15H Cp*Me). ^{13}C NMR (101 MHz, CD_3OD) δ 185.4 (CHOO), 172.1 ($CONH_2$), 83.8 (Cp*), 55.1 (αCH), 36.8 (CH_2) , 7.1 (Cp*Me).

HRMS/ESI+ (*m/z*): [M+H]+ calcd for $C_{14}H_{23}Cl[^{193}Ir]N_2O_3$ 495.1021, Found 495.1017

Anal. Calcd for $C_{14}H_{23}ClIrN_2O_3$; C, 34.04; H, 4.49; Found C, 34.31; H, 4.69

8.2.1.5. Synthesis of (Cp*)Ir(L-asp)Cl (**1c**)

Following the general procedure: $[IrCp^*Cl_2]_2$ (0.100 g, 0.126 mmol), L-aspartic acid (0.071 g (0.533 mmol), and KOH (0.03g 0.533 mmol) were reacted in methanol (30 mL) to give **1c** (0.107 g 86%) (mol ratio of diastereomers 51/49): Major Isomer: ^{1}H NMR (400 MHz, CD_3OD) δ 5.57 (s br, 1H NH*H*), 5.33 (s br, 1H N*H*H), 3.67 (m, 1H CHOO), 2.73 (m, 2H CH_2), 1.69 (s, 15H Cp*Me). ^{13}C NMR (101 MHz, $CDCl_3$) δ 84.1 (Cp*), 53.4 (Cα), 29.5 (COH_2), 9.1 (Cp*Me). Minor Isomer: 1H NMR (400 MHz, CD_3OD) δ 6.16 (s br, 1H NH*H*), 5.66 (s br, 1H N*H*H), 4.16 (m, 1H CHOO), 2.87 (m, 2H CH_2), 1.69 (s, 15H Cp*Me). ^{13}C NMR (101 MHz, CD_3OD) δ 187.1 (CHOO), 176.0 (CHOO), 84.3 (Cp*), 48.8 (αCH), 37.8 (CH_2), 8.0 (Cp*Me).

HRMS/ESI+ (*m/z*): [M+H]+ calcd for$C_{14}H_{22}Cl[^{193}Ir]NO_4$ 496.0861, Found 496.0814

(CH analysis was consistently low for this compound. The pendant carboxylic acid may be responsible for holding on to solvents such as water very tightly. It is one in a series of many compounds made using exactly the same procedure and which yielded proper CH analyses.)
Anal Calcd for $C_{14}H_{21}ClIrNO_2$: C, 38.97; H, 4.28. Found: C, 25.42; H, 3.99

8.2.1.6. Synthesis of (Cp*)Ir(gly)Cl (**1d)**

Following the general procedure: $[IrCp^*Cl_2]_2$ (0.150 g, 0.189 mmol), glycine (0.058 g ,0.773 mmol), and KOH (0.043 g 0.766 mmol) were reacted in methanol (25 mL) to give **1d** (0.131 g, 0.300 mmol, 80%): ^{1}H NMR (400 MHz, $CDCl_3$) δ 6.49 (br s, 2H, NH_2), 3.45 (d, J = 6.0 Hz, 2H) CH_2, 1.71 (s, 15H, Cp*Me). ^{13}C NMR (101 MHz, $CDCl_3$) δ 183.4 (COO), 84.1 (CP*), 45.3 (CH_2), 9.2 (Cp*Me). Single crystals suitable for X-ray diffraction were grown from slow diffusion of ether into dichloromethane.

HRMS/ESI+ (*m/z*): [M+H]+ calcd for $C_{12}H_{19}NO_2[^{193}Ir]$ 402.104; found, 402.1059

Anal Calcd for $C_{12}H_{19}ClIrNO_2 \bullet H_2O$: C, 31.68; H, 4.65. Found: C, 31.64; H, 4.45

8.2.1.7. Synthesis of (Cp*)Ir(*N*-Me-gly)Cl (**1e**)

Following the general procedure: $[IrCp^*Cl_2]_2$ (0.100 g, 0.126 mmol), *N*-methyl-glycine (0.0454 g, 0.510 mmol), and KOH (0.0284 g, 0.510 mmol) were reacted in methanol (50 mL) to give **1e** (0.0824 g, 0.183 mmol, 73%), (mol ratio of diastereomers 72/28): Major Isomer: ^{1}H NMR (400 MHz, $CDCl_3$) δ 6.41 (br s, 1H, NH), 3.45 (dd, *J* = 14.7, 10.2 Hz, 1H, C*H*H), 3.37 (dd, *J* = 14.7, 5.8 Hz, 1H, CH*H*), 2.81 (d, *J* = 5.7 Hz, 3H, N- CH_3), 1.68 (s, 15H, Cp*Me). ^{13}C NMR (101 MHz, $CDCl_3$) δ 183.4 (COO), 83.9 (Cp*), 55.7 (CH), 39.9 (NCH_3), 8.8 (Cp*Me). Minor Isomer: ^{1}H NMR (400

MHz, $CDCl_3$) δ 4.39 (br s, 1H, NH), 3.88 (dd, *J* = 15.6, 5.7 Hz, 1H, C*H*H), 3.18 (dd, *J* = 15.6, 9.2 Hz, 1H, CH*H*), 3.02 (d, *J* = 6.2 Hz, 3H, N-Me), 1.68 (s, 15H, Cp*Me, overlap with major isomer). ^{13}C NMR (101 MHz, $CDCl_3$) δ 179.5 (COO), 84.5 (Cp*), 57.9 (αC), 43.5 (NCH_3), 9.2 (Cp*Me).

HRMS/ESI+ (*m/z*): [M+Na]+ calcd for $C_{13}H_{21}Cl[^{193}Ir]NNaO_2$ 474.0782; found 474.079

Anal. Calcd for $C_{13}H_{21}ClIrNO_2$; C, 34.62; H, 4.69; Found: C, 35.00; H, 4.83

8.2.1.8. Synthesis of (Cp*)Ir(*N*,*N*-Me-gly)Cl (**1f**)

Following the general procedure: $[IrCp^*Cl_2]_2$ (0.100 g, 0.126 mmol), *N*, *N*-dimethyl-glycine (0.053 g, 0.510 mmol), and KOH (0.0284 g, 0.510 mmol) were reacted in methanol (30 mL) to give **1f** (0.082 g, 0.177 mmol, 71%): ^{1}H NMR (400 MHz, $CDCl_3$) δ 4.09 (d, J = 14.6 Hz, 1H, CH), 3.10 (s, 3H, NCH_3), 3.00 (d, J = 14.6 Hz, 1H, CH), 2.94 (s, 3H, NCH_3), 1.62 (s, 15H, Cp*Me). ^{13}C NMR (101 MHz, $CDCl_3$) δ 180.5 (COO), 84.3 (Cp*), 66.3 (CH_2), 56.3 (NCH_3), 50.6 (NCH_3), 9.0 (Cp*Me).

HRMS/ESI+ (*m/z*): [M+Na]+ calcd for $C_{14}H_{24}Cl[^{193}Ir]NO_2$ 466.1119; found 466.1117

Anal. Calcd for $C_{14}H_{23}ClIrNO_2$; C, 36.16; H, 4.99; Found: C, 35.57; H, 4.95

8.2.1.9. Synthesis of (Cp*)Ir(L-glu)Cl (**1g**)

Following the general procedure: $[IrCp^*Cl_2]_2$ (0.100 g, 0.126 mmol), L-glutamic acid (0.0800 g, 0.544 mmol), and KOH (0.030 g, 0.535 mmol) were reacted in methanol (30 mL) to give **1g** (0.103 g, 0.203 mmol, 81%): ^{1}H NMR (400 MHz, $CDCl_3$) δ 5.74 (br s, 1H, NH), 4.11 (br s, 1H, NH), 3.63 – 3.52 (m, 1H, CH), 2.64 – 2.50 (m, 2H, CH_2), 2.08 – 1.97 (m, 2H, CH_2), 1.70 (s, 15H, Cp*Me). ^{13}C NMR (101 MHz, $CDCl_3$) δ 184.2 (COO), 176.8 (COO), 84.0 (Cp*), 55.7 (CH), 32.4 (CH_2), 27.7 (CH_2), 9.0 (Cp*Me).

HRMS/ESI+ (m/z): [M+H]+ calcd for $C_{15}H_{24}[^{193}Ir]NO_4$ 475.1329; found 475.1343

Anal. Calcd for $C_{15}H_{23}ClIrNO_4$: C, 35.39; H, 4.55: Found; C, 35.91; H, 4.83

8.2.1.10. Synthesis of (Cp*)Ir(L-his)Cl (**1h)**

Following the general procedure: $[IrCp^*Cl_2]_2$ (0.100 g, 0.126 mmol), L-histidine (0.0409 g, 0.264 mmol), and sodium bicarbonate (0.0221 g 0.264 mmol) were reacted in methanol (30 mL) to give **1h** (0.0677 g, 0.131 mmol, 52%): ^{1}H NMR (400 MHz, CD_3OD) δ 8.13 (m, 1H, ArH), 7.11 (m, 1H, ArH), 6.36 (br s, 1H, NH), 5.99 (br s, 1H, NH), 4.18 (m 1H, αCH), 3.25 – 3.11 (m, 2H, CH_2), 1.76 (s, 15H, Cp*Me). ^{13}C NMR (101 MHz, CD_3OD) δ 185.0 (COO), 137.9 (ArC), 132.6 (ArC), 115.8 (ArC,) 85.4 (Cp*), 53.2 (αC), 26.7 (CH_2), 7.5 (Cp*Me). Single crystals suitable for X-ray diffraction were grown from slow diffusion of ether into dichloromethane.

HRMS/ESI+ (m/z): [M+H]+ calcd for $C_{16}H_{24}Cl[^{193}Ir]N_3O_2$ 518.1181; found 518.1171

Anal. Calcd for $C_{16}H_{23}ClIrN_3O_2 \bullet H_2O$: C, 35.92; H, 4.71: Found; C, 36.11; H, 4.78

8.2.1.11. Synthesis of (Cp*)Ir(D-his)Cl (**1i**)

Following the general procedure: $[IrCp^*Cl_2]_2$ (0.150 g, 0.189 mmol), D-histidine (0.120 g, 0.773 mmol), and KOH (0.0434 g, 0.773 mmol) were reacted in methanol (50 mL) to give **1i** (0.0800 g, 0.155 mmol, 41%): ^{1}H NMR (400 MHz, CD_3OD) δ 8.16 (m, 1H, ArH), 7.12 (s, 1H, ArH), 4.21 (br s, 1H, NH), 3.28 – 3.21 (m, 2H, CH_2), 1.77 (s, 15H, Cp*Me). ^{13}C NMR (101 MHz, CD_3OD) δ 185.1 (COO), 137.6 (ArC), 132.4 (ArC), 115.5 (ArC), 85.2 (Cp*), 53.2 (CH), 26.6 (CH_2), 7.6 (Cp*Me).

HRMS/ESI+ (m/z): [M+H]+ calcd for $C_{16}H_{24}Cl[^{193}Ir]N_3O_2$ 518.1181; found 518.1158

Anal. Calcd for $C_{16}H_{23}ClIrN_3O_2$: C, 37.10; H, 4.67: Found; C, 37.36; H, 5.10

8.2.1.12. Synthesis of (Cp*)Ir(L-ile)Cl (**1j**)

Following the general procedure: $[IrCp^*Cl_2]_2$ (0.150 g, 0.189 mmol), L-isoleucine (0.101 g, 0.773 mmol), and KOH (0.0434 g, 0.773 mmol) were reacted in methanol (30 mL) to give **1j** (0.107 g, 0.217 mmol, 58%) (mol ratio of diastereomers 50/50): ^{1}H NMR (400 MHz, Chloroform-*d*) δ 4.39 (br s, 1H, NH), 4.02 (brs, 1H, NH), 3.87 (brs, 1H, NH), 3.69 (br s, 1H, NH), 3.51 – 3.35 (m, 1H, αCH), 3.23 – 3.12 (m, 1H, αCH), 2.29 – 2.17 (m, 1H, CH), 2.17 – 2.08 (m, 1H, CH, 1H), 1.72 (s, 15H, Cp*Me), 1.70 (s, 15H, Cp*Me), 1.52 – 1.37 (m, 2H, CH_2), 1.20 – 1.06 (m, 2H, CH_2), 1.04 (d, *J* = 2.6 Hz, 3H, CH_3), 1.02 (d, *J* = 2.6 Hz, 3H, CH_3), 0.96 (t, *J* = 6.4 Hz, 3H, CH_3), 0.92 (t, *J* = 6.5 Hz, 3H, CH_3).

HRMS/ESI+ (*m/z*): [M+H]+ calcd for $C_{16}H_{26}[^{193}Ir]NO_2$ 458.162; found 458.1675

Anal. Calcd for $C_{16}H_{27}ClIrNO_2$; C, 38.98; H, 5.52, Found C, 38.88; H, 5.36

8.2.1.13. Synthesis of (Cp*)Ir(L-leu)Cl (**1k**)

Following the general procedure: $[IrCp^*Cl_2]_2$ (0.150 g, 0.189 mmol), L-leucine (0.101 g, 0.773 mmol), and KOH (0.0434 g, 0.773 mmol) were reacted in methanol (30 mL) to give **1k** (0.107 g, 58%): ^{1}H NMR (400 MHz, $CDCl_3$) δ 6.58 (br s, 1H, NH), 4.75 (br s, 1H, NH), 4.25 (br s, 1H, NH), 3.54 (br s, 1H, NH), 3.34 (s, 2H, 2xCHOO), 1.83 (dd, *J* = 10.0, 4.4 Hz, 4H, 2xCH_2), 1.69 (s, 30H, 2XCp*Me), 1.53 (m, 2H, 2x CH), 0.94 (dd, *J* = 17.4, 6.1 Hz, 12H, 4xCH3). ^{13}C NMR (101 MHz, $CDCl_3$) δ 184.0 (COO), 183.6 (COO), 84.0 (Cp*), 84.0 (Cp*), 55.0 (αC), 54.4 (αC), 44.5 (CH_2), 41.9 (CH_2), 24.7 (CH), 24.5 (CH), 23.4 (CH_3), 23.2 (CH_3), 21.56 (CH_3), 21.5 (CH_3), 9.2 (Cp*Me).

HRMS/ESI+ (*m/z*): [M+H]+ calcd for $C_{16}H_{26}[^{193}Ir]NO_2$ 458.162; found 458.1638

Anal. Calcd for $C_{16}H_{27}ClIrNO_2$: C, 38.98; H, 5.52. Found: C; 38.87, H; 5.51

8.2.1.14. Synthesis of (Cp*)Ir(L-met)Cl (**1l**)

Following the general procedure: $[IrCp^*Cl_2]_2$ (0.150 g, 0.189 mmol), L-methionine (0.101 g, 0.773 mmol), and KOH (0.0434 g, 0.773 mmol) were reacted in methanol (50 mL) to give **1l** (0.179 g, 0.351 mmol, 93%), (mol ratio of diastereomers 61/39): Major Isomer: ^{1}H NMR (400 MHz, CD_3OD) δ 4.09 (br s, 1H NH), 3.48 – 3.42 (m, 1H, CHOO), 3.27 – 3.21 (br s, 1H NH), 2.80 (s, 3H SCH_3), 2.62 – 2.56 (m, 2H CH_2), 2.09 – 2.02 (m, 1H C*H*H), 1.95 – 1.85 (m, 1H CH*H*), 1.75 (s, 15H Cp*Me). ^{13}C NMR (101 MHz, CD_3OD) δ 89.7 (Cp*), 54.8 (CH), 33.3 (CH_2), 28.6 (CH_2), 13.7 (SCH_3), 7.2 (Cp*Me). Minor Isomer: ^{1}H NMR (400 MHz, CD_3OD) δ 4.04 (d, *J* = 4.7 Hz, 1H NH*H*), 3.29 – 3.26 (m, 1H N*H*H), 2.94 (dt, *J* = 13.7, 6.7 Hz, 1H CHOO), 2.48 (s, 3H SCH_3), 2.39 (d, *J* = 6.4 Hz, 2H CH_2), 2.09 – 2.01 (m, 2H CH_2), 1.77 (S, 15H Cp*Me). ^{13}C NMR (101 MHz, CD_3OD) δ 89.66 (Cp*). Single crystals suitable for X-ray diffraction were grown from slow diffusion of hexanes into dichloromethane.

HRMS/ESI+ (*m/z*): $[M+NH_4]^+$ calcd for $C_{15}H_{28}[^{193}Ir]N_2O_2S$ 493.1495; found 493.1475

Anal. Calcd for $C_{15}H_{25}ClIrNO_2S$: C, 35.25; H, 4.93; Found: C, 35.01; H, 5.02

8.2.1.15. Synthesis of (Cp*)Ir(L-phe)Cl (**1m**)

Following the general procedure: $[IrCp^*Cl_2]_2$ (0.150 g, 0.189 mmol), L-phenylalanine (0.128 g, 0.773 mmol), and KOH (0.0434 g, 0.773 mmol) were reacted in methanol (50 mL) to give **1m** (0.175 88%), (mol ratio of diastereomers 69/31): Major Isomer: ^{1}H NMR (400 MHz, $CDCl_3$) δ 7.35 – 7.21 (m, 5H ArH), 4.40 – 4.22 (br s, 1H, NH), 4.07 – 3.94 (br s, 1H, NH), 3.92 – 3.79 (m, 1H, αCH)., 3.30 (dd, *J* = 14.3, 6.0 Hz, 1H C*H*H), 3.03 (dd, *J* = 14.3, 4.9 Hz, 1H CH*H*), 1.47 (s, 15H Cp*Me). ^{13}C NMR (101 MHz, $CDCl_3$) δ 129.7 (ArC), 129.4 (ArC), 129.3 (ArC), 83.9 (Cp*), 55.1 (αC), 38.4 (CH_2), 8.8 (Cp*Me). Minor Isomer: ^{1}H NMR (400 MHz, $CDCl_3$) δ 7.35 – 7.21 (m, ArH, 5H), 4.06 (br s, 1H NH), 3.57 (br s, 1H NH), 3.50 – 3.44 (m, 1H CHOO), 3.70 – 3.59 (m, 1H C*H*H), 3.46 –

3.34 (m, 1H CH*H*), 1.60 (s, 15H Cp*Me). ^{13}C NMR (101 MHz, $CDCl_3$) δ 84.2 (Cp*), 9.1 (Cp*Me). Single crystals suitable for X-ray diffraction were grown from slow diffusion of ether into dichloromethane.

HRMS/ESI+ (*m/z*): [M+H]+ calcd for $C_{19}H_{24}[^{193}Ir]NO_2$ 492.1464; found 492.1476

Anal. Calcd for $C_{19}H_{25}ClIrNO_2$: C, 43.3%; H, 4.78%. Found: C, 42.71%; H, 4.78% (While outside the normally acceptable range, all other analyses indicate a pure compound and the D-isomer made by the same procedure yields proper CH analysis.)

8.2.1.16. Synthesis of (Cp*)Ir(D-phe)Cl (**1n**)

Following the general procedure: $[IrCp^*Cl_2]_2$ (0.100 g, 0.126 mmol), D-phenylalanine (0.087 g, 0.514 mmol), and KOH (0.029 g, 0.514 mmol) were reacted in methanol (50 mL) to give **1n** (0.117g, 0.222 mmol, 88%), (mol ratio of diastereomers 70/30): Major Isomer: ^{1}H NMR (400 MHz, $CDCl_3$) δ 7.38 – 7.29 (m, 5H ArH), 4.59 (br s, 1H NH), 4.16 (br s, 1H NH), 3.64 – 3.54 (m, 1H CHOO), 3.38 (dd, *J* = 14.3, 5.7 Hz, 1H C*H*H), 3.11 (dd, *J* = 14.3, 4.7 Hz, 1H CH*H*), 1.53 (s, 15H Cp*Me). ^{13}C NMR (101 MHz, $CDCl_3$) δ 182.6 (COO), 136.4 (ArC), 129.9 (ArC), 129.5 (ArC), 127.7 (ArC), 84.1 (Cp*), 55.2 (αC), 38.5 (CH_2), 8.9 (Cp*Me). Minor Isomer: ^{1}H NMR (400 MHz, $CDCl_3$) δ 7.40 – 7.27 (m, 5H ArH), 3.50 – 3.44 (dd, J = 14.7, 3.57, 1H C*H*H), 3.03 (dd, *J* = 14.7, 9.2 Hz, 1H CH*H*), 1.66 (s, 15H Cp*Me). ^{13}C NMR (101 MHz, $CDCl_3$) δ 129.6 (ArC), 84.3 (Cp*), 9.3 (Cp*Me). Single crystals suitable for X-ray diffraction were grown from slow diffusion of ether into dichloromethane.

HRMS/ESI+ (*m/z*): [M+H]+ calcd for $C_{19}H_{24}[^{193}Ir]NO_2$ 492.1464; found 492.1476

Anal. Calcd for $C_{19}H_{25}ClIrNO_2$: C, 43.3%; H, 4.78%. Found: C; 43.56, H; 4.88

8.2.1.17. Synthesis of (Cp*)Ir(L-phengly)Cl (**1o**)

Following the general procedure: $[IrCp^*Cl_2]_2$ (0.100 g, 0.126 mmol), L-phenylglycine (0.043 g, 0.0287 mmol), and KOH (0.0211 g, 0.287 mmol) were reacted in methanol (30 mL) to give **1o** (0.107 g, 0.208 mmol, 83%) (mol ratio of diastereomers 52/48): Major Isomer: ^{1}H NMR (400 MHz, $CDCl_3$) δ 7.180 – 7.119 (m, 5H ArH), 6.50 (br s, 1H NH), 4.22 – 4.14 (m, 1H CHOO), 3.52 (br s, 1H NH), 1.63 (s, 15H Cp*Me). ^{13}C NMR (101 MHz, $CDCl_3$) δ 180.9 (COO), 140.7 (ArC), 129.3 (ArC), 128.9 (ArC), 128.0 (ArC), 84.3 (Cp*), 58.9 (αCH), 9.3 (Cp*Me). Minor Isomer: ^{1}H NMR (400 MHz, $CDCl_3$) δ 7.35 – 7.26 (m, 5H ArH), 4.71 (Br s, 1H NH), 4.52 – 4.45 (m, 1H CHOO), 4.11 (br s, 1H NH), 1.50 (s, 15H Cp*Me). ^{13}C NMR (101 MHz, $CDCl_3$) δ 181.5 (COO), 138.7 (ArC), 129.8 (ArC), 128.4 (ArC), 128.1 (ArC), 84.2 (Cp*), 61.0 (αCH), 9.1 (Cp*Me). Single crystals suitable for X-ray diffraction were grown from slow diffusion of hexanes into dichloromethane.

HRMS/ESI+ (*m/z*): [M+H]+ calcd for $C_{18}H_{23}NO_2[^{193}Ir]$ 478.1353; found 478.1389

Anal. Calcd for $C_{18}H_{23}ClIrNO_2$: C, 42.14%; H, 4.52%. Found: C; 42.23, H; 4.55

8.2.1.18. Synthesis of (Cp*)Ir(*N*-Me-L-phengly)Cl (**1p**)

Following the general procedure: $[IrCp^*Cl_2]_2$ (0.100 g, 0.126 mmol), N-methyl-L-phenylglycine (0.0474 g, 0.277 mmol), and sodium bicarbonate (0.0264 g, 0.277 mmol) were reacted in methanol (30 mL) to give **1p** (0.128 g, 96%) mol ratio of diastereomers (63/47): Major Isomer: ^{1}H NMR (400 MHz, $CDCl_3$) δ 7.39 – 7.21 (m, 5H, ArH), 4.62-4.45 (m, 1H, NH), 3.93 (d, *J* = 11.4 Hz, 1H, CH), 2.82 (d, *J* = 6.1 Hz, 3H, N-CH_3), 1.68 (s, 15H, Cp*Me). ^{13}C NMR (101 MHz, $CDCl_3$) δ 177.9 (COO), 137.3 (ArC), 129.2 (ArC) , 128.7 (ArC) , 128.7 (ArC), 84.8 (Cp*), 72.7 (αC), 41.2 (N-Me), 9.4 (Cp*Me). Minor Isomer: ^{1}H NMR (400 MHz, $CDCl_3$) δ 7.38 – 7.13 (m, 5H, ArH), 4.62-4.45 (m, NH, 1H), 4.33 (d, *J* = 10.4 Hz, 1H, CH), 2.76 (d, *J* = 5.7 Hz, 3H, N-CH_3), 1.65 (s, 15H, Cp*Me). ^{13}C NMR (101 MHz, $CDCl_3$) δ 180.2 (COO), 137.7 (ArC), 129.2 ArC, 129.0 (ArC), 128.5 (ArC), 84.1

(Cp*), 69.2 (αC), 38.9 (N-Me), 8.9 (Cp*Me). Single crystals suitable for X-ray diffraction were grown from slow diffusion of hexanes into dichloromethane

HRMS/ESI+ (m/z): calcd for $C_{19}H_{26}Cl[^{193}Ir]NO_2$ 528.1276; 528.1314

Anal. Calcd for $C_{19}H_{25}ClIrNO_2$: C, 43.3%; H, 4.78%. Found: C, 43.23%; H, 4.95%

8.2.1.19. Synthesis of (Cp*)Ir(L-Pro)Cl (**1q**)

Following the general procedure: $[IrCp^*Cl_2]_2$ (0.100 g, 0.126 mmol), L-proline (0.0434 g, 0.377 mmol), and KOH (0.0211g, 0.377 mmol) were reacted in methanol (30 mL) to give **1q** (0.107g, 0.224 mmol, 89%) (mol ratio of diastereomers 93/7): Major Isomer: ^{1}H NMR (400 MHz, $CDCl_3$) δ 4.64 (br s, 1H NH), 4.12 – 4.00 (m, 1H, CHOO), 3.64 – 3.53 (m, 1H NCH), 3.02 – 2.88 (m, 1H NCH), 2.31 – 2.19 (m, 1H C*H*H), 2.11 – 2.00 (m, 1H CH*H*), 1.98 – 1.87 (m, 1H C*H*H), 1.78 – 1.71 (m, 1H CH*H*), 1.67 (s, 15H Cp*Me). ^{13}C NMR (101 MHz, $CDCl_3$) δ 184.2 (COO), 84.2 (Cp*), 62.4 (αCH), 54.7 (CH_2), 28.7 (CH_2), 27.1 (CH_2), 9.2 (Cp*Me). Minor Isomer: ^{1}H NMR (400 MHz, $CDCl_3$) δ 6.73 (br s, 1H NH), 4.25 – 4.18 (m, 1H CHOO), 3.80 – 3.66 (m, 1H, NCH), 3.42 – 3.29 (m, 1H NCH), 3.27 – 3.21 (m, 1H CH), 2.11 – 1.99 (m, 2H, CH_2), 1.70 (s, 15H, Cp*Me). ^{13}C NMR (101 MHz, $CDCl_3$) δ 9.0 (CpMe). Single crystals suitable for X-ray diffraction were grown from slow diffusion of hexanes into dichloromethane

HRMS/ESI+ (*m/z*): [M+H]+ calcd for $C_{15}H_{24}Cl[^{193}Ir]NO_2$ 478.1119; found 478.113

Anal. Calcd for $C_{15}H_{23}ClIrNO_2$: C, 37.77; H, 4.86. Found: C, 37.79%; H, 5.06%

8.2.1.20. Synthesis of (Cp*)Ir(D-pro)Cl (**1r**)

Following the general procedure: $[IrCp^*Cl_2]_2$ (0.100 g, 0.126 mmol), D-proline (0.0434 g, 0.377 mmol), and KOH (0.0211 g, 0.377 mmol) were reacted in methanol (30 mL) to give **1r** (0.104 g, 0.217 mmol, 867%), (mol ratio of diastereomers 93/7): Major Isomer: ^{1}H NMR (400 MHz, $CDCl_3$) δ

4.71 (br s, 1H NH), 4.08 – 3.99 (m, 1H CHOO), 3.66 – 3.53 (m, 1H NCH), 3.02 – 2.87 (m, 1H NCH), 2.30 – 2.20 (m, 1H C*H*H), 2.09 – 2.00 (m, 1H CH*H*), 2.00 – 1.90 (m, 1H C*H*H), 1.81 – 1.71 (m, 1H CH*H*), 1.67 (s, 15H Cp*Me). ^{13}C NMR (101 MHz, $CDCl_3$) δ 184.2 (COO), 84.2 (Cp*), 62.3 (CH), 54.7 (CH_2), 28.7 (CH_2), 27.1 (CH_2), 9.2 (Cp*Me). Minor Isomer: ^{1}H NMR (400 MHz, $CDCl_3$) δ 6.79 (br s, 1H NH), 3.77- 3.67 (m, 1H CHOO), 3.28 – 3.17 (m, 1H NCH), 2.19 – 2.11 (m, 2H CH_2), 1.69 (s, 15H Cp*Me). ^{13}C NMR (101 MHz, $CDCl_3$) δ 83.8 (Cp*), 9.0 (Cp*Me).

HRMS/ESI+ (*m/z*): [M+H]+ calcd for $C_{15}H_{24}Cl[^{193}Ir]NO_2$ 478.1119; found 478.1117

Anal. Calcd. for $C_{15}H_{24}ClIrNO_2$: C, 37.69; H, 5.06. Found: C; 37.74, H; 5.08.

8.2.1.21. Synthesis of (Cp*)Ir(L-Trans-4-Hydroxy-pro)Cl (**1s**)

Following the general procedure: $[IrCp^*Cl_2]_2$ (0.100 g, 0.126 mmol), L-trans-4-hydroxy-proline (0.0702 g, 0.536 mmol), and KOH (0.0300 g, 0.535 mmol) were reacted in methanol (30 mL) to give 1s (0.110 g, 0.224 mmol, 89%), (mol ratio of diastereomers 73/27): Major: ^{1}H NMR (400 MHz, acetone) δ 5.40 (br s, 1H NH), 4.42 – 4.36 (m, 1H C*H*-OH), 4.06 – 3.98 (m, 1H CHOO), 3.64 (td, *J* = 11.9, 5.1 Hz, 1H NCH), 3.02 (td, *J* = 11.9, 3.3 Hz, 1H NCH), 2.10 – 2.07 (m, 2H CH_2), 1.68 (s, 15H Cp*Me). ^{13}C NMR (101 MHz, $CDCl_3$) δ 185.6 (COO), 84.3 (Cp*), 71.9 (C-O), 61.9 (αCH), 61.5 (CH), 38.2 (CH), 9.3 (Cp*Me). Minor Isomer: ^{1}H NMR (400 MHz, acetone) δ 7.00 (br s, 1H NH), 4.33 – 4.28 (m, 1H C*H*-OH), 4.18 – 4.09 (m, 2H NCH_2), 3.96 – 3.88 (m, 1H CHOO), 3.17 – 3.10 (m, 1H CH*H*), 2.25 – 2.15 (m, 2H CH_2), 1.71 (s, 15H Cp*Me). ^{13}C NMR (101 MHz, $CDCl_3$) δ 84.2 (Cp*), 9.1 (Cp*Me).

HRMS/ESI+ (*m/z*): [M+H]+ calcd for $C_{15}H_{24}Cl[^{193}Ir]NO_3$ 494.1068; found 494.1057

Anal. Calcd for $C_{15}H_{23}ClIrNO_3$: C, 36.54; H, 4.70; Found: C, 37.06; H, 4.86

8.2.1.22. Synthesis of (Cp*)Ir(L-Trans-4-F-pro)Cl (**1t**)

Following the general procedure: $[IrCp^*Cl_2]_2$ (0.100 g, 0.126 mmol), L-Trans-4-fluoro-proline (0.042 g, 0.314 mmol), and KOH (0.0176 g, 0.314 mmol) were reacted in methanol (30 mL) to give **1t** (0.0903 g 73%), (mol ratio of diastereomers 70/30): Major Isomer: ^{1}H NMR (400 MHz, $CDCl_3$) δ 5.24 (dm J = 52.1 Hz, 1H CF*H*) 4.98 – 4.88 (m, 1H NH), 4.38 – 4.28 (m, 1H, CHOO), 3.78 – 3.64 (m, 1H NCH), 3.10 – 2.90 (m, 1H NCH), 2.49 – 2.39 (m, 2H CH_2), 1.66 (s, 15H Cp*Me). ^{13}C NMR (101 MHz, $CDCl_3$) δ 183.1 (COO), 95.0 – 93.1 (d, J = 176.38, C-F), 84.4 (Cp*), 61.1 (αC), 59.6 (d, J = 21.5 Hz, C-C-F), 36.2 (d, J = 21.5 Hz, C-C-F), 9.21 (Cp*Me). Minor Isomer: ^{1}H NMR (400 MHz, $CDCl_3$) 7.24 – 7.15 (m, 1H NH), 5.14 (dm, J = 52.1 Hz), 4.28 – 4.21 (m, 1H CHOO), 4.12 – 3.90 (m, 1H NCH), 3.55 – 3.41 (m, 1H NCH), 2.39 – 2.28 (m, 2H CH_2), 1.68 (s, 15H Cp*Me). ^{13}C NMR (101 MHz, $CDCl_3$) δ 184.2 (COO), 84.1 (Cp*), 95.6 (d, J = 176.38 Hz C-F, 61.81 (αCH), 57.8 (d, *J* = 21.5 Hz **C**-C-F), 37.8 (d, *J* = 21.5 Hz **C**-C-F), 9.0 (Cp*Me). Single crystals suitable for X-ray diffraction were grown from slow diffusion of hexanes into dichloromethane

HRMS/ESI+ (*m/z*): [M+H]+ calcd for $C_{15}H_{23}ClF[^{193}Ir]NO_2$ 496.1025, Found 496.1

Anal. Calcd for $C_{15}H_{22}ClFIrNO_2$: C, 36.40%; H, 4.48%. Found: C, 36.18%; H, 4.35%

8.2.1.23. Synthesis of (Cp*)Ir(D-*N*-Me-pro)Cl (**1u**)

Following the general procedure: $[IrCp^*Cl_2]_2$ (0.1000 g, 0.126mmol), N-methyl-D-proline (0.0434 g (0.377 mmol), and KOH (0.0211g 0.377 mmol) were reacted in methanol (30 mL) to give **1u** (0.0895g, 72.6%): ^{1}H NMR (400 MHz, $CDCl_3$) δ 4.05 – 3.96 (m, 1H), 3.40 – 3.19 (m, 2H), 2.94 (s, 3H), 2.49 – 2.36 (m, 1H), 2.15 – 2.03 (m, 1H), 2.03 – 1.91 (m, 1H), 1.89 – 1.80 (m, 1H), 1.64 (s, 15H). ^{13}C NMR (101 MHz, $CDCl_3$) δ 182.9 (COO), 84.1 (Cp*), 71.8 (αCH), 63.6 (CH_2), 47.0 (NCH_3), 24.2 (CH_2), 22.4 (CH_2), 9.2 (Cp*Me). Single crystals suitable for X-ray diffraction were grown from slow diffusion of hexanes into dichloromethane

HRMS/ESI+ (*m/z*): [M+H]+ calcd for $C_{16}H_{26}[^{193}Ir]NO_2$ 457.1531; found 457.1542

Anal. Calcd. for $C_{16}H_{25}ClIrNO_2$: C, 39.14; H, 5.13. Found: C; 39.06, H; 5.22.

8.2.1.24. Synthesis of (Cp*)Ir(L-ser)Cl (**1v**)

Following the general procedure: $[IrCp^*Cl_2]_2$ (0.150 g, 0.188 mmol), L-serine (0.0813 g, 0.779 mmol), and KOH (0.0813 g, 0.773 mmol) were reacted in methanol (50 mL) to give 1v (0.151 g, 0.3229 mmol, 85.6%), (mol ratio of diastereomers 62/38): Major Isomer: ^{1}H NMR (400 MHz, DMSO-d_6) δ 5.32 (br s, 1H, NH), 5.06 (br s, 1H, Br), 3.67 – 3.51 (m, 3H, CHOO, CH_2), 1.59 (s, 15H, Cp*Me). ^{13}C NMR (101 MHz, $CDCl_3$) δ 181.6 (COO), 84.5 (Cp*), 63.1 (C-OH), 58.8 (αCH), 9.2 (Cp*Me). Minor Isomer: ^{1}H NMR (400 MHz, DMSO-*d*6) δ 6.26 (br s 1H NH), 4.93 – 4.76 (m, 1H, CHOO), 4.06 (br s, 1H NH), 3.27 – 3.12 (m, 2H, CH_2), 1.60 (s, 1H Cp*Me). ^{13}C NMR (101 MHz, $CDCl_3$) δ 183.5 (COO), 84.2 (Cp*), 62.1 (CH_2-OH), 57.4 (αCH), 9.0 (Cp*Me). Single crystals suitable for X-ray diffraction were grown from slow evaporation of dichloromethane

HRMS/ESI+ (*m/z*): [M+H]+ calcd for $C_{13}H_{21}[^{193}Ir]NO_3$ 433.1178; found 433.1178

Anal. Calcd for $C_{13}H_{21}ClIrNO_3$: C, 33.44; H, 4.53; Found: C, 33.37; H, 4.30

8.2.1.25. Synthesis of (Cp*)Ir(L-thr)Cl (**1w**)

Following the general procedure: $[IrCp^*Cl_2]_2$ (0.100 g, 0.126 mmol), L-threonine (0.061 g, 0.51 mmol), and KOH (0.029 g, 0.51 mmol) were reacted in methanol (30 mL) to give 1w (0.0918g, 0.1908 mmol, 76%), (mol ratio of diastereomers 72/28): Major Isomer: ^{1}H NMR (400 MHz, DMSO-d_6) δ 5.42 (br s, 1H, NH), 5.00 (d, *J* = 5.4 Hz, 1H, CHOO), 4.65 (br s, 1H, NH), 4.15 – 3.91 (m, 1H, O-CH), 1.59 (s, 15H, Cp*Me), 1.12 (d, *J* = 6.6 Hz, 3H, CH_3). ^{13}C NMR (101 MHz, DMSO-d_6) δ 181.9 (COO), 83.3 (Cp*), 66.4 (C-OH), 60.3 (αC), 21.3 (CH_3), 8.9 (Cp*Me).Minor Isomer: ^{1}H NMR (400 MHz, DMSO-*d*6) δ 5.98 (br s, 1H, NH), 4.88 (d, *J* = 5.0 Hz, 1H, CHOO), 2.94 (br s, 1H, NH),

2.91 – 2.82 (m, 1H, O-CH), 1.60 (s, 15H, Cp*Me), 1.15 (d, J = 6.7 Hz, 3H, CH_3). ^{13}C NMR (101 MHz, DMSO-d_6) δ 83.8 (Cp*), 9.0 (Cp*Me).

HRMS/ESI+ (*m/z*): [M+H]+ calcd for $C_{14}H_{24}[^{193}Ir]NO_3$ 482.1068; found 482.102

Anal. Calcd for $C_{14}H_{23}ClIrNO_3$: C, 34.96; H, 4.82; Found: C, 34.61; H, 4.74

8.2.1.26. Synthesis of (η^5-Cp)*Ir(L-val)Cl (**1x**)

Following the general procedure: $[IrCp^*Cl_2]_2$ (0.150 g, 0.188 mmol), L-valine (0.091 g, 0.773 mmol), and KOH (0.043 g, 0.773 mmol) were reacted in methanol (50mL) to give **1x** (0.145 g, 0.303 mmol, 80%) mol ratio of diastereomers 53/47: Major Isomer: ^{1}H NMR (400 MHz, $CDCl_3$) δ 4.01 (s, 1H, NH), 3.86 (s, 1H, NH), 3.27 – 3.12 (m, 1H, CHOO), 2.48 – 2.38 (m, 1H, CH-$(CH_3)_2$), 1.72 (s, 15H), 1.08 – 1.03 (m, 6H, 2CH_3, overlapping doublets). ^{13}C NMR (101 MHz, DMSO-*d6*) δ 182.4 (COO), 83.3 (Cp*), 61.7 (αCH), 31.3 (CH_2), 19.3 (CH_3), 17.4 (CH_3), 8.9 (Cp*Me). Minor Isomer: ^{1}H NMR (400 MHz, DMSO-*d6*) δ 6.05 – 5.95 (m, 1H, NH), 3.61 – 3.53 (m, 1H, NH), 3.02 – 2.93 (m, 1H, αCH), 2.12 – 2.04 (m, 1H C*H*-$(CH_3)_2$), 1.61 (s, 15H, Cp*Me), 0.93 – 0.90 (m, 3H, CH_3), 0.90 – 0.89 (m, 3H, CH_3). ^{13}C NMR (101 MHz, DMSO-*d6*) δ 180.2 (COO), 83.8 (Cp*), 60.1 (αCH), 31.1 (CH_2), 19.4 (CH_3), 17.2 (CH_3), 9.0 (Cp*Me). Single crystals suitable for X-ray diffraction were grown from slow evaporation of dichloromethane

HRMS/ESI+ (m/z): calcd for $C_{15}H_{25}NO_2[^{193}Ir]$ 445.1542; found 445.1564

Anal. Calcd for $C_{15}H_{25}ClIrNO_2$; C, 37.61; H, 5.26; Found: C, 37.34; H, 5.34

8.2.1.27. Synthesis of (Cp*)Ir(L-Aze)Cl (**1y**)

Following the general procedure: $[IrCp^*Cl_2]_2$ (0.100 g, 0.126 mmol), L-azetidine-2-carboxylic acid (0.0267g, 0.267 mmol), and sodium bicarbonate (0.0221 g, 0.267 mmol) were reacted in methanol (30 mL) to give **1y** (0.109 g, 0.236 mmol, 94%), mol ratio of diastereomers 93/7. (Cp*)Ir(L-Aze)Cl

was identified based on the following information: Major Isomer: ^{1}H NMR (400 MHz, $CDCl_3$) δ 5.46 (br s, 1H, NH), 4.53 – 4.40 (m, 1H, CHOO), 4.36 – 4.20 (m, 1H, N-CH), 3.91 – 3.81 (m, 1H, N-CH), 2.98 – 2.86 (m, 1H), C*H*H), 2.50 – 2.40 (m, 1H, CH*H*), 1.68 (s, 15H, Cp*me). ^{13}C NMR (101 MHz, $CDCl_3$) δ 185.8 (COO), 84.0 (Cp*), 60.6 (αCH), 51.0 (CH_2), 26.2 (CH_2), 9.0 (Cp*Me). Minor Isomer: ^{1}H NMR (400 MHz, $CDCl_3$) δ 6.99 (brs, 1H, NH), 4.88 – 4.77 (m, 1H, CHOO), 4.10 – 4.00 (m, 1H, N-CH*H*), 4.00 – 3.92 (m, 1H, N-C*H*H), 2.73 – 2.64 (m, 1H, CH*H*), 2.64 – 2.52 (m, 1H, C*H*H), 1.66 (s, 15H, Cp*Me). ^{13}C NMR (101 MHz, $CDCl_3$) δ 8.9 (Cp*Me). Single crystals suitable for X-ray diffraction were grown from slow evaporation of dichloromethane

HRMS/ESI+ (*m/z*): [M+H]+ calcd for $C_{14}H_{22}Cl[^{193}Ir]NO_2$ 464.0963; found 464.0952

Anal Calc for: $C_{14}H_{21}ClIrNO_2$; C, 36.32; H, 4.57; Found: C, 36.33; H, 4.78

8.2.1.28. Synthesis of (Cp*)Ir(L-pip)Cl (**1z**)

Following the general procedure: $[IrCp^*Cl_2]_2$ (0.100 g, 0.126 mmol), L-azetidine-2-carboxylic acid (0.0340 g, 0.267 mmol), and sodium bicarbonate (0.0221 g, 0.267 mmol) were reacted in methanol (30 mL) to give **1z** (0.115 g, 0.235 mmol, 94%) mol ratio of diastereomers (74/26): Major Isomer: ^{1}H NMR (400 MHz, $CDCl_3$) δ 3.92 – 3.80 (m, 1H, NH), 3.55 – 3.47 (m, 1H, N-CH*H*, 3.15 – 3.06 (m, 1H, CHOO), 3.06 – 2.94 (m, 1H, N-C*H*H), 2.28 – 2.20 (m, 1H, C*H*H), 2.03 – 1.93 (m, 1H, CH*H*), 1.86 – 1.79 (m, 2H, CH_2), 1.66 (s, 15H, Cp*Me), 1.58 – 1.46 (m, 4H, CH_2-CH_2). ^{13}C NMR (101 MHz, $CDCl_3$) δ 177.8 (COO) , 84.4 (Cp*), 66.2 (αCH), 53.7 (N-CH_2), 30.8 (CH_2), 27.8 (CH_2), 23.6 (CH_2), 9.3 (Cp*Me). Minor Isomer: ^{1}H NMR (400 MHz, $CDCl_3$) δ 5.03 – 4.92 (m, NH), 3.80 – 3.72 (m, 1H, CHOO), 3.28 – 3.15 (m, 2H, N-CH_2), 2.15 – 2.07 (m, 1H, CH*H*), 1.72 – 1.67 (m, 1H, C*H*H), 1.64 (s, 15H, Cp*Me), 1.46 – 1.37 (m, 4H, CH_2-CH_2). ^{13}C NMR (101 MHz, $CDCl_3$) δ 84.0 (Cp*), 62.5 (αCH), 53.4 (N-CH_2), 28.5 (CH_2), 26.8 (CH_2), 23.9 (CH_2), 8.9 (Cp*Me). Single crystals suitable for X-ray diffraction were grow from slow diffusion of ether into dichloromethane.

HRMS/ESI+ (m/z): calcd for $C_{16}H_{25}NO_2[^{193}Ir]$ 492.1276; found 492.1253

Anal Calc for: $C_{16}H_{25}ClIrNO_2$: C, 39.14; H, 5.13; Found: C, 39.26; H, 5.62

8.2.1.29. Synthesis of $[Cp^*Ir(gly)PF_6]_8$ (**1aa**)

To a RBF flask, 0.050g (0.114 mmol) of [(Cp*)Ir(gly)Cl] was added and dissolved in 20 mL of water. 0.042 g (0.12) mmol of thallium hexaflourophospate was added. The solution was stirred and a white precipitate formed over the course of 30 minutes. Solvent was removed and the product was extracted with dichloromethane and filtered. **1aa** was recrystallized with dichloromethane and hexanes to yield a yellow powder (0.362g, 58%): ^{1}H NMR (400 MHz, CD_3OD) δ 5.64 – 5.52 (m, 1H, NH), 5.41 – 5.27 (m, 1H, NH), 3.85 – 3.71 (m, 1H, C*H*H), 3.27 – 3.19 (m, 1H, CH*H*), 1.74 (s, 15H, Cp*Me). ^{13}C NMR (101 MHz, CD_3OD) δ 189.0 (CHOO), 84.3 (Cp*), 45.0 (αC), 8.3 (Cp*Me).

HRMS/ESI+ (m/z): calcd for $C_{12}H_{19}NO_2[^{193}Ir]$ 402.1045; found 402.0960

Anal. Calcd for $C_{96}H_{152}F_{48}Ir_8N_8O_{16}P_8$•2($C_6H_{14}$); C, 28.55; H, 3.99; Found: C, 29.19; H, 3.91. Hexanes from isolation are contained in the lattice. **1aa** was placed under a vacuum for 2 h at 110 °C prior to analysis.

8.2.2. Synthesis of HCp^{*R} ligands

Unless otherwise stated, all reactions were conducted under an N_2 atmosphere.

8.2.2.1. Synthesis of (2,3,4,5-tetramethylcyclopenta-2,4-dien-1-yl)benzene (**2a**)

To a stirred solution of 2,3,4,5-tetramethyl-2-cyclopentenone (2.00 g, 15.2 mmol) in anhydrous THF (20mL) was added a solution of phenylmagnesium bromide (6.4 mL of a 3.0 M solution 19.1 mmol) in THF. The mixture was refluxed for 3 h. Then cooled to 0 °C and quenched with HCl (20 mL of a

1.0M solution, 20 mmol). This solution was warmed to room temperature and agitated for 1 h. The mixture was diluted with diethyl ether (30 mL). The products were washed with water (30mL x 3), and the organic layer was dried over $MgSO_4$. The products were concentrated under reduced pressure, and purified by column chromatography (Silica gel, hexanes) to afford 2.0639g (69%) **2a** as an orange liquid.

Major Isomer: ^{1}H NMR (400 MHz, Chloroform-*d*) δ 7.38 – 7.28 (m, 2H), 7.25 – 7.14 (m, 3H), 3.19 (dddt, *J* = 9.3, 7.6, 5.8, 1.7 Hz, 1H), 2.02 (d, *J* = 1.8 Hz, 3H), 1.93 (d, *J* = 1.0 Hz, 3H), 1.86 (dt, *J* = 2.4, 1.1 Hz, 3H), 0.95 (d, *J* = 7.7 Hz, 3H). ^{13}C NMR (101 MHz, Chloroform-*d*) δ 142.70, 140.68, 137.14, 134.97, 128.42, 128.05, 125.35, 50.08, 14.72, 12.65, 11.90, 11.07.

HRMS/ESI+ (*m/z*): Cacld for $C_{15}H_{19}$ 199.1481; Found 199.1475

8.2.2.2. Synthesis of ((2,3,4,5-tetramethylcyclopenta-2,4-dien-1-yl)methyl)benzene (**2b**)

To a stirred solution of 2,3,4,5-tetramethyl-2-cyclopentenone (5.00 g, 36.2 mmol) in anhydrous THF (20 mL) was added a solution of benzylmagnesium bromide (45.3 mL of a 1.0 M solution 45.3 mmol) in THF. The mixture was refluxed for 4 h. Then cooled to 0 ℃ and quenched with HCl (15 mL of a 1.0M solution, 15 mmol). This solution was warmed to room temperature and agitated for 1 h. The mixture was diluted with diethyl ether (30 mL). The products were washed with water (30mL x 3), and the organic layer was dried over $MgSO_4$. The products were concentrated under reduced pressure, and purified by column chromatography (Silica gel, hexanes) to afford 7.12 g (93%) of **2b** as a yellow liquid.

Isomer 1: ^{1}H NMR (400 MHz, $CDCl_3$) δ 7.43 – 7.04 (m, 5H), 6.10 (s, 1H), 2.52 (q, *J* = 7.7 Hz, 2H), 1.90 (s, 3H), 1.61 (s, 3H), 1.06 (d, *J* = 2.3 Hz, 3H), 1.04 (d, *J* = 2.2 Hz, 3H).

Isomer 2: ^{1}H NMR (400 MHz, $CDCl_3$) δ 7.43 – 7.04 (m, 5H), 3.68 – 3.53 (m, 2H), 2.60 (q, *J* = 7.4 Hz, 1H), 1.80 (s, 6H), 1.79 (s, 3H), 1.75 (s, 3H).

Isomer 3: ^{1}H NMR (400 MHz, $CDCl_3$) δ 7.46 – 7.03 (m, 5H), 3.76 (d, *J* = 15.3 Hz, 1H), 3.44 (d, *J* = 15.2 Hz, 1H), 2.98 – 2.88 (m, 1H), 1.89 – 1.86 (m, 3H), 1.79 (d, *J* = 1.6 Hz, 3H), 1.76 – 1.74 (m, 3H), 0.98 (d, *J* = 7.6 Hz, 3H).

HRMS/ESI+ (*m/z*): Calcd for $C_{16}H_{21}$ 213.1638; Found 213.1635

8.2.2.3. Synthesis of 5-isopropyl-1,2,3,4-tetramethylcyclopenta-1,3-diene (**2c**)

To a stirred solution of 2,3,4,5-tetramethyl-2-cyclopentenone (2.5 0g, 18.1 mmol) in anhydrous THF (30 mL) was added a solution of isopropylmagnesium bromide (7.34 mL of a 2.9 M solution, 22.60 mmol) in THF. The mixture was refluxed for 24 h. The mixture was cooled to 0 °C and quenched with HCl (30 mL of a 1.0M solution, 30 mmol). This solution was then stirred for 1.5 h. The mixture was diluted with diethyl ether (30 mL). The organic phase was washed with water (30mL x 3), and the organic layer was dried over $MgSO_4$. The products were concentrated under reduced pressure and purified by column chromatography (Silica gel, hexanes) to afford 1.102 g (37 %) of **2c** as a yellow liquid.

HRMS/ESI+ (*m/z*): Calcd for $C_{12}H_{21}$ 165.1638; Found 165.1627

8.2.2.4. Synthesis of (2,3,4,5-tetramethylcyclopenta-2,4-dien-1-yl)cyclohexane (**2d**)

To a stirred solution of 2,3,4,5-tetramethyl-2-cyclopentenone (4.00 g, 28.9 mmol) in anhydrous THF (20 mL) was added a solution of octylmagnesium chloride (18.1 mL of a 2.0 M solution, 36.2 mmol) in THF. The mixture was refluxed for 2 h. The mixture was cooled to 0 °C and quenched with HCl

(40 mL of a 1.0M solution, 40 mmol). This solution was then stirred for 1 h. The mixture was diluted with diethyl ether (30 mL) and separated. The organic phase was washed with water (30mL x 3), and the organic layer was dried over $MgSO_4$. The products were concentrated under reduced pressure and purified by column chromatography (Silica gel, hexanes) to afford 4.83 g (71%) **2d** as a yellow liquid.

^{1}H NMR (400 MHz, Chloroform-*d*) δ 2.66 – 2.55 (m, 1H), 2.38 – 2.26 (m, 1H), 2.13 (dq, *J* = 26.6, 6.1, 5.2 Hz, 1H), 1.89 – 1.72 (m, 8H), 1.53 – 1.10 (m, 12H), 1.08 – 0.93 (m, 4H), 0.91 – 0.84 (m, 3H). ^{13}C NMR (101 MHz, Chloroform-*d*) δ 142.87, 138.88, 138.00, 135.48, 135.22 , 134.07, 133.72, 51.41, 49.36, 30.62 , 30.18, 27.80 , 26.24 , 25.79, 23.53, 22.65, 11.82, 11.58.

HRMS/ESI+ (*m/z*): Calcd for $C_{17}H_{31}$ 235.242; Found 235.2424

8.2.2.5. Synthesis of 1,2,3,4-tetramethyl-5-octylcyclopenta-1,3-diene (**2e**)

To a stirred solution of 2,3,4,5-tetramethyl-2-cyclopentenone (4.00 g, 28.9 mmol) in anhydrous THF (20 mL) was added a solution of octylmagnesium chloride (18.1 mL of a 2.0 M solution, 36.2 mmol) in THF. The mixture was refluxed for 2 h. The mixture was cooled to 0 °C and quenched with HCl (40 mL of a 1.0M solution, 40 mmol). This solution was then stirred for 1 h. The mixture was diluted with diethyl ether (30 mL) and separated. The organic phase was washed with water (30mL x 3), and the organic layer was dried over $MgSO_4$. The products were concentrated under reduced pressure and purified by column chromatography (Silica gel, hexanes) to afford 4.83 g (72 %) **2e** as a yellow liquid.

^{1}H NMR (400 MHz, Chloroform-*d*) δ 2.66 – 2.55 (m, 1H), 2.38 – 2.26 (m, 1H), 2.13 (dq, *J* = 26.6, 6.1, 5.2 Hz, 1H), 1.89 – 1.72 (m, 8H), 1.53 – 1.10 (m, 12H), 1.08 – 0.93 (m, 4H), 0.91 – 0.84 (m,

3H). ^{13}C NMR (101 MHz, Chloroform-*d*) δ 142.87, 138.88, 138.00, 135.48, 135.22 , 134.07, 133.72, 51.41, 49.36, 30.62 , 30.18, 27.80 , 26.24 , 25.79, 23.53, 22.65, 11.82, 11.58.

HRMS/ESI+ (*m/z*): Calcd for $C_{17}H_{31}$ 235.242; Found 235.2424

8.2.2.6. Synthesis of 1,2,3,4-tetramethylcyclopenta-5-dodecyl-1,3-diene (**2f**)

To a stirred solution of 2,3,4,5-tetramethyl-2-cyclopentenone (2.00 g, 14.5 mmol) in anhydrous THF (20 mL) was added a solution of dodecylmagnesium chloride (21.75 mL of a 1.0 M solution, 21.75 mmol). The mixture was refluxed for 4 h. The mixture was cooled to 0 °C and quenched with HCl (25 mL of a 1.0 M solution, 25 mmol). The organic products were extracted from the aqueous phase with ether, (3 x 20 mL). The organic layer was dried over $MgSO_4$ and filtered. The organic layer was concentrated under reduced pressure and purified by column chromatohraphy (Silica gel, hexanes) to afford a yellow liquid. Excess dodecane was removed via short path distillation under reduced pressure, with the residue being subjected to column chromatohraphy (Silica gel, hexanes) **2f** as a yellow liquid.

HRMS/ESI+ (*m/z*): Calcd for $C_{21}H_{39}$ 291.3046; Found 291.3071

8.2.3. Synthesis of Iridium Cp*-Phenyl (aa) Cl complexes

8.2.3.1. Synthesis of $(Cp^{*Ph})IrCpCl_2]_2$ (**3a**)

0.200g (0.569 mmol) of $IrCl_3$ x $3H_2O$ was combined with **2a** (0.135 g 0.683 mmol) in methanol (1mL) in a microwave pressure tube. The reaction mixture was heated to 115 °C at 150 watts and 88 psi and held there fo1r 30 minutes. Upon cooling, an orange powder formed and was collected by filtration. This orange powder was washed with cold methanol and hexanes to give **3a** 0.119 g (45 %). ^{1}H NMR (400 MHz, $CDCl_3$) δ 7.62 – 7.53 (m, 2H), 7.4. – 7.32 (m, 3H), 1.72 (s, 6H), 1.63 (s, 6H). ^{13}C NMR (101 MHz, $CDCl_3$) δ 130.18, 129.79, 128.62, 128.42, 93.43, 85.48, 10.33, 9.60.

HRMS/ESI+ (*m/z*): Calcd for C_{30} H_{34} [193Ir]$_2$ Cl_3 885.0979; Found 885.1018

Anal calc. for $C_{30}H_{34}Cl_4Ir_2$, C, 39.13; H 3.72; Found, C 38.07; H, 3.65

8.2.3.2. Synthesis of (Cp*^{Ph})Ir(L-ala)Cl (**3b**)

Following the general procedure: 0.100 g (0.109 mmol) of **3a** was combined with 0.0203 g (0.228 mmol) of L-alanine and 0.0192 g (0.228 mmol) of sodium bicarbonate in methanol (30 mL) to give **3b** as a yellow solid, 0.0578 g (52% yield): Major Isomer: ^{1}H NMR (400 MHz, Chloroform-*d*) δ 7.51 – 7.43 (m, 2H, ArH), 7.39 – 7.30 (m, 3H, ArH), 6.23 (br s, 1H, NH), 3.54 (br s, 1H, NH), 3.47 – 3.33 (m, 1H, αCH), 1.69 (s, 6H, $(CpMe)_2$), 1.67 (s, 3H, CpMe), 1.65 (s, 3H, CpMe), 1.43 (d, *J* = 6.9 Hz, 3H, CH_3). ^{13}C NMR (101 MHz, Chloroform-*d*) δ 182.70 (COO), 130.43 (ArC), 130.29 (ArC), 128.84 (ArC), 128.75 (ArC), 91.97 (CpC), 91.45 (CpC), 82.92 (CpC), 82.83 (CpC), 81.94 (CpC), 53.04, (CH), 21.61, CH_3, 10.04 (CpMe), 9.89 (CpMe), 9.35 (CpMe), 9.26 (CpMe). Minor Isomer: ^{1}H NMR (400 MHz, Chloroform-*d*) δ 7.52 – 7.43 (m, 2H, ArH), 7.40 – 7.30 (m, 3H, ArH), 4.48 (d, *J* = 6.3 Hz, 2H, NH_2), 3.45 – 3.35 (m, 1H, CH), 1.82 (s, 3H, CpMe), 1.80 (s, 3H, CpMe), 1.77 (s, 3H, CpMe), 1.77 (s, 3H, CpMe), 1.34 (d, *J* = 7.2 Hz, 3H, CH_3). ^{13}C NMR (101 MHz, Chloroform-*d*) δ 184.44 (COO), 130.72 (ArC), 130.54 (ArC), 128.48 (ArC), 128.34 (ArC), 92.53 (CpC), 91.70 (CpC), 82.33 (CpC), 81.50 (CpC), 81.31 (CpC), 51.50 (CH), 19.86 (CH_3), 9.97 (CpMe), 9.94 (CpMe), 9.35 (CpMe), 9.15 (CpMe).

HRMS/ESI+ (*m/z*): Calcd for $C_{18}H_{23}$[^{193}Ir]NO_2; 478.1358; Found 478.1391

Anal calc. for $C_{18}H_{23}ClIrNO_2 \cdot H_2O$, C, 40.71; H, 4.74: Found C, 40.62; H, 4.47

8.2.3.3. Synthesis of (Cp*^{Ph})Ir(L-Phenylglycine)Cl (**3c)**

Following the general procedure: 0.100 g (0.109 mmol) of **3a** was combined with 0.0345 (0.228 mmol) of L-phenylglycine and 0.0192 g (0.228 mmol) of sodium bicarbonate with methanol (30 mL)

to give **3c** as a yellow solid, 0.1176 g (94.2% yield): Major Isomer: ^{1}H NMR (400 MHz, Acetone-d_6) δ 7.69 – 7.61 (m, 2H, ArH), 7.43 – 7.36 (m, 3H, ArH), 7.36 – 7.22 (m, 5H, ArH), 6.98 – 6.84 (m, 1H, NH), 4.42 – 4.29 (m, 1H, αCH), 4.16 – 4.03 (m, 1H, NH), 1.89 (s, 3H, CpMe), 1.78 (s, 3H, CpMe), 1.73 (s, 3H, CpMe), 1.69 (s, 3H, CpMe). ^{13}C NMR (101 MHz, DMSO-d_6) δ 181.61 (COO), 140.56 (ArC), 131.66 (ArC), 131.02 (ArC), 129.44 (ArC), 128.73 (ArC), 128.54 (ArC), 128.38 (ArC), 127.94 (ArC), 92.14 (CpMe), 90.72 (CpMe), 83.07 (CpMe), 81.29 (CpMe), 81.06 (CpMe), 59.40 (CH), 9.14 (CpMe), 9.05 (CpMe), 8.94 (CpMe). Minor Isomer: ^{1}H NMR (400 MHz, Acetone-d_6) δ 7.71 – 7.61 (m, 2H, ArH), 7.43 – 7.36 (m, 3H, ArH), 7.36 – 7.22 (m, 5H, ArH), 5.54 – 5.42 (m, 1H, NH), 5.32 – 5.18 (m, 1H, NH), 4.63 – 4.53 (m, 1H, αCH), 1.74 (s, 3H, CpMe), 1.72 (s, 3H, CpMe), 1.66 (s, 3H, CpMe), 1.65 (s, 3H, CpMe). ^{13}C NMR (101 MHz, DMSO-d_6) δ 181.61 (COO), 141.54 (ArC), 131.64 (ArC), 131.05 (ArC), 129.14 (ArC), 128.84 (ArC), 128.66 (ArC), 128.45 (ArC), 92.08 (CpC), 90.28 (CpC), 82.52 (CpC), 81.65 (CpC), 80.72(CpC), 60.68 (CH), 10.11 (CpMe), 9.88 (CpMe), 9.79 (CpMe), 9.73 (CpMe).

HRMS/ESI+ (*m/z*): Cacld for $C_{23}H_{25}Cl[^{193}Ir]Cl$; 575.1198; Found 575.1238

Anal calc. for $C_{23}H_{25}ClIrNO_2 \bullet H_2O$, C, 46.57; H, 4.59: Found C, 46.91; H, 4.41

8.2.3.4. Synthesis of (Cp*^{Ph})Ir(L-Phenylalanine)Cl (**3d**)

Following the general procedure: 0.100 g (0.109 mmol) of **3a** was combined with 0.0377 (0.228 mmol) of L-phenylalanine and 0.0192g (0.228 mmol) of sodium bicarbonate in methanol (30 mL) to give **3d** as a yellow solid, 0.0550 g (43% yield): Major Isomer: ^{1}H NMR (400 MHz, $CDCl_3$) δ 7.46 – 7.19 (m, 8H, ArH), 7.18 – 7.10 (m, 2H, ArH), 4.12 (br s, 1H, NH), 3.98 – 3.84 (m, 1H, αCH), 3.76 (br s, 1H, NH), 3.24 (dd, *J* = 14.4, 6.6 Hz, 1H, C*H*H), 3.06 (dd, *J* = 14.4, 5.2 Hz, 1H, CH*H*), 1.63 (s, 3H, CpMe), 1.62 (s, 3H, CpMe), 1.58 (s, 3H, CpMe), 1.49 (s, 3H, CpMe). ^{13}C NMR (101 MHz, $CDCl_3$) δ 182.42 (COO), 135.87 (ArC), 130.08 (ArC), 129.70 (ArC), 129.34 (ArC), 129.22 (ArC),

128.92 (ArC), 128.47 (ArC), 127.49 (ArC), 90.57 (CpC), 89.89 (CpC), 84.30 (CpC), 81.92 (CpC), 81.42 (CpC), 55.03 αC, 38.47, CH_2, 9.66 (CpMe), 9.58 (CpMe), 8.81 (CpMe), 8.79 (CpMe). Note* significant overlap is observed between benzyl protons in the spectra. Minor Isomer: ^{1}H NMR (400 MHz, $CDCl_3$) δ 7.44 – 7.19 (m, 8H, ArH), 7.18 – 7.10(m, 2H, ArH), 4.43 – 4.24 (m, 1H, NH), 3.71 – 3.61 (m, 1H, NH), 3.57 – 3.48 (m, 1H, αCH), 3.00 (d, *J* = 9.9 Hz, 1H, CH*H*), 1.77 (s, 3H, CpMe), 1.75 (s, 3H, CpMe), 1.67 (s, 3H, CpMe), 1.63 (s, 3H, CpMe). ^{13}C NMR (101 MHz, $CDCl_3$) δ 180.32 (COO), 136.88 (ArC), 130.27 (ArC), 130.06 (ArC), 129.40 (ArC), 129.17 (ArC), 129.10 (ArC), 128.58 (ArC), 91.10 (CpC), 90.59 (CpC), 83.80 (CpC), 82.32 (CpC), 58.44 αC, 40.73 CH_2, 9.95 (CpMe), 9.80 (CpMe), 9.17 (CpMe), 9.09 (CpMe).

HRMS/ESI+ (*m/z*): Calcd for C_{24} H_{27} N O_2 [^{193}Ir] 554.1666; Found 554.1632

8.2.3.5. Synthesis of (Cp*^{Ph})Ir(L-Proline)Cl (**3e**)

Following the general procedure: 0.100 g (0.109 mmol) of **3a** was combined with 0.0281 (0.244 mmol) of L-proline and 0.0205g (0.244 mmol) of sodium bicarbonate in methanol (30 mL) to give **3e** as a yellow solid, 0.1102 g (94.1% yield): Major Isomer:^{1}H NMR (400 MHz, Chloroform-*d*) δ 7.47 – 7.41 (m, 2H, ArH), 7.40 – 7.33 (m, 3H, ArH), 4.79 – 4.65 (m, 1H, NH), 4.11 – 3.98 (m, 1H, αCH), 3.31 – 3.20 (m Hz, 1H N-CH), 2.75 – 2.62 (m, 1H, N-CH), 2.25 – 2.14 (m, 1H, CH*H*), 2.04 – 1.92 (m, 1H, C*H*H), 1.77 (s, 3H, CpMe), 1.75 (s, 3H, CpMe), 1.74 (s, 3H, CpMe), 1.66 (s, 3H, CpMe), 1.65 – 1.54 (m, 2H, CH_2). ^{13}C NMR (101 MHz, $CDCl_3$) δ 184.45 (COO), 130.52 (ArC), 130.10 (ArC), 128.88 (ArC), 128.51 (ArC), 91.44 (CpC), 91.12 (CpC), 85.38 (CpC), 80.90 (CpC), 80.68 (CpC), 62.54 (αC), 54.53 (N-C), 29.09 (CH_2), 26.94 (CH_2), 10.52 (CpMe), 9.68 (CpMe), 9.16 (CpMe), 9.09 (CpMe). Minor Isomer:^{1}H NMR (400 MHz, $CDCl_3$) δ 1.79 (s, 3H, CpMe), 1.68 (s, 3H, CpMe), 1.67 (s, 3H, CpMe). (significant overlap with major isomer obscures other peaks).

HRMS/ESI+ (*m/z*): Calcd for $C_{20}H_{26}NO_2[^{193}Ir]Cl$ 540.1276; Found 540.1231

Anal calc. for $C_{20}H_{25}ClIrNO_2 \bullet H_2O$; C, 43.12; H, 4.88: found C, 43.52; H, 4.88

8.2.3.6. Synthesis of (Cp^{*Ph})Ir(L-piperidine-2carboxylic acid)Cl (**3f**)

Following the general procedure: 0.100 g (0.109 mmol) of 3a was combined with 0.0295 (0.228 mmol) of L-pipecolic acid and 0.0192 g (0.228 mmol) of sodium bicarbonate in methanol (30 mL) to give **3f** as a yellow solid, 0.1133 g (94.3% yield): Major Isomer:^{1}H NMR (400 MHz, CDCl3) d 7.54–7.47 (m, 2H, ArH), 7.41–7.32 (m, 3H, ArH), 4.00 (br s, 1H, NH), 3.46–3.33 (m, 1H, N-CH), 3.09 (td, J = 11.8, 3.1 Hz, 1H, aCH), 2.82 (qd, J = 12.4, 3.1 Hz, 1H, NCH), 2.28–2.13 (m, 1H, CHH), 2.08–1.83 (m, 1H, CHH), 1.77 (s, 3H, CpMe), 1.73 (s, 3H, CpMe), 1.68 (s, 3H, CpMe), 1.65 (s, 3H, CpMe), 1.58–1.38 (m, 4H, CH_2–CH_2) ppm. ^{13}C NMR (101 MHz, $CDCl_3$) d 177.93 (COO), 130.34 (ArC), 130.28 (ArC), 128.79 (ArC), 128.46 (ArC), 94.89 (CpC), 93.02 (CpC), 82.46 (CpC), 81.44 (CpC), 79.33 (CpC), 66.15 (aC), 53.27 (N–C), 30.83 (CH_2), 27.71 (CH_2), 23.57 (CH_2), 10.56 (CpMe), 10.05 (CpMe), 9.38 (CpMe), 9.13 (CpMe)ppm. Minor Isomer: ^{1}H NMR (400 MHz, $CDCl_3$) d 7.56–7.47 (m, 2H, ArH), 7.40–7.31 (m, 3H, ArH), 4.36 (br s, 1H, NH), 3.90–3.76 (m, 1H, N-CH), 3.30–3.16 (m, 1H, N-CH), 3.04–2.94 (m, 1H, aCH), 2.28–2.13 (m, 1H, CHH), 2.00–1.92 (m, 1H, CHH), 1.75 (s, 3H, CpMe), 1.70 (s, 3H, CpMe), 1.69 (s, 3H, CpMe), 1.64 (s, 3H, CpMe), 1.57–1.38 (m, 4H, CH_2–CH_2) ppm. ^{13}C NMR (101 MHz, $CDCl_3$) 180.92 (COO), 130.73 (ArC), 130.14 (ArC), 128.46 (ArC), 128.32 (ArC), 91.96 (CpC), 83.64 (CpC), 81.42 (CpC), 62.48 (aC), 52.24 (N–C), 31.53 (CH_2), 29.00 (CH_2), 23.70 (CH_2), 9.70 (CpMe), 9.55 (CpMe), 8.90 (CpMe), 8.74 (CpMe) ppm.

HRMS/ESI+ (*m/z*): Calcd for $C_{21}H_{27}O_2[^{193}Ir]$ 518.1666; Found 518.1677

Anal calc. for $C_{21}H_{27}ClIrNO_2 \bullet CH_2Cl_2$; C, 41.48; H, 4.58: Found C, 40.63; H, 4.50

8.2.4. Synthesis of Iridium Cp*-Benzyl (aa) Cl complexes

8.2.4.1. Synthesis of $[(Cp^{*Bn})IrCpCl_2]_2$ (**4a**)

1.00 g (2.84 mmol) of $IrCl_3$ x $3H_2O$ was combined with 2b 0.9033g (4.25 mmol) in methanol (30 mL) in a 100 mL Schlenk flask. The reaction was refluxed for 48 h. Upon cooling, an orange powder formed and was collected by filtration. This orange powder was washed with cold methanol and hexanes (0.354 g). Solvent was removed to half volume and the flask was stored overnight with refrigeration and a second crop of crystals were collected (0.188 g) for a combined yield of 0.5421 g of **4a** (42 %, 0.571 mmol). ^{1}H NMR (400 MHz, $CDCl_3$) δ 7.29 – 7.24 (m, 4H, ArH), 7.22 – 7.16 (m, 2H, ArH), 7.12 – 7.05 (m, 4H, ArH), 3.55 (s, 4H, $(CH_2)_2$), 1.63 (s, 12H, $(CpMe)_2$), 1.61 (s, 12H, $(CpMe)_2$). ^{13}C NMR (101 MHz, $CDCl_3$) δ 136.79 (ArC), 128.70 (ArC), 128.21 (ArC), 126.73 (ArC), 87.52 (CpC), 86.76 (CpC), 85.80 (CpC), 30.41 (CH_2), 9.78 (CpMe), 9.35 (CpMe).

HRMS/ESI+ (*m/z*): Calcd for $C_{32}H_{38}Cl_3Ir_2$ 913.1298; Found 913.1347

Anal calc. for $C_{32}H_{38}Cl_4Ir_2$; C, 40.50; H, 4.04: Found; C, 40.40; H, 3.98

8.2.4.2. Synthesis of (Cp^{*Bn})Ir(L-phenylalanine)Cl (**4b**)

0.100 g (0.105 mmol) of **4a** was combined with 0.0360 g (0.221 mmol) of L-phenylalanine and 0.0186 g (0.221 mmol) of sodium bicarbonate with methanol (20 mL) to give **4b** as a yellow solid, 0.119 g (93% yield, 0.197 mmol): Major Isomer: ^{1}H NMR (400 MHz, Chloroform-*d*) δ 7.40 – 7.25 (m, 6H, ArH), 7.24 – 7.21 (m, 2H, ArH), 7.05 – 7.01 (m, 2H, ArH), 4.30 (br s, 1H, NH), 4.01 (br s, 1H, NH), 3.94 – 3.83 (m, 1H, αCH), 3.40 (dd, *J* = 14.2, 6.1 Hz, 1H, CH*H*), 3.33 – 3.21 (m, 2H, CH_2), 3.10 (dd, *J* = 14.2, 5.2 Hz, 1H, C*H*H), 1.57 (s, 3H, CpMe), 1.55 (s, 3H, CpMe), 1.54 (s, 3H, CpMe), 1.53 (s, 3H, CpMe). ^{13}C NMR (101 MHz, Chloroform-*d*) δ 182.76 (COO), 137.16 (ArC), 136.20 (ArC), 129.90 (ArC), 129.28 (ArC), 128.72 (ArC), 128.09 (ArC), 126.77 (ArC), 86.17 (CpC), 85.68

(CpC), 84.39 (CpC), 83.81 (CpC), 83.17 (CpC), 55.06 (αC), 38.47 (Cp-***C***H_2-Ar), 29.71 (CH_2), 9.16 (CpMe), 8.82 (CpMe). Minor Isomer: ^{1}H NMR (400 MHz, $CDCl_3$) δ 7.42 – 7.25 (m, 6H, ArH), 7.24 – 7.13 (m, 2H, ArH), 7.10 – 7.06 (m, 2H, ArH), 5.11 (br s, 1H, NH), 3.71 – 3.58 (m, 1H, NH), 3.62 – 3.51 (m, 1H, αCH), 3.46 (s, 2H, CH_2), 1.71 (s, 3H, CpMe), 1.69 (s, 3H, CpMe), 1.68 (s, 3H, CpMe), 1.67 (s, 3H, CpMe). ^{13}C NMR (101 MHz, $CDCl_3$) δ 136.77 (ArC), 137.13 (ArC), 129.58 (ArC), 129.10 (ArC), 128.70 (ArC), 128.19 (ArC), 127.53 (ArC), 85.63 (CpC), 84.66 (CpC), 84.16 (CpC), 58.49 (αC), 40.45(CH_2), 30.03 (Cp-***C***H_2-Ar), 9.49 (CpMe), 9.12 (CpMe).

HRMS/ESI+ (*m/z*): Calcd for $C_{25}H_{29}ClIrNO_2$; 603.1511: Found 603.1597

Anal calc. for $C_{25}H_{29}ClIrNO_2$; C, 49.78; H, 4.85: Found C, 50.01; H, 5.04

8.2.4.3. Synthesis of (Cp*^{Bn})Ir(L-proline)Cl (**4c**)

Following the general procedure: 0.100 g (0.105 mmol) of **4a** was combined with 0.0255 (0.221 mmol) of L-proline and 0.0186g (0.221 mmol) of sodium bicarbonate in round bottom flask with methanol (20 mL) to give **4c** as a yellow solid, 0.1032 g (89% yield, 0.187 mmol): Major Isomer: ^{1}H NMR (400 MHz, $CDCl_3$) δ 7.30 – 7.25 (m, 2H, ArH), 7.23 – 7.16 (m, 1H, ArH), 7.13 – 7.05 (m, 3H, ArH), 4.92 (br s, 1H, NH), 4.10 – 3.98 (m, 1H, N-CH), 3.63 – 3.56 (m, 1H, N-CH), 3.49 (s, 2H, CH_2), 2.93 (qd, *J* = 11.0, 5.8 Hz, 1H, CH***H***), 2.32 – 2.18 (m, 2H, CH_2), 2.17 – 1.81 (m, 2H, CH_2), 1.70 (s, 3H CpMe), 1.69 (s, 3H CpMe), 1.67 (s, 3H CpMe), 1.67 (s, 3H, CpMe). ^{13}C NMR (101 MHz, Chloroform-*d*) δ 184.55 (COO), 137.02 (ArC), 128.75 (ArC), 128.10 (ArC), 126.79 (ArC), 86.25 (CpC), 85.71 (CpC), 84.41 (CpC), 84.36 (CpC), 83.73 (CpC), 62.53 (N-C), 54.98 (αC), 30.14 (Cp-***C***H_2-Ar), 28.79 (CH_2), 27.12 (CH_2), 9.64 (CpMe), 9.55 (CpMe), 9.29 (CpMe), 9.23 (CpMe).

Minor Isomer: ^{1}H NMR (400 MHz, $CDCl_3$) δ 1.73 (s, 3H, CpMe), 1.72 (s, 3H, CpMe), 1.71 (s, 3H, CpMe).

HRMS/ESI+ (*m/z*): Calcd for $C_{21}H_{28}Cl[^{193}Ir]NO_2$; 554.1432: Found 554.1431

Anal calc. for $C_{21}H_{27}ClIrNO_2 \bullet CH_2Cl_2$; C, 41.41; H, 4.58: Found C, 41.27; H, 4.74

8.2.4.4. Synthesis of (Cp^{*Bn})Ir(L-piperdine-2-carboxylic acid)Cl (**4d**)

Following the general procedure: 0.100 g (0.105 mmol) of **4a** was combined with 0.0224 g (0.221 mmol) of L-pipecolic acid and 0.0186g (0.221 mmol) of sodium bicarbonate in round bottom flask with methanol (20 mL) to give **4d** as a yellow solid, 0.110 g (92% yield, 0.194 mmol): Major Isomer: ^{1}H NMR (400 MHz, Chloroform-*d*) δ 7.31 – 7.25 (m, 2H, ArH), 7.24 – 7.17 (m, 1H, ArH), 7.10 – 7.04 (m, 3H, ArH), 3.92 (br s, 1H, NH), 3.61 – 3.50 (m, 1H, N-CH), 3.48 (s, 2H, CH_2), 3.18 – 3.10(m, 1H, αCH), 2.30 – 2.20 (m, 1H, N-CH), 2.03 – 1.91 (m, 1H, CH*H*), 1.88 – 1.75 (m, 2H, CH_2), 1.69 (s, 3H, CpMe), 1.69 (s, 3H CpMe), 1.68 (s, 3H CpMe), 1.67 (s, 3H, CpMe), 1.59 – 1.37 (m, 4H, CH_2-CH_2). ^{13}C NMR (101 MHz, $CDCl_3$) δ 177.76 (COO), 136.72 (ArC), 128.82 (ArC), 127.99 (ArC), 126.91 (ArC), 86.35 (CpC), 86.20 (CpC), 84.76 (CpC), 84.25 (CpC), 83.96 (CpC), 66.39 (N-C), 53.85 (αC), 30.79 (CH_2), 30.29 (Cp-***C***H_2-Ar), 27.82 (CH_2), 23.62 (CH_2), 9.73 (CpMe), 9.65 (CpMe), 9.36 (CpMe).

Minor Isomer: ^{1}H NMR (400 MHz, $CDCl_3$) δ 7.32 – 7.25 (m, 2H, ArH), 7.24 – 7.17 (m, 1H, ArH), 7.15 – 7.11 (m, 2H, ArH), 3.82 – 3.71 (m, 1H, N-C*H*), 3.45 – 3.37 (m, 1H, αCH), 3.10 – 2.97 (m, N-CH), 2.13 – 2.05 (m, 1H, CH*H*), 1.72 (s, 3H, CpMe), 1.67 (s, 3H, CpMe), 1.64 (s, 3H, CpMe), 1.59 – 1.38 (m, 4H, CH_2-CH_2). ^{13}C NMR (101 MHz, $CDCl_3$) δ 128.90 (ArC), 128.48 (ArC), 9.25 (CpMe).

HRMS/ESI+ (*m/z*): Calcd for $C_{22}H_{29}[^{193}Ir]NO_2$; 532.1822: Found 532.1830

Anal calc. for $C_{22}H_{29}IrNO_2 \bullet H_2O$; C, 45.16; H, 5.34: Found C, 45.78; H, 5.43

8.2.4.5. Synthesis of (Cp^{*Bn}) Ir(L-azetidine-2-carboxylic acid)Cl (**4e**)

Following the general procedure: 0.100 g (0.105 mmol) of **4a** was combined with 0.0255 (0.221 mmol) of L-azetidine-2-carboxylic acid and 0.0186g (0.221 mmol) of sodium bicarbonate with methanol (10 mL) to give **4e** as a yellow solid, 0.936 g (82% yield, 0.174 mmol): Major Isomer: ^{1}H NMR (400 MHz, $CDCl_3$) δ 7.30 – 7.25 (m, 2H, ArH), 7.23 – 7.16 (m, 1H, ArH), 7.13 – 7.06 (m, 2H, ArH), 5.55 (br s, 1H, NH), 4.62 – 4.43 (m, 1H, αCH), 4.35 – 4.24 (m, 1H, N-CH), 3.95 – 3.83 (m, 1H, N-CH), 3.52 (s, 2H, CH_2), 3.04 – 2.90 (m, 1H, CH*H*), 2.50 – 2.36 (m, 1H, C*H*H), 1.73 (s, 3H, CpMe), 1.71 (s, 3H, CpMe), 1.71 (s, 3H, CpMe), 1.70 (s, 3H, CpMe). ^{13}C NMR (101 MHz, $CDCl_3$) δ 137.09 (ArC), 128.74 (ArC), 128.10 (ArC), 126.78 (ArC), 86.06 (CpC), 85.40 (CpC), 84.28 (CpC), 84.23 (CpC), 83.72 (CpC), 60.76 (N-C), 51.29 (αC), 30.03 (Cp-***C***H_2-Ar), 26.26 (CH_2), 9.43 (CpMe), 9.38 (CpMe), 9.08 (CpMe), 9.06 (CpMe).

Minor Isomer: ^{1}H NMR (400 MHz, $CDCl_3$) δ 4.96-4.80 (m, 1H, N-CH), 4.16 – 3.99 (m, 1H, NH), 2.77-2.64 (m, 1H, CH*H*), 2.64 – 2.55 (m, 1H, C*H*H), 1.68 (s, 3H, CpMe), 1.67 (s, 3H, CpMe).

HRMS/ESI+ (*m/z*): Calcd for $C_{20}H_{26}Cl[^{193}Ir]NO_2$; 540.1276: Found 540.1258

Anal calc. for $C_{20}H_{25}ClIrNO_2$; C, 44.56; H, 4.67: Found C, 44.41; H, 4.76

8.2.5. Synthesis of Iridium Cp*Isopropyl (aa) Cl complexes

8.2.5.1. Synthesis of [(Cp^{*iPr})$IrCl_2$]$_2$ (**5a**)

1.00g (2.84 mmol) of $IrCl_3$ x $3H_2O$ was combined with **2c** 0.699 g 4.25 mmol in methanol (30mL) with stirring. The mixture was refluxed for 48hrs. Solvent was removed to half volume and the reaction was cooled to 0°C produce an orange solid. The product was isolated by filtration and washed with cold methanol to yield 1.37 g of **5a** (56 %). ^{1}H NMR (400 MHz, $CDCl_3$) δ 2.47 (p, *J* = 7.1 Hz, 2H, $(CMe)_2$C*H*), 1.67 (s, 12H, $(CpMe)_2$), 1.59 (s, 12H, $(CpMe)_2$), 1.28 (d, *J* = 7.1 Hz, 12H,

$(CHMe_2)_2$). ^{13}C NMR (101 MHz, $CDCl_3$) δ 25.24 $(CMe)_2CH$), 20.58 $(CMe)_2CH$), 10.21 (CpMe), 9.51 (CpMe).

HRMS/ESI+ (*m/z*): Calcd for $C_{24}H_{38}Cl_4[^{193}Ir]_2$ Na; 875.0878: Found 875.0898

Anal calc. for $C_{24}H_{36}Cl_4Ir_2$; C, 33.8; H, 4.49: Found C, 33.98; H, 4.62

8.2.5.2. Synthesis of (Cp^{*iPr})Ir(Glycine)Cl (**5b**)

Following the general procedure: 0.100 g (0.173 mmol) of **5a** was combined with 0.0198 g (0.246 mmol) of glycine and 0.0207g (0.246 mmol) of sodium bicarbonate in methanol (30 mL) to give **5b** as a yellow solid, 0.0963 g (88% yield): ^1H NMR (400 MHz, Methanol-d_4) δ 3.49 – 3.27 (m, 2H, CH_2), 2.63 (sept, *J* = 7.1 Hz, 1H, (Me_2C***H***), 1.75 (s, 3H, CpMe), 1.73 (s, 3H, CpMe), 1.68 – 1.64 (br s, 6H, 2CpMe), 1.31 (overlapping doublets, $J_1 \approx J_2 =$ 7.0 Hz, 6H, $CHMe_2$) ppm. ^{13}C NMR (101 MHz, Methanol-d_4) δ 185.47 (COO), 88.37 (CpC), 88.27 (CpC), 85.99 (CpC), 83.65 (CpC), 82.59 (CpC), 44.19 (αC), 24.93 (Me_2**C**H), 20.09 (CH_3), 19.84 (CH_3), 8.51 (CpMe), 8.25 (CpMe), 7.53 (CpMe), 7.43 (CpMe).

HRMS/ESI+ (*m/z*): Calcd for $C_{24}H_{38}Cl_4[^{193}Ir]_2$ Na; 875.0878: Found 875.0898

Anal calc. for $C_{14}H_{23}ClIrNO_2$; C, 36.16; H, 4.99: Found C, 35.98; H, 4.94

8.2.5.3. Synthesis of (Cp^{*iPr})Ir(N,N-dimethyl-Glycine)Cl (**5c**)

0.100 g (0.173 mmol) of **5a** was combined with 0.0254 g (0.246 mmol) of N,N-dimethyl-glycine and 0.0207 g (0.246 mmol) of sodium bicarbonate in round bottom flask with methanol (30 mL) to give **5c** as a yellow solid, 0.0859 g (74% yield): ^1H NMR (400 MHz, $CDCl_3$) δ 4.06 (d, *J* = 14.6, 1H, CH***H***), 3.07 (s, 3H, N-CH_3), 2.95 (d, *J* = 14.6 Hz, 1H, C***H***H), 2.92 (s, 3H, N-CH_3), 2.58 (sept, *J* = 7.4 Hz, 1H, $(CMe)_2C$***H***)), 1.68 (s, 3H, CpMe), 1.65 (s, 3H, CpMe), 1.57 (s, 3H, CpMe), 1.56 (s, 3H,

CpMe), 1.29 (overlapping doublets, *J* = 7.4 Hz, 6H, CH**Me**$_2$) ppm. ^{13}C NMR (101 MHz, $CDCl_3$) δ 180.40 (COO), 87.73 (CpC), 87.47 (CpC), 86.77 (CpC), 85.10 (CpC), 81.88 (CpC), 66.32 (αC), 56.26 (N-CH_3), 50.65 (N-CH_3), 25.16 (Me_2**C**H), 20.58 (CH_3), 20.35 (CH_3), 9.91 (CpMe), 9.42 (CpMe), 9.23 (CpMe), 9.02 (CpMe).

HRMS/ESI+ (*m/z*): Calcd for $C_{16}H_{28}Cl[^{193}Ir]NO_2$; 494.1432: Found 494.1455

Anal calc. for $C_{16}H_{27}ClIrNO_2$; C, 38.98; H, 5.52: Found C, 39.01; H, 5.43

8.2.5.4. Synthesis of (Cp*^{iPr})Ir(L-Alanine)Cl (**5d**)

Following the general procedure: 0.100 g (0.173 mmol) of **5a** was combined with 0.0220 g (0.246 mmol) of L-alanine and 0.0207 g (0.246 mmol) of sodium bicarbonate in round bottom flask with methanol (30 mL) to give **5d** as a yellow solid, 0.0762 g (68% yield): Significant signal overlap is observed for this complex for the iso-propyl portion of the Cp ring. Major Isomer: ^{1}H NMR (400 MHz, $CDCl_3$) δ 6.65 (br s, 1H, NH), 3.46 (m, 1H, NH), 3.41 – 3.33(m, 1H, αCH), 2.63 (sept, *J* = 7.3 Hz, 1H, Me_2C***H***), 1.71 – 1.64 (m, 12H, $(CpMe)_4$), 1.44 (d, *J* = 6.7 Hz, 3H, CH_2), 1.28 (overlapping doublets, *J* = 7.3 Hz, 6H, CH**Me**$_2$) ppm. ^{13}C NMR (101 MHz, $CDCl_3$) δ 183.21 (COO), 89.01 (CpC), 88.77 (CpC, 85.77 (CpC), 83.18 (CpC), 82.40 (CpC), 52.97 (αC), 25.07 (Me_2**C**H), 21.71 (CH_3), 21.32 (CH_3), 10.03 (CpMe), 9.87 (CpMe), 9.26 (CpMe), 9.19 (CpMe).

Minor Isomer: ^{1}H NMR (400 MHz, $CDCl_3$) δ 4.94 (br s, 1H, NH), 4.45 – 4.23 (m, Hz, 1H, NH), 3.70 – 3.56 (m, 1H, αCH), 2.63 (sept, *J* = 7.1, 1H, $(CMe)_2$C***H***)), 1.78 – 1.71 (m, 12H, $(CpMe)_4$)), 1.40 (d, *J* = 7.2 Hz, 3H, CH_3), 1.28 (overlapping doublets, *J* = 7.1, 6H, CH**Me**$_2$). ^{13}C NMR (101 MHz, $CDCl_3$) δ 184.72 (COO), 88.97 (CpC), 88.71 (CpC), 85.58 (CpC), 83.06 (CpC), 82.55 (CpC), 51.60 (αC), 21.35 (CH_3), 21.26 (CH_3), 19.63 (CH_3), 10.08 (CpMe), 9.85 (CpMe), 9.30 (CpMe), 9.13 (CpMe).

Anal Calc. for $C_{15}H_{25}ClIrNO_2$; C, 3.61; H, 5.26: Found C, 37.37; H, 5.36

8.2.5.5. Synthesis of (Cp^{*iPr})Ir(L-Phenylalanine)Cl (**5e**)

Following the general procedure: 0.100 g (0.173 mmol) of **5a** was combined with 0.0410 g (0.246 mmol) of L-phenylalanine and 0.0207 g (0.246 mmol) of sodium bicarbonate in methanol (30 mL) to give **5e** as a yellow solid, 0.107 g (82% yield): Major Isomer: ^{1}H NMR (400 MHz, $CDCl_3$) δ 7.37 – 7.25 (m, 5H, ArH), 4.20 (br s, 1H, NH), 3.97 – 3.91 (m, 1H, NH), 3.87 (tt, *J* = 7.6, 5.3 Hz, 1H, αCH), 3.39 (dd, *J* = 14.3, 5.3 Hz, 1H, CH), 3.06 (dd, *J* = 14.3, 5.3 Hz, 1H, CH), 2.43 (sept, *J* = 7.1 Hz, 1H, $Me_2C\boldsymbol{H}$)), 1.59 (s, 3H, CpMe), 1.55 (s, 3H, CpMe), 1.49 (s, 3H, CpMe), 1.48 (s, 3H, CpMe), 1.16 (overlapping doublets, *J* = 7.1 Hz, 6H, CH$\mathbf{Me}_2$). ^{13}C NMR (101 MHz, $CDCl_3$) δ 182.34 (COO), 136.12 (ArC), 129.90 (ArC), 129.25 (ArC), 127.49 (ArC), 88.40 (CpC), 87.79 (CpC), 85.88 (CpC), 83.44 (CpC), 82.38 (CpC), 54.88 (αC), 38.40 (CH_2), 25.05 ($Me_2\mathbf{C}H$), 21.14 (CH_3), 21.04 (CH_3), 9.58 (CpMe), 9.54 (CpMe), 8.79 (CpMe), 8.76 (CpMe). Minor Isomer: ^{1}H NMR (400 MHz, $CDCl_3$) δ 7.36 – 7.25 (m, 5H, ArH), 4.88 – 4.75 (m, 1H, NH), 3.66 – 3.51(m, 2H, NH, αCH), 3.45 (dd, *J* = 14.7, 3.1 Hz, 1H, CH), 3.04 (dd, *J* = 14.7, 3.1 Hz, 1H, CH), 2.56 (sept, *J* = 7.1 Hz, 1H, $Me_2C\boldsymbol{H}$),1.71 (s, 3H, CpMe), 1.68 (s, 3H CpMe), 1.64 (s, 3H CpMe), 1.63 (s, 3H CpMe), 1.26 (overlapping doublets, *J* = 7.1 Hz, 6H, CH$\mathbf{Me}_2$). ^{13}C NMR (101 MHz, $CDCl_3$) δ 180.52 (COO), 136.99 (ArC), 129.47 (ArC), 129.10 (ArC), 127.09 (ArC), 88.67 (CpC), 88.46 (CpC), 86.17 (CpC), 83.16 (CpC), 82.68 (CpC), 58.50 (αC), 40.67 (CH_2), 25.12 ($Me_2\mathbf{C}H$), 21.29 (CH_3), 21.26 (CH_3), 9.84 (CpMe), 9.81 (CpMe), 9.15 (CpMe), 9.11 (CpMe).

HRMS/ESI+ (*m/z*): Calcd for $C_{21}H_{28}Cl[^{193}Ir]NNaO_2$; 577.133: Found, 577.1385

Anal calc. for $C_{21}H_{29}ClIrNO_2$; C, 45.44; H, 5.27: Found C, 45.67; H, 5.25

8.2.5.6. Synthesis of (Cp*^{iPr})Ir(L-proline)Cl (**5f**)

Following the general procedure: 0.100 g (0.173 mmol) of **5a** was combined with 0.0339 (0.293 mmol) of L-proline and 0.0246g (0.293 mmol) of sodium bicarbonate in methanol (20 mL) to give **5f** as a yellow solid, 0.0839 g (70.8% yield): Major Isomer: ^{1}H NMR (400 MHz, $CDCl_3$) δ 4.68 (br s, 1H, NH), 4.08 – 3.98 (m, 1H, αCH), 3.64 – 3.52 (m, 1H, N-CH), 3.00 – 2.86 (m, 1H, N-CH), 2.57 (sept, *J* = 7.1 Hz, 1H, $Me)_2C\boldsymbol{H}$), 2.30 – 2.17 (m, 1H, CH*H*), 2.06 – 1.86 (m, 3H, CH_2-C*H*H), 1.71 (s, 3H, CpMe), 1.70 (s, 3H, CpMe), 1.65 (s, 3H, CpMe), 1.62 (s, 3H, CpMe), 1.29 (overlapping doublets, *J* = 7.1 Hz, 6H, CH**Me**$_2$). ^{13}C NMR (101 MHz, $CDCl_3$) δ 184.41 (COO), 89.20 (CpC), 87.81 (CpC), 86.16 (CpC), 84.18 (CpC), 82.24 (CpC), 62.46 (αC), 54.92 (NC), 28.83 (CH_2), 27.19 (CH_2), 25.07 (Me_2**C**H), 21.03 (CH_3), 20.92 (CH_3), 9.96 (CpMe), 9.83 (CpMe), 9.26 (CpMe), 9.20 (CpMe). Minor Isomer: ^{1}H NMR (400 MHz, $CDCl_3$) δ 4.42 – 4.25 (m, 1H, NH), 3.82 – 3.62 (m, 1H, αCH), 3.82 – 3.65 (m, 1H, N-CH), 2.79 – 2.62 (m, 1H, C*H*H), 1.75 (s, 3H, CpMe), 1.73 (d, 3H, CpMe), 1.68 (s, 3H, CpMe), 1.66 (s, 3H, CpMe).

HRMS/ESI+ (*m/z*): Calcd for $C_{17}H_{28}Cl[^{193}Ir]Cl$; 506.1432: Found 506.1432

Anal calc. for $C_{17}H_{27}ClIrNO_2$; C, 40.43; H, 5.39: Found C, 40.82; H, 5.56

8.2.6. Synthesis of Iridium Cp*cyclohexyl (aa) Cl complexes

8.2.6.1. Synthesis of [(Cp*^{Cy})$IrCl_2]_2$: (**6a**)

2.00 g (5.67 mmol) of $IrCl_3$ x $3H_2O$ was combined with 1.74 g (8.51 mmol) of **2d** in 50mL of methanol with stirring. The mixture was refluxed for 48 h. After 48 h the reaction mixture was cooled in an ice bath to produce an orange powder. The powder was isolated on a frit and washed with cold methanol and ether (1.23g). Removal of solvent and overnight storage at 4 °C produced a

second crop of crystals what were isolated as stated previously, (0.05g). Combined yield of **6a** was 49%.

^{1}H NMR (400 MHz, $CDCl_3$ δ 2.03 (tt, *J* = 12.1, 3.2 Hz, 2H, CH_2), 1.96 – 1.85 (m, 4H, $2CH_2$), 1.80 – 1.70 (m, 4H, $2CH_2$), 1.66 (s, 12H, 2CpMe), 1.62 – 1.59 (m, 2H, CH_2), 1.58 (s, 12H, 2CpMe), 1.43 – 1.19 (m, 8H, $4CH_2$), 1.13 (tt, *J* = 12.6, 3.5 Hz, 2H, CH_2).

^{13}C NMR (101 MHz, $CDCl_3$) δ 90.57 (CpC), 85.85 (CpC), 84.73 (CpC), 35.60 (Cp-***C***H), 30.72 (CH_2), 26.93 (CH_2), 26.03 (CH_2), 10.51 (CpMe), 9.56 (CpMe).

HRMS/ESI+ (*m/z*): Calcd for $C_{30}H_{50}Cl_4[^{193}Ir]_2N$ 950.195: Found 950.1946

Anal Calc for $C_{30}H_{46}Cl_4Ir_2$ C, 38.62; H, 4.970: Found C, 38.77; H, 4.92

8.2.6.2. Synthesis of (Cp^{*Cy})Ir(Glycine)Cl (**6b**)

Following the general procedure: 0.100 g (0.107 mmol) of **6a** was combined with 0.0170 g (0.225 mmol) of glycine and 0.019 g (0.225 mmol) of sodium bicarbonate in round bottom flask with methanol (30 mL) to give **6b** as a yellow solid, 0.0634g (58% yield: ^{1}H NMR (400 MHz, Methanol-d_4) δ 5.82 (br s, 1H, NH), 4.92 (br s, 1H, NH), 3.51 – 3.39 (m, 1H, CH*H*), 3.39 – 3.31 (m, 1H, C*H*H), 2.21 (tt, *J* = 12.4, 3.2 Hz, 1H, Cp-C***H***), 1.92 – 1.83 (m, 2H, CH_2), 1.83 – 1.77 (m, 2H, CH_2), 1.75 (s, 3H, CpMe), 1.73 (s, 3H, CpMe), 1.67 – 1.62 (m, 6H, 2CpMe), 1.58 – 1.43 (m, 2H, CH_2), 1.42 – 1.15 (m, 4H, $2CH_2$). ^{13}C NMR (101 MHz, Methanol-d_4) δ 185.46 (COO), 88.62 (CpC), 84.28 (CpC), 83.61 (CpC), 44.31 (αC), 35.46 (Cp-***C***H), 31.08 (CH_2), 30.94 (CH_2), 26.70 (CH_2), 25.71 (CH_2), 8.80 (CpMe), 8.50 (CpMe), 7.47 (CpMe).

HRMS/ESI+ (*m/z*): Calcd for $C_{17}H_{31}$ 235.242; Found 235.2424

Anal Calc for $C_{17}H_{27}ClIrNO_2 \bullet H_2O$: C, 39.03; H, 5.59: Found C, 39.05; H, 5.54

8.2.6.3. Synthesis of (Cp*^{Cy})Ir(L-alanine)Cl (**6c**)

Following the general procedure: 0.100g (0.107 mmol) of **6a** was combined with 0.0210 g (0.225 mmol) of glycine and 0.019 g (0.225 mmol) of sodium bicarbonate in methanol (30 mL) to give **6c** as a yellow solid, 0.0089 g (80% yield): Major Isomer: ^{1}H NMR (400 MHz, $CDCl_3$) δ 6.15 (br s, 1H, NH), 3.52 – 3.34 (m, 2H, NH, αCH), 2.17 (ddt, *J* = 15.6, 12.4, 3.1 Hz, 1H, Cp-C***H***), 1.88 – 1.77 (m, 4H, $2CH_2$), 1.77 – 1.71 (m, 12H, 4CpMe), 1.47 (d, *J* = 6.7 Hz, 3H, CH_3), 1.45 – 1.41 (m, 1H, CH*H*), 1.36 – 1.22 (m, 4H, $2CH_2$), 1.15 (ddd, *J* = 16.3, 8.3, 3.6 Hz, 1H, C*H*H). ^{13}C NMR (101 MHz, $CDCl_3$) δ 183.20 (COO), 89.77 (CpC), 89.28 (CpC), 83.97 (CpC), 82.86 (CpC), 82.22 (CpC), 52.97 (aC), 35.42 (Cp-***C***H), 31.56 (CH_2), 27.00 (CH_2), 25.99 (CH_2), 21.70 (CH_3), 10.34 (CpMe), 10.15 (CpMe), 9.27 (CpMe), 9.22 (CpMe). Minor Isomer: ^{1}H NMR (400 MHz, $CDCl_3$) δ 4.59 – 4.48 (m, 1H, NH), 4.46 – 4.32 (m, 1H, NH), 3.75 – 3.62 (m, 1H, αCH), 2.17 (tt, *J* = 12.4, 3.2 Hz, 1H, Cp-C***H***), 1.88 – 1.77 (m, 4H, $2CH_2$), 1.71 – 1.64 (m, 12H, 4CpMe), 1.45 – 1.41 (m, 2H, CH_2), 1.40 (d, *J* = 7.2 Hz, 3H, CH_3), 1.30 (ddt, *J* = 17.2, 13.9, 6.9 Hz, 2H, CH_2), 1.16 (tt, *J* = 12.8, 3.2 Hz, 2H, CH_2). ^{13}C NMR (101 MHz, $CDCl_3$) δ 184.73 (COO), 89.68 (CpC), 89.32 (CpC), 83.72 (CpC), 82.79, 82.35 (CpC), 51.60 (αC), 35.48 (Cp-***C***H), 31.51 (CH_2), 27.00 (CH_2), 25.99 (CH_2), 19.65 (CH_3), 10.38 (CpMe), 10.12 (CpMe), 9.32 (CpMe), 9.15 (CpMe).

HRMS/ESI+ (*m/z*): Calcd for $C_{18}H_{30}Cl[^{193}Ir]NO_2$ 520.1589: Found 520.1603

Anal Calc for $C_{18}H_{29}ClIrNO_2 \bullet H_2O$: C, 40.25; H, 5.82: Found C, 41.00; H, 5.78

8.2.6.4. Synthesis of (Cp*^{Cy})Ir(L-phenylglycine)Cl (**6d**)

Following the general procedure: 0.100 g (0.107 mmol) of **6a** combined with 0.0342 g (0.225 mmol) of L-phenylglycine and 0.019 g (0.225 mmol) of sodium bicarbonate in methanol (30 mL) to give **6d**

as a yellow solid, 0.1072 g (86% yield): Major Isomer: ^{1}H NMR (400 MHz, $CDCl_3$) δ 7.38 – 7.31 (m, 2H, ArH), 7.24 – 7.16 (m, 3H, ArH), 6.39 (br s, 1H, NH), 4.20 (dd, *J* = 10.0, 7.6 Hz, 1H, αCH), 3.65 (br s, 1H, NH), 2.18 (tt, *J* = 12.2, 3.1 Hz, 1H, Cp-C***H***), 1.89 – 1.75 (m, 4H, $2CH_2$), 1.73 (s, 3H, CpMe), 1.71 (s, 3H, CpMe), 1.68 (s, 3H, CpMe), 1.65 (s, 3H, CpMe), 1.32 – 1.22 (m, 4H, $2CH_2$), 1.20 – 1.06 (m, 2H, CH_2). ^{13}C NMR (101 MHz, $CDCl_3$) δ 181.24 (COO), 140.63 (ArC), 129.28 (ArC), 128.90 (ArC), 128.86 (ArC), 128.06 (ArC), 89.74 (CpC), 89.37 (CpC), 84.20 (CpC), 83.60 (CpC), 82.55 (CpC), 58.76 (αC), 35.50 (Cp-***C***H), 31.60 (CH_2), 27.01 (CH_2), 25.86 (CH_2), 10.33 (CpMe), 10.19 (CpMe), 10.17 (CpMe), 10.11 (CpMe). Minor Isomer: ^{1}H NMR (400 MHz, $CDCl_3$) δ 7.35 – 7.32 (m, 2H, ArH), 7.24 – 7.16 (m, 3H, ArH), 4.73 (br s, 1H, NH), 4.53 (dd, *J* = 7.9, 4.9 Hz, 1H, αCH), 4.11 (br s, 1H, NH), 2.09 (tt, *J* = 12.4, 3.2 Hz, 1H, Cp-C***H***), 1.89 – 1.76 (m, 4H, $2CH_2$), 1.64 (s, 3H, CpMe), 1.60 (s, 3H, CpMe), 1.55 (s, 3H, CpMe), 1.52 (s, 3H, CpMe), 1.48 – 1.32 (m, 4H, $2CH_2$), 1.18 – 1.06 (m, 2H, CH_2). ^{13}C NMR (101 MHz, $CDCl_3$) δ 180.70 (COO), 138.90 (ArC), 129.28 (ArC), 128.86 (ArC), 128.77 (ArC), 128.06 (ArC), 89.70 (CpC), 89.64 (CpC), 83.60 (CpC), 82.96 (CpC), 82.69 (CpC), 61.08 (αC), 35.39 (Cp-***C***H), 31.57 (CH_2), 26.93 (CH_2), 26.01 (CH_2), 10.17 (CpMe), 10.11 (CpMe), 9.27 (CpMe), 9.00 (CpMe).

HRMS/ESI+ (*m/z*): Calcd for $C_{23}H_{32}Cl[^{193}Ir]O_2$ 582.1745: Found 582.1726

Anal Calc for $C_{23}H_{31}ClIrNO_2 \bullet H_2O$: C, 46.10; H, 5.55: Found C, 46.39: H, 5.50

8.2.6.5. Synthesis of (Cp*^{Cy})Ir(L-phenylalanine)Cl (**6e**)

Following the general procedure: 0.100 g (0.107 mmol) of **6a** was combined with 0.0373 g (0.225 mmol) of L-phenylalanine and 0.019 g (0.225 mmol) of sodium bicarbonate in methanol (30 mL) to give **6e** as a yellow solid, 0.108 g (845% yield): Major Isomer: ^{1}H NMR (400 MHz, $CDCl_3$) δ 7.42 – 7.25 (m, 5H, ArH), 4.25 – 4.07 (m, 1H, NH), 3.97 – 3.76 (m, 2H, NH, αCH), 3.38 (dd, *J* = 14.3, 4.9

Hz, 1H, CH*H*), 3.06 (dd, *J* = 14.3, 4.6 Hz, 1H, C*H*H), 2.02 (tt, *J* = 12.2, 3.1 Hz, 1H, Cp-C***H***), 1.84 – 1.71 (m, 4H, $2CH_2$), 1.60 (s, 3H, CpMe), 1.55 (s, 3H, CpMe), 1.49 (s, 3H, CpMe), 1.48 (s, 3H, CpMe), 1.44 – 1.03 (m, 6H, $3CH_2$). ^{13}C NMR (101 MHz, $CDCl_3$) δ 182.22 (COO), 136.07 (ArC), 129.87 (ArC), 129.23 (ArC), 127.51 (ArC), 88.91 (CpC), 88.16 (CpC), 84.16 (CpC), 83.34 (CpC), 82.27 (CpC), 54.85 (αC), 38.43 (CH_2), 35.47 (Cp-***C***H), 31.46 (CH_2), 31.29 (CH_2), 26.96 (CH_2), 25.89 (CH_2), 9.89 (CpMe), 9.87 (CpMe), 8.81 (CpMe), 8.77 (CpMe). Minor Isomer: ^{1}H NMR (400 MHz, $CDCl_3$) δ 7.43 – 7.25 (m, 5H, ArH), 3.64 – 3.56 (m, 1H, NH), 3.55 – 3.42 (m, 2H, NH, αCH), 3.03 – 2.98 (m, 1H, CH*H*), 2.11 (ddd, *J* = 12.3, 9.1, 3.1 Hz, 1H, Cp-C***H***), 1.83 – 1.71 (m, 4H, $2CH_2$), 1.70 (s, 3H, CpMe), 1.67 (s, 3H, CpMe), 1.65 (s, 3H, CpMe), 1.63 (s, 3H, CpMe), 1.45 – 1.01 (m, 6H, $3CH_2$). ^{13}C NMR (101 MHz, $CDCl_3$) δ 180.23 (COO), 137.08 (ArC), 129.38 (ArC), 129.14 (ArC), 127.12 (ArC), 89.29 (CpC), 84.54 (CpC), 82.75 (CpC), 58.70 (αC), 40.79 (CH_2), 35.58 (Cp-***C***H), 31.56 (CH_2), 27.01 (CH_2), 26.95 (CH_2), 10.13 (CpMe), 9.18 (CpMe), 9.12 (CpMe).

HRMS/ESI+ (*m/z*): Calcd for $C_{24}H_{33}Cl[^{193}Ir]NO_2$ 595.1824; Found 595.1871

Anal Calc for $C_{24}H_{33}ClIrNO_2$: C, 48.43; H, 5.59: Found C, 48.38; H, 5.77

8.2.6.6. Synthesis of (Cp^{*Cy})Ir(L-proline)Cl (**6f**)

Following the general procedure: 0.100 g (0.107 mmol) of **6a** was combined with 0.0259 g (0.225 mmol) of L-proline and 0.019 g (0.225 mmol) of sodium bicarbonate in round bottom flask with methanol (30 mL) to give **6f** as a yellow solid, 0.0810 g (68% yield): Major Isomer: ^{1}H NMR (400 MHz, $CDCl_3$) δ 4.56 (br s, 1H, NH), 4.10 – 3.97 (m, 1H, αCH), 3.60 – 3.51 (m, 1H, N-CH), 2.98 – 2.85 (m, 1H, N-CH), 2.29 – 2.17 (m, 1H, CH*H*), 2.12 (tt, *J* = 12.4, 3.0 Hz, 1H, Cp-C***H***), 2.06 – 1.89 (m, 2H, CH_2), 1.89 – 1.75 (m, 4H, $2CH_2$), 1.71 (s, 3H, CpMe), 1.70 (s, 3H, CpMe), 1.69 – 1.65 (m, 2H, CH_2), 1.64 (s, 3H, CpMe), 1.62 (s, 3H, CpMe), 1.51 – 1.35 (m, 2H, CH_2), 1.36 – 1.21 (m 2H,

CH_2), 1.21 – 1.09 (m, 1H, C*H*H). ^{13}C NMR (101 MHz, $CDCl_3$) δ 184.16 (COO), 90.11 (CpC), 88.29 (CpC), 84.15 (CpC), 83.98 (CpC), 81.92 (CpC), 62.44 (αC), 54.83 (CH_2), 35.73 (Cp-***C***H), 31.35 (CH_2), 31.30 (CH_2), 28.79 (CH_2), 27.22 (CH_2), 27.06 (CH_2), 26.03 (CH_2), 10.31 (CpMe), 10.09 (CpMe), 9.32 (CpMe), 9.22 (CpMe). Minor Isomer: ^{1}H NMR (400 MHz, $CDCl_3$) δ 6.53 (br s, 1H, NH), 3.81 – 3.72 (m, 1H, αCH), 3.24 – 3.11 (m, N-CH, 1H), 1.73 (s, 3H, CpMe), 1.72 (s, 3H, CpMe), 1.66 (s, 3H, CpMe). Other signals not detectable due to signal overlap.

HRMS/ESI+ (m/z): Calc. for $C_{24}H_{33}Cl[^{193}Ir]NO_2$ 595.1824. Found: 595.1871.

Anal Calc for $C_{20}H_{31}ClIrNO_2$: C, 44.06; H, 5.73; Found C, 44.72; H, 6.01

8.2.7. Synthesis of Iridium Cp*n-propyl (aa) Cl complexes

8.2.7.1. Synthesis of $[(Cp^{*n\text{-propyl}})IrCl_2]_2$ (**7a**)

1.00g (2.836 mmol) of $IrCl_3$ x $3H_2O$ was combined with $HCp^{*n\text{-propyl}}$ (0.702 g 4.28 mmol) in methanol (100 mL) with stirring. The mixture was refluxed for 48hrs. No product formed upon cooling, so the solvent was removed and the product was crystalized with dichloromethane and ether. The product was isolated by filtration and washed with cold ether to yield **7a**, 1.11 g (92 %). ^{1}H NMR (400 MHz, $CDCl_3$) δ 2.15 – 2.06 (m, 4H, $2CH_2$), 1.59 (s, 12H, 4CpMe), 1.57 (s, 12H, 4CpMe), 1.48 – 1.37 (m, 4H, $2CH_2$), 0.91 (t, *J* = 7.4 Hz, 6H, $2CH_3$). ^{13}C NMR (101 MHz, $CDCl_3$) δ 87.89 (CpC), 86.45 (CpC), 86.43 (CpC), 26.05 (CH_2), 20.85 (CH_2), 14.22 (CH_2), 9.41 (CpMe), 9.32 (CpMe).

HRMS/ESI+ (*m/z*): Calcd for $C_{24}H_{38}Cl_3[^{193}Ir_2]$ 817.1298; Found 817.1272

8.2.7.2. Synthesis of (Cp*$^{\text{-n-propyl}}$)Ir(L-alanine)Cl (**7b**)

Following the general procedure: 0.100 g (0.117 mmol) of **7a** was combined with 0.0219 g (0.246 mmol) of L-alanine and 0.0207 g (0.246 mmol) in methanol (30mL) to give **7b** as a yellow solid, 0.0567 g (50.5% yield): ^{1}H NMR (400 MHz, D_2O) δ 3.49 (d, *J* = 7.2 Hz, 1H, αCH), 2.02 (t, *J* = 7.5 Hz, 2H), 1.58 (s, 6H), 1.56 (s, 6H), 1.43 (h, *J* = 7.4 Hz, 3H), 1.27 (d, *J* = 7.2 Hz, 3H), 0.81 (t, *J* = 7.4 Hz, 3H). Signals for Diastereomers are isochronic in D_2O.

HRMS/ESI+ (*m/z*): Calcd for C15H25[^{193}]IrNO2: 444.1515; Found 444.0269i

8.2.7.3. Synthesis of (Cp*$^{\text{n-propyl}}$)Ir(L-phenylglycine)Cl (**7c**)

Following the general procedure: 0.100 g (0.117 mmol) of **7a** was combined with 0.0444 g (0.293 mmol) of L-phenylglycine and 0.0246g (0.291 mmol) in methanol (30mL) gave **7c** as a yellow solid, 0.108g (85% yield): Major Isomer: ^{1}H NMR (400 MHz, $CDCl_3$) δ 7.35 – 7.27 (m, 2H, ArH), 7.22 – 7.10 (m, 3H, ArH), 6.97 (t, *J* = 8.8 Hz, 1H, NH), 4.22 (t, *J* = 8.6 Hz, 1H, αCH), 3.41 (t, *J* = 10.2 Hz, 1H, NH), 2.13 (td, *J* = 7.3, 2.1 Hz, 2H, CH_2), 1.68 (s, 12H, 4CpMe), 1.45 (p, *J* = 7.5 Hz, 2H, CH_2), 0.93 (t, *J* = 7.4 Hz, 3H, CH_3). ^{13}C NMR (101 MHz, $CDCl_3$) δ 181.47 (COO), 140.71 (ArC), 129.12 (ArC), 128.90 (ArC), 128.74 (ArC), 128.03 (ArC), 85.95 (CpC), 84.99 (CpC), 84.92 (CpC), 84.31 (CpC), 84.26 (CpC), 60.87 (αC), 25.85 (CH_2), 21.66 (CH_2), 14.09 (CH_2), 9.32 (CpMe), 9.24 (CpMe).

Minor Isomer: ^{1}H NMR (400 MHz, $CDCl_3$) δ 7.35 – 7.26 (m, 2H, ArH), 7.22 – 7.10 (m, 3H, ArH), 4.82 (t, *J* = 9.2 Hz, 1H, NH),4.48 (dd, *J* = 7.3, 4.1 Hz, 1H, NH), 4.42 (dd, *J* = 10.6, 4.4 Hz, 1H, αCH), 1.97 – 1.87 (m, 2H, CH_2), 1.52 (t, *J* = 2.6 Hz, 12H, 4CpMe), 1.41 – 1.34 (m, 2H, CH_2), 0.88 (t, *J* = 7.4 Hz, 3H, CH_3). ^{13}C NMR (101 MHz, $CDCl_3$) δ 181.68 (COO), 138.57 (ArC), 128.66 (ArC), 127.90 (ArC), 85.80 (CpC), 84.95 (CpC), 84.65 (CpC), 84.35 (CpC), 59.00 (αC), 25.77 (CH_2), 21.53 (CH_2), 14.07 (CH_2), 9.09 (CpMe), 9.08 (CpMe), 9.00 (CpMe), 8.99 (CpMe).

HRMS/ESI+ (*m/z*): Calcd for $C_{20}H_{26}NO_2[^{193}Ir]H$ 506.1666; Found 506.1640

8.2.7.4. Synthesis of (Cp*$^{n\text{-propyl}}$)Ir(L-proline)Cl (**7d**)

Following the general procedure: 0.100 g (.117 mmol) of **7a** was combined with 0.0338g (0.29 mmol) of L-proline and 0.0244g (0.29 mmol) in methanol (30 mL) to give **7d** as a yellow solid, 0.066 g (59% yield): Major Isomer: ^{1}H NMR (400 MHz, $CDCl_3$) δ 4.73 (brs, 1H, NH), 4.07 – 3.98 (m, 1H, CH-N), 3.63 – 3.51 (m, 1H, αCH), 2.96 – 2.84 (m, 1H, N-CH), 2.28 – 2.16 (m, 1H, CH**H**), 2.14 – 2.03 (m, 1H, CH_2), 2.04 – 1.87 (m, 1H, C**H**H), 1.67 (s, 3H, CpMe), 1.66 (s, 3H, CpMe), 1.65 (s, 3H, CpMe), 1.53 – 1.39 (m, 2H, CH_2), 0.94 (t, *J* = 7.3 Hz, 3H, CH_3). ^{13}C NMR (101 MHz, $CDCl_3$) δ 184.31 (COO), 85.86 (CpC), 84.69 (CpC), 84.59 (CpC), 84.17 (CpC), 62.45 (αC), 54.88 (N-C), 26.11 (CH_2), 21.44 (CH_2), 14.20 (CH_3), 9.33 (CpMe), 9.23 (CpMe), 9.14 (CpMe).

Minor Isomer: ^{1}H NMR (400 MHz, $CDCl_3$) δ 1.63 (s, 3H, CpMe), 1.62 (s, 3H, CpMe), 1.62 (s, 6H, 2CpMe), 0.95 (t, *J* = 7.4 Hz, 3H, CH_3). ^{13}C NMR (101 MHz, $CDCl_3$) δ 183.13 (COO), 86.11 (CpC), 84.80 (CpC), 84.27 (CpC), 63.79 (αC), 26.21 (CH_2), 21.29 (CH_2), 14.24 (CpMe), 9.08 (CpMe).

HRMS/ESI+ (*m/z*): Calcd for $C_{17}H_{27}NO_2[^{193}Ir]$ 470.1666; Found 470.1656.

8.2.7.5. Synthesis of (Cp*$^{n\text{-propyl}}$)Ir(L-aze)Cl (**7e**)

Following the general procedure: 0.100 g (.117 mmol) of **7a** was combined with 0.0338g (0.29 mmol) of L-aze and 0.0244g (0.29 mmol) in methanol (30 mL) to give **7e** as a yellow solid, 0.066 g (59% yield)Major Isomer: ^{1}H NMR (400 MHz, $CDCl_3$) δ 5.77 (brs, 1H, NH), 4.43 – 4.33 (m, 1H, N-CH), 4.32 – 4.22 (m, 1H, αCH), 3.93 – 3.81 (m, 1H, N-CH), 3.00 – 2.84 (m, 1H, C**H**H), 2.47 – 2.31 (m, 1H, CH**H**), 2.20 – 2.08 (m, 2H, CH_2), 1.73 – 1.68 (m, 12H, 4CpMe), 1.47 (hept, *J* = 7.0, 6.6 Hz,

2H, CH_2), 0.95 (t, *J* = 7.5, 3H, CH_3). ^{13}C NMR (101 MHz, $CDCl_3$) δ 184.82 (COO), 85.69 (CpC), 84.50 (CpC), 84.48 (CpC), 84.40(CpC), 83.94 (CpC), 60.64 (αC), 51.16 (N-C), 26.34 (CH_2), 25.85 (CH_2), 14.15 (CH_3), 9.12 (CpMe), 9.08 (CpMe), 9.02 (CpMe), 9.00 (CpMe).

Minor Isomer: ^{1}H NMR (400 MHz, $CDCl_3$) δ 6.66 (brs, 1H, NH), 4.76 – 4.65 (m, 1H, αCH), 3.73 – 3.64 (m, 1H, NCH), 2.62 – 2.48 (m, 1H, C**H**H), 1.68 – 1.65 (m, 12H, 4CpMe). ^{13}C NMR (101 MHz, $CDCl_3$) δ 174.23 (COO), 87.33 (CpC), 86.86 (CpC), 86.45 (CpC), 85.63 (CpC), 85.30 (CpC), 60.87 (αC), 48.07 (N-C), 26.83 (CH_2), 25.67 (CH_2), 14.11 (CH_3), 9.22 (CpMe), 9.17 (CpMe).

HRMS/ESI+ (*m/z*): Calcd for $C_{16}H_{26}Cl[^{193}Ir]NO_2$ 492.1276; Found 492.1283

8.2.8. Synthesis of Iridium Cp*-n-octyl (aa) complexes

8.2.8.1. Synthesis of $[(Cp^{*n\text{-octyl}})IrCl_2]_2$ (**8a**)

2.00 g (5.67 mmol) of $IrCl_3$ x $3H_2O$ was combined with **2f** (1.99 g 8.51 mmol) in methanol (50 mL) with stirring. The mixture was refluxed for 48hrs. Upon reduction of solvent and cooling an orange precipitate formed. The product was isolated by filtration and washed with cold hexanes to yield **8a**, 1.6259 g (57.8 %). Single crystals suitable for X-ray diffraction were grown from hot hexanes.

^{1}H NMR (400 MHz, $CDCl_3$) δ 2.16 – 2.03 (m, 4H, $2CH_2$), 1.59 (s, 12H, 4CpMe), 1.58 (s, 12H, 4CpMe), 1.46 – 1.15 (m, 24H, $6CH_2$), 0.91 – 0.80 (m, 6H, $2CH_3$). ^{13}C NMR (101 MHz, $CDCl_3$) δ 88.19 (CpC), 86.44 (CpC), 86.38 (CpC), 31.76 (CH_2), 29.70 (CH_2), 29.29 (CH_2), 29.08 (CH_2), 27.62 (CH_2), 24.11 (CH_2), 14.03 (CH_3), 9.39 (CpMe), 9.35 (CpMe).

HRMS/ESI+ (m/z): Calcd for C34H58Cl3$[^{193}]Ir_2$ 957.0115; Found 957.0124

Anal Calc for $C_{34}H_{58}Cl_4Ir_2 \bullet CH_3OH$: C, 41.01; H, 6.10; Found C, 40.86; H, 5.84

8.2.8.2. Synthesis of ($Cp^{*n\text{-}octyl}$)Ir(Glycine)Cl (**8b**)

Following the general procedure: 0.100 g (0.101 mmol) of **8a** combined with 0.0159 (0.212 mmol) of glycine and 0.018 g (0.212 mmol) of sodium bicarbonate in methanol to give **8b** as a yellow powder. 0.0851 g (79% yield): ^{1}H NMR (400 MHz, $CDCl_3$) δ 5.84 (br s, 1H, NH), 3.67 (br s, 1H, NH), 3.58 – 3.28 (m, 2H, CH_2), 2.13 (t, *J* = 6.9, 6.2 Hz, 2H, CH_2), 1.70 (s, 12H, 4CpMe), 1.46 – 1.16 (m, 12H, $6CH_2$), 0.90 – 0.82 (m, 3H, CH_3). ^{13}C NMR (101 MHz, $CDCl_3$) δ 86.27 (CpC), 84.50 (CpC), 31.80 (CH_2), 29.62 (CH_2), 29.38 (CH_2), 29.12 (CH_2), 28.38 (CH_2), 23.93 (CH_2), 22.60 (CH_2), 14.05 (CH_3), 9.13 (CpMe), 9.08 (CpMe).

HRMS/ESI+ (m/z): Calcd for C20H35[^{193}Ir]NO2 514.2297; Found 514.2324

8.2.8.3. Synthesis of ($Cp^{*n\text{-}octyl}$)Ir(L-alanine)Cl (**8c**)

Following the general procedure: 0.100 g (0.101 mmol) of **8a** was combined with 0.0189 g (0.212 mmol) of L-alanine and 0.0180 g (0.212 mmol) of sodium bicarbonate in methanol (30 mL) to give **8c** as a yellow powder. 0.0925g (83.4% yield): Major Isomer: ^{1}H NMR (400 MHz, $CDCl_3$) δ 6.32 (s, 1H, NH), 3.79 – 3.56 (m, 1H, NH), 3.41 (q, *J* = 8.6, 8.1 Hz, 1H, αCH), 2.20 – 2.05 (m, 2H, CH_2), 1.70 (s, 12H, 4CpMe), 1.39 (d, *J* = 7.0 Hz, 3H, CH_3), 1.41 – 1.15 (m, 12H, $6CH_2$), 0.92 – 0.79 (m, 3H, CH_3). ^{13}C NMR (101 MHz, $CDCl_3$) δ 182.70 (COO), 86.34 (CpC), 84.45 (CpC), 84.28 (CpC), 53.18 (αC), 31.79 (CH_2), 29.62 (CH_2), 29.38 (CH_2), 29.12 (CH_2), 28.46 (CH_2), 24.04 , 22.59 (CH_2), 21.67 (CH_3), 14.04 (CH_3), 9.25 (CpMe). Minor Isomer: ^{1}H NMR (400 MHz, $CDCl_3$) δ 4.83 – 4.64 (m, 1H, NH), 4.46 – 4.22 (m, 1H, NH), 3.41 (q, *J* = 8.6, 8.1 Hz, 1H, αCH), 2.13 (t, *J* = 7.7 Hz, 2H, CH_2), 1.70 (s, 12H, 4CpMe), 1.44 (d, *J* = 5.9 Hz, 3H, CH_3), 1.42 – 1.15 (m, 12H, $4CH_2$), 0.91 –

0.81 (m, 3H, CH_3). ^{13}C NMR (101 MHz, $CDCl_3$) δ 184.52 (COO), 86.26 (CpC), 84.50 (CpC), 84.34 (CpC), 51.74 (αC), 29.62 (CH_2), 28.46(CH_2), 24.11(CH_2), 19.68(CH_3), 9.20 (CpMe).

HRMS/ESI+ (m/z): Calcd for $C_{20}H_{36}Cl[^{193}Ir]NO_2$ 550.2058; Found 550.2048

8.2.8.4. Synthesis of ($Cp^{*n\text{-octyl}}$)Ir(L-phenylglycine)Cl (**8d**)

0.100 g (0.101 mmol) of **8a** combined with 0.0320 g (0.212 mmol) of L-phenlyglycine and 0.0180 g (0.212 mmol) of sodium bicarbonate in methanol (30 mL) to give **8d** as a yellow powder. 0.116 g (94% yield). Major Isomer: ^1H NMR (400 MHz, $CDCl_3$) δ 7.38 – 7.31 (m, 1H, ArH), 7.24 – 7.15 (m, 4H, ArH), 6.40 (t, *J* = 8.9 Hz, 1H, NH), 4.17 (dd, *J* = 10.1, 7.4 Hz, 1H, αCH), 3.58 (t, *J* = 10.4 Hz, 1H, NH, CH2), 2.13 (dd, *J* = 8.8, 6.6 Hz, 2H, CH_2), 1.69 (s, 12H, 4CpMe), 1.46 – 1.16 (m, 12H, 6CH_2), 0.89 – 0.83 (m, 3H, CH_3). ^{13}C NMR (101 MHz, $CDCl_3$) δ 180.55 (COO), 140.61 (ArC), 129.27 (ArC), 128.86 (ArC), 128.79 (ArC), 127.92 (ArC), 86.35 (CpC), 84.71 (CpC), 84.51 (CpC), 84.35 (CpC), 84.30 (CpC), 58.79 (αC), 31.81 (CH_2), 29.61 (CH_2), 29.29 (CH_2), 29.15 (CH_2), 28.49 (CH_2), 23.96 (CH_2), 22.61 (CH_2), 14.06 (CH_3), 9.27 (CpMe), 9.09 (CpMe), 9.04 (CpMe).

Minor Isomer: ^1H NMR (400 MHz, $CDCl_3$) δ 7.38 – 7.32 (m, 1H, ArH), 7.24 – 7.15 (m, 4H, ArH), 4.73 (t, *J* = 9.3 Hz, 1H, NH), 4.51 (dd, *J* = 7.8, 4.3 Hz, 1H, αCH), 4.10 (dd, *J* = 10.9, 4.3 Hz, 1H, NH), 1.93 (dd, *J* = 8.9, 6.5 Hz, 2H, CH_2), 1.57 (d, *J* = 0.8 Hz, 6H, 2CpMe), 1.56 (s, 3H, CpMe), 1.55 (s, 3H, CpMe), 1.45 – 1.14 (m, 12H, 6CH_2), 0.93 – 0.83 (m, 3H, CH_3). ^{13}C NMR (101 MHz, $CDCl_3$) δ 180.55 (COO), 140.61 (ArC), 129.27 (ArC), 128.78 (ArC), 128.07 (ArC), 86.20 (CpC), 84.74 (CpC), 84.68 (CpC), 84.39 (CpC), 84.30 (CpC), 61.11 (αC), 31.78 (CH_2), 29.59 (CH_2), 29.42 (CH_2), 29.09 (CH_2), 28.34 (CH_2), 24.03 (CH_2), 22.59 (CH_2), 14.04 (CH_3), 9.23 (CpMe), 9.07 (CpMe), 9.02 (CpMe).

HRMS/ESI+ (m/z): Calcd for $C_{25}H_{38}Cl[^{193}Ir]NO_2$ 612.2215; Found 612.2249

8.2.8.5. Synthesis of (Cp*$^{n\text{-octyl}}$)Ir(L-proline)Cl (**8e**)

0.100 g (0.101 mmol) of **8a** combined with 0.0243 (0.212 mmol) of L-proline and 0.0180 g (0.212 mmol) of sodium bicarbonate in methanol (30mL) to give **8e** as a yellow powder. 0.0740 g (64% yield): Major Isomer: ^{1}H NMR (400 MHz, $CDCl_3$) δ 4.53 (s, 1H, NH), 4.11 – 3.97 (m, 1H, αCH), 3.56 (dt, *J* = 11.6, 6.3 Hz, 1H, N-CH), 2.92 (dq, *J* = 11.1, 5.3 Hz, 1H, N-CH), 2.29 – 2.18 (m, 2H, CH_2), 2.14 – 2.07 (m, 2H, CH_2), 2.06 – 1.89 (m, 2H, CH_2), 1.68 – 1.65 (m, 12H, 4CpMe), 1.47 – 1.18 (m, 12H, 6CH_3), 0.91 – 0.83 (m, 3H, CH_3). ^{13}C NMR (101 MHz, $CDCl_3$) δ 184.09 (COO), 86.33 (CpC), 84.66 (CpC), 84.50 (CpC), 84.48 (CpC), 84.22 (CpC), 62.38 (αC), 54.81 (N-C), 31.77 (CH_2), 29.71 (CH_2), 29.31 (CH_2), 29.09 (CH_2), 28.67 (CH_2), 28.24 (CH_2), 27.21 (CH_2), 24.21 (CH_2), 22.59 (CH_2), 14.03 (CH_3), 9.29 (CpMe), 9.19 (CpMe), 9.14 (CpMe), 9.13 (CpMe). Minor Isomer: ^{1}H NMR (400 MHz, $CDCl_3$) δ 4.31 (s, 1H, NH), 3.41 (d, *J* = 7.0 Hz, 2H, N-CH), 1.71 (s, 3H, CpMe), 1.70 (s, 3H, CpMe).

HRMS/ESI+ (m/z): Calcd for $C_{22}H_{38}Cl[^{193}Ir]NO_2$ 576.2215; Found 576.2229

8.2.8.6. Synthesis of (Cp*$^{n\text{-octyl}}$)Ir(L-Aze)Cl (**8f**)

0.100 g (0.101 mmol) of **8a** was combined with 0.0210 g (0.212 mmol) of L-azetidine-2-carboxlic acid and 0.0180 g (0.212 mmol) of sodium bicarbonate in methanol (30mL) to give **8f** as a yellow powder. 0.0857 g (76% yield): Major Isomer: ^{1}H NMR (400 MHz, $CDCl_3$) δ 5.30 – 5.19 (m, 1H, NH), 4.47 (ddd, *J* = 9.9, 7.3, 5.8 Hz, 1H, αCH), 4.25 (p, *J* = 9.1 Hz, 1H, N-CH), 3.85 (p, *J* = 8.4 Hz, 1H, N-CH), 2.90 (dtd, *J* = 11.5, 9.8, 7.5 Hz, 1H, CH*H*), 2.40 (ddt, *J* = 12.1, 8.9, 6.2 Hz, 1H, C*H*H), 2.14 – 2.08 (m, 2H, CH_2), 1.69 (s, 6H, 2CpMe), 1.68 (s, 6H, 2CpMe), 1.46 – 1.14 (m, 12H, 6CH_2),

0.90 – 0.80 (m, 3H, CH_3). ^{13}C NMR (101 MHz, $CDCl_3$) δ 184.72 (COO), 86.14 (CpC), 84.53 (CpC), 84.37 (CpC), 84.06 (CpC), 60.66 (αC), 51.02 (N-C), 31.76 (CH_2), 29.69 (CH_2), 29.30 (CH_2), 29.08 (CH_2), 28.29 (CH_2), 26.09 (CH_2), 23.95 (CH_2), 22.58 (CH_2), 14.03 (CH_3), 9.09 (CpMe), 9.04 (CpMe), 9.02 (CpMe), 9.00 (CpMe).

8.2.9. Synthesis of Iridium Cp*-n-dodecyl (aa) complexes

8.2.9.1. Synthesis of [(Cp*$^{n\text{-dodecyl}}$)$IrCl_2$]$_2$ (**9a**)

1.00 g (2.84 mmol) of $IrCl_3$ x $3H_2O$ was combined with **2g** (1.2358 g 4254 mmol) in methanol (50 mL) with stirring. The mixture was refluxed for 48hrs. After 48 h, the solution turned orange, with a black precipitate. The solution was filtered to remove the black precipitate, and the remaining orange solution was concentrated down and stored overnight in the freezer. The product was isolated by filtration and washed with cold ether (freezer temperature) to give **9a**, 0.426 g (14 %): ^{1}H NMR (400 MHz, $CDCl_3$) δ 2.18 – 1.97 (m, 4H, $2CH_2$), 1.58 (s, 12H), 1.57 (s, 12H, 4CpMe), 1.45 – 1.15 (m, 40H, $20CH_2$), 0.96 – 0.77 (m, 6H, $2CH_3$). ^{13}C NMR (101 MHz, $CDCl_3$) δ 88.16 CpC, 86.41 CpC, 86.35 CpC, 31.86 CH_2, 29.69 CH_2, 29.59 CH_2, 29.56 CH_2, 29.54 CH_2, 29.42 CH_2, 29.32 CH_2, 29.28 CH_2, 27.62 CH_2, 24.10 CH_2, 22.64 CH_2, 14.06 CH_3, 9.38 CpMe, 9.33 CpMe.

HRMS/ESI+ (m/z): Calcd for $C_{42}H_{74}Cl_4[^{193}Ir]_2 \bullet NH_4$ 1123.4175; Found 1123.3998

8.2.9.2. Synthesis of (Cp*$^{n\text{-dodecyl}}$)Ir(L-Phengly)Cl (**9b**)

0.100 g (0.0905 mmol) of **9a** was combined with 0.0342 g (0.226 mmol) of L-phenylglycine and 0.0190 g (0.226 mmol) of sodium bicarbonate in methanol (30mL) to give **9b** as a yellow/orange glass. 0.00657g (54% yield): Major Isomer: ^{1}H NMR (400 MHz, $CDCl_3$) δ 7.40 – 7.29 (m, 3H, ArH),

7.25 (s, 2H, ArH), 4.77 (s, 1H, NH), 4.59 (s, 1H, αCH), 4.26 (s, 1H, NH), 1.95 (t, *J* = 7.7 Hz, 2H, CH_2), 1.70 (s, 12H, 4CpMe), 1.49 – 1.13 (m, 20H, $10CH_2$), 0.86 (t, *J* = 6.8 Hz, 3H, CH_3).

HRMS/ESI+ (m/z): Calcd for $C_{29}H_{45}Cl[^{193}]IrNO_2$ 667.2768; Found 667.2753

8.2.9.3. Synthesis of (Cp*$^{n\text{-dodecyl}}$)Ir(L-Phe)Cl (**9c**)

0.100 g (0.0905 mmol) of **9a** was combined with 0.0448 (0.271 mmol) of L-phenylalanine and 0.0228g (0.271 mmol) of sodium bicarbonate in methanol (30mL) to give **9b** as a yellow/orange glass. 0.0611g (54% yield): Major Isomer:^{1}H NMR (400 MHz, $CDCl_3$) δ 7.41 – 7.25 (m, 5H, ArH), 4.10 (s, 1H, NH), 3.97 – 3.79 (m, 2H, NH, αCH), 3.41 – 3.30 (m, 1H, CH*H*), 3.11 – 3.04 (m, 1H, C*H*H), 1.86 (t, *J* = 7.6 Hz, 2H, CH_2), 1.54 (s, 6H, 2CpMe), 1.52 (s, 3H, CpMe), 1.50 (s, 3H, CpMe), 1.44 – 1.12 (m, 20H), 0.86 (t, *J* = 6.8 Hz, 3H, CH_3). Minor Isomer: ^{1}H NMR (400 MHz, $CDCl_3$) δ 7.41 – 7.25 (m, 5H), 4.39 (br s, 1H, NH), 3.64 – 3.51 (m, 2H, NH, αCH), 3.32 – 3.17 (m, 1H, CH*H*), 3.01 – 2.94 (m, 1H, C*H*H), 2.09 – 2.00 (m, 2H, CH_2), 1.67 – 1.62 (m, 12H, 4CpMe), 1.44 – 1.12 (m, 20H, $10CH_2$), 0.86 (t, *J* = 6.8 Hz, 3H, CH_3).

HRMS/ESI+ (m/z): Calcd for $C_{30}H_{48}Cl[^{193}Ir]NO_2$ 682.2997; Found 682.2982

8.2.9.4. Synthesis of (Cp*$^{n\text{-dodecyl}}$)Ir(L-pro)Cl (**9d**)

0.100g (0.0905 mmol) of **9a** was combined with 0.0219 g (0.190 mmol) of L-proline and 0.0160 g (0.190 mmol) of sodium bicarbonate in round bottom flask. Upon addition of 20mL and a magnetic stir bar the mixture slowly turned yellow over the course of 20 minutes with slight heating. Solvent was removed and the product extracted away using dichlormethane (3 x 10 mL). This was solution was filtered to remove any excess amino acid or sodium bicarbonate. The solvent was removed to produce a yellow/orange glass which was purified on silica gel with methanol/DCM (10/90) to give

9d, 0.0784g (69% yield): Major Isomer: ^{1}H NMR (400 MHz, $CDCl_3$) δ 4.60 (brs, 1H, NH), 4.09 – 3.99 (m, 1H, N-CH), 3.60 – 3.50 (m, 1H, αCH), 2.98 – 2.83 (m, 1H, N-CH), 2.31 – 2.15 (m, 1H, CH**H**), 2.14 – 2.07 (m, 2H, CH_2), 2.05 – 1.88 (m, 1H, CH**H**), 1.68 – 1.65 (m, 12H, 4CpMe), 1.45 – 1.18 (m, 20H, $10CH_2$), 0.85 (t, *J* = 6.7 Hz, 3H, CH_3). ^{13}C NMR (101 MHz, $CDCl_3$) δ 184.26 (COO), 86.35 (CpC), 84.67 (CpC), 84.54 (CpC), 84.51 (CpC), 84.26 (CpC), 62.43 (αC), 54.83 (NC), 31.86 (CH_2), 29.60 (CH_2), 29.57 (CH_2), 29.56 (CH_2), 29.44 (CH_2), 29.28 (CH_2), 28.69 (CH_2), 28.23 (CH_2), 27.18 (CH_2), 24.20 (CH_2), 22.64 (CH_2), 14.07 (CH_3), 9.29 (CpMe), 9.14 (CpMe), 9.13 (CpMe). Minor Isomer: ^{1}H NMR (400 MHz, Chloroform-*d*) δ 4.36 – 4.26 (m, 1H, NH), 3.84 – 3.72 (m, 1H, NCH), 1.74 – 1.68 (m, 12H, 4CpMe). ^{13}C NMR (101 MHz, $CDCl_3$) δ 29.34 (CH_2), 24.11(CH_2), 9.31 (CpMe), 9.26 (CpMe).

HRMS/ESI+ (m/z): Calcd for $C_{26}H_{45}NO_2[^{193}Ir]Cl$ 631.2763; Found 631.2804

8.2.9.5. Synthesis of ($Cp^{*n\text{-dodecyl}}$)Ir(D-pro)Cl (**9e**)

0100 g (0.0905 mmol) of **9a** was combined with 0.0219 g (0.190 mmol) of D-proline and 0.0160 g (0.190 mmol) of sodium bicarbonate in methanol (30mL) to give **9e** as a yellow/orange glass. 0.0912g (80% yield). : Major Isomer: ^{1}H NMR (400 MHz, $CDCl_3$) δ 4.60 (brs, 1H, NH), 4.09 – 3.99 (m, 1H, N-CH), 3.60 – 3.50 (m, 1H, αCH), 2.98 – 2.83 (m, 1H, N-CH), 2.31 – 2.15 (m, 1H, CH**H**), 2.14 – 2.07 (m, 2H, CH_2), 2.05 – 1.88 (m, 1H, CH**H**), 1.68 – 1.65 (m, 12H, 4CpMe), 1.45 – 1.18 (m, 20H, $10CH_2$), 0.85 (t, *J* = 6.7 Hz, 3H, CH_3). ^{13}C NMR (101 MHz, $CDCl_3$) δ 184.26 (COO), 86.35 (CpC), 84.67 (CpC), 84.54 (CpC), 84.51 (CpC), 84.26 (CpC), 62.43 (αC), 54.83 (NC), 31.86 (CH_2), 29.60 (CH_2), 29.57 (CH_2), 29.56 (CH_2), 29.44 (CH_2), 29.28 (CH_2), 28.69 (CH_2), 28.23 (CH_2), 27.18 (CH_2), 24.20 (CH_2), 22.64 (CH_2), 14.07 (CH_3), 9.29 (CpMe), 9.14 (CpMe), 9.13 (CpMe). Minor Isomer: ^{1}H NMR (400 MHz, $CDCl_3$) δ 4.36 – 4.26 (m, 1H, NH), 3.84 – 3.72 (m, 1H, NCH), 1.74 –

1.68 (m, 12H, 4CpMe). ^{13}C NMR (101 MHz, $CDCl_3$) δ 29.34 (CH_2), 24.11(CH_2), 9.31 (CpMe), 9.26 (CpMe).

HRMS/ESI+ (m/z): Calcd for $C_{26}H_{45}NO_2[^{193}Ir]Cl$ 631.2763; Found 631.2799

8.3. Synthesis of Ruthenium Arene amino acid complexes

8.3.1. General Procedure for synthesis of (Arene)Ru(aa)Cl complexes

A round bottom flask was charged with appropriate amounts of $[(Arene)RuCl_2]_2$, amino acid, base (KOH or $NaHCO_3$), and MeOH with magnetic stirring. The initially orange solution changed to yellow over the course of 30 min to 2 h depending on the amino acid used. The solvent was removed via reduced pressure. The complex was extracted with 3x10 mL of DCM and filtered to remove excess amino acid and base. The complexes were recrystallized with dichloromethane and ether or hexanes and collected on a frit as yellow crystalline powders.

8.3.1.1. Synthesis of $[(p\text{-}MeC_6H_4iPr)RuCl_2]_2$ (**10a**)

1.00 g (3.82 mmol) of $RuCl_3•H_2O$ was combined with a molar excess of α-phellandrene with 150 mL of ethanol in a schlenk flask. The mixture was refluxed for 4 h. Solvent was reduced to about half volume and the mixture was cooled in an ice bath, producing orange crystals. The product as isolated via filtration and washed with cold ethanol and ether to yield **10a**, 1.124 g 90.6% (1.735 mmol). ^{1}H NMR (400 MHz, $CDCl_3$) δ 5.44 – 5.24 (m, 8H, ArH), 2.86 (p, J = 6.9 Hz, 2H, C***H***-Me), 2.09 (s, 6H, Me), 1.21 (d, J = 7.0 Hz, 12H, CH***Me***).

HRMS/ESI+ (m/z): Calcd for $C_{20}H_{28}Cl_3[^{102}Ru_2]$ 576.9344; Found 576.9356

8.3.1.2. Synthesis of (*p*-MeC_6H_4*iPr*)Ru(L-phengly)Cl (**10b**)

Following the general procedure: 0.100 g (0.163 mmol) of **10a** was combined with 0.0518 g (0.343 mmol) of L-phenylglycine and 0.0289 g (0.343 mmol) sodium bicarbonate and reacted in MeOH (15 mL) to give **10b**, 0.124 g 56% (0.183 mmol): Major Isomer: ^{1}H NMR (400 MHz, $CDCl_3$) δ 7.75 (s, 1H, NH), 7.31 – 7.25 (m, 1H, Ar-H), 7.19 – 7.05 (m, 4H, Ar-H), 5.53 (d, *J* = 5.8 Hz, 1H, H_AH_B of *p*-MeC_6H_4*iPr*), 5.47 – 5.37 (m, 2H, overlap of H_AH_B of *p*-MeC_6H_4*iPr*), 5.27 (d, *J* = 5.6 Hz, 1H, H_AH_B of *p*-MeC_6H_4*iPr*), 4.23 (t, *J* = 8.8 Hz, 1H, αCH), 2.67 (p, *J* = 6.9 Hz, 1H, $CHMe_2$), 2.52 (t, *J* = 9.8 Hz, 1H, NH), 2.03 (s, 3H, Me), 1.17 (d, *J* = 6.9 Hz, 3H, CHMe*Me*), 1.14 (d, *J* = 6.9 Hz, 3H, CH*Me*Me). ^{13}C NMR (101 MHz, $CDCl_3$) δ 180.55 COO, 140.26 ArC, 128.72 ArC, 128.45 ArC, 100.95 ArC, 95.10 ArC, 82.03 ArC, 81.21 ArC, 80.33 ArC, 79.71 ArC, 60.97 αC, 30.81 *C*H-Me_2, 22.71 CH-Me, 22.05 CH-*Me*, 18.23 Me. Minor Isomer: ^{1}H NMR (400 MHz, $CDCl_3$) δ 7.31 – 7.25 (m, 1H, Ar-H), 7.18 – 7.06 (m, 4H, Ar-H), 5.95 (t, *J* = 8.3 Hz, 1H, NH), 5.22 (d, *J* = 5.8 Hz, 1H, H_AH_B of *p*-MeC_6H_4*iPr*), 4.09 (t, *J* = 7.0 Hz, 1H, αCH), 3.88 (t, *J* = 10.0 Hz, 1H, NH), 2.65 – 2.58 (m, 1H, C*H*Me_2), 1.93 (s, 3H, Me), 1.09 (d, *J* = 6.9 Hz, 3H, CH*Me*Me). ^{13}C NMR (101 MHz, $CDCl_3$) δ 128.87 ArC, 128.13 ArC, 127.85 ArC, 101.23 ArC, 30.76 *C*H-Me_2, 22.41 CH-*Me*, 22.28 CH-*Me*, 18.08 Me.

HRMS/ESI+ (m/z): Calcd for $C_{18}H_{23}ClNO_2{}^{102}Ru$ 422.0455; Found 422.0438

8.3.1.3. Synthesis of (*p*-MeC_6H_4*iPr*)Ru(L-Phe)Cl (**10c**)

Following the general procedure: 0.100 g (0.163 mmol) of **10a** was combined with 0.0566 g (0.343 mmol) of L-Phenalanine and 0.0289 g (0.343 mmol) sodium bicarbonate and reacted in MeOH (20 mL) to give **10c**, 0.129 g 91% (0.297 mmol): ^{1}H NMR (400 MHz, $CDCl_3$) δ 7.43 – 7.25 (m, 4H, ArH), 7.23 – 7.14 (m, 1H, ArH), 5.51 – 5.48 (m, 1H, H_AH_B of *p*-MeC_6H_4*iPr*), 5.46 – 5.41 (m, 1H,

H_AH_B of *p*-MeC_6H_4*iPr*), 5.30 – 5.26 (m, 1H, H_AH_B of *p*-MeC_6H_4*iPr*), 5.18 – 5.14 (m, 1H, H_AH_B of *p*-MeC_6H_4*iPr*), 3.99 – 3.84 (m, 1H, NH), 3.65 (p, *J* = 7.8 Hz, 1H, αCH), 3.29 (dd, *J* = 14.5, 4.6 Hz, 1H, C*H*H), 3.19 (t, *J* = 6.2 Hz, 1H, NH), 3.00 (dd, *J* = 14.5, 8.0 Hz, 1H, CH*H*), 2.67 (p, *J* = 6.8 Hz, 1H, C*H*-Me_2), 2.02 (s, 3H, Me), 1.16 (d, *J* = 6.8, Hz, 3H, CH-Me), 1.14 (d, *J* = 6.8, Hz, 3H, CH-Me). ^{13}C NMR ($CDCl_3$) δ 181.52 COO, 137.02 ArC, 130.01 ArC, 128.96 ArC, 127.15 ArC, 100.69 ArC, 96.59 ArC, 82.24 ArC, 80.38 ArC, 79.89 ArC, 79.38 ArC, 55.76 αC, 38.48 CH_2, 30.73 *C*H-Me_2, 22.76 CH-Me*Me*, 22.15 CH-*Me*Me, 18.15 Me. Minor Isomer: ^{1}H NMR (400 MHz, $CDCl_3$) δ 7.43 – 7.25 (m, 4H, ArH), 7.22 – 7.13 (m, 1H, ArH), 7.06 (t, *J* = 8.5 Hz, 1H, NH), 5.61 (dd, *J* = 8.9, 5.9 Hz, 2H, overlap of H_AH_B of *p*-MeC_6H_4*iPr*), 5.39 (d, *J* = 5.6 Hz, 1H, H_AH_B of *p*-MeC_6H_4*iPr*), 5.25 – 5.19 (m, 1H, NH), 3.19 (dd, *J* = 35.0, 5.7 Hz, 1H, CH*H*), 2.80 (p, *J* = 6.8 Hz, 1H, C*H*-Me_2), 2.10 (s, 3H, Me), 1.25 (d, *J* = 6.8 Hz, 3H, CH-Me), 1.23 (d, *J* = 6.8 Hz, 3H, CH-Me).

HRMS/ESI+ (m/z): Calcd for $C_{19}H_{25}ClNO_2{}^{102}Ru$ 436.0612; Found 436.064

8.3.1.4. Synthesis of (*p*-MeC_6H_4*iPr*)Ru(L-pro)Cl (**10d**)

Following the general procedure: 0.100 g (0.163 mmol) of **10a** was combined with 0.039 g (0.343 mmol) of L-proline and 0.0289 g (0.343 mmol) sodium bicarbonate and reacted in MeOH (20 mL) to give **10d** 0.1243 g 90.9 % (0.2970 mmol); Major Isomer: ^{1}H NMR (400 MHz, $CDCl_3$) δ 5.52 (d, *J* = 5.9 Hz, 1H, H_AH_B of *p*-MeC_6H_4*iPr*), 5.47 (d, *J* = 5.9 Hz, 1H, H_AH_B of *p*-MeC_6H_4*iPr*), 5.40 (d, *J* = 5.9, 1.1 Hz, 1H, H_AH_B of *p*-MeC_6H_4*iPr*), 5.25 (d, *J* = 5.7 Hz, 1H, H_AH_B of *p*-MeC_6H_4*iPr*), 4.41 (br S, *J* = 14.8 Hz, 1H, NH), 3.92 (dt, *J* = 11.2, 6.2 Hz, 1H, N-CH), 3.69 – 3.56 (m, 1H, αCH), 3.05 (qd, *J* = 10.8, 5.5 Hz, 1H, N-CH), 2.88 (dp, *J* = 11.9, 6.8 Hz, 1H, $CHMe_2$), 2.22 (s, 3H, Me), 2.10 – 1.69 (m, 4H, CH_2), 1.32 (d, *J* = 6.9 Hz, 3H, CH*Me*Me), 1.27 (d, *J* = 6.9 Hz, 3H, CHMe*Me*). ^{13}C NMR (101 MHz, $CDCl_3$) δ 182.92 COO, 101.43 ArC, 95.81 ArC, 82.83 ArC, 82.43 ArC, 79.43 ArC, 79.17 ArC, 62.06 αC, 57.02 N-C, 30.80 CH_2, 28.82 CH_2, 27.17 CH_2, 22.58 Me, 22.20 Me, 18.32 Me.

HRMS/ESI+ (m/z): Calcd for $C_{15}H_{22}ClNO_2{}^{102}Ru$; 386.0455; Found 386.0427

8.3.1.5. Synthesis of (*p*-MeC_6H_4*iPr*)Ru(L-pip)Cl (**10e**)

Following the general procedure: 0.100 g (0.163 mmol) of **10a** was combined with 0.039 g (0.343 mmol) L-pipecolic acid and 0.021 g (0.343 mmol) sodium bicarbonate and reacted in MeOH (20 mL) to give **10e** 0.0926 g, 71%, (0.232 mmol): Major Isomer: ^{1}H NMR (400 MHz, $CDCl_3$) δ 6.88 – 6.71 (m, 1H, NH), 6.17 (d, *J* = 6.2 Hz, 1H, 1H, H_AH_B of *p*-MeC_6H_4*iPr*), 5.99 (d, *J* = 5.8 Hz, 1H, 1H, H_AH_B of *p*-MeC_6H_4*iPr*), 5.79 (d, *J* = 6.2 Hz, 1H, 1H, H_AH_B of *p*-MeC_6H_4*iPr*), 5.67 (d, *J* = 5.8 Hz, 1H, 1H, H_AH_B of *p*-MeC_6H_4*iPr*), 3.78 – 3.69 (m, 1H, N-CH), 2.77 (hept, *J* = 7.1 Hz, 1H, C*H*-Me_2), 2.71 – 2.58 (m, 1H, N-CH), 2.48 (s, 3H, Me), 1.95 – 1.69 (m, 4H, $2CH_2$), 1.69 – 1.50 (m, 2H, CH_2), 1.26 (d, *J* = 7.1 Hz, 3H, CH-Me), 1.24 (d, *J* = 7.1 Hz, 3H, CH-Me). ^{13}C NMR (101 MHz, $CDCl_3$) δ 185.30 COO, 122.01 ArC, 118.83 ArC, 98.54 ArC, 97.41 ArC, 81.53 ArC, 81.38 ArC, 61.98 αC, 53.80 N-C, 30.80 CH_2, 27.09 CH_2, 25.56 CH_2, 23.81 CH_2, 22.47 Me, 22.33 Me, 18.63 Me.

8.3.1.6. Synthesis of $[(C_6H_3Me_3)RuCl_2]_2$ (**11a**)

2.00 g (7.65 mmol) of $RuCl_3$•H_2O was combined with 1.169 g (9.562 mmol) 1,3,5-trimethylcyclohexa-1,4-diene with in 100mL of ethanol in a schlenk flask. The mixture was refluxed for 16 h. Solvent was reduced to about half volume and the mixture was cooled in an ice bath, producing a deep red powder. The product as isolated via filtration and washed with cold ethanol and ether to yield **11a**, 2.148 g, 96%, 3.6751 mmol.

8.3.1.7. Synthesis of $(C_6H_3Me_3)$Ru(L-pip)Cl (**11b**)

Following the general procedure: 0.100 g (0.171 mmol) of **11a** was combined with 0.0464g (0.359 mmol) of L-pipecolic acid and 0.0302g (0.302 mmol) of sodium bicarbonate were reacted in H_2O (15

mL) to give **11b**, 0.112 g 85% yield (0.291 mmol): Major Isomer: ^{1}H NMR (400 MHz, Methanol-d_4) δ 5.00 (s, 3H, ArH), 3.50 – 3.42 (m, 1H, αCH), 3.15 (dd, *J* = 12.1, 2.7 Hz, 1H, N-CH*H*), 3.03 (ddd, *J* = 13.2, 9.5, 7.3 Hz, 1H, N-C*H*H), 2.18 (s, 9H, ArMe), 1.87 (ddt, *J* = 14.2, 12.7, 3.7 Hz, 2H, CH_2), 1.77 – 1.65 (m, 2H, CH_2), 1.58 – 1.45 (m, 2H, CH_2). ^{13}C NMR (101 MHz, Methanol-d_4) δ 181.40 COO, 102.55 ArC, 74.00 ArC, 62.15 αC, 53.26 N-C, 27.18 CH_2, 26.56 CH_2, 23.69 CH_2, 17.12 ArMe. Minor Isomer: ^{1}H NMR (400 MHz, Methanol-d_4) δ 5.29 (s, 3H, ArH), 2.20 (s, 9H, Me). ^{13}C NMR (101 MHz, Methanol-d_4) δ 77.91 ArC, 17.54 ArMe.

HRMS/ESI+ (m/z): Calcd for $C_{15}H_{22}NO_2[^{102}Ru]$ 350.0689; Found 350.0666

8.3.1.8. Synthesis of $(C_6H_3Me_3)Ru(L\text{-}pro)Cl$ (**11c**)

Following the general procedure: 0.100 g (0.171 mmol) of **11a** was combined with 0.0414 g (0.359 mmol) of L-proline and 0.0302g (0.302 mmol) of sodium bicarbonate were reacted in MeOH (20 mL) to **11c**, 0.105 g 82% yield (0.281 mmol): Major Isomer ^{1}H NMR (400 MHz, $CDCl_3$) δ 4.99 (s, 3H, Ar-H), 4.47 (s, 1H, NH), 3.95 – 3.81 (m, 1H, αCH), 3.74 – 3.59 (m, 1H, N-CH), 3.03 – 2.84 (m, 1H, N-CH), 2.22 (s, 9H, Ar-Me), 1.98 – 1.61 (m, 4H, CH_2). ^{13}C NMR (101 MHz, $CDCl_3$) δ 182.68 COO, 98.67 Ar-C, 77.80 Ar-C, 62.63 αC, 56.31 N-C, 28.30 CH_2, 26.94 CH_2, 18.95 ArMe.

HRMS/ESI+ (m/z): Calcd for $C_{14}H_{21}ClNO_2[^{102}Ru]$ 372.0299; Found 372.0277

8.3.1.9. Synthesis of $[(C_6Me_6)RuCl_2]_2$ (**12a**)

2.00 g (3.27 mmol) of $[(p\text{-}MeC_6H_4iPr)RuCl_2]_2$ was combined with 10.0 g (61.6 mmol) of hexamethyl benzene in a 10 mL Ace Glass pressure tube. The mixture was melted at 180 °C for 8 h. The resulting orange mixture was purified by column chromatography, first flushed with hexanes, then elution of the red/orange band by 10% MeOH/DCM mixture. Upon removal of solvent a red/orange powder formed, **12a** 1.023 g 47% yield (1.53 mmol).

^{1}H NMR (400 MHz, Chloroform-*d*) δ 2.01 (s, 18H).

HRMS/ESI+ (m/z): Calcd for $C_{24}H_{26}Cl_3[^{102}Ru]_2$ 632.9970; Found 632.9984

8.3.1.10. Synthesis of (C_6Me_6)Ru(L-pro)Cl (**12b**)

Following the general procedure: 0.100 g (0.150 mmol) of **12a** was combined with 0.0362 g (0.314 mmol) of L-proline and 0.0264g (0.314 mmol) of sodium bicarbonate were reacted in MeOH (30 mL) to give **12b**, 0.0917g 74% yield (0.222 mmol): Major Isomer: ^{1}H NMR (400 MHz, $CDCl_3$) δ 3.84 (s, 1H, NH), 3.69 – 3.51 (m, 2H, αCH, N-CH), 2.78 (qd, *J* = 11.2, 5.5 Hz, 1H, N-CH), 2.11 (s, 18H, 6Me), 1.97 – 1.77 (m, 2H, CH_2), 1.70 – 1.55 (m, 1H, CH). ^{13}C NMR (101 MHz, $CDCl_3$) δ 181.94 COO, 90.45 **C**-Ru, 62.85 N-C, 53.56 αC, 28.14 CH_2, 27.14 CH_2, 15.98 Ar-Me.

Minor Isomer: ^{1}H NMR (400 MHz, $CDCl_3$) δ 5.70 (s, 1H, NH), 3.74 (m, 1H, αCH), 3.41 (s, 2H, CH_2), 1.99 (s, 18H, 6Me).

HRMS/ESI+ (m/z): Calcd for $C_{17}H_{26}NO_2[^{102}Ru]$ 379.1002; Found 379.0974

8.3.1.11. Synthesis of (C_6Me_6)Ru(L-phengly)Cl (**12c**)

Following the general procedure: 0.100 g (0.150 mmol) of **12a** was combined with 0.0475 g (0.314 mmol) of L-phenylglycine and 0.0264g (0.314 mmol) of sodium bicarbonate were reacted in MeOH (30 mL) to give **12c**, 0.118 g 74% yield (0.263 mmol): Major Isomer: ^{1}H NMR (400 MHz, $CDCl_3$) δ 7.38 – 7.29 (m, 2H, ArH), 7.24 – 7.19 (m, 1H, ArH), 7.19 – 7.08 (m, 2H, ArH), 4.31 – 4.17 (m, 1H, NH), 4.17 – 4.08 (m, 1H, αCH), 3.23 (br s, 1H, NH), 2.02 (s, 18H, ArMe). ^{13}C NMR (101 MHz, $CDCl_3$) δ 129.37 ArC, 128.82 ArC, 128.61 ArC, 127.94 ArC, 90.32 **C**-Ru, 15.66 Ar-Me. Minor Isomer: ^{1}H NMR (400 MHz, $CDCl_3$) δ 7.42 – 7.26 (m, 2H), 7.23 – 7.18 (m, 1H), 7.18 – 7.08 (m,

2H), 5.54 (br s, 1H, NH), 4.07 – 3.96 (m, 1H, αCH), 3.17 – 3.02 (m, 1H, NH), 2.11 (s, 18H, ArMe). ^{13}C NMR (101 MHz, $CDCl_3$) δ 129.37 ArC, 128.82 ArC, 128.61 ArC, 127.90 ArC, 90.15 C-Ru, 15.87 Ar-Me.

HRMS/ESI+ (m/z): Calcd for $C_{20}H_{27}ClNO_2[^{102}Ru]$ 450.0768; Found 450.0777

8.3.1.12. Synthesis of $(C_6Me_6)Ru(L\text{-}phe)Cl$ (**12d**)

Following the general procedure: 0.100 g (0.150 mmol) of **12a** was combined with 0.0452 g (0.314 mmol) of L-phenylalanine and 0.0264 g (0.314 mmol) of sodium bicarbonate were reacted in MeOH (30 mL) to give **12d**, 0.119 g 86% yield (0.258 mmol), and was identified by the following information: Major Isomer: ^{1}H NMR (400 MHz, $CDCl_3$) δ 7.44 – 7.11 (m, 5H Ar-H), 3.52 – 3.31 (m, 1 αH), 2.80 (s, 2H CH_2), 1.87 (s, 18H Ar-Me). ^{13}C NMR (101 MHz, $CDCl_3$) δ 136.41 (ArC), 130.23 (ArC), 129.22 (ArC), 127.47 (ArC), 89.95 (ArC-Ru), 38.36 (CH_2), 15.28 (ArMe).

HRMS/ESI+ (m/z): calcd for $C_{21}H_{29}ClNO_2[^{102}Ru]$ 464.0925; Found 464.0961

8.3.1.13. Synthesis of $(C_6Me_6)Ru(L\text{-}pip)Cl$ (**12e**)

Following the general procedure: 0.100 g (0.150 mmol) of **12a** was combined with 0.0406 g (0.314 mmol) of L-phenylalanine and 0.0264 g (0.314 mmol) of sodium bicarbonate were reacted in MeOH (30 mL) to give **12e**, 0.103 g 80% yield (0.240mmol): Major Isomer: ^{1}H NMR (400 MHz, $CDCl_3$) δ 3.40 – 3.32 (m, 2H, N-CH_2), 3.11 – 2.98 (m, 1H, αCH), 2.90 (t, *J* = 12.5 Hz, 1H, NH), 2.27 – 2.20 (m, 1H, CH*H*), 2.19 – 2.14 (m, 1H, C*H*H), 2.11 (s, 18H, Ar-Me), 1.51 – 1.35 (m, 4H, CH_2-CH_2). ^{13}C NMR (101 MHz, $CDCl_3$) δ 176.45 COO, 90.46 Ru-C, 65.63 αC, 52.46 N-C, 30.81 CH_2, 27.78 CH_2 , 23.83 CH_2, 15.99 Ar-Me. Minor Isomer: ^{1}H NMR (400 MHz, $CDCl_3$) δ 3.27 – 3.16 (m, 2H, N-CH_2),

2.08 (s, 18H, Ar-Me), 1.32 – 1.19 (m, 4H, CH_2-CH_2). ^{13}C NMR (101 MHz, $CDCl_3$) δ 90.18 Ru-C, 15.49 Ar-Me.

HRMS/ESI+ (m/z): Calcd for $C_{18}H_{29}ClNO_2[^{102}Ru]$ 428.0925; Found 428.0929

8.3.2. Synthesis of Rhodium Complexes

8.3.2.1. Synthesis of $[(Cp^*)RhCl_2]_2$ (**13a**)

$[(Cp^*)RhCl_2]_2$ was synthesized by a previously reported method. 1.00 g (3.79 mmol) of $RhCl_3•3H_2O$ was combined with 0.776 g (5.69 mmol) of 1,2,3,4,5-pentamethylcyclopenta-1,3-diene with 90 mL of MeOH and refluxed for 36 h to give **13a**, 0.845 g 72% (1.37 mmol).

8.3.2.2. General Procedure for Synthesis of Rhodium Amino Acid Complexes

A RBF was charged with appropriate amounts of $[RhCp^*Cl_2]_2$, amino acid, base (KOH or NaHCO3), and MeOH with magnetic stirring. The initially orange solution changed to yellow over the course of 30 min to 2 h depending on the amino acid used. The solvent was removed via reduced pressure. The complex was extracted with 3x10 mL of DCM and filtered to remove excess amino acid and base. The complexes were recrystallized with dichloromethane and ether or hexanes and collected on a frit as orange to red crystalline powders.

8.3.2.3. Synthesis of (Cp*)Rh(L-phe)Cl (**13b**)

Following the general procedure: Following the general procedure: 0.100 g (0.162 mmol) of **13a** was combined with 0.0563g (0.340 mmol) of L-phe and 0.0285g (0.340 mmol) of $NaCHO_3$ and reacted in methanol (20 mL) for 30 minutes to give **13b**, 0.0954g 67.1% (0.217 mmol): Major Isomer: ^{1}H NMR (400 MHz, $CDCl_3$) δ 7.42 – 7.27 (m, 5H, ArH), 3.77 – 3.66 (m, 1H, NH), 3.54 – 3.46 (m, 1H, NH), 3.42 (dd, *J* = 14.2, 6.0 Hz, 1H, C*H*H), 3.04 (dd, *J* = 14.2, 5.6 Hz, 1H, CH*H*), 1.54 (s, 15H,

Cp*Me). ^{13}C NMR (101 MHz, $CDCl_3$) δ 179.71 COO, 136.76 ArC, 129.97 ArC, 129.15 ArC, 127.29 ArC, 92.77 (d, *J* = 8.7 Hz, Cp*), 56.46 αC, 38.97 CH_2, 8.77 Cp*Me. Minor Isomer: ^{1}H NMR (400 MHz, $CDCl_3$δ 7.38 – 7.25 (m, 5H), 3.79 (m, 1H, NH), 2.97 – 2.87 (m, 1H, CH*H*), 1.66 (s, 15H, Cp*Me). ^{13}C NMR (101 MHz, $CDCl_3$) δ 129.07 ArC, 126.98 ArC, 92.94 (d, 8.7 Hz, Cp*), 59.61 αC, 9.06 Cp*Me.

HRMS/ESI+ (m/z): Calcd for $C_{19}H_{26}ClNO_2Rh$ 438.0702; Found 438.0713

8.3.2.4. Synthesis of (Cp*)Rh(L-pro)Cl (**13c**)

Following the general procedure: 0.100g (0.162 mmol) of 13a was combined with 0.0391 g (0.340 mmol) of L-proline and 0.0285g (0.340 mmol) of $NaCHO_3$ and reacted in methanol (20 mL) for 30 minutes to give 13c, 0.1134g 90% (0.293 mmol): Major Isomer: ^{1}H NMR (400 MHz, $CDCl_3$) δ 4.25 (s, 1H, NH), 3.86 (q, *J* = 8.2, 7.5 Hz, 1H, αCH), 3.59 (dt, *J* = 12.0, 6.7 Hz, 1H, N-CH), 2.87 (qd, *J* = 10.9, 5.9 Hz, 1H, N-CH), 2.19 – 1.89 (m, 4H, CH_2), 1.69 (s, 15H, Cp*Me). ^{13}C NMR (101 MHz, $CDCl_3$) δ 181.43 COO, 93.01 (d, *J* = 8.8 Hz) Cp-C, 63.79 αC, 52.12 N-C, 28.60 CH_2, 26.71 CH_2, 9.17 Cp*Me. Minor isomer is not observable due to low abundance and signal overlap.

HRMS/ESI+ (m/z): Calcd for $C_{15}H_{23}NO_2RhCl$ 387.0467; Found 387.0496

8.3.2.5. Synthesis of (Cp*)Rh(L-pip)Cl (**13d**)

Following the general procedure: 0.100 g (0.162 mmol) of 13a was combined with 0.0439g (0.340 mmol) of L-pip and 0.0285g (0.340 mmol) of $NaCHO_3$ and reacted in methanol (20 mL) for 30 minutes to give 13d, 0.111 g 88% (0.285 mmol): Major Isomer: ^{13}C NMR (101 MHz, $CDCl_3$) δ 176.70 COO, 93.10 (d, *J* = 8.9 Hz) Cp*-C, 66.30 αC, 51.62 N-C, 31.01 CH_2, 27.90 CH_2, 23.95 CH_2,

9.21 Cp*Me. Minor Isomer: ^{13}C NMR (101 MHz, $CDCl_3$) δ 92.78 (d, *J* = 8.8 Hz), Cp*C, 63.49 αC, 51.28 N-C, 29.05 CH_2, 27.27 CH_2, 23.99 CH_2, 8.86 Cp*Me.

HRMS/ESI+ (m/z): Calcd for $C_{16}H_{26}ClNO_2Rh$ 402.0702; Found 402.068

8.3.2.6. Synthesis of (Cp*)Rh(L-Phengly)Cl (**13e**)

Following the general procedure: 0.100 g (0.162 mmol) of **13a** was combined with 0.0439 g (0.340 mmol) of L-pip and 0.0285 g (0.340 mmol) of $NaCHO_3$ and reacted in methanol (20 mL) for 30 minutes to give **13e**, 0.111 g 88% (0.285 mmol): Major Isomer: ^{1}H NMR (400 MHz, $CDCl_3$) δ 7.45 – 7.27 (m, 2H, ArH), 7.23 – 7.09 (m, 3H, ArH), 6.46 (t, *J* = 8.8 Hz, 1H, NH), 4.45 – 4.35 (m, 1H, αCH), 2.86 (t, *J* = 10.1 Hz, 1H, NH), 1.67 (s, 15H, CpMe). ^{13}C NMR (101 MHz, $CDCl_3$) δ 179.68 COO, 141.49 ArC, 128.63 ArC, 128.13 ArC, 93.03 (d, *J* = 7.7 Hz, Cp*C), 61.64 αC, 9.19 Cp*Me.

Minor Isomer: ^{1}H NMR (400 MHz, $CDCl_3$) δ 7.46 – 7.27 (m, 2H, ArH), 7.22 – 7.08 (m, 3H ArH), 4.35 (t, *J* = 6.6 Hz, 1H, NH), 4.24 (t, *J* = 9.3 Hz, 1H, NH), 4.05 – 3.88 (m, 1H, αCH), 1.53 (s, 15H, Cp*Me). ^{13}C NMR (101 MHz, $CDCl_3$) δ 128.97 ArC, 128.63 ArC, 128.35 ArC, 60.51 αC, 9.02 Cp*Me.

HRMS/ESI+ (m/z): Calcd for $C_{18}H_{24}ClNO_2Rh$ 424.0545; 424.054

8.4. Catalytic Conditions and Separation of Enantiomers

8.4.1. General procedure for the reduction of ketones in aqueous media

The catalyst (4 x 10^{-4} mmol) was added to a vial (1 or 2 dram) and DI water was added (1 mL to 4 mL). The resulting mixture was stirred for 1 h at the required temperature. Sodium formate (0.2 mmol) was then added, and after further stirring the ketone (0.04 mmol) was injected. The reaction

was maintained at set temperature until the total reduction of the ketone was achieved or conversion of the ketone had ceased as monitored by GC. The product was extracted with diethyl ether (3 x 2 mL), and dried over $MgSO_4$, and evaporated under reduced pressure. The product was purified by TLC with hexanes/ethyl acetate mixture if require. Enantiomeric excess was determined by chiral GC.

8.4.2. General procedure for the reduction of ketones in alcohols

The catalyst (4 x 10^{-4} mmol) was added to a Teflon sealed vial and the atmosphere was evacuated and backfilled with N_2 three times. Dry, degassed 2-propanol was added via syringe and the solution was stirred at the set temperature for 1 h. The base was then added (8 x 10^{-4} mmol as an aqueous solution), and after further stirring the ketone (0.04 mmol) was injected. The reaction was maintained at set temperature until the total reduction of the ketone was achieved or conversion of the ketone had ceased as monitored by GC. Solvent was then removed and water was added to the reaction vial. The product was extracted with dethyl ether (3 x 2 mL), and dried over $MgSO_4$, and evaporated under reduced pressure. The product was purified by TLC with hexanes/ethyl acetate mixture if require. Enantiomeric excess was determined by chiral GC.

8.5. Alcohol Products

8.5.1. 1-phenylethan-1-ol:

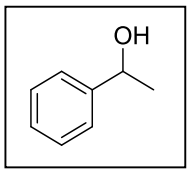

^{1}H NMR (400 MHz, $CDCl_3$) δ 7.33 – 7.25 (m, 3H), 7.23 – 7.18 (m, 2H), 4.83 (q, *J* = 6.5 Hz, 1H), 1.43 (d, *J* = 6.5 Hz, 3H). T = 140°C, P = 15 psi retention times: tR = 8.471 min, tS = 9.137 min

8.5.2. 2,2-dimethyl-1-phenylpropan-1-ol:

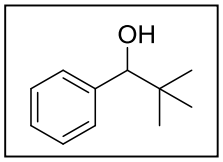

^{1}H NMR (400 MHz, $CDCl_3$) δ 7.30 – 7.28 (m, 5H), 4.38 (s, 1H), 0.91 (s, 12H). T = 120°C, P = 15 psi, retention times, tR = 9.633 min, tS = 10.016 min

8.5.3. 3,3-dimethylbutan-2-ol:

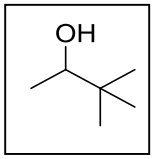

^{1}H NMR (400 MHz, $CDCl_3$) δ 3.45 (q, *J* = 6.4 Hz, 1H), 1.44 (s, 1H), 1.10 (d, *J* = 6.4 Hz, 3H), 0.87 (s, 9H). T = 75°C, P = 15 psi, retention times: tR = 7.163 min, tS = 7.384 min

8.5.4. 3-methylbutan-2-ol

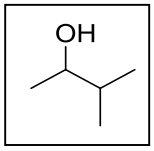

^{1}H NMR (400 MHz, $CDCl_3$) δ 3.53 (p, *J* = 6.3 Hz, 1H), 1.58 (heptd, *J* = 6.8, 5.6 Hz, 1H), 1.11 (d, *J* = 6.3 Hz, 3H), 0.89 (d, *J* = 6.8 Hz, 3H), 0.87 (d, *J* = 6.8 Hz, 3H). Retention times: tR = 9.061 min, tS = 9.476 min

8.5.5. butan-2-ol:

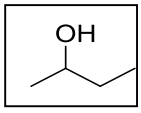

^{1}H NMR (400 MHz, $CDCl_3$) δ 3.70 (h, *J* = 6.2 Hz, 1H), 1.52 – 1.38 (m, 2H), 1.16 (d, *J* = 6.2 Hz, 3H), 0.91 (t, *J* = 7.5 Hz, 3H). T = 40°C, P = 15 psi, retention times: tR = 6.537 min, tS = 6.773 min

8.5.6. heptan-2-ol*:

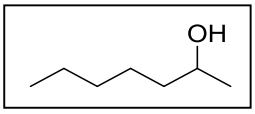

*hept-2-ol was converted to octan-2-yl acetate via reaction with acetyl chloride for proper separation

^{1}H NMR (400 MHz, $CDCl_3$) δ 3.79 (dt, *J* = 12.2, 6.0 Hz, 1H), 1.51 – 1.22 (m, 8H), 1.17 (d, *J* = 6.2 Hz, 3H), 0.87 (t, *J* = 6.6 Hz, 3H). T = 70 °C, P = 15 psi, retention times: tR = 7.5 min, tS = 8.2 min

8.5.7. octan-2-ol*

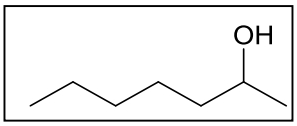

*octan-2-ol was converted to octan-2-yl acetate via reaction with acetyl chloride for proper separation.

^{1}H NMR (400 MHz $CDCl_3$) δ 3.83 – 3.73 (m, 1H), 1.37 – 1.22 (m, 8H), 1.17 (d, *J* = 6.2 Hz, 3H), 0.87 (t, *J* = 3.2 Hz, 3H).

T = 80°C, P = 15 psi, retention times: tR = 13.384 min, tS = 16.040 min

8.5.8. 2-methyl-1-phenylpropan-1-ol

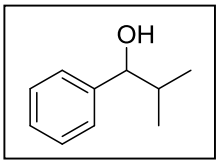

^{1}H NMR (400 MHz, $CDCl_3$) δ 7.57 – 7.27 (m, 5H), 4.35 (d, *J* = 6.9 Hz, 1H), 1.94 (dq, *J* = 13.5, 6.8 Hz, 1H), 1.20 (d, *J* = 6.9 Hz, 6H)

T = 130°C, P = 15 psi, retention times: tR = 5.853 min, tS = 6.078 min

8.5.9. 1-phenylpropan-1-ol

^{1}H NMR (400 MHz, $CDCl_3$): δ 7.28–7.33 (m, 5H, Ph), 4.59 (t, 1H, J= 6.5Hz, CH), 1.76 (m, 2H, CH_2), 0.91 (t, 3H ,J= 7.5 Hz, CH_3)

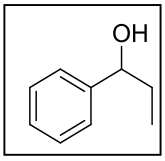

T = 120°C, P = 15 psi, retention times: tR = 7.825, tS = 8.076

8.5.10. cyclohexyl(phenyl)methanol

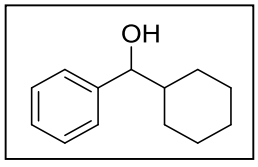

^{1}H NMR (400 MHz, $CDCl_3$) δ 7.32-7.42 (m, 5H), 4.42 (d, J =7.2 hz, 1H), 2.04-2.07 (m, 1H), 1.95 (s, 1H), 1.80-1.87 (m, 1H), 1.60-1.79 (m, 3H), 1.42-1.46 (m, 1H), 1.24-1.33 (m, 5H).

8.5.11. 1-cyclohexylethan-1-ol

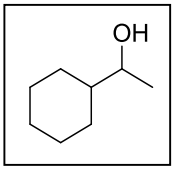

^{1}H NMR (400 MHz, $CDCl_3$) δ 3.53 (p, *J* = 6.2 Hz, 1H), 1.36 – 1.15 (m, 8H), 1.14 (d, *J* = 6.3 Hz, 3H), 1.06 – 0.89 (m, 2H). T = 100°C, P = 15 psi, retention times: tR = 8.645 min, tS = 9.457 min

8.5.12. 1-(4-fluorophenyl)ethan-1-ol

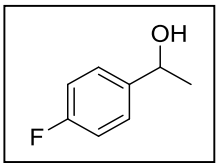

^{1}H NMR (400 MHz, $CDCl_3$) δ 7.34 – 7.26 (m, 2H), 7.03 – 6.94 (m, 2H), 4.84 (q, *J* = 6.4 Hz, 1H), 1.44 (d, *J* = 6.5 Hz, 3H). T = 120°C, P = 15 psi, retention times: tR = 7.354 min, tS = 7.710 min

8.5.13. 2,2,2-trifluoro-1-phenylethan-1-ol

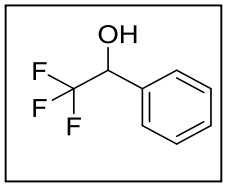

T = 120°C, P = 15 psi, retention times: tR = 4.187 min, tS = 7.862 min

(1) Knight, Julian G. *Advanced Synthesis & Catalysis* **2001**, *343*, 141.
(2) Noyori; John Wiley & Sons: 1994.
(3) Gladiali, S.; Alberico, E. *Chemical Society Reviews* **2006**, *35*, 226.
(4) Patel, R. N.; McNamee, C. G.; Banerjee, A.; Howell, J. M.; Robison, R. S.; Szarka, L. J. *Enzyme and Microbial Technology* **1992**, *14*, 731.
(5) Schenk, D.; Games, D.; Seubert, P. *J Mol Neurosci* **2001**, *17*, 259.
(6) Noyori, R. *Angewandte Chemie International Edition* **2002**, *41*, 2008.
(7) Campbell, E. J.; Zhou, H.; Nguyen, S. T. *Angewandte Chemie International Edition* **2002**, *41*, 1020.
(8) Evans, D. A.; Nelson, S. G.; Gagne, M. R.; Muci, A. R. *J. Am. Chem. Soc.* **1993**, *115*, 9800.
(9) Fujii, A.; Hashiguchi, S.; Uematsu, N.; Ikariya, T.; Noyori, R. *J. Am. Chem. Soc.* **1996**, *118*, 2521.
(10) Wu, X. F.; Wang, C.; Xiao, J. L. *Platin. Met. Rev.* **2010**, *54*, 3.
(11) Nordin, S. J. M.; Roth, P.; Tarnai, T.; Alonso, D. A.; Brandt, P.; Andersson, P. G. *Chem.-Eur. J.* **2001**, *7*, 1431.
(12) Noyori, R.; Hashiguchi, S. *Accounts Chem. Res.* **1997**, *30*, 97.
(13) Hayes, A.; Clarkson, G.; Wills, M. *Tetrahedron: Asymmetry* **2004**, *15*, 2079.
(14) Hayes, A. M.; Morris, D. J.; Clarkson, G. J.; Wills, M. *J. Am. Chem. Soc.* **2005**, *127*, 7318.
(15) Cheung, F. K.; Lin, C. X.; Minissi, F.; Criville, A. L.; Graham, M. A.; Fox, D. J.; Wills, M. *Organic Letters* **2007**, *9*, 4659.
(16) Matharu, D. S.; Martins, J. E. D.; Wills, M. *Chem.-Asian J.* **2008**, *3*, 1374.
(17) Everaere, K.; Mortreux, A.; Carpentier, J.-F. *Advanced Synthesis & Catalysis* **2003**, *345*, 67.
(18) Takehara, J.; Hashiguchi, S.; Fujii, A.; Inoue, S.-i.; Ikariya, T.; Noyori, R. *Chemical Communications* **1996**, *0*, 233.
(19) Hashiguchi, S.; Fujii, A.; Takehara, J.; Ikariya, T.; Noyori, R. *J. Am. Chem. Soc.* **1995**, *117*, 7562.
(20) Ohkuma, T.; Ooka, H.; Hashiguchi, S.; Ikariya, T.; Noyori, R. *J. Am. Chem. Soc.* **1995**, *117*, 2675.
(21) Ohkuma, T.; Hattori, T.; Ooka, H.; Inoue, T.; Noyori, R. *Organic Letters* **2004**, *6*, 2681.
(22) Noyori, R.; Koizumi, M.; Ishii, D.; Ohkuma, T. *Pure and Applied Chemistry* **2001**, *73*, 227.
(23) Wu, J.; Chen, H.; Kwok, W.; Guo, R. W.; Zhou, Z. Y.; Yeung, C.; Chan, A. S. C. *Journal of Organic Chemistry* **2002**, *67*, 7908.
(24) Burk, M. J.; Hems, W.; Herzberg, D.; Malan, C.; Zanotti-Gerosa, A. *Organic Letters* **2000**, *2*, 4173.
(25) Yamakawa, M.; Ito, H.; Noyori, R. *J. Am. Chem. Soc.* **2000**, *122*, 1466.
(26) Haack, K. J.; Hashiguchi, S.; Fujii, A.; Ikariya, T.; Noyori, R. *Angew. Chem.-Int. Edit. Engl.* **1997**, *36*, 285.
(27) Yamakawa, M.; Yamada, I.; Noyori, R. *Angew. Chem.-Int. Edit.* **2001**, *40*, 2818.
(28) Wu, X. F.; Liu, J. K.; Di Tommaso, D.; Iggo, J. A.; Catlow, C. R. A.; Bacsa, J.; Xiao, J. L. *Chem.-Eur. J.* **2008**, *14*, 7699.
(29) Dub, P. A.; Ikariya, T. *J. Am. Chem. Soc.* **2013**, *135*, 2604.
(30) Pavlova, A.; Meijer, E. J. *ChemPhysChem* **2012**, *13*, 3492.
(31) Yamada, I.; Noyori, R. *Organic Letters* **2000**, *2*, 3425.
(32) Sandoval, C. A.; Ohkuma, T.; Muniz, K.; Noyori, R. *J. Am. Chem. Soc.* **2003**, *125*, 13490.
(33) Abdur-Rashid, K.; Faatz, M.; Lough, A. J.; Morris, R. H. *J. Am. Chem. Soc.* **2001**, *123*, 7473.
(34) Dub, P. A.; Henson, N. J.; Martin, R. L.; Gordon, J. C. *J. Am. Chem. Soc.* **2014**, *136*, 3505.

(35) Rautenstrauch, V.; Hoang-Cong, X.; Churlaud, R.; Abdur-Rashid, K.; Morris, R. H. *Chem.-Eur. J.* **2003**, *9*, 4954.

(36) Ohkuma, T.; Utsumi, N.; Tsutsumi, K.; Murata, K.; Sandoval, C.; Noyori, R. *J. Am. Chem. Soc.* **2006**, *128*, 8724.

(37) Sandoval, C. A.; Bie, F.; Matsuoka, A.; Yamaguchi, Y.; Naka, H.; Li, Y.; Kato, K.; Utsumi, N.; Tsutsumi, K.; Ohkuma, T.; Murata, K.; Noyori, R. *Chem.-Asian J.* **2010**, *5*, 806.

(38) Wu, X.; Corcoran, C.; Yang, S.; Xiao, J. *ChemSusChem* **2008**, *1*, 71.

(39) Bubert, C.; Blacker, J.; Brown, S. M.; Crosby, J.; Fitzjohn, S.; Muxworthy, J. P.; Thorpe, T.; Williams, J. M. J. *Tetrahedron Letters* **2001**, *42*, 4037.

(40) Thorpe, T.; Blacker, J.; Brown, S. M.; Bubert, C.; Crosby, J.; Fitzjohn, S.; Muxworthy, J. P.; Williams, J. M. J. *Tetrahedron Letters* **2001**, *42*, 4041.

(41) Wu, X.; Li, X.; Hems, W.; King, F.; Xiao, J. *Organic & Biomolecular Chemistry* **2004**, *2*, 1818.

(42) Wu, X.; Li, X.; Zanotti-Gerosa, A.; Pettman, A.; Liu, J.; Mills, A. J.; Xiao, J. *Chemistry – A European Journal* **2008**, *14*, 2209.

(43) Wu, X.; Li, X.; King, F.; Xiao, J. *Angewandte Chemie* **2005**, *117*, 3473.

(44) Corey, E. J.; Bakshi, R. K.; Shibata, S.; Chen, C. P.; Singh, V. K. *J. Am. Chem. Soc.* **1987**, *109*, 7925.

(45) Ohkuma, T.; Sandoval, C. A.; Srinivasan, R.; Lin, Q.; Wei, Y.; Muniz, K.; Noyori, R. *J. Am. Chem. Soc.* **2005**, *127*, 8288.

(46) Reetz, M. T.; Li, X. G. *J. Am. Chem. Soc.* **2006**, *128*, 1044.

(47) Schlatter, A.; Woggon, W. D. *Advanced Synthesis & Catalysis* **2008**, *350*, 995.

(48) Boukachabia, M.; Zeror, S.; Collin, J.; Fiaud, J. C.; Zouioueche, L. A. *Tetrahedron Letters* **2011**, *52*, 1485.

(49) Li, J. H.; Tang, Y. F.; Wang, Q. W.; Li, X. F.; Cun, L. F.; Zhang, X. M.; Zhu, J.; Li, L. C.; Deng, J. G. *J. Am. Chem. Soc.* **2012**, *134*, 18522.

(50) A. Tomita, H. H., S. Makishima *Inorg. Chem.* **1967**, *6*, 1746.

(51) A. Tomita, H. H., S. Makishima *Inorganic Nuclear Chemistry Letters* **1968**, *4*, 715.

(52) Kovalev, Y. G.; Ioganson, A. A. *Zhurnal Obshchei Khimii* **1985**, *55*, 1211.

(53) Darensbourg, D. J.; Atnip, E. V.; Klausmeyer, K. K.; Reibenspies, J. N. *Inorg. Chem.* **1994**, *33*, 5230.

(54) Beck, W.; Petri, W.; Meder, J. *Journal of Organometallic Chemistry* **1980**, *191*, 73.

(55) Maksakov, V. A.; Ershova, V. A.; Kirin, V. P. *Koord. Khimiya* **1996**, *22*, 424.

(56) Severin, K.; Sunkel, K.; Beck, W. *Chemische Berichte* **1994**, *127*, 615.

(57) Werner, H.; Daniel, T.; Nürnberg, O.; Knaup, W.; Meyer, U. *Journal of Organometallic Chemistry* **1993**, *445*, 229.

(58) Severin, K.; Mihan, S.; Beck, W. *Chemische Berichte* **1995**, *128*, 1127.

(59) Hauck, T.; Sunkel, K.; Beck, W. *Inorganica Chimica Acta* **1995**, *235*, 391.

(60) Potvin, C.; Davignon, L.; Pannetier, G. *Bulletin de la Société chimique de France* **1975**, 507.

(61) Sheldrick, W. S.; Exner, R. *Inorganica Chimica Acta* **1989**, *166*, 213.

(62) Schmidt, D.; Gilav, E. *Journal of Organometallic Chemistry* **1986**, *307*, 377.

(63) Carmona, D.; Viguri, F.; Pilar Lamata, M.; Ferrer, J.; Bardaji, E.; Lahoz, F. J.; Garcia-Orduna, P.; Oro, L. A. *Dalton Transactions* **2012**, *41*, 10298.

(64) Carmona, D.; Lahoz, F. J.; Garcia-Orduna, P.; Oro, L. A.; Lamata, M. P.; Viguri, F. *Organometallics* **2012**, *31*, 3333.

(65) Krämer, R.; Polborn, K.; Wanjek, H.; Zahn, I.; Beck, W. *Chemische Berichte* **1990**, *123*, 767.

(66) Bergs, R.; Sunkel, K.; Beck, W. *Chemische Berichte-Recueil* **1993**, *126*, 2429.
(67) Schuhmann, E.; Robl, C.; Beck, W. *Z.Naturforsch.(B)* **1994**, *49*, 1569.
(68) Roy, C. P.; Huff, L. A.; Barker, N. A.; Berg, M. A. G.; Merola, J. S. *Journal of Organometallic Chemistry* **2006**, *691*, 2270.
(69) Sheldrick, W. S.; Exner, R. *Inorganica Chimica Acta* **1990**, *175*, 261.
(70) Fu, C.; Wenzel, M.; Treutlein, E.; Harms, K.; Meggers, E. *Inorg. Chem.* **2012**, *51*, 10004.
(71) Perekalin, D. S.; Karslyan, E. E.; Petrovskii, P. V.; Nelyubina, Y. V.; Lyssenko, K. A.; Kononikhin, A. S.; Nikolaev, E. N.; Kudinov, A. R. *Chem.-Eur. J.* **2010**, *16*, 8466.
(72) Chernova, N. N.; Kurskii, I. G.; Strukov, V. V. *Zhurnal Neorganicheskoi Khimii* **1978**, *23*, 430.
(73) Pneumatikakis, G.; Psaroulis, P. *Inorganica Chimica Acta-Bioinorganic Chemistry* **1980**, *46*, 97.
(74) Rosenberg, B. *Nature (London)* **1969**, *222*, 385.
(75) Gallerani, E.; Bauer, J.; Hess, D.; Boehm, S.; Droege, C.; Jeckelmann, S.; Miani, M.; Herrmann, R.; Marsoni, S.; Sperka, S.; Sessa, C. *Acta Oncologica* **2011**, *50*, 1105.
(76) Wheate, N. J.; Walker, S.; Craig, G. E.; Oun, R. *Dalton Transactions* **2010**, *39*, 8113.
(77) Karpin, G. W.; Merola, J. S.; Falkinham, J. O., III *Antimicrobial Agents and Chemotherapy* **2013**, *57*, 3434.
(78) Leung, C.-H.; Zhong, H.-J.; Chan, D. S.-H.; Ma, D.-L. *Coordination Chemistry Reviews* **2013**, *257*, 1764.
(79) Gasser, G.; Metzler-Nolte, N. *Curr. Opin. Chem. Biol.* **2012**, *16*, 84.
(80) Barry, N. P. E.; Sadler, P. J. *Chemical Society Reviews* **2012**, *41*, 3264.
(81) Morris, R. E.; Aird, R. E.; Murdoch, P. D.; Chen, H. M.; Cummings, J.; Hughes, N. D.; Parsons, S.; Parkin, A.; Boyd, G.; Jodrell, D. I.; Sadler, P. J. *Journal of Medicinal Chemistry* **2001**, *44*, 3616.
(82) Allardyce, C. S.; Dyson, P. J.; Ellis, D. J.; Heath, S. L. *Chemical Communications* **2001**, 1396.
(83) White, C. *Inorganic syntheses* **1992**, *29*, 228.
(84) Carmona, D.; Pilar Lamata, M.; Viguri, F.; San José, E.; Mendoza, A.; Lahoz, F. J.; García-Orduña, P.; Atencio, R.; Oro, L. A. *Journal of Organometallic Chemistry* **2012**, *717*, 152.
(85) Carmona, D.; Lahoz, F. J.; Atencio, R.; Oro, L. A.; Lamata, M. P.; San José, E. *Tetrahedron: Asymmetry* **1993**, *4*, 1425.
(86) Carmona, D.; Mendoza, A.; Lahoz, F. J.; Oro, L. A.; Lamata, M. P.; Jose, E. S. *Journal of Organometallic Chemistry* **1990**, *396*, C17.
(87) Lampeka, R.; Bergs, R.; Kramer, R.; Polborn, K.; Beck, W. *Z.Naturforsch.(B)* **1994**, *49*, 225.
(88) Carmona, D.; Vega, C.; Lahoz, F. J.; Atencio, R.; Oro, L. A.; Lamata, M. P.; Viguri, F.; San Jose, E. *Organometallics* **2000**, *19*, 2273.
(89) Carmona, D.; Lahoz, F. J.; Atencio, R.; Oro, L. A.; Lamata, M. P.; Viguri, F.; San José, E.; Vega, C.; Reyes, J.; Joó, F.; Kathó, Á. *Chemistry – A European Journal* **1999**, *5*, 1544.
(90) Sunkel, K.; Hoffmuller, W.; Beck, W. *Z.Naturforsch.(B)* **1998**, *53*, 1365.
(91) Kathó, Á.; Carmona, D.; Viguri, F.; Remacha, C. D.; Kovács, J.; Joó, F.; Oro, L. A. *Journal of Organometallic Chemistry* **2000**, *593–594*, 299.
(92) Wöckel, S.; Plessow, P.; Schelwies, M.; Brinks, M. K.; Rominger, F.; Hofmann, P.; Limbach, M. *ACS Catalysis* **2013**, *4*, 152.
(93) Liu, Z.; Habtemariam, A.; Pizarro, A. M.; Fletcher, S. A.; Kisova, A.; Vrana, O.; Salassa, L.; Bruijnincx, P. C. A.; Clarkson, G. J.; Brabec, V.; Sadler, P. J. *Journal of Medicinal Chemistry* **2011**, *54*, 3011.
(94) Reichardt, C. In *Pure and Applied Chemistry* 1982; Vol. 54, p 1867.
(95) Agilent; Agilent Technologies: Oxford, UK, 2012.
(96) Sheldrick, G. M. *Acta Crystallographica Section A* **2008**, *64*, 112.

(97) Dolomanov, O. V.; Bourhis, L. J.; Gildea, R. J.; Howard, J. A. K.; Puschmann, H. *Journal of Applied Crystallography* **2009**, *42*, 339.

Appendix

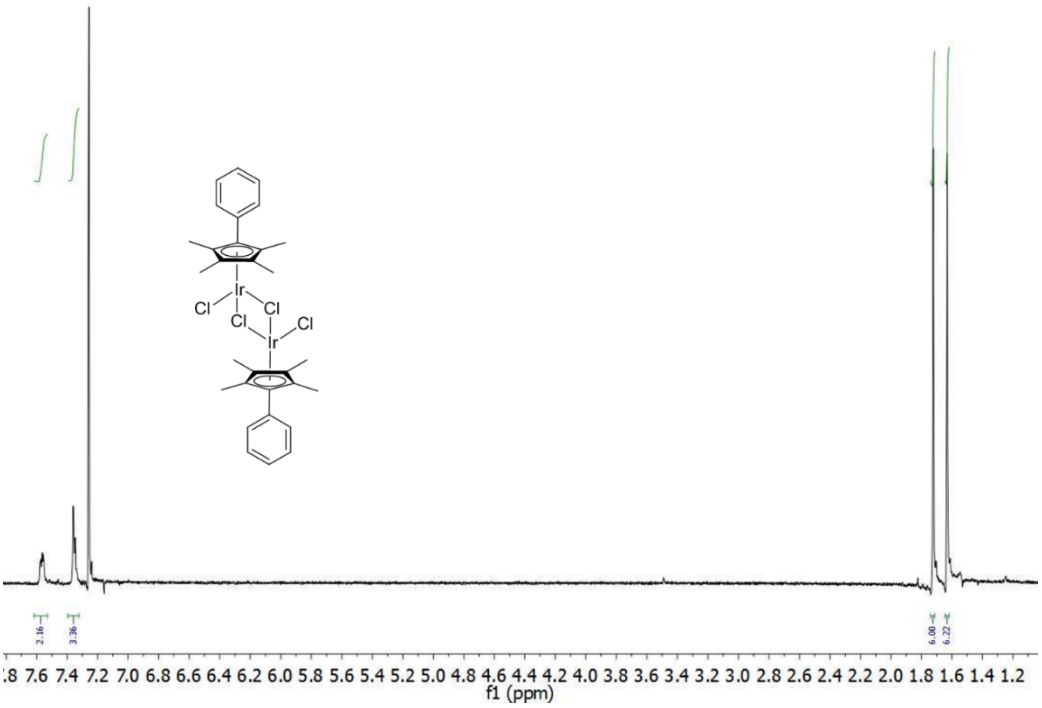

Figure A1: ^{1}H Spectra of $(\eta^5\text{-}C_5Me_4C_6H_5)IrCpCl_2]_2$

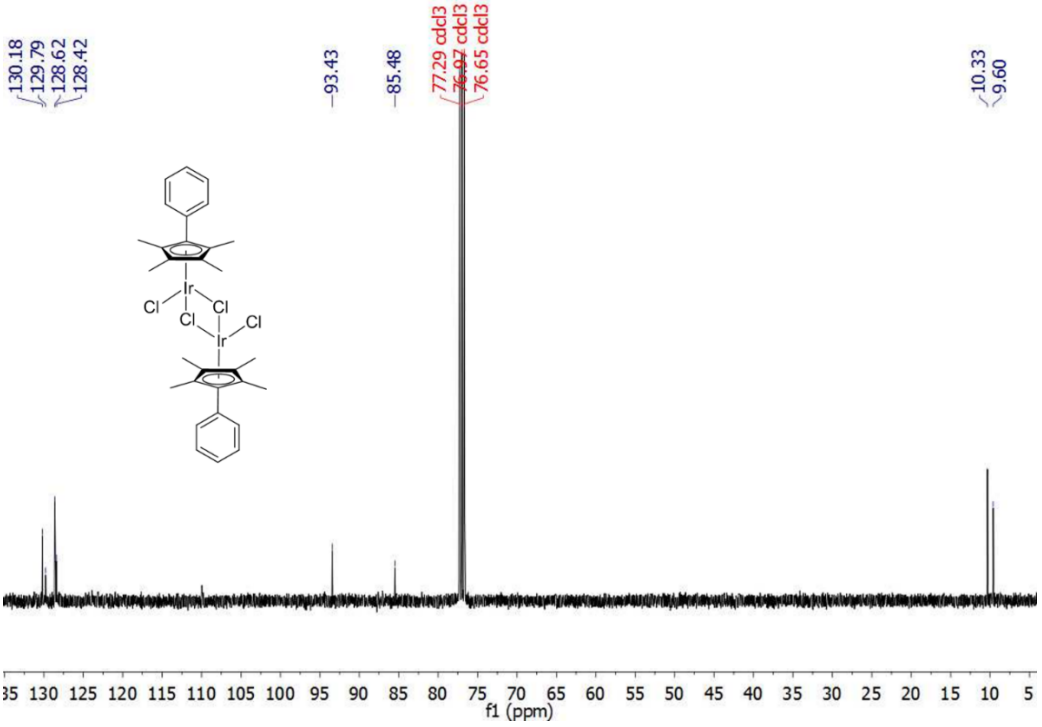

Figure A2: ^{13}C Spectra of $(\eta^5\text{-}C_5Me_4C_6H_5)IrCpCl_2]_2$

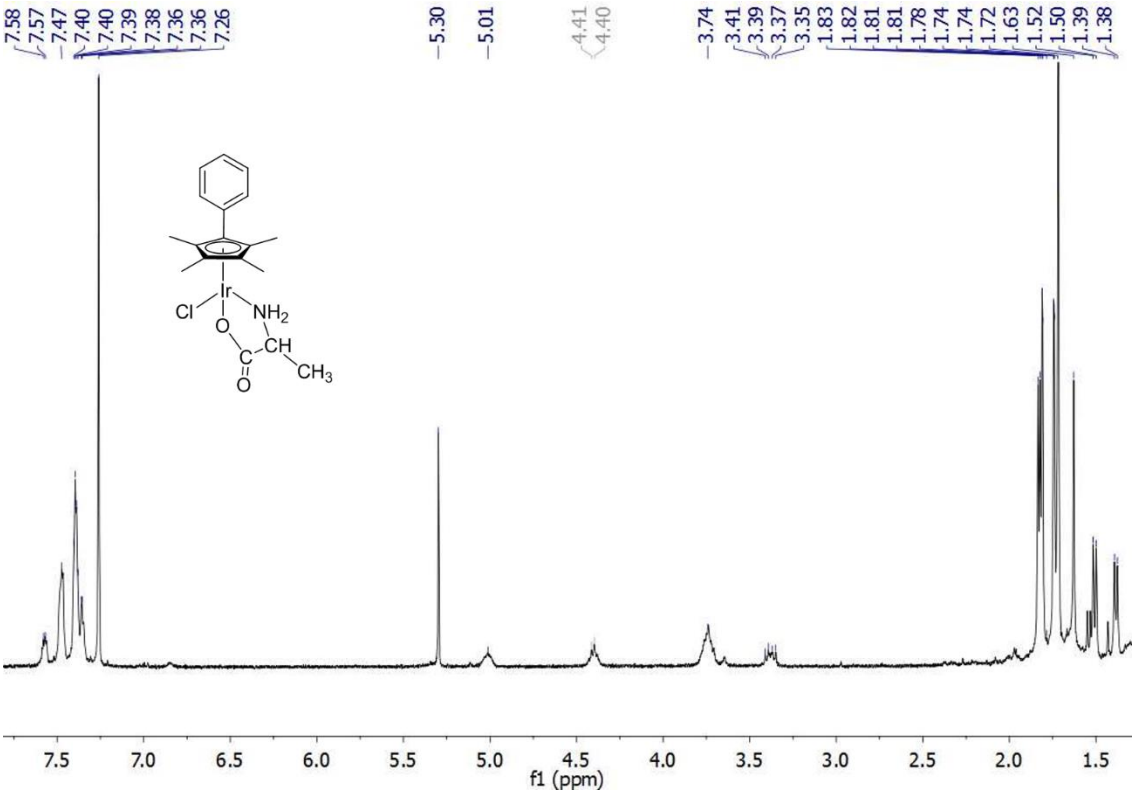

Figure A3: ^{1}H Spectra of (η^5-$C_5Me_4C_6H_5$)Ir(L-ala)Cl

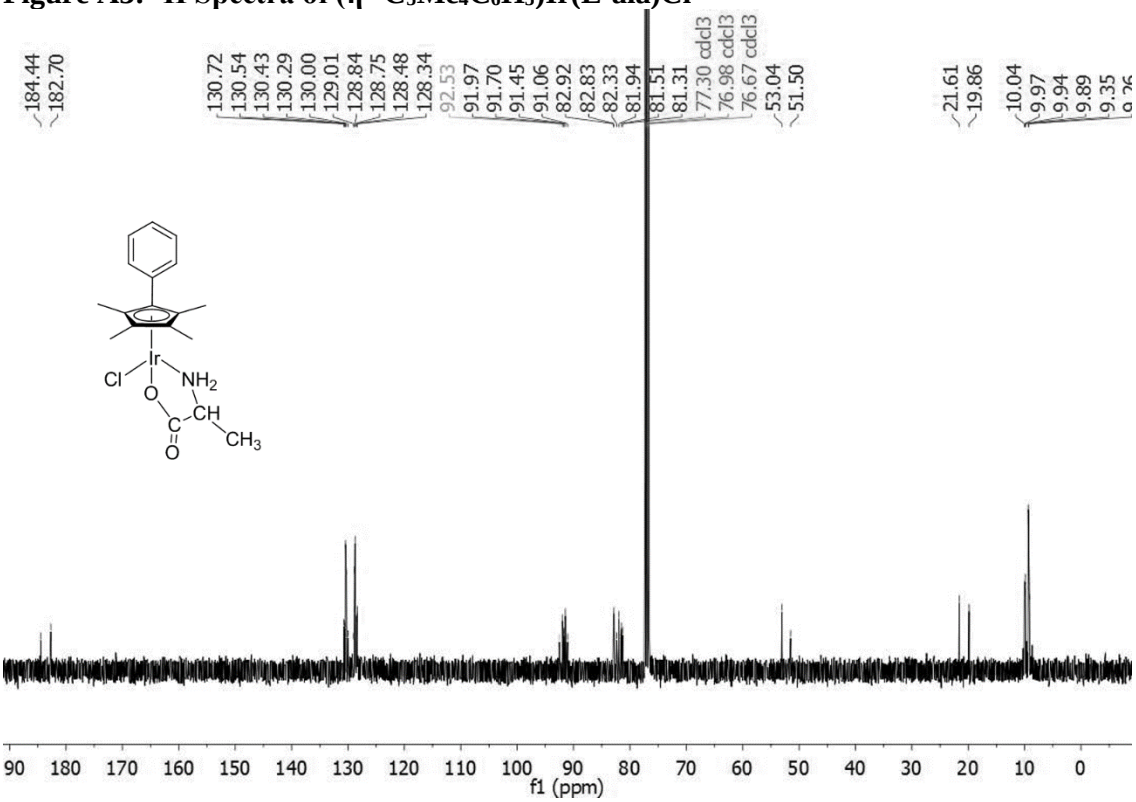

Figure A4: ^{13}C Spectra of (η^5-$C_5Me_4C_6H_5$)Ir(L-ala)Cl

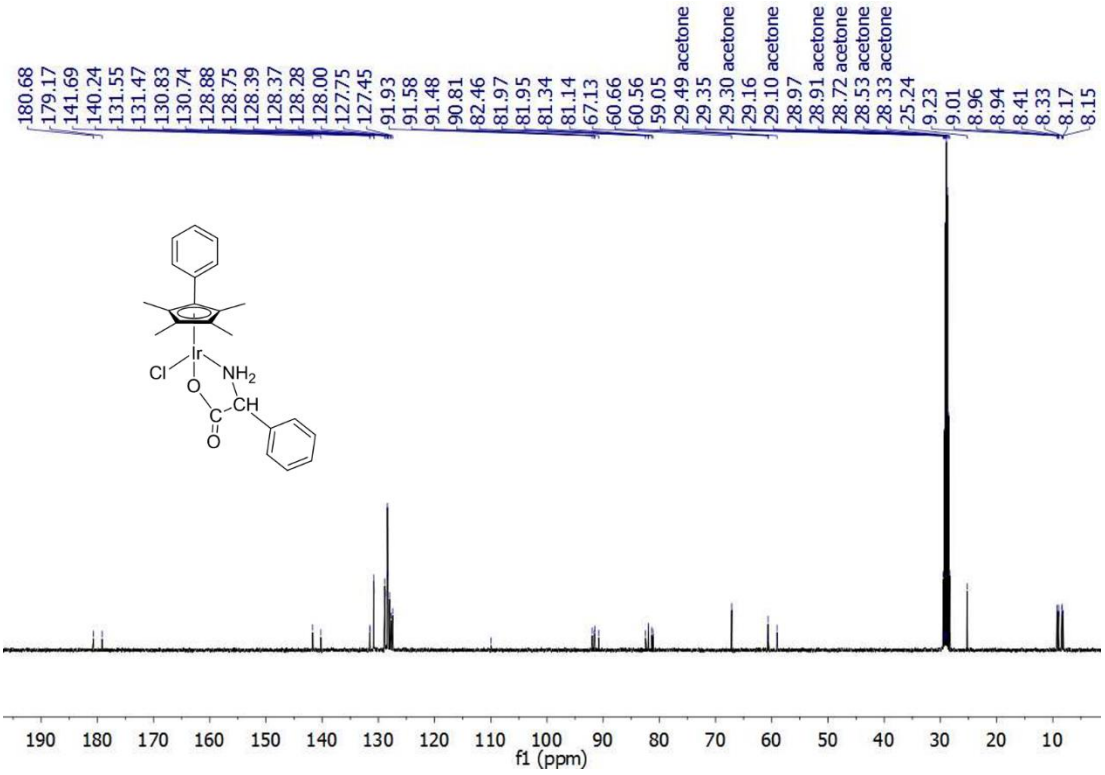

Figure A5: ^{1}H Spectra of (η^5-$C_5Me_4C_6H_5$)Ir(L-Phenylglycine)Cl

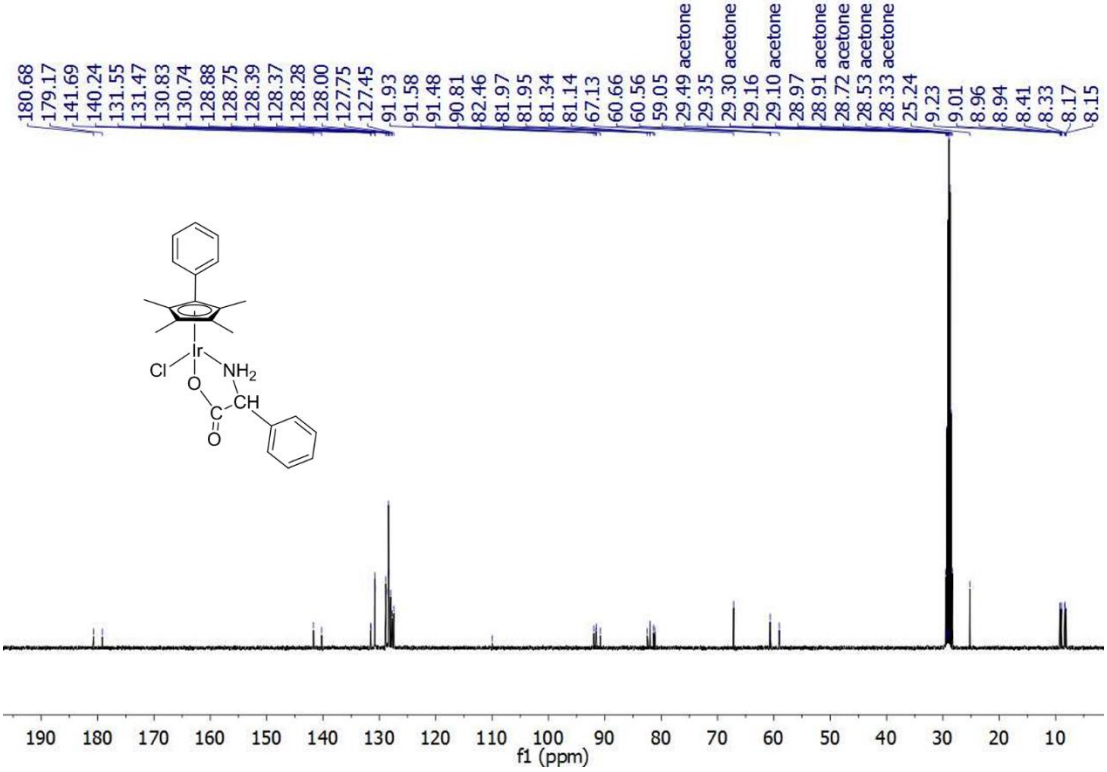

Figure A6: ^{13}C Spectra of (η^5-$C_5Me_4C_6H_5$)Ir(L-Phenylglycine)Cl

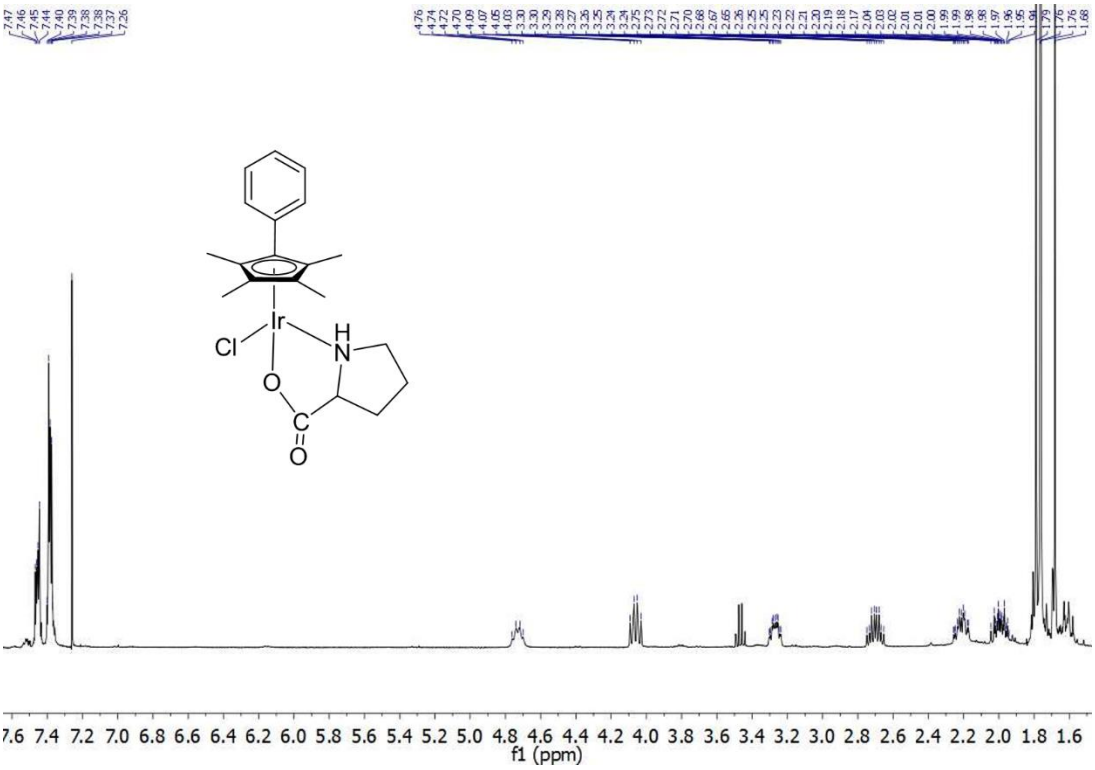

Figure A9: ^{1}H Spectra of (η^5-$C_5Me_4C_6H_5$)Ir(L-Pro)Cl

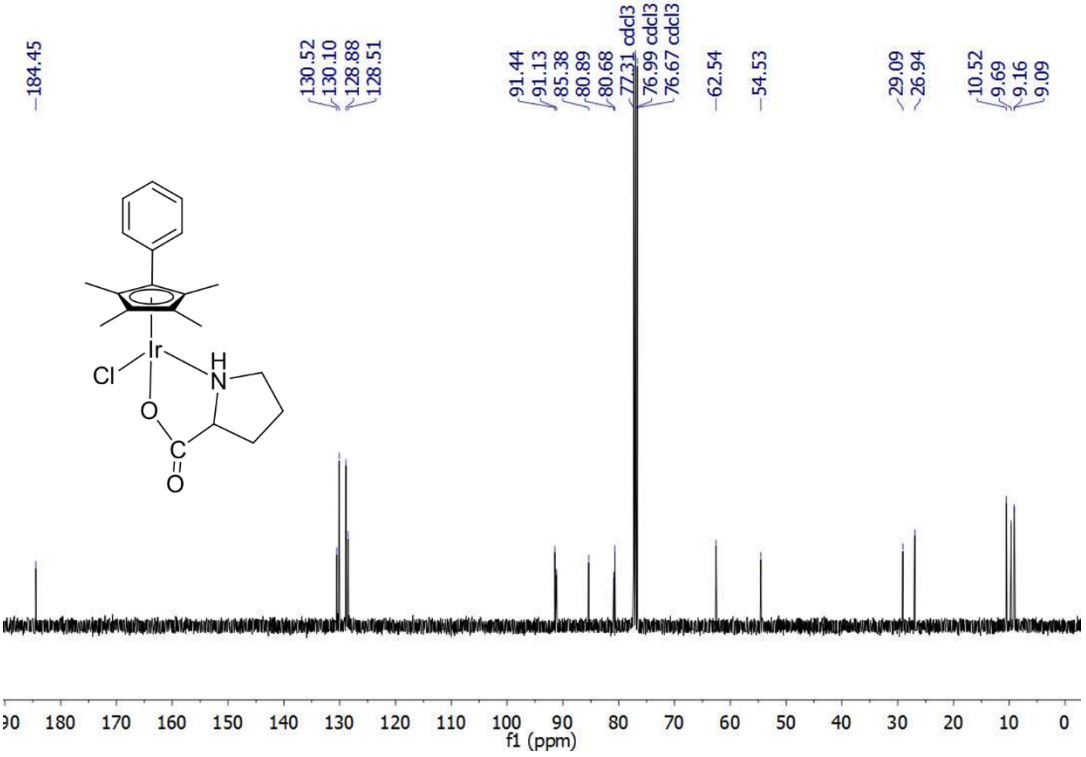

Figure A10: ^{13}C Spectra of (η^5-$C_5Me_4C_6H_5$)Ir(L-Pro)Cl

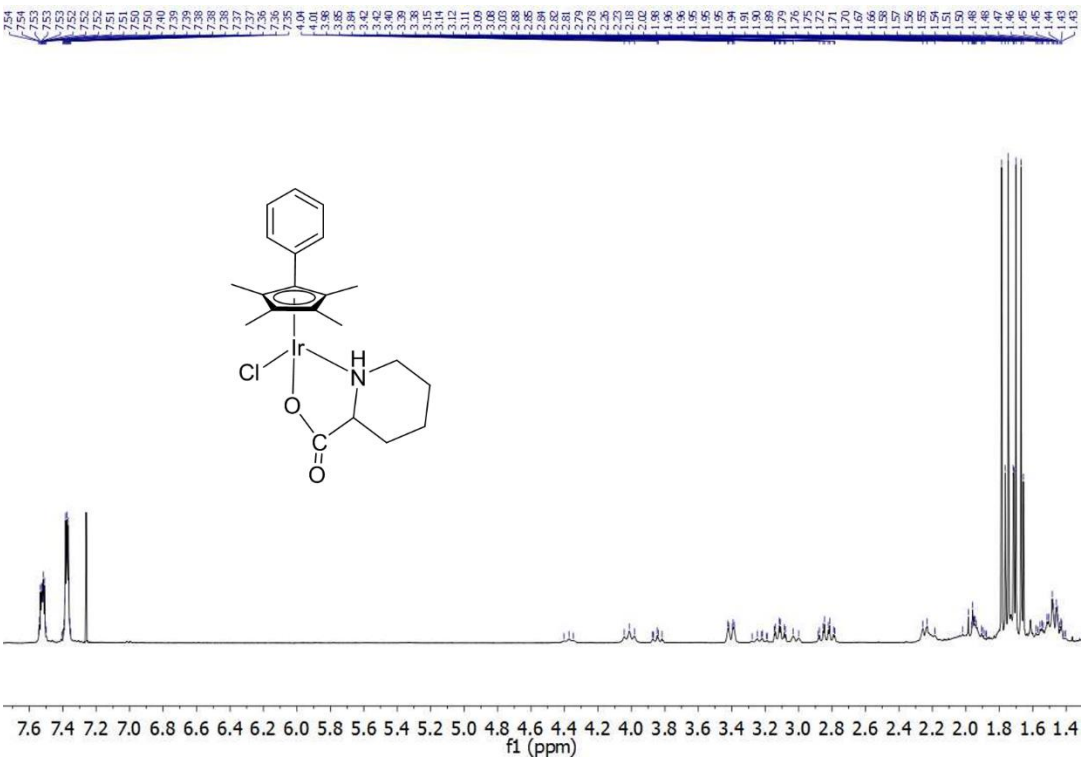

Figure A11: ^{1}H Spectra of (η^5-$C_5Me_4C_6H_5$)Ir(L-pip)Cl

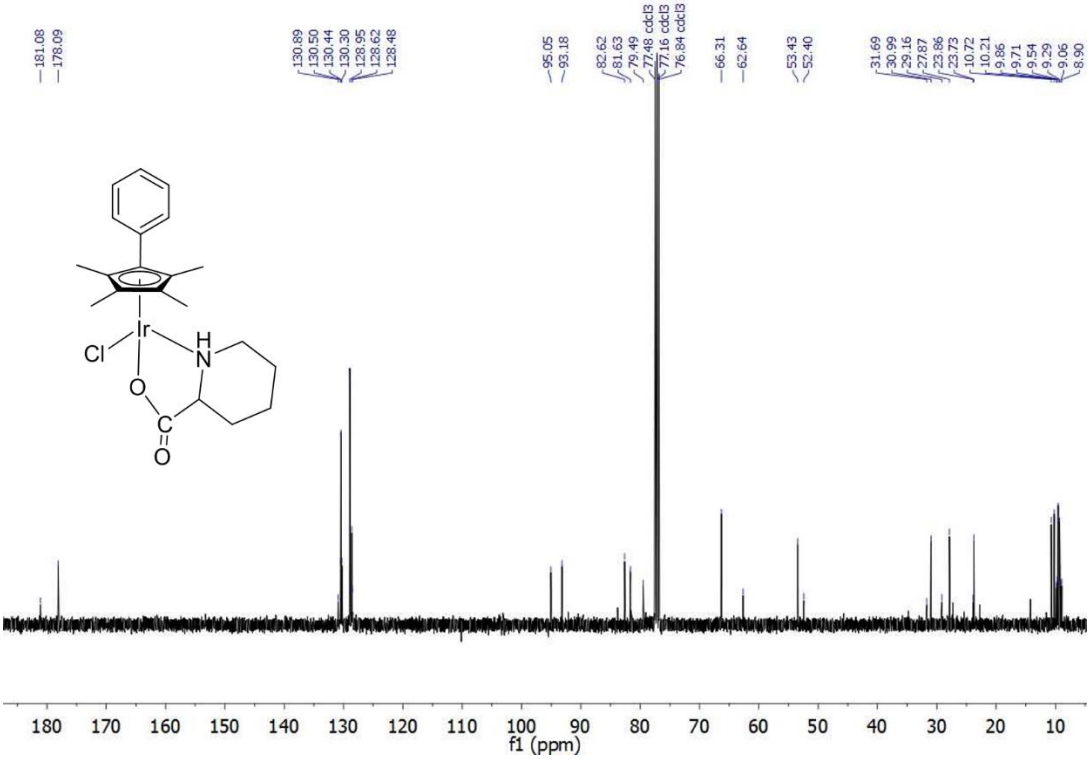

Figure A12: ^{13}C Spectra of (η^5-$C_5Me_4C_6H_5$)Ir(L-Pip)Cl

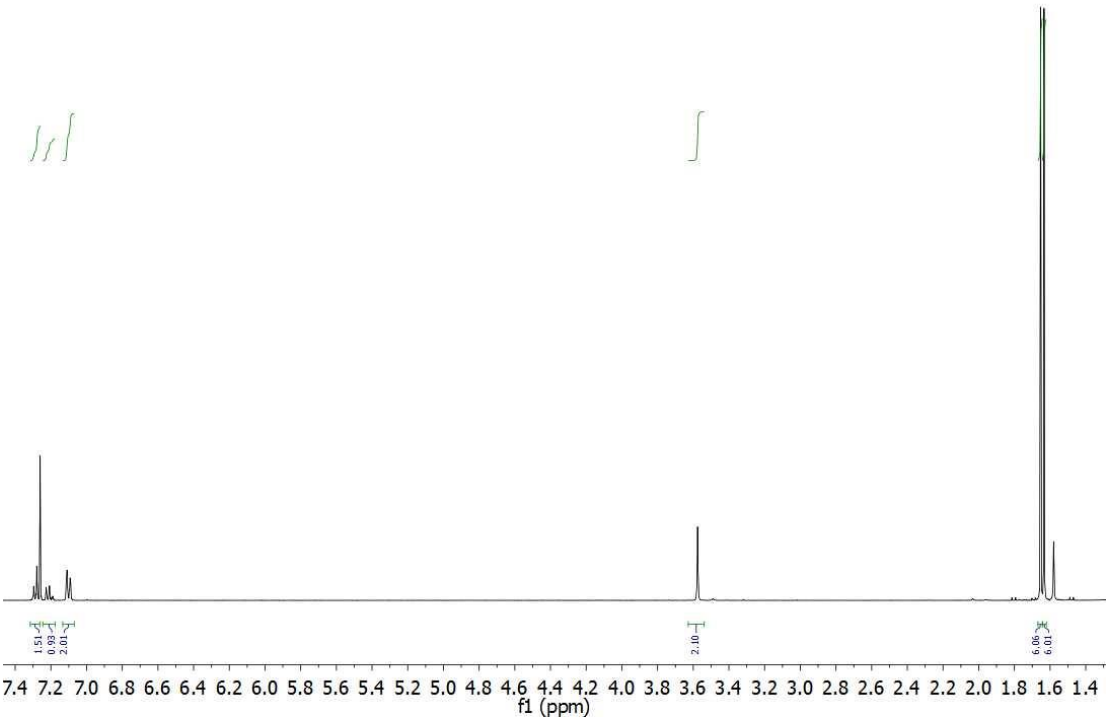

Figure A13: ^{1}H Spectra of $[(\eta^5\text{-}C_5Me_4CH_2C_6H_5)IrCpCl_2]_2$

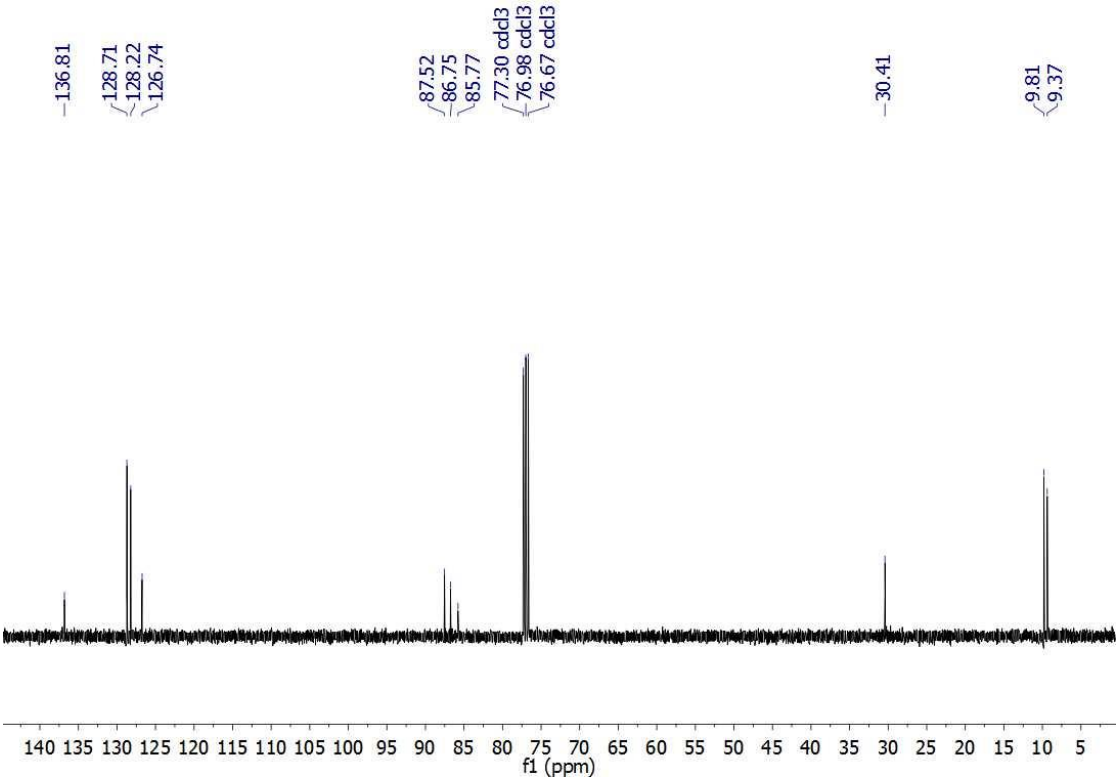

Figure A13: ^{1}H Spectra of $[(\eta^5\text{-}C_5Me_4CH_2C_6H_5)IrCpCl_2]_2$

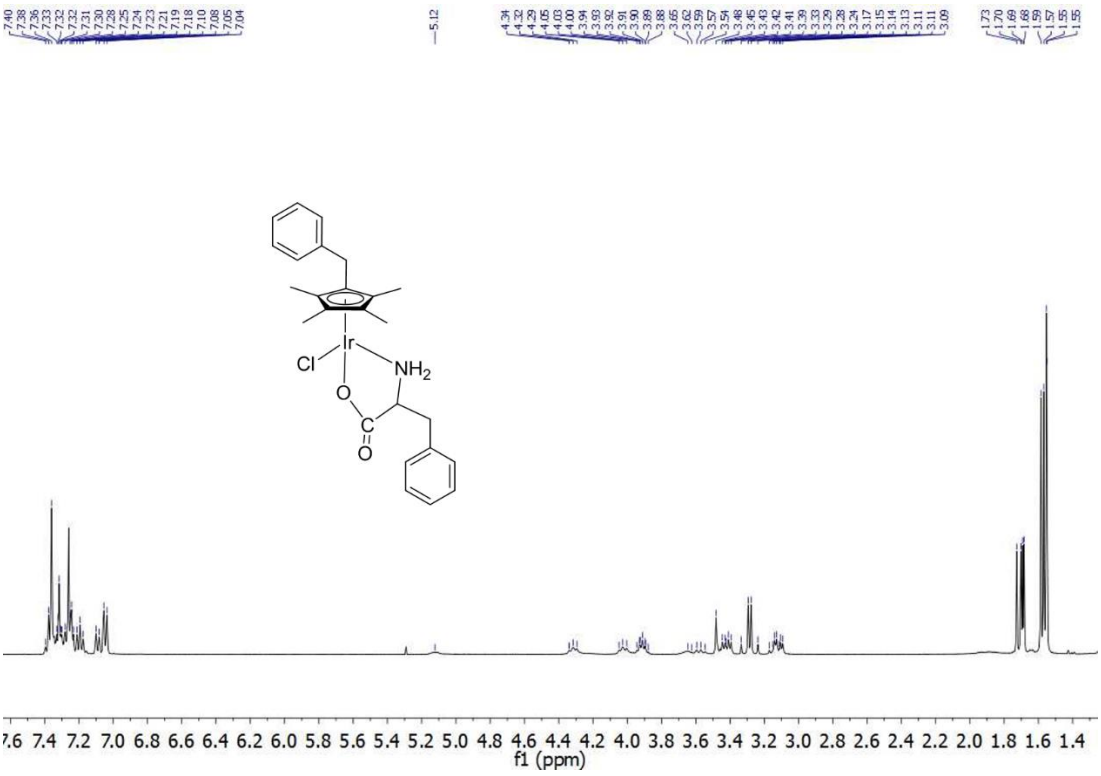

Figure A14: ^{1}H Spectra of (η^5-$C_5Me_4CH_2C_6H_5$)Ir(L-phenylalanine)Cl

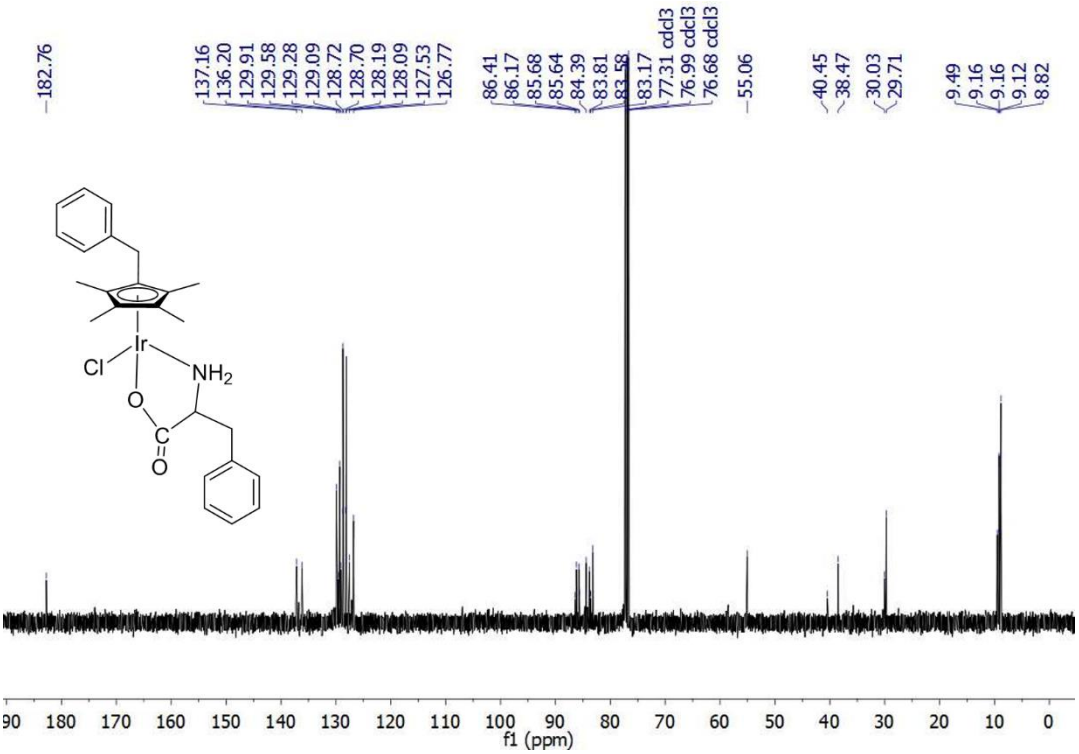

Error! No text of specified style in document.

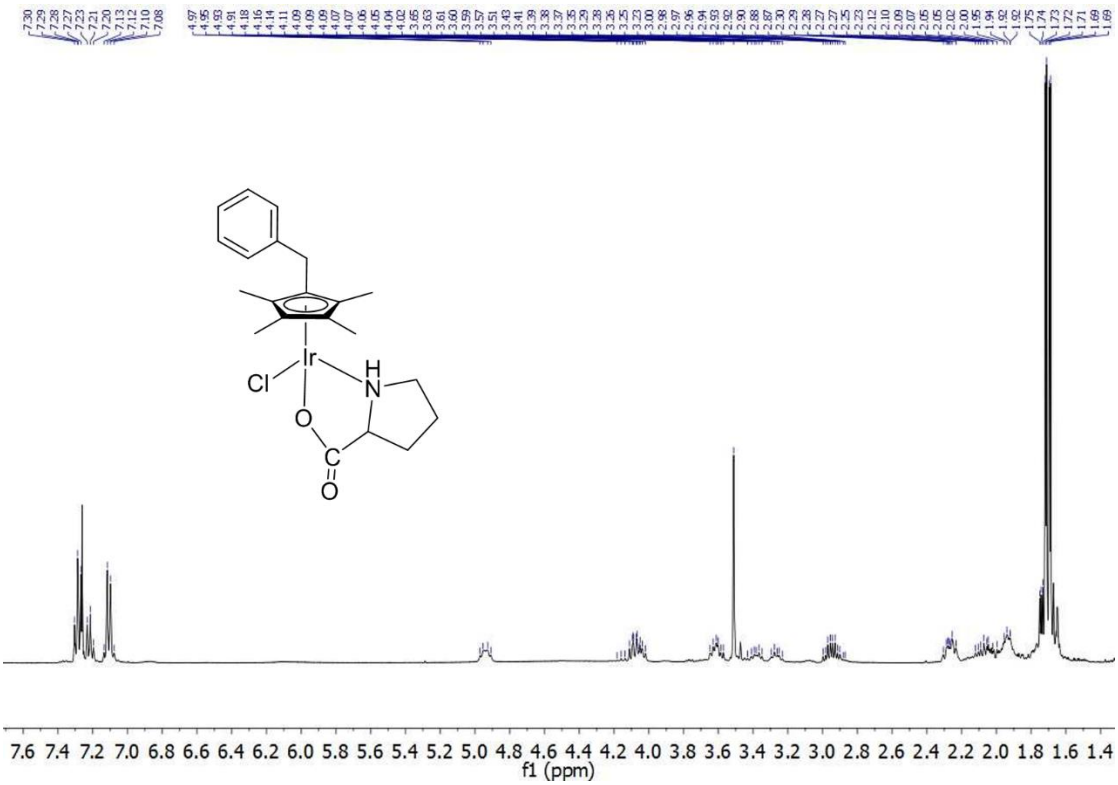

Figure A16: ^{1}H Spectra of (η^5-$C_5Me_4CH_2C_6H_5$)Ir(L-proline)Cl

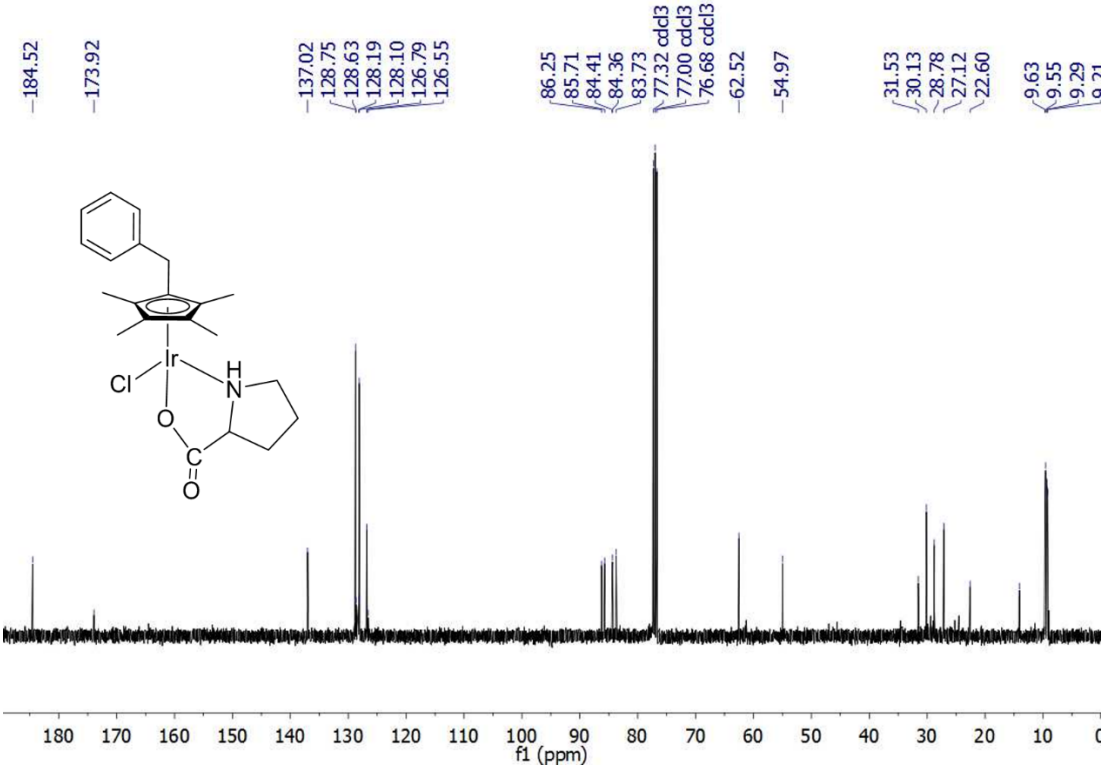

Figure A17: ^{13}C Spectra of (η^5-$C_5Me_4CH_2C_6H_5$)Ir(L-proline)Cl

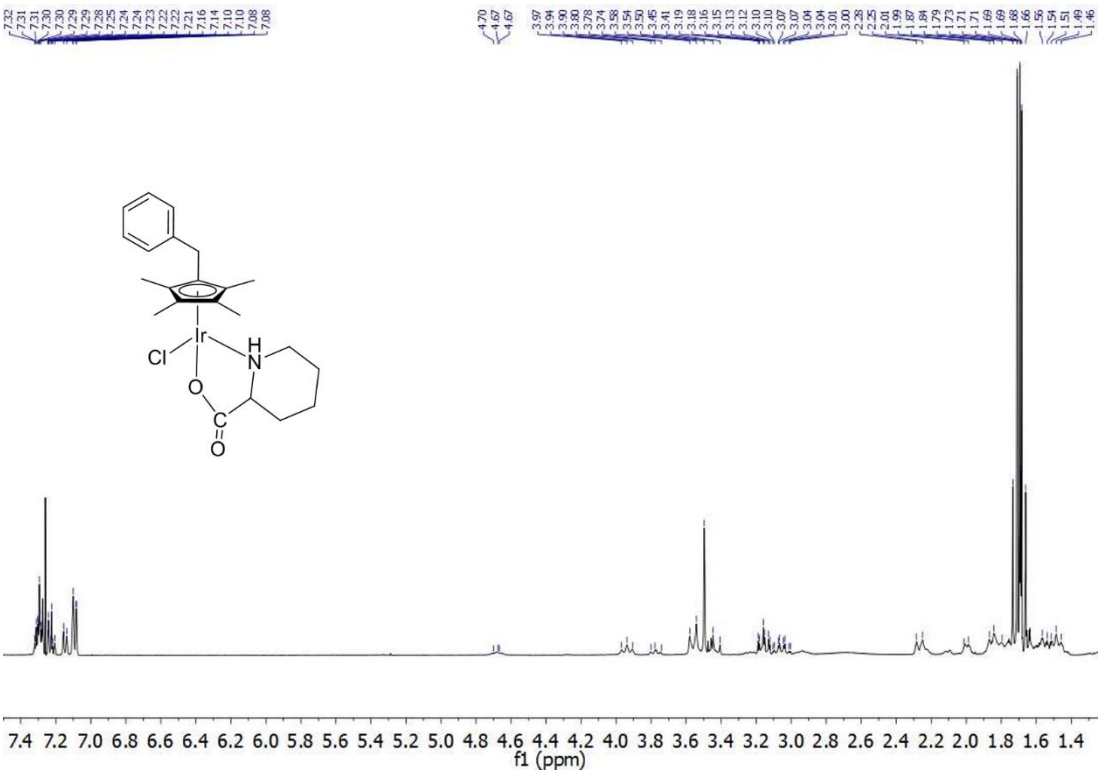

Figure A18: ^{1}H Spectra of (η^5-$C_5Me_4CH_2C_6H_5$)Ir(L-pip)Cl

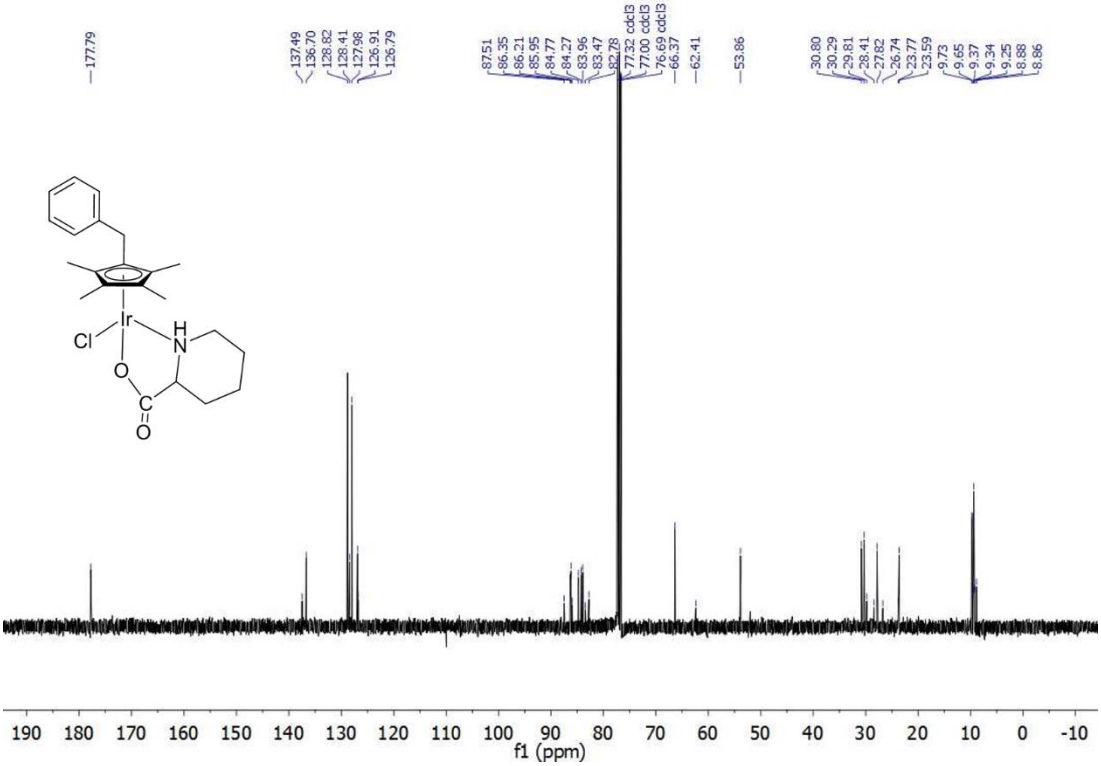

Figure A19: ^{13}C Spectra of (η^5-$C_5Me_4CH_2C_6H_5$)Ir(L-pip)Cl

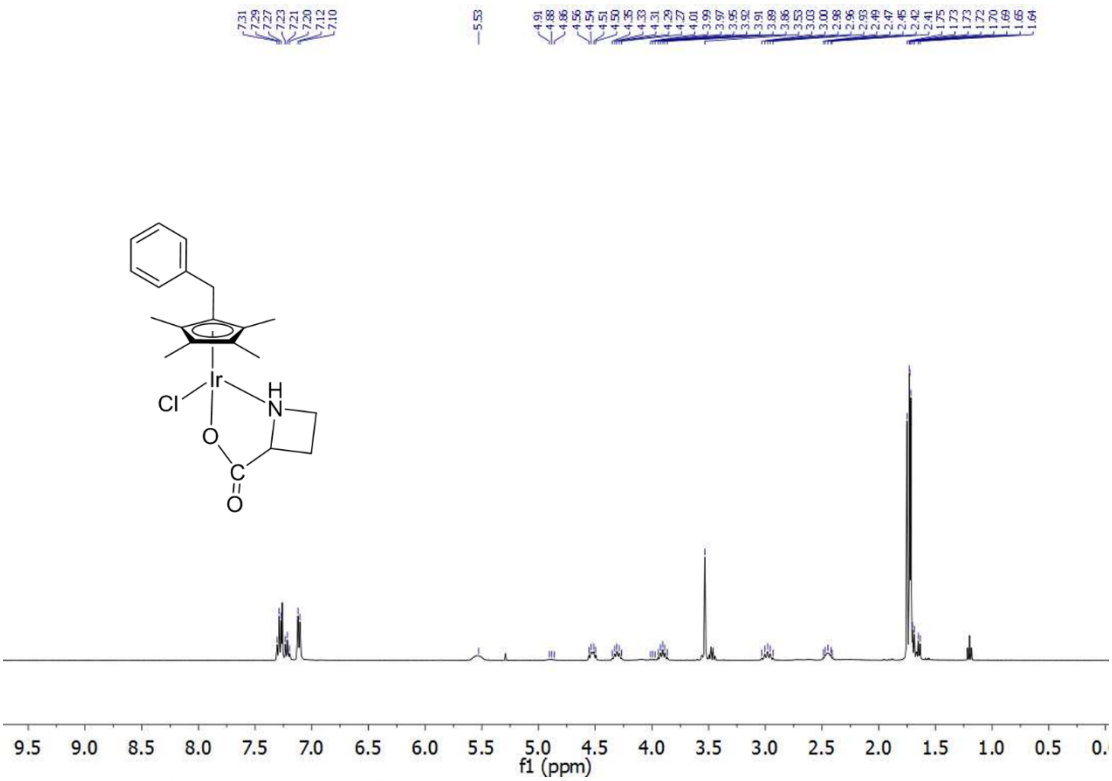

Figure A20: ^{1}H Spectra of (η^5-$C_5Me_4CH_2C_6H_5$)Ir(L-aze)Cl

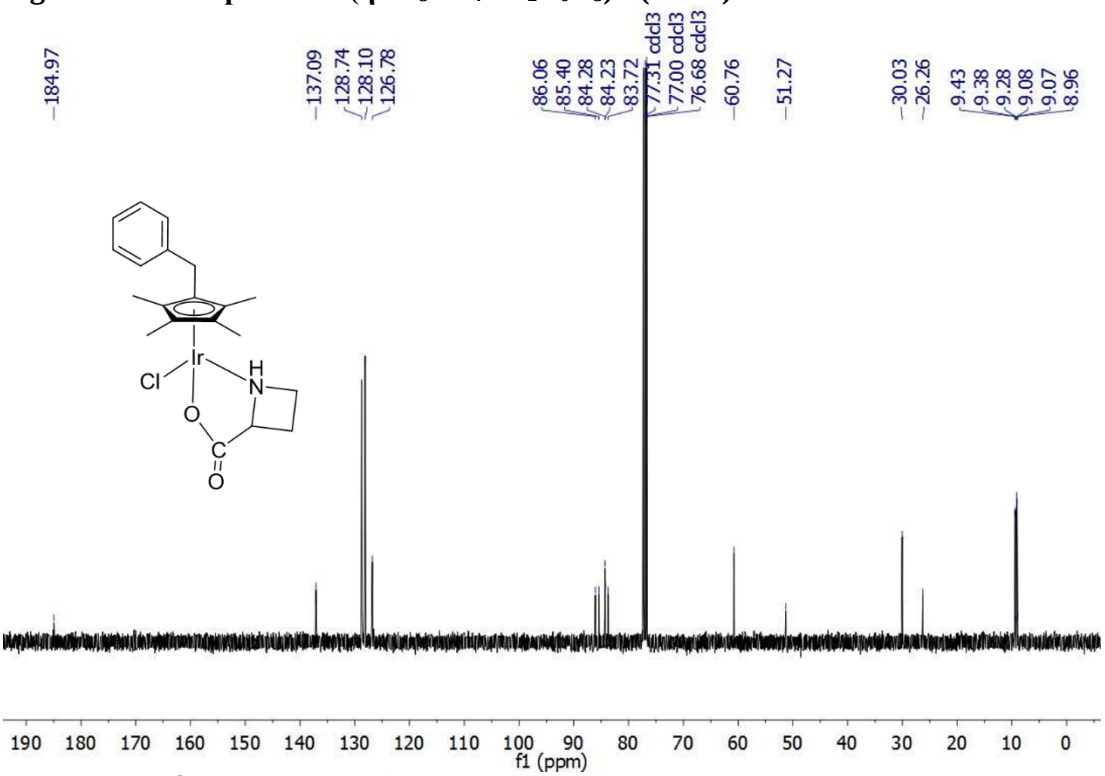

Figure A21: ^{13}C Spectra of (η^5-$C_5Me_4CH_2C_6H_5$)Ir(L-aze)Cl

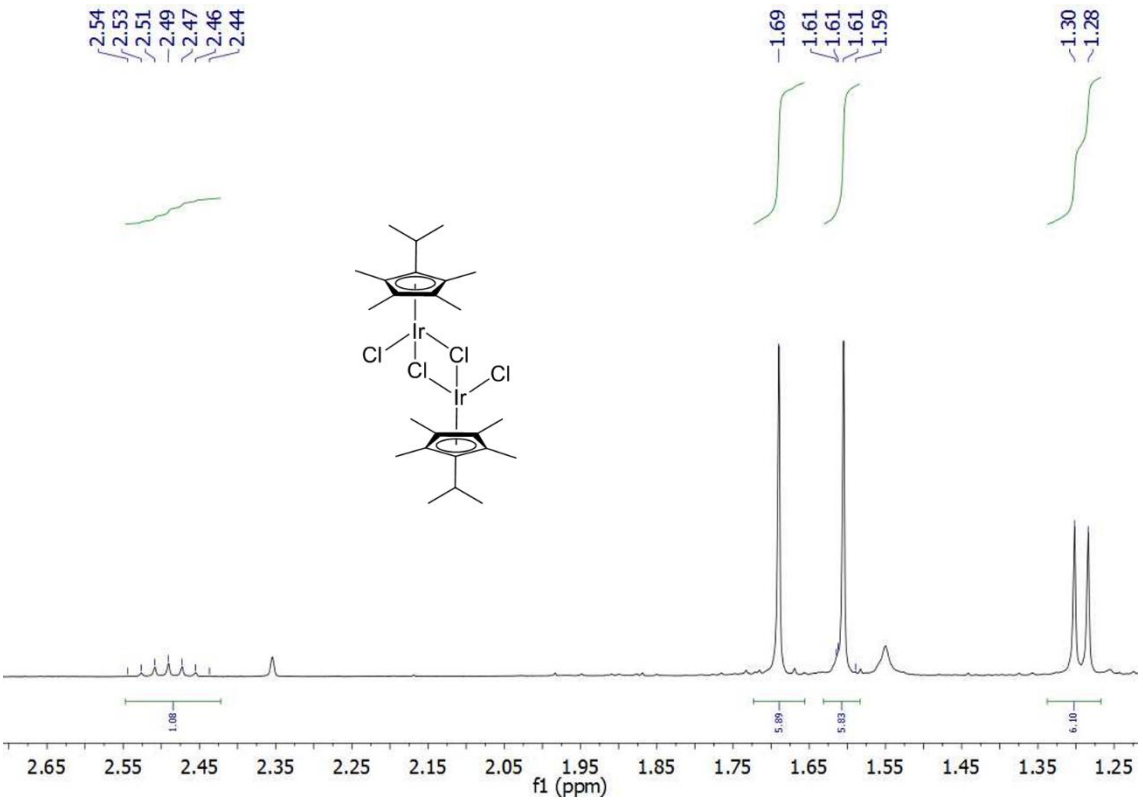

Figure A22: ^{1}H Spectra of [(η^5-C_5Me_4iPr)$IrCl_2$]$_2$

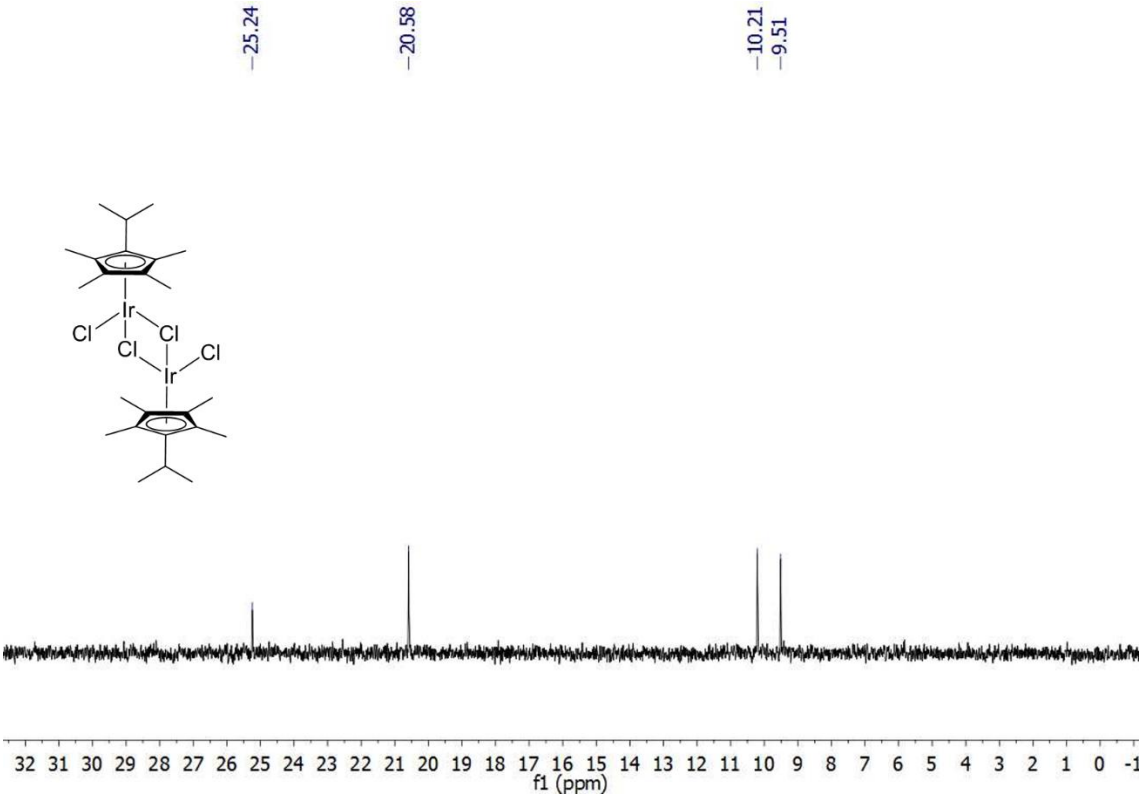

Figure A23: ^{13}C Spectra of [(η^5-C_5Me_4iPr)$IrCl_2$]$_2$

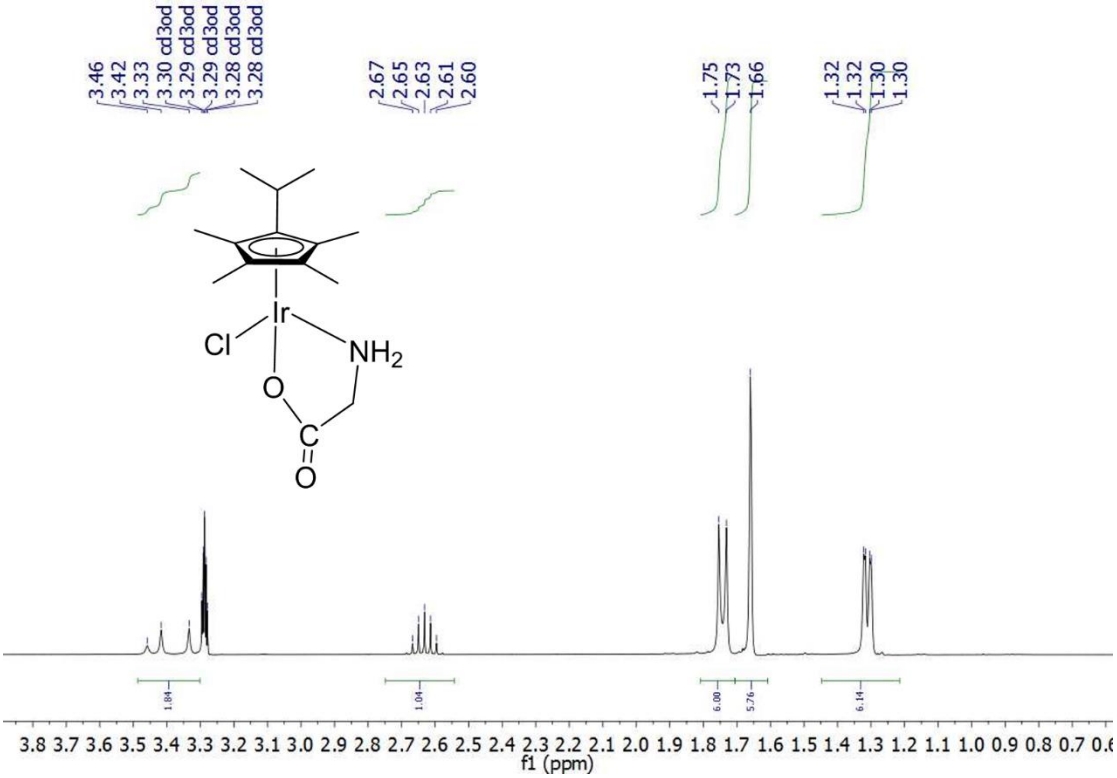

Figure A24: ^{1}H Spectra of (η^5-C_5Me_4iPr)Ir(Glycine)Cl Complex

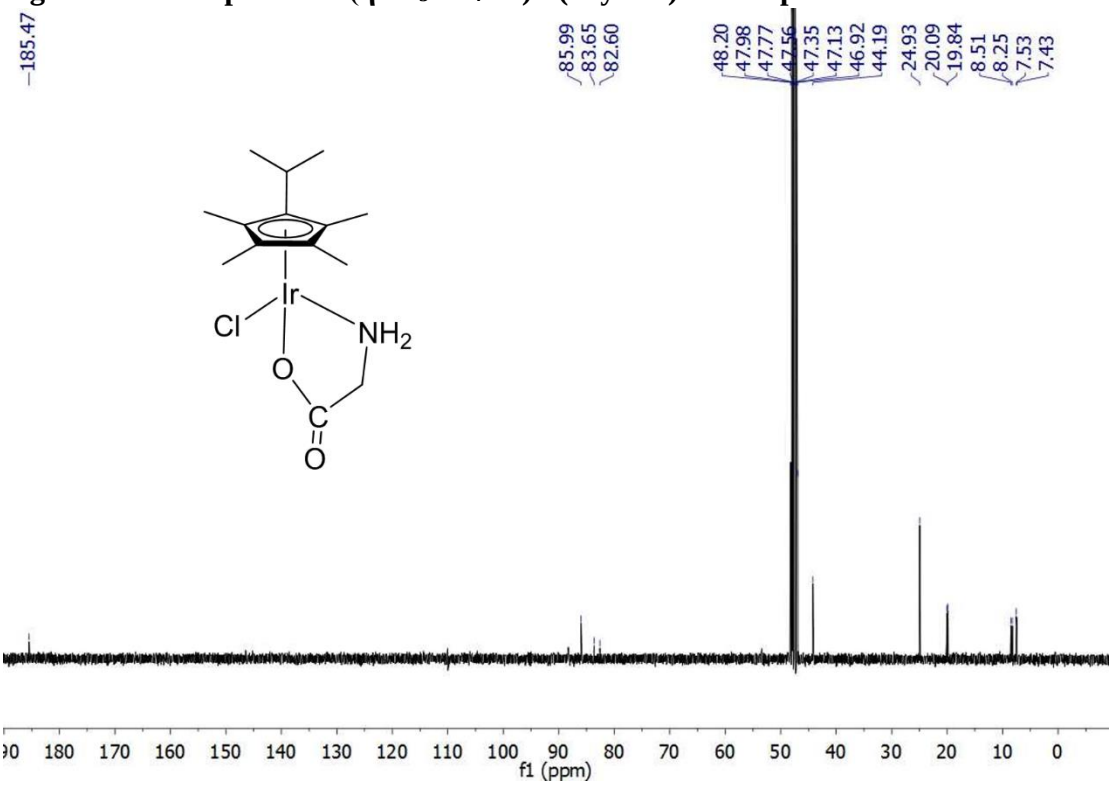

Figure A25: ^{13}C Spectra of (η^5-C_5Me_4iPr)Ir(Glycine)Cl Complex

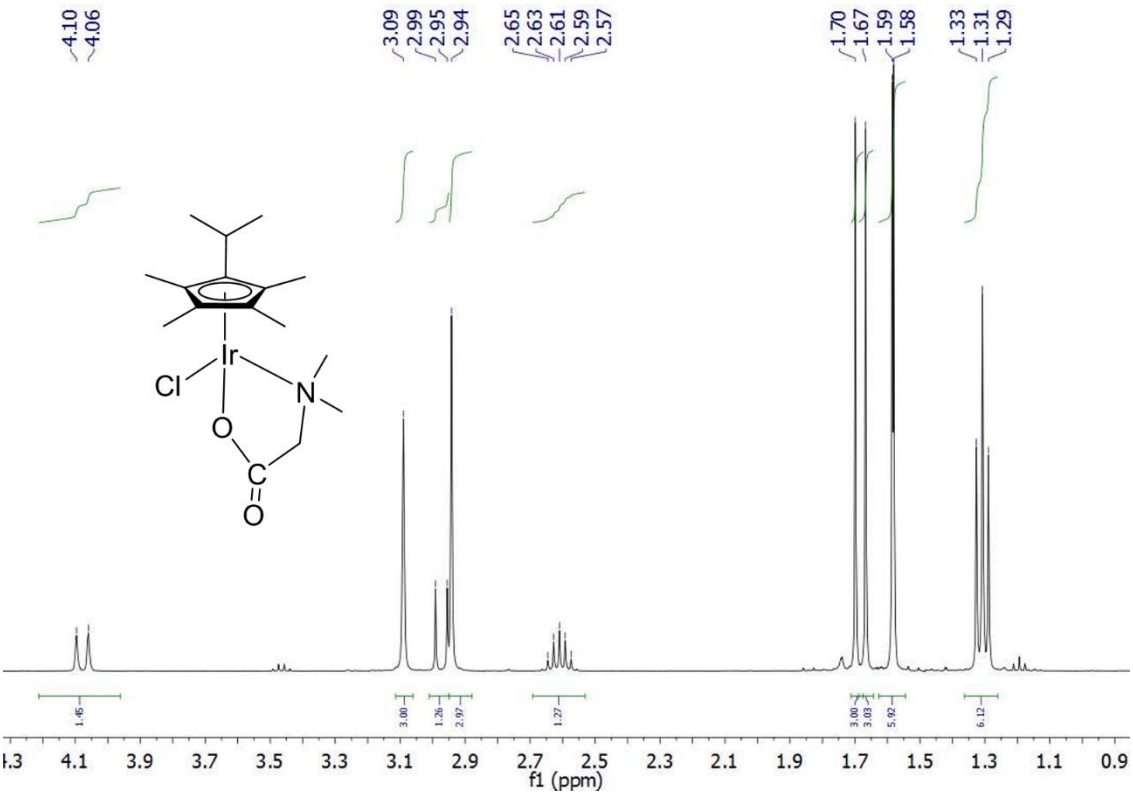

Figure A26: ^{1}H Spectra of (η^5-C_5Me_4iPr)Ir(N,N-dimethyl-Glycine)Cl Complex

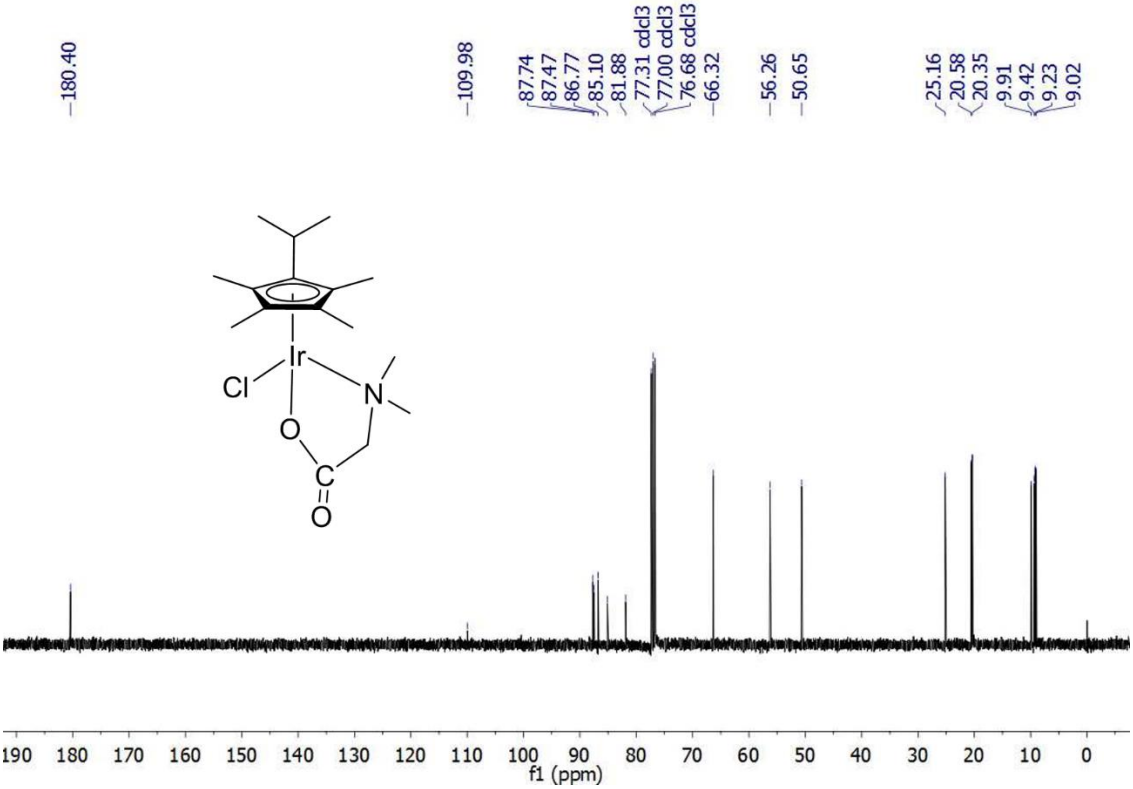

Figure A27: ^{13}C Spectra of (η^5-C_5Me_4iPr)Ir(N,N-dimethyl-Glycine)Cl Complex

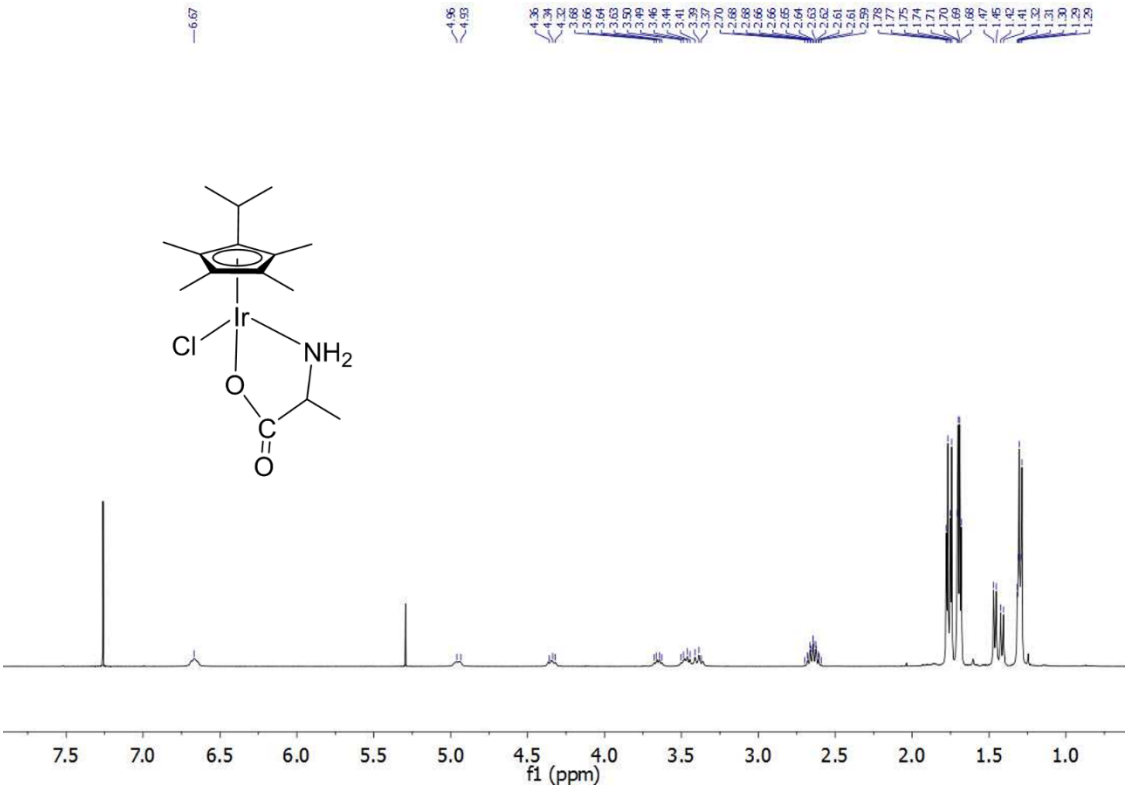

Figure A28: ^{1}H Spectra of (η^5-C_5Me_4iPr)Ir(L-Alanine)Cl Complex

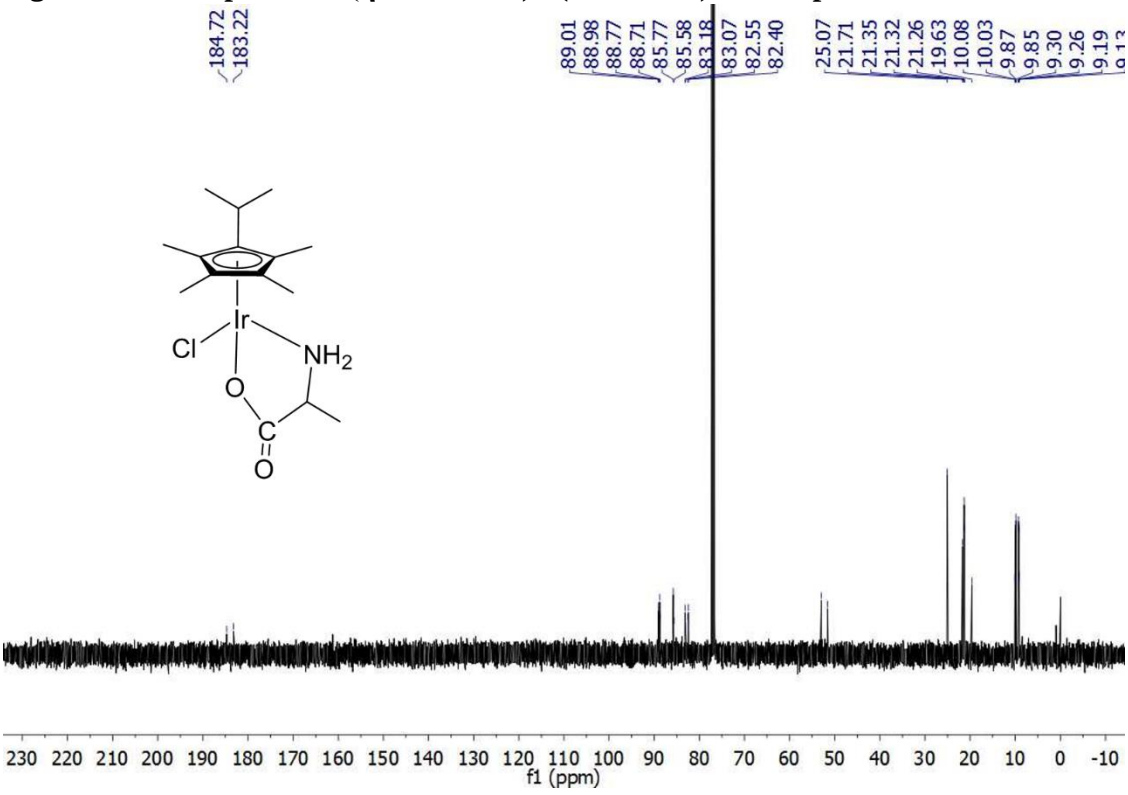

Figure A29: ^{13}C Spectra of (η^5-C_5Me_4iPr)Ir(L-Alanine)Cl Complex

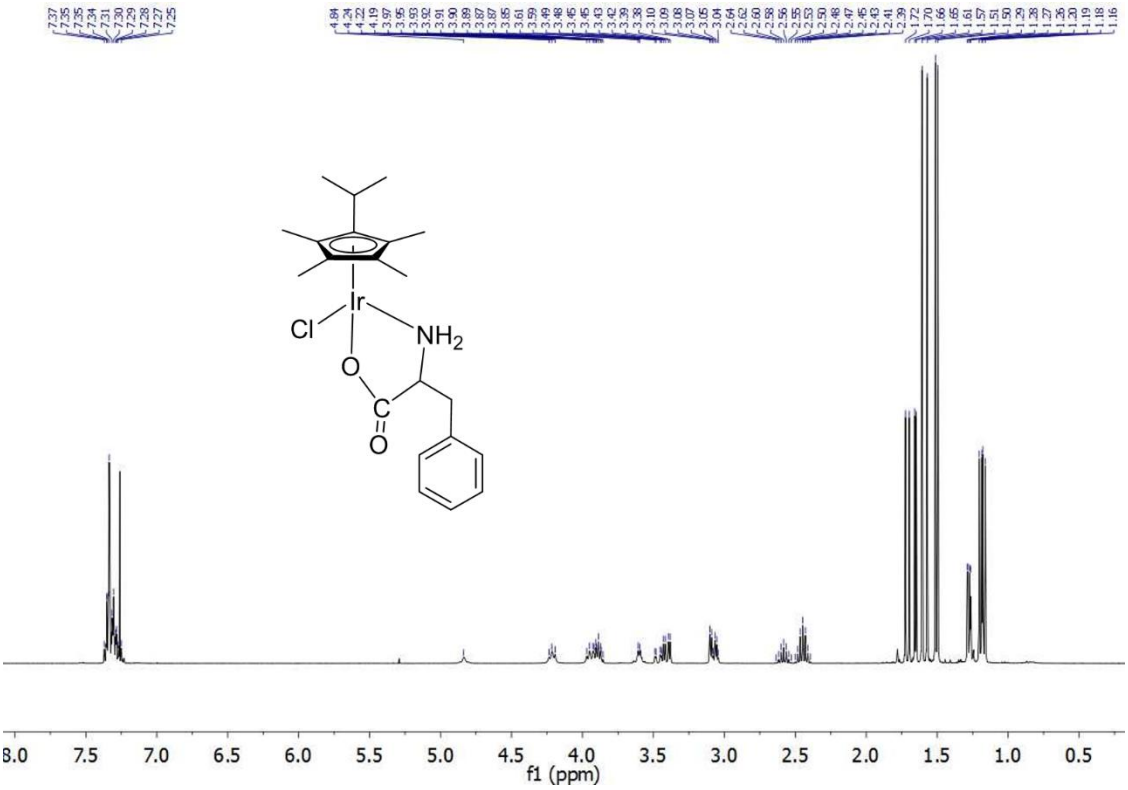

Figure A30: ^{1}H Spectra of (η^5-C_5Me_4iPr)Ir(L-Phenylalanine)Cl Complex

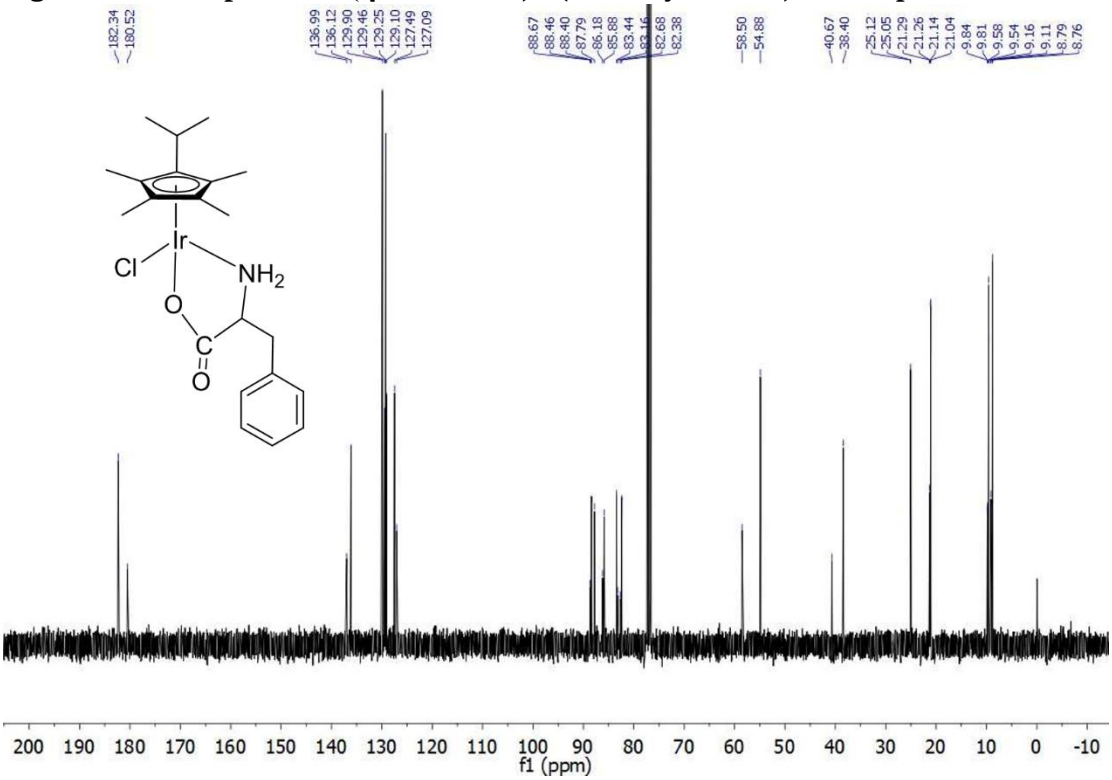

Figure A31: ^{13}C Spectra of (η^5-C_5Me_4iPr)Ir(L-Phenylalanine)Cl Complex

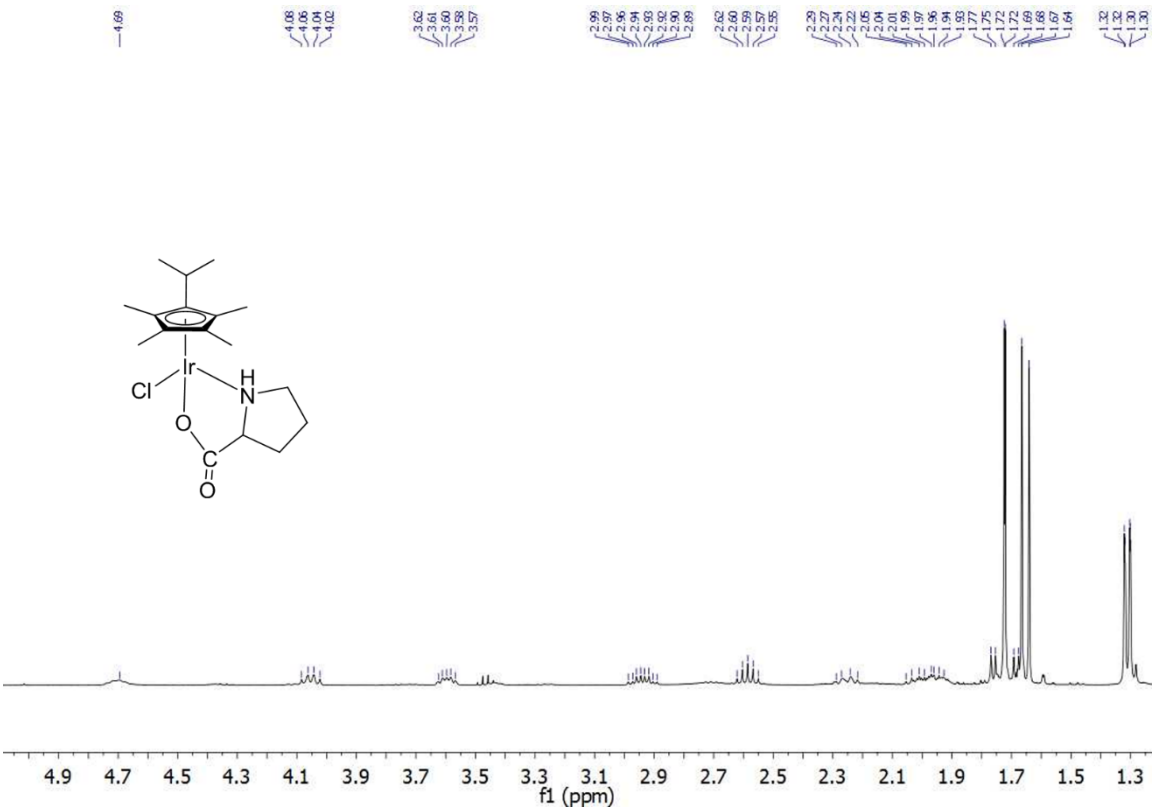

Figure A32: ^{1}H Spectra of (η^5-C_5Me_4iPr)Ir(L-proline)Cl Complex

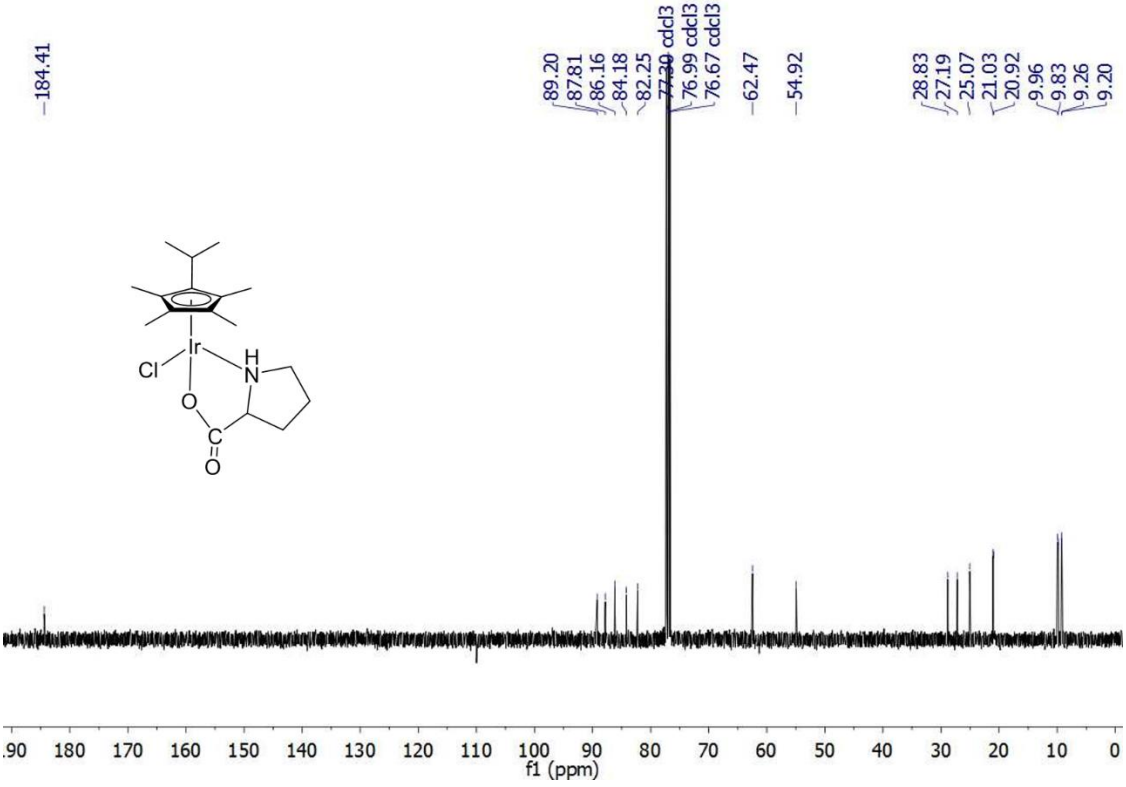

Figure A33: ^{13}C Spectra of (η^5-C_5Me_4iPr)Ir(L-proline)Cl Complex

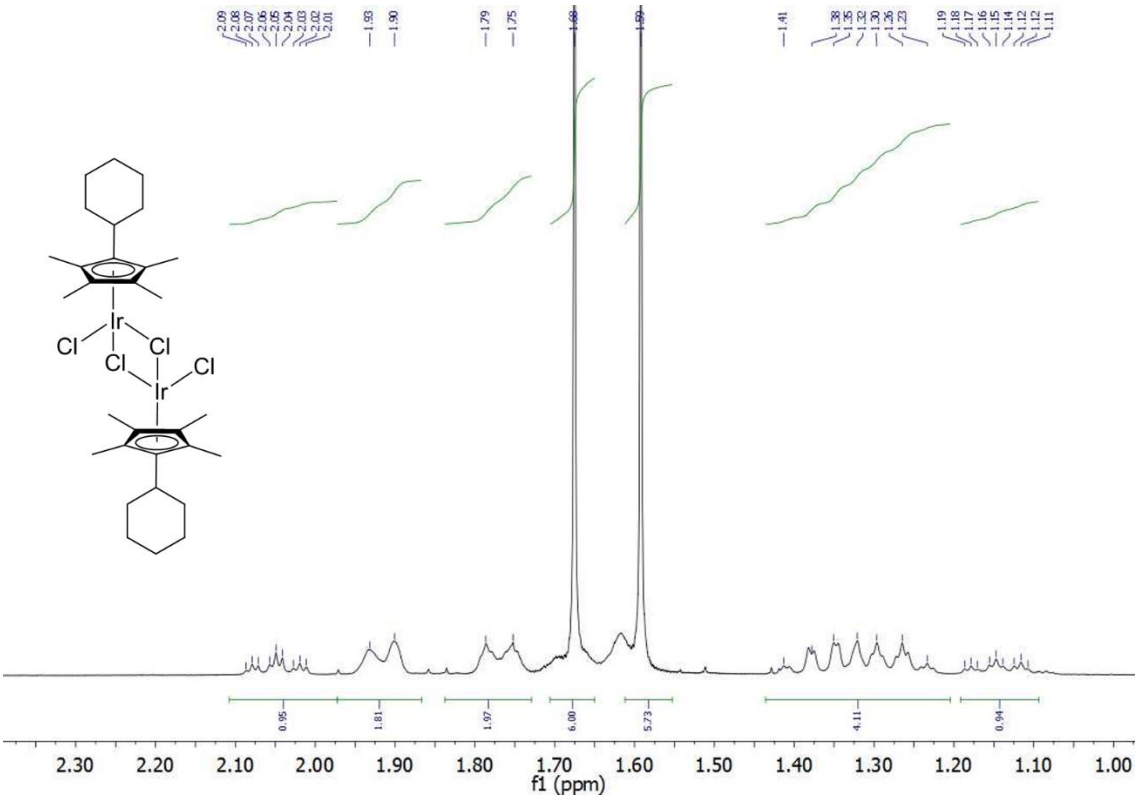

Figure A34: ^{1}H Spectra of $[(\eta^5\text{-}C_5Me_4C_6H_{10})IrCl_2]_2$

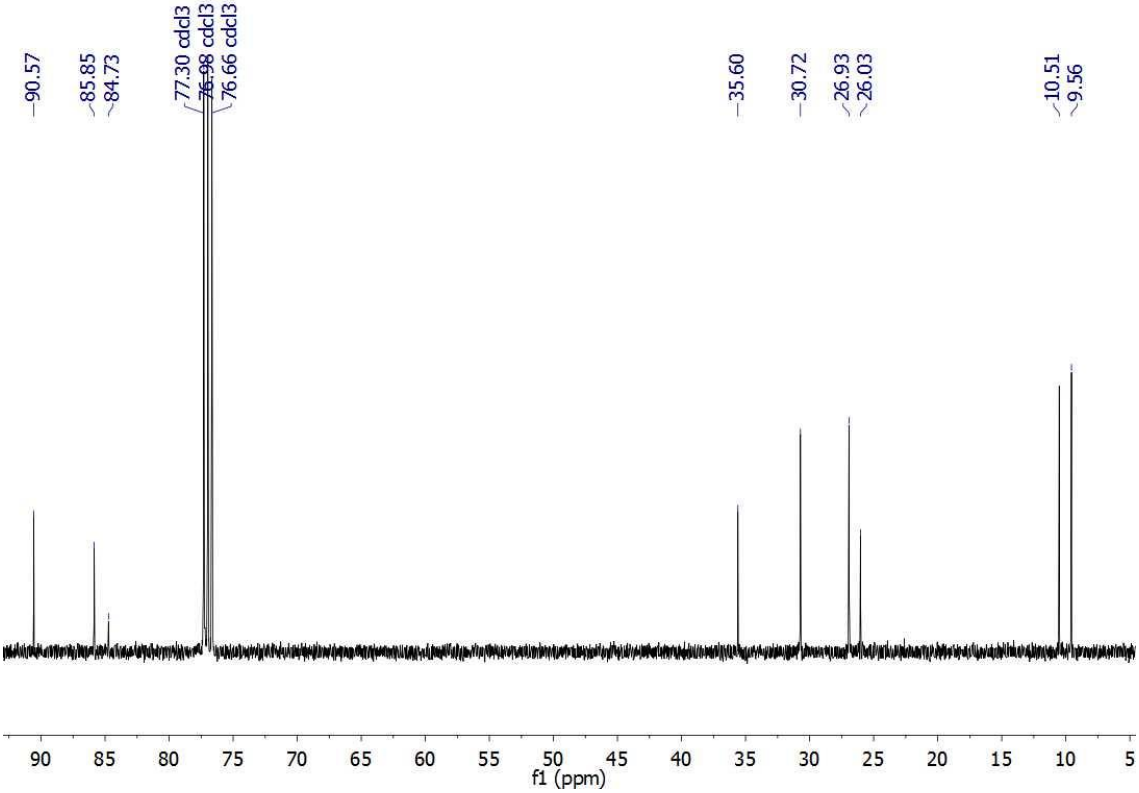

Figure A35: ^{13}C Spectra of $[(\eta^5\text{-}C_5Me_4C_6H_{10})IrCl_2]_2$

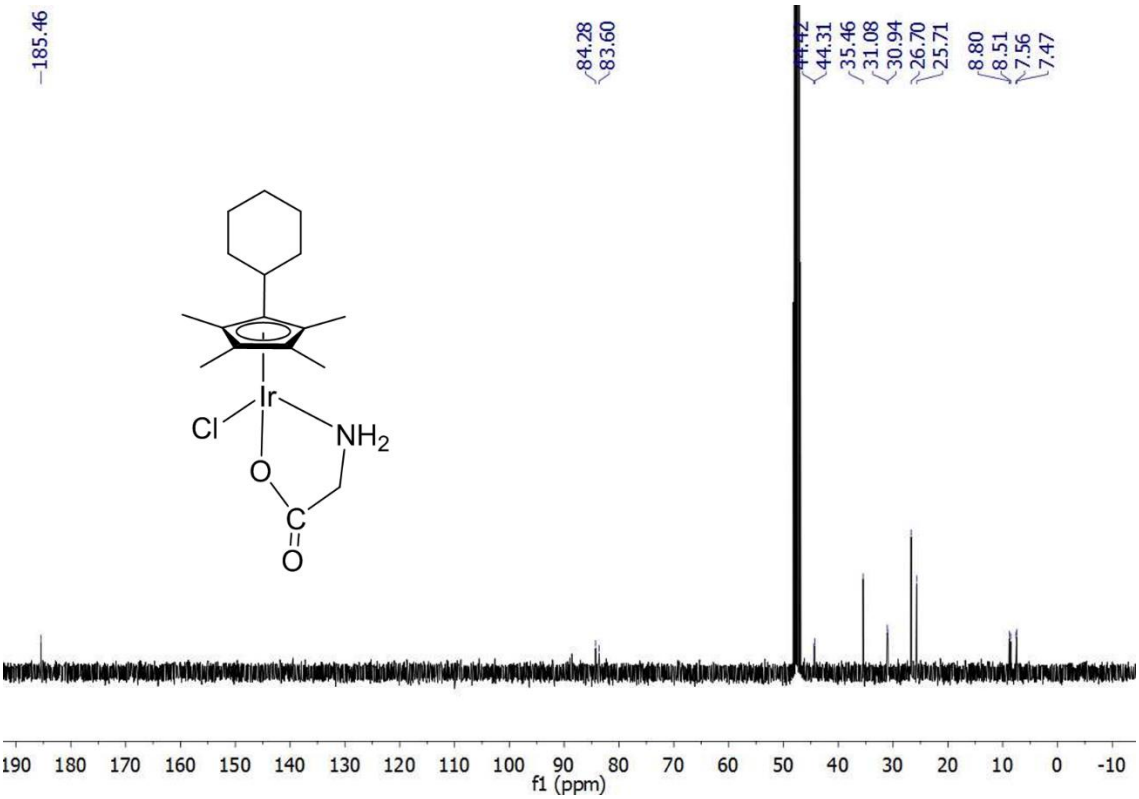

Figure A36: ^{1}H Spectra of (η^5-$C_5Me_4C_6H_{10}$)Ir(Glycine)Cl Complex

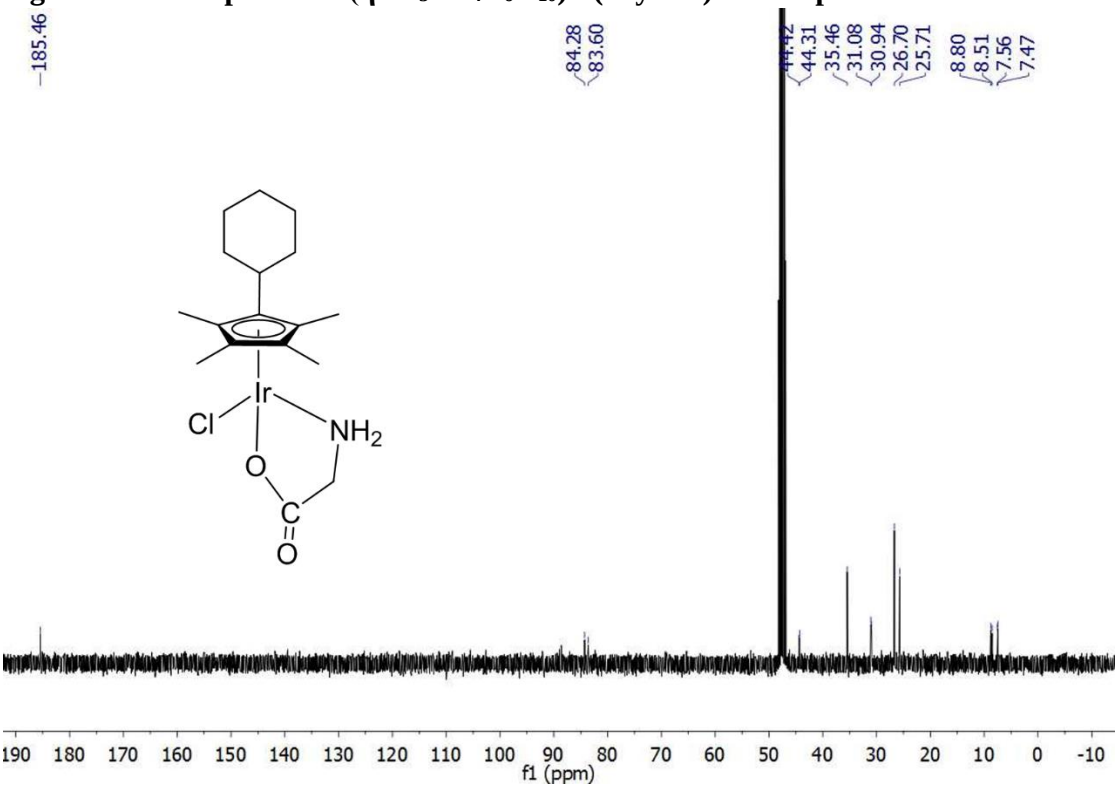

Figure A37: ^{13}C Spectra of (η^5-$C_5Me_4C_6H_{10}$)Ir(Glycine)Cl Complex

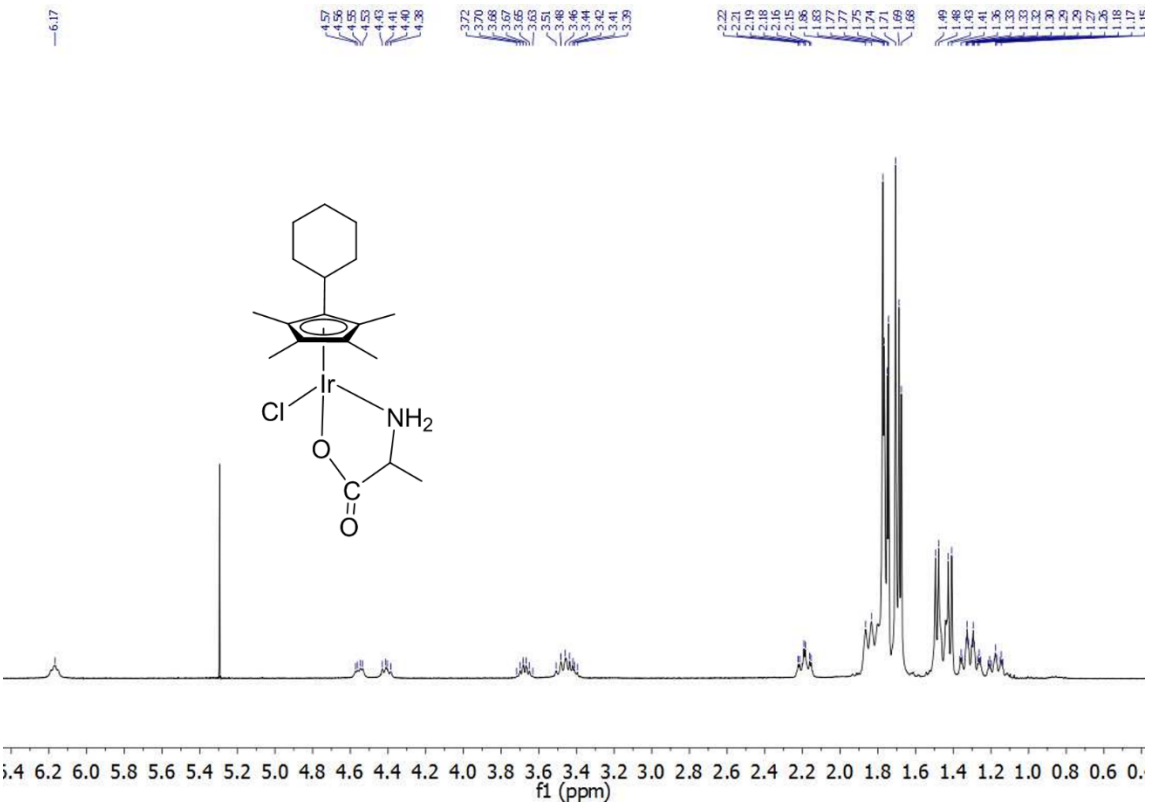

Figure A38: ^{1}H Spectra of (η^5-$C_5Me_4C_6H_{10}$)Ir(L-alanine)Cl Complex

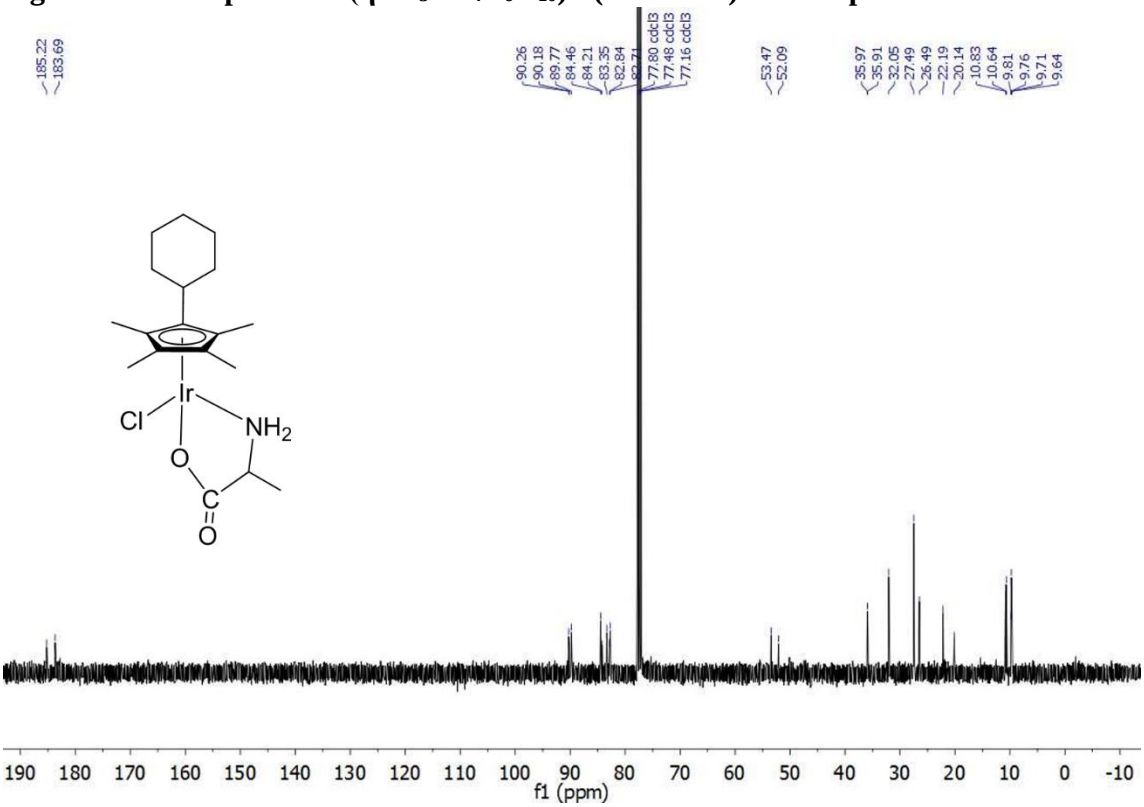

Figure A39: ^{13}C Spectra of (η^5-$C_5Me_4C_6H_{10}$)Ir(L-alanine)Cl Complex

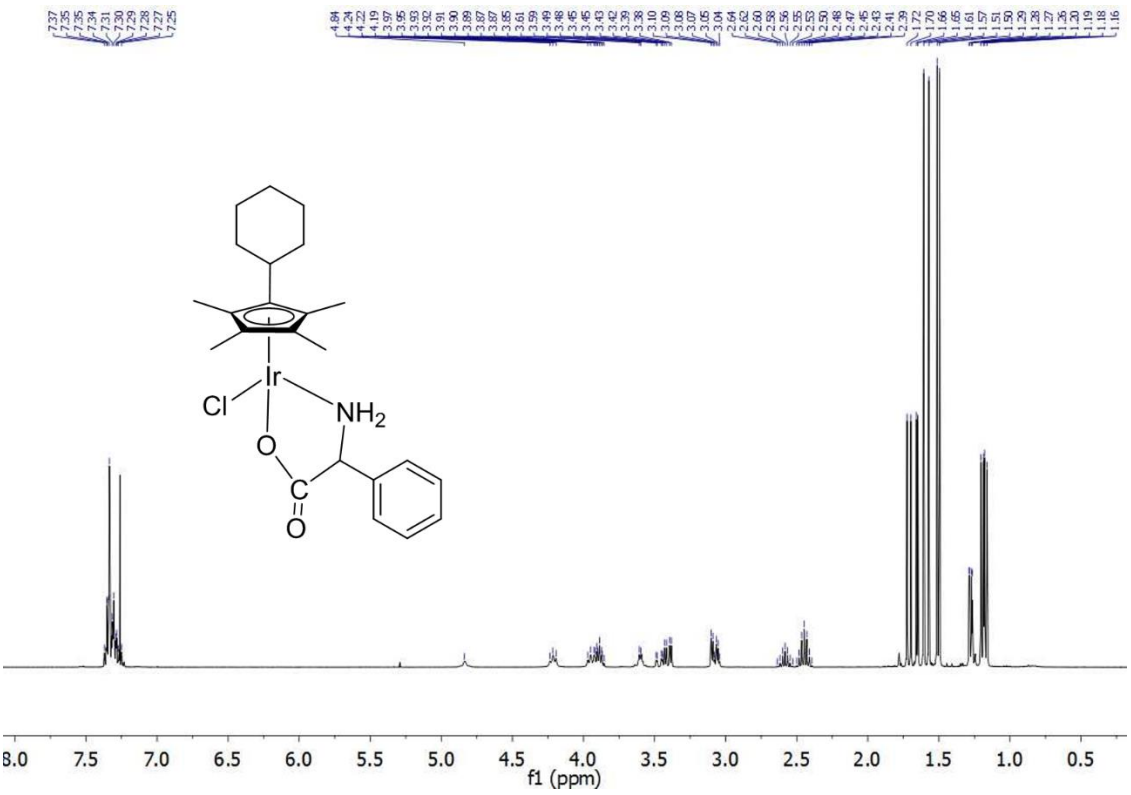

Figure A40: ^{1}H Spectra of (η^5-$C_5Me_4C_6H_{10}$)Ir(L-phenylglycine)Cl complex

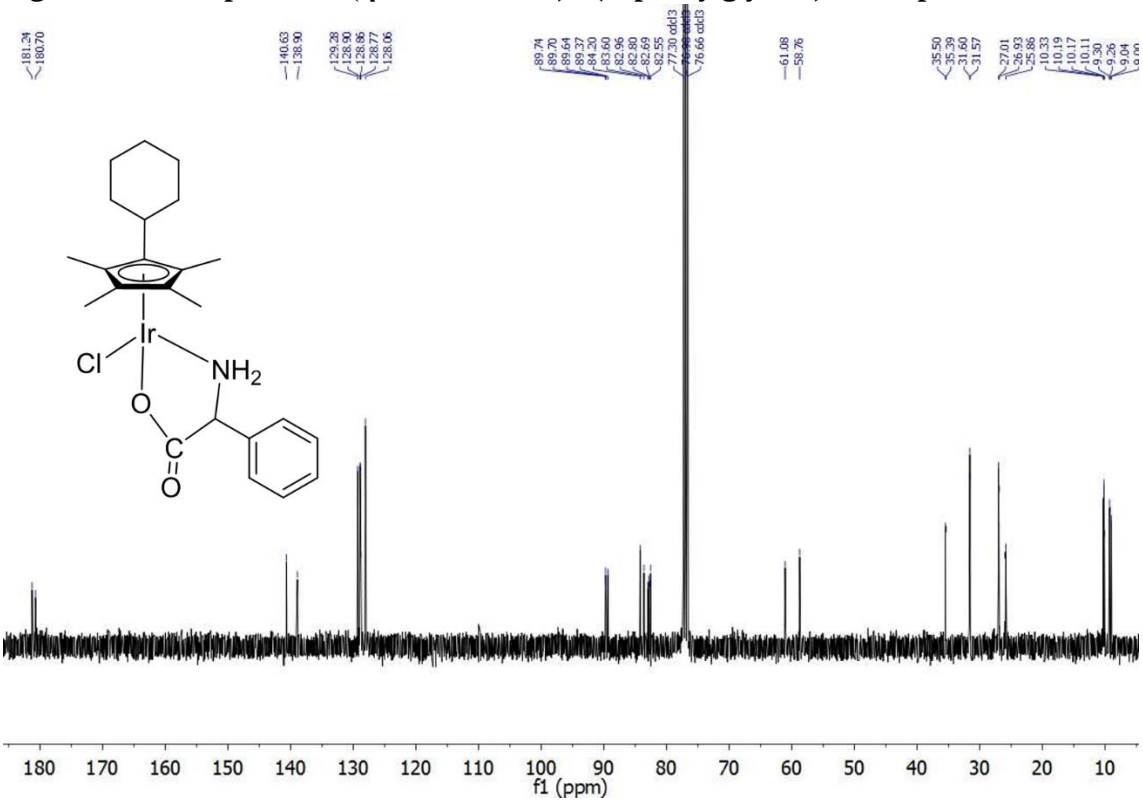

Figure A41: ^{13}C Spectra of (η^5-$C_5Me_4C_6H_{10}$)Ir(L-phenylglycine)Cl complex

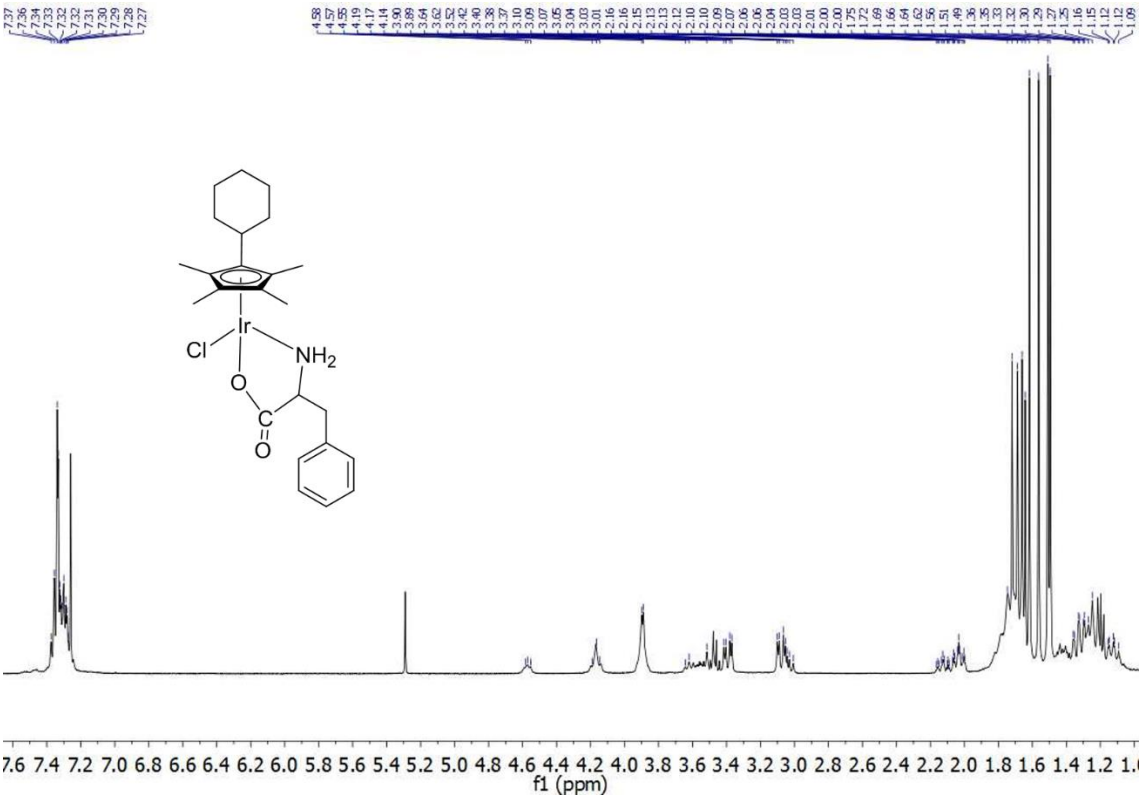

Figure A42: ^{1}H Spectra of (η^5-$C_5Me_4C_6H_{10}$)Ir(L-phenylalanine)Cl

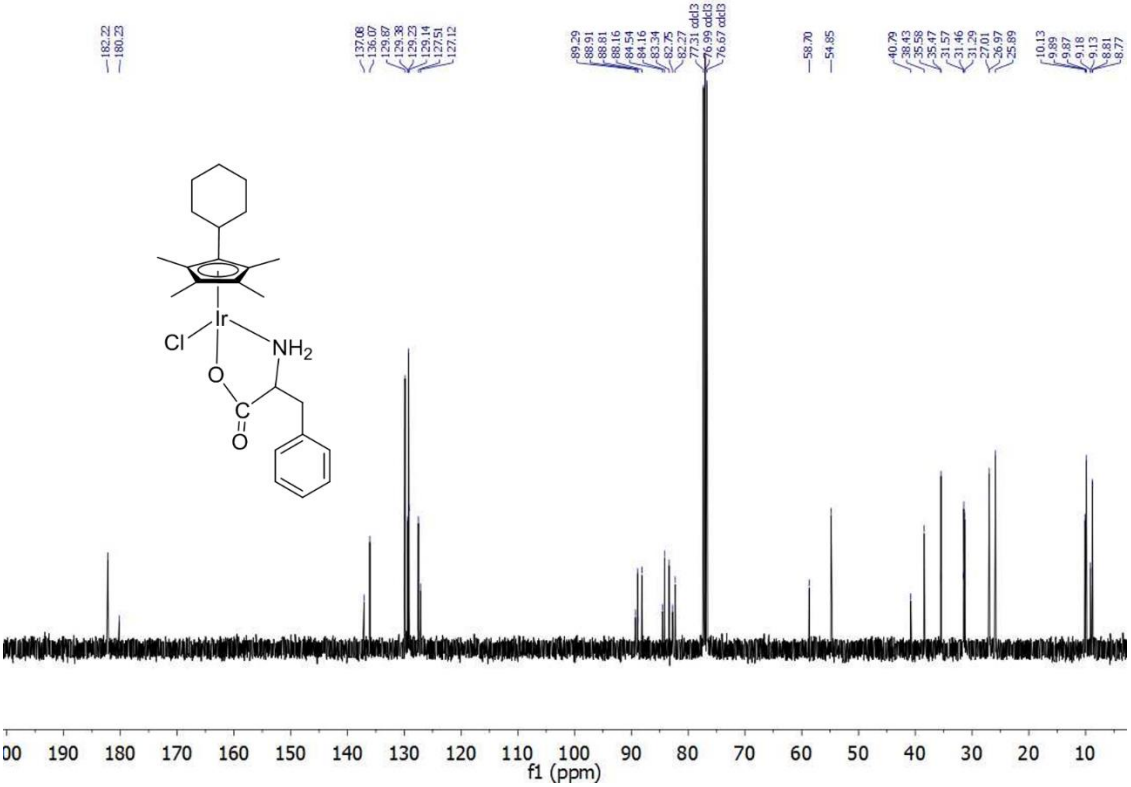

Figure A43: ^{13}C Spectra of (η^5-$C_5Me_4C_6H_{10}$)Ir(L-phenylalanine)Cl

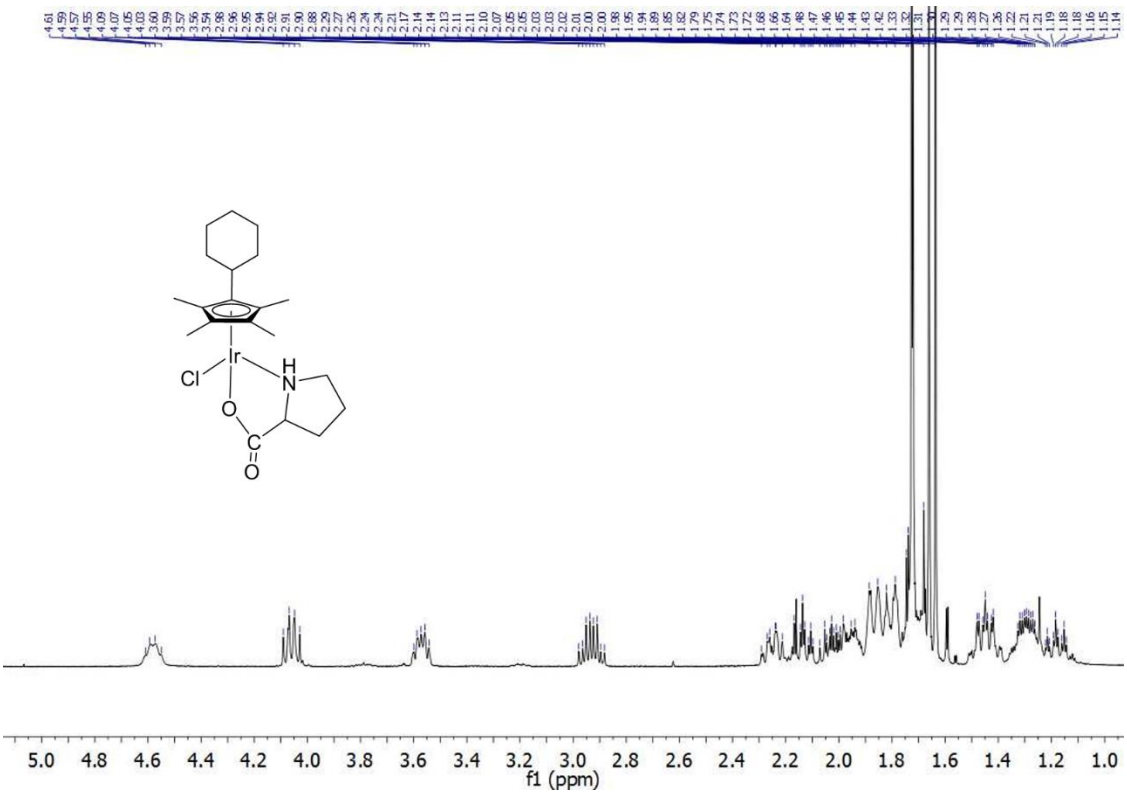

Figure A44: ^{1}H Spectra of (η^5-$C_5Me_4C_6H_{10}$)Ir(L-proline)Cl complex

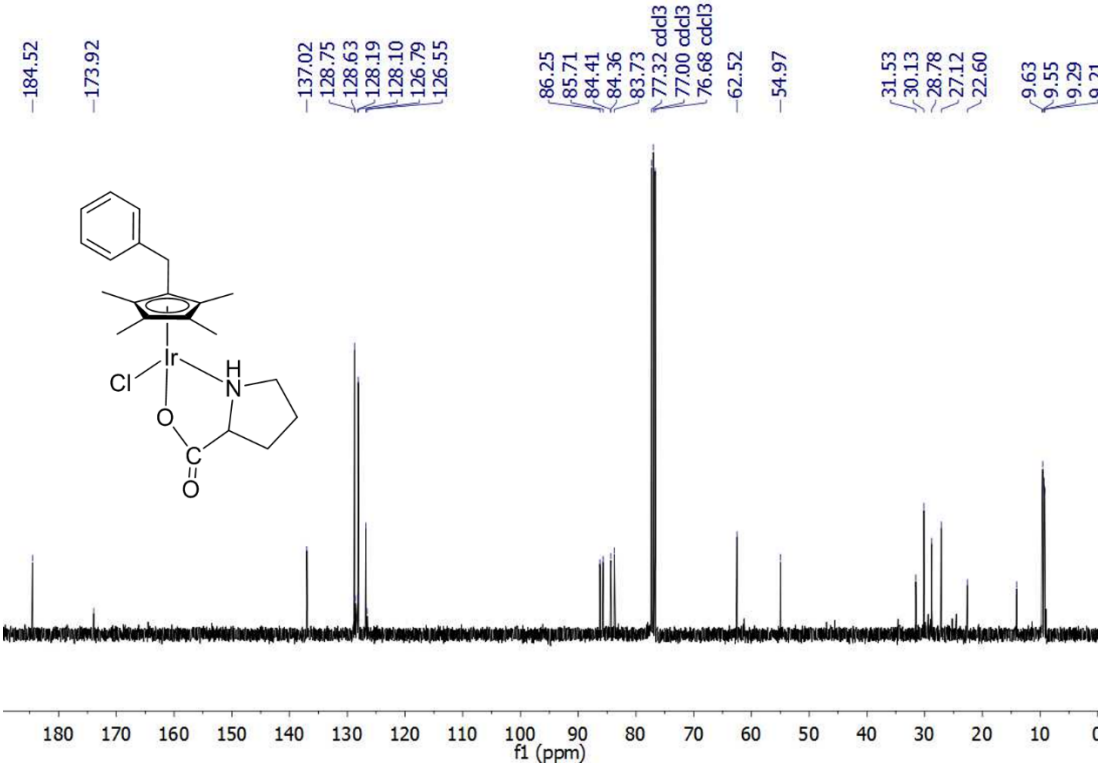

Figure A45: ^{13}C Spectra of (η^5-$C_5Me_4C_6H_{10}$)Ir(L-proline)Cl complex

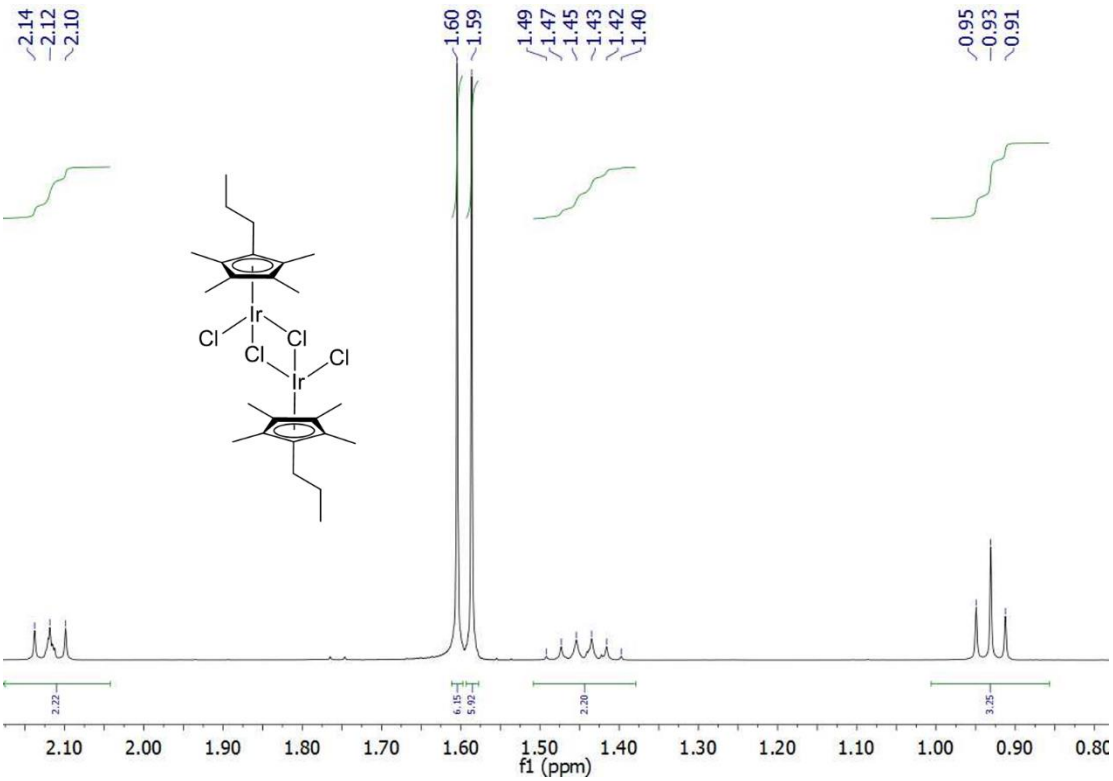

Figure A46: ^{1}H Spectra of [(η^5-C_5Me_4-n-propyl)$IrCl_2]_2$

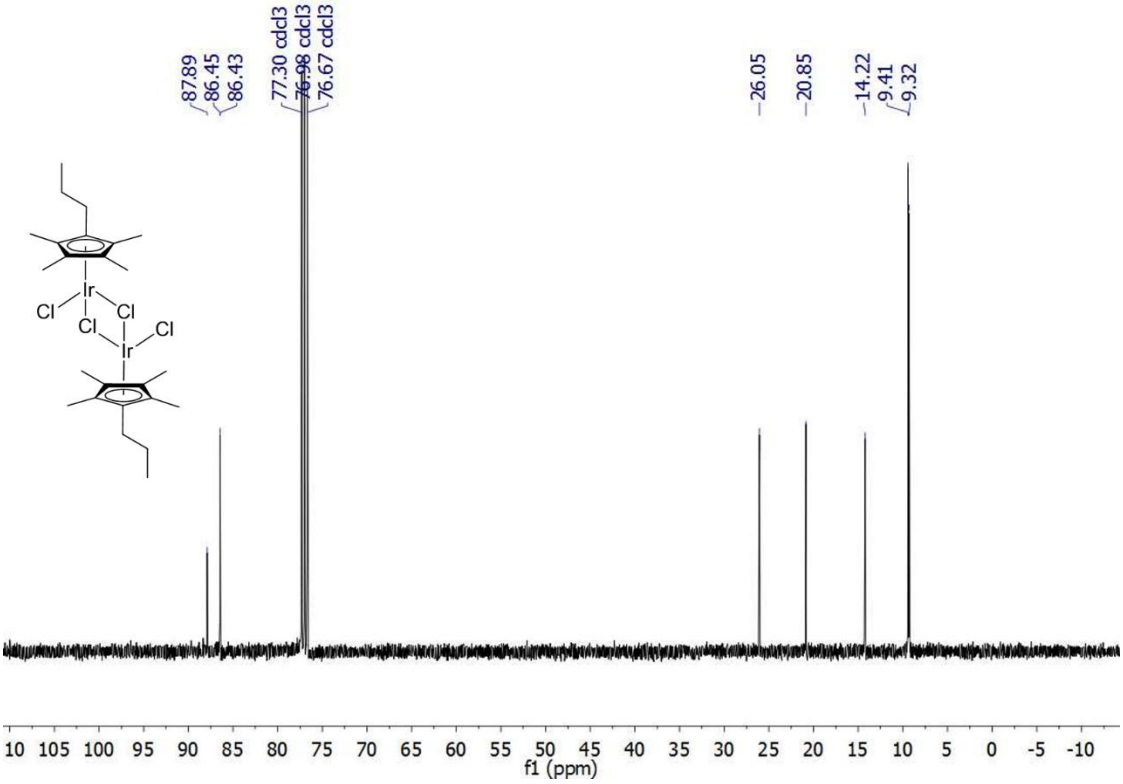

Figure A47: ^{13}C Spectra of [(η^5-C_5Me_4-n-propyl)$IrCl_2]_2$

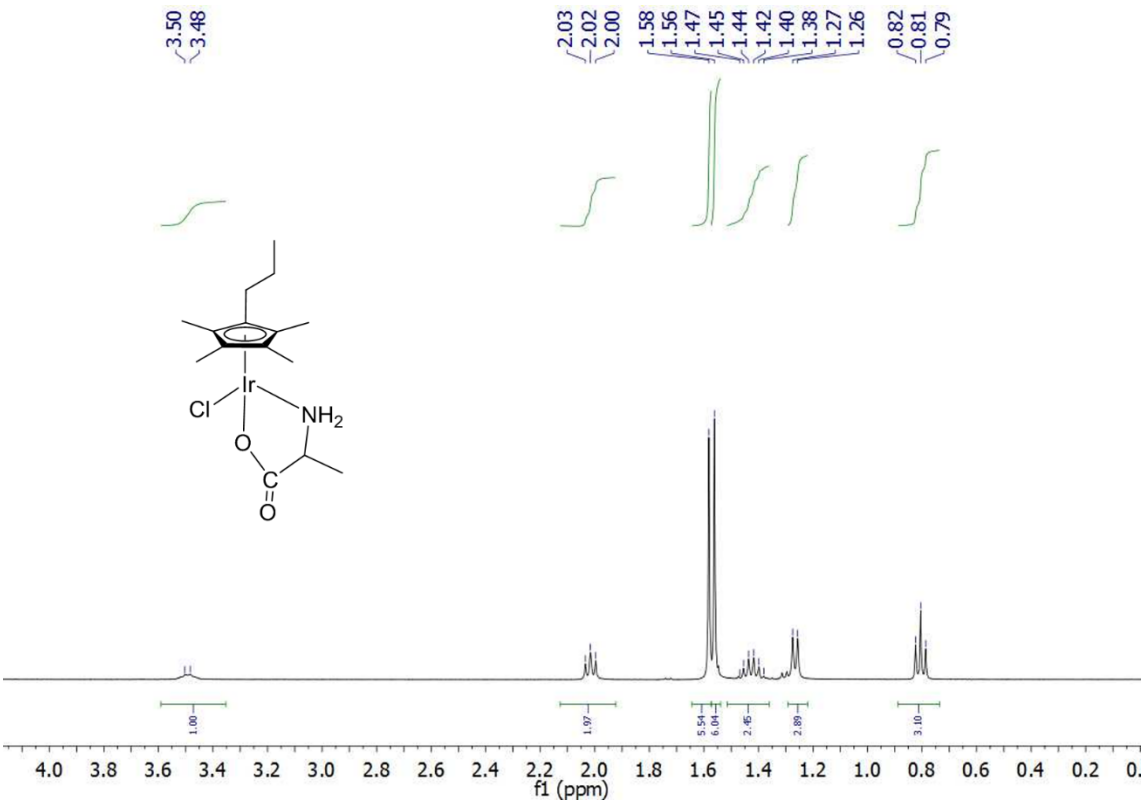

Figure A48: ^{1}H Spectra of (η^5-C_5Me_4-n-propyl)Ir(L-alanine)Cl Complex

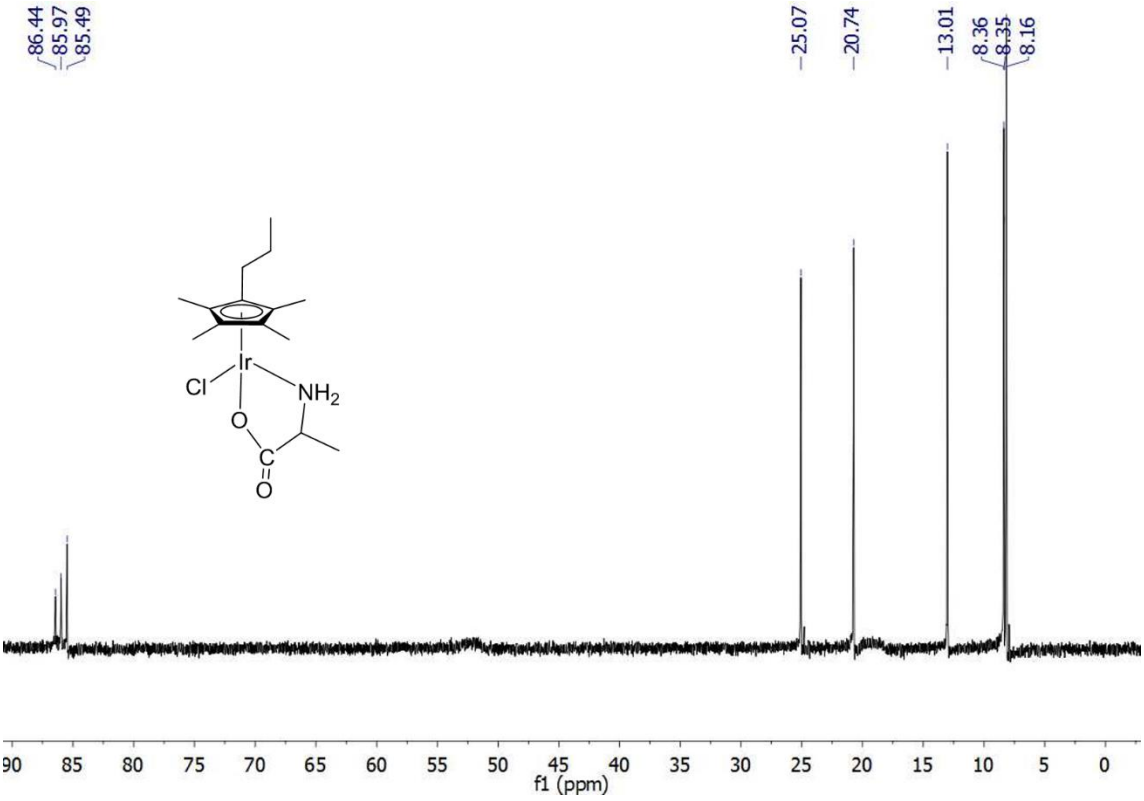

Figure A49: ^{13}C Spectra of (η^5-C_5Me_4-n-propyl)Ir(L-alanine)Cl Complex

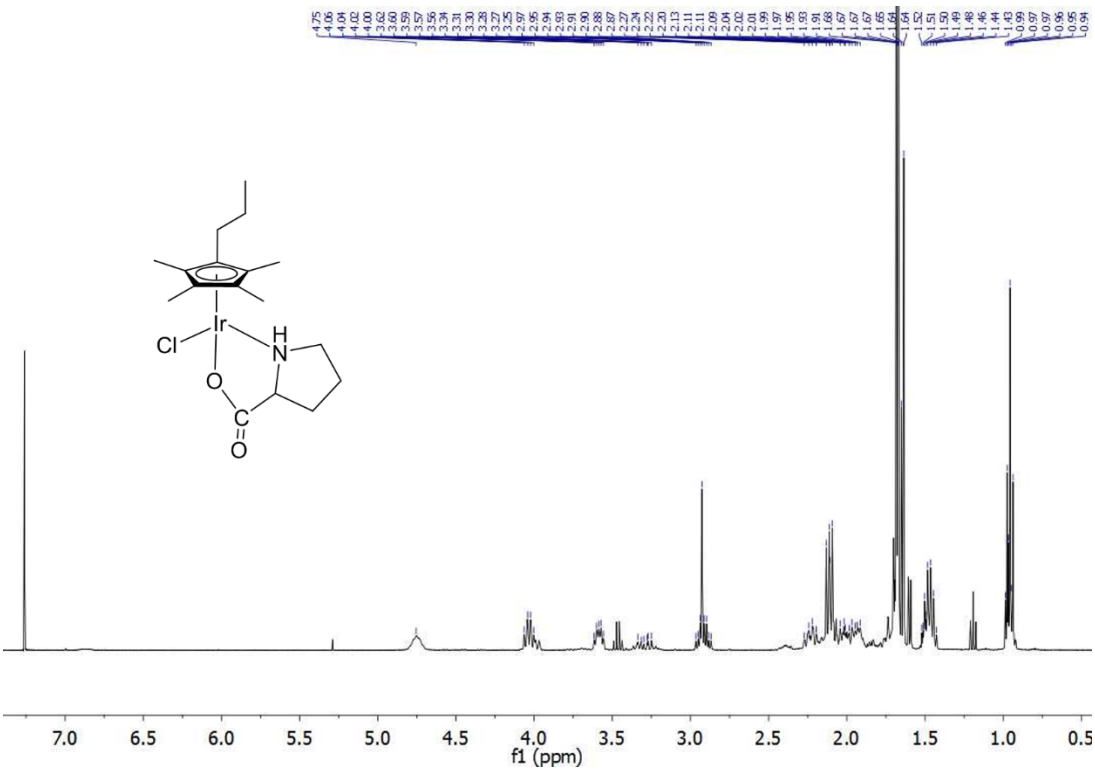

Figure A50: ^{1}H Spectra of (η^5-C_5Me_4-n-propyl)Ir(L-proline)Cl

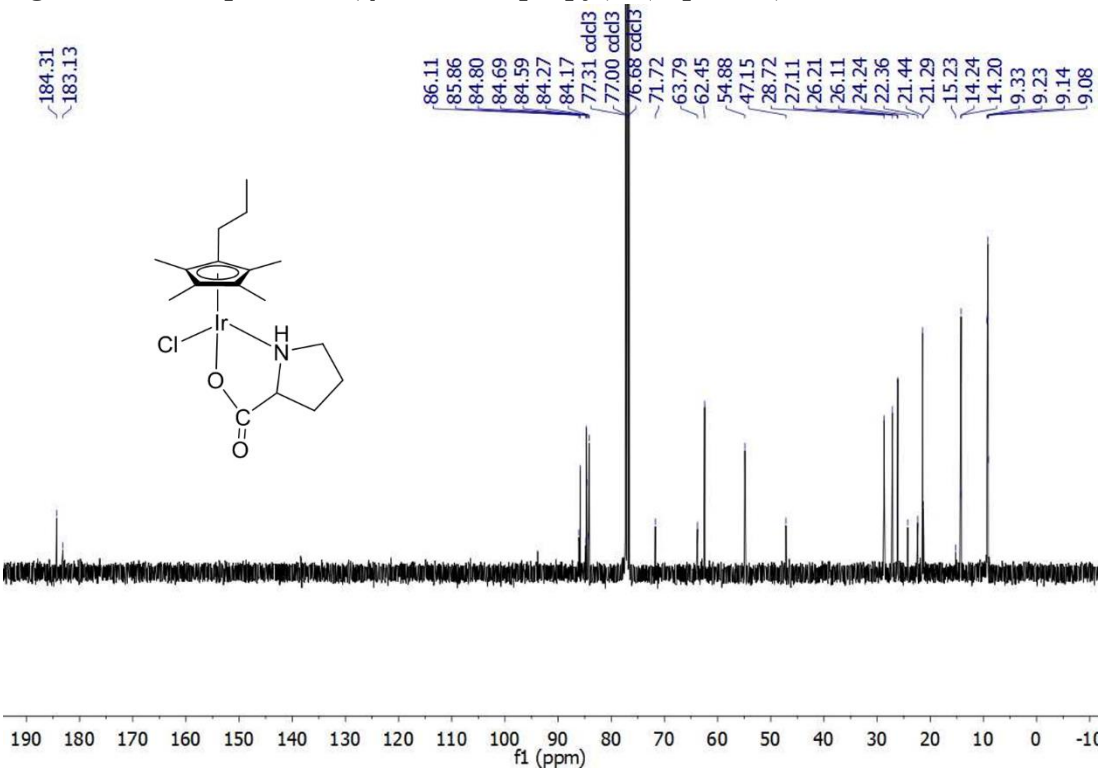

Figure A51: ^{13}C Spectra of (η^5-C_5Me_4-n-propyl)Ir(L-proline)Cl

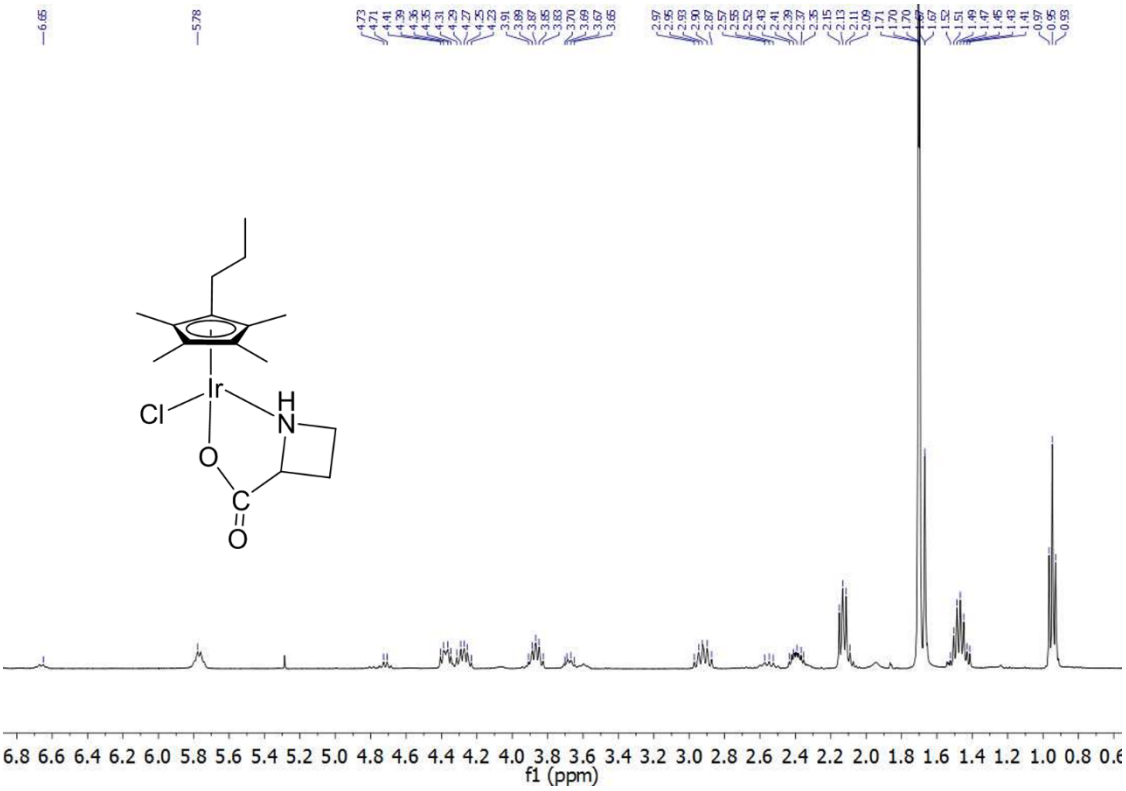

Figure A52: ^{1}H Spectra of (η^5-C_5Me_4-n-propyl)Ir(L-aze)Cl Complex

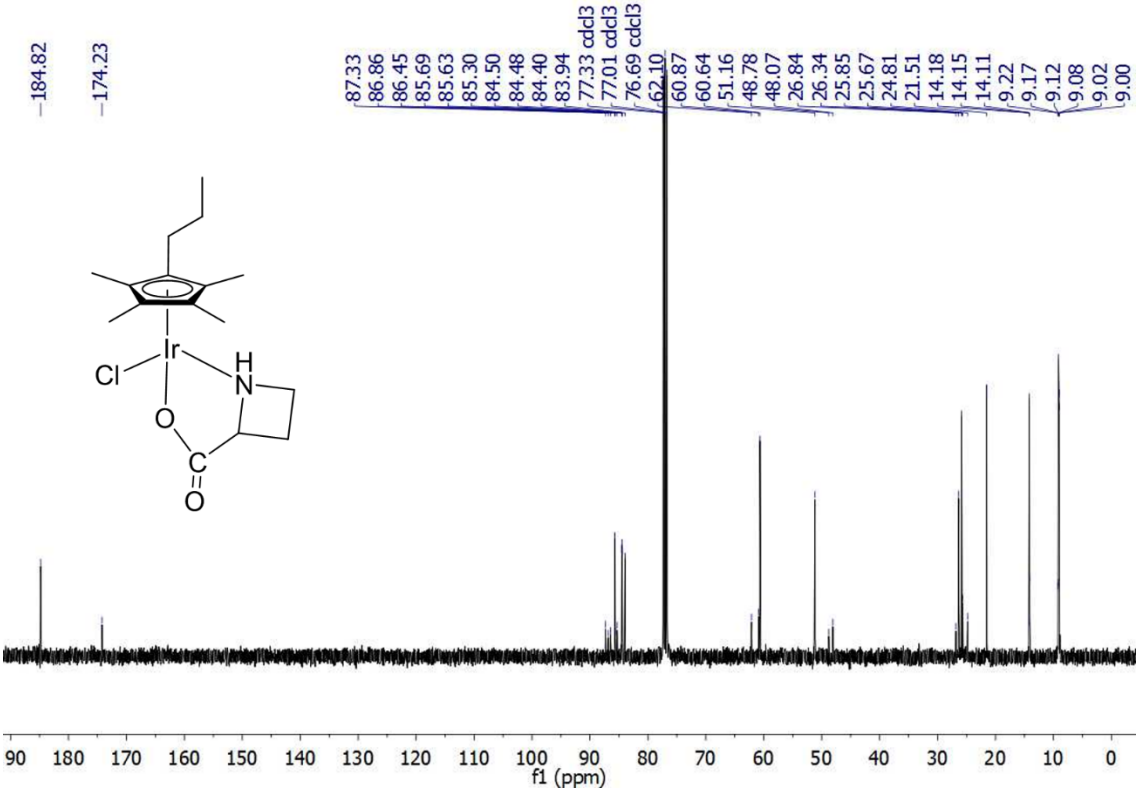

Figure A53: ^{13}C Spectra of (η^5-C_5Me_4-n-propyl)Ir(L-aze)Cl Complex

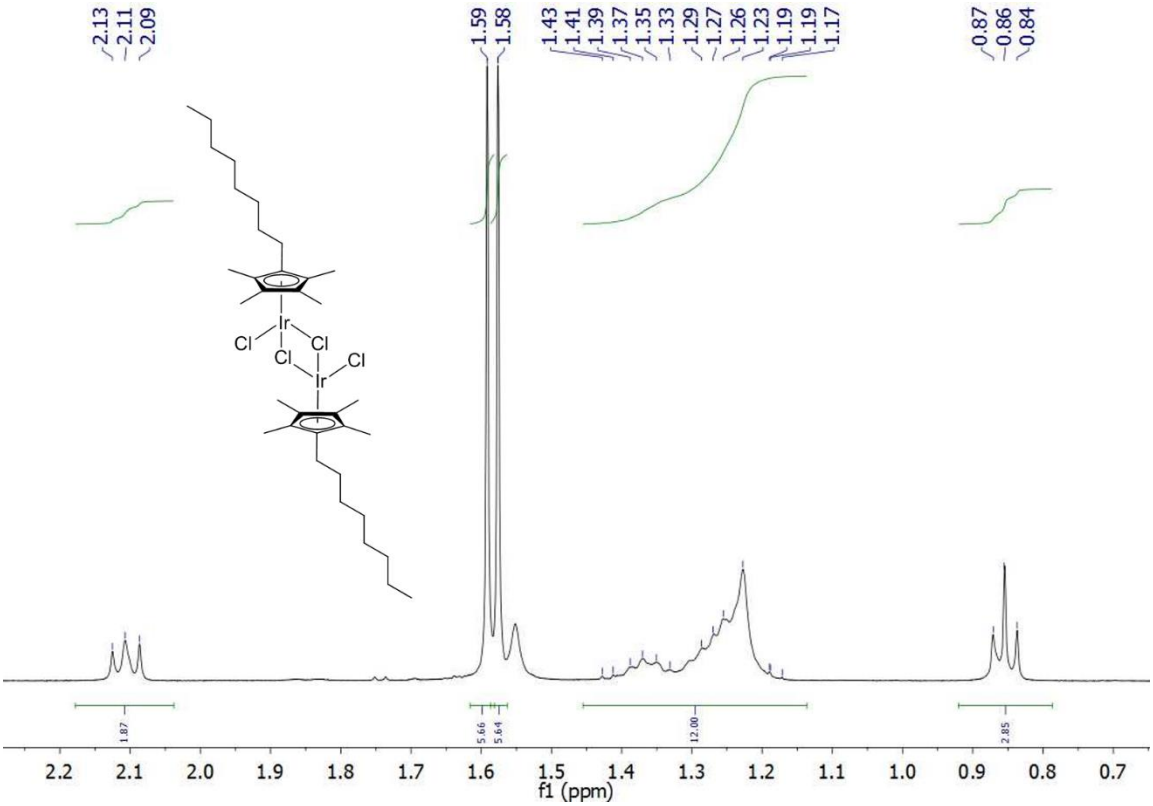

Figure A54: ^{1}H Spectra of [(η^5-C_5Me_4-n-octyl)$IrCl_2$]$_2$

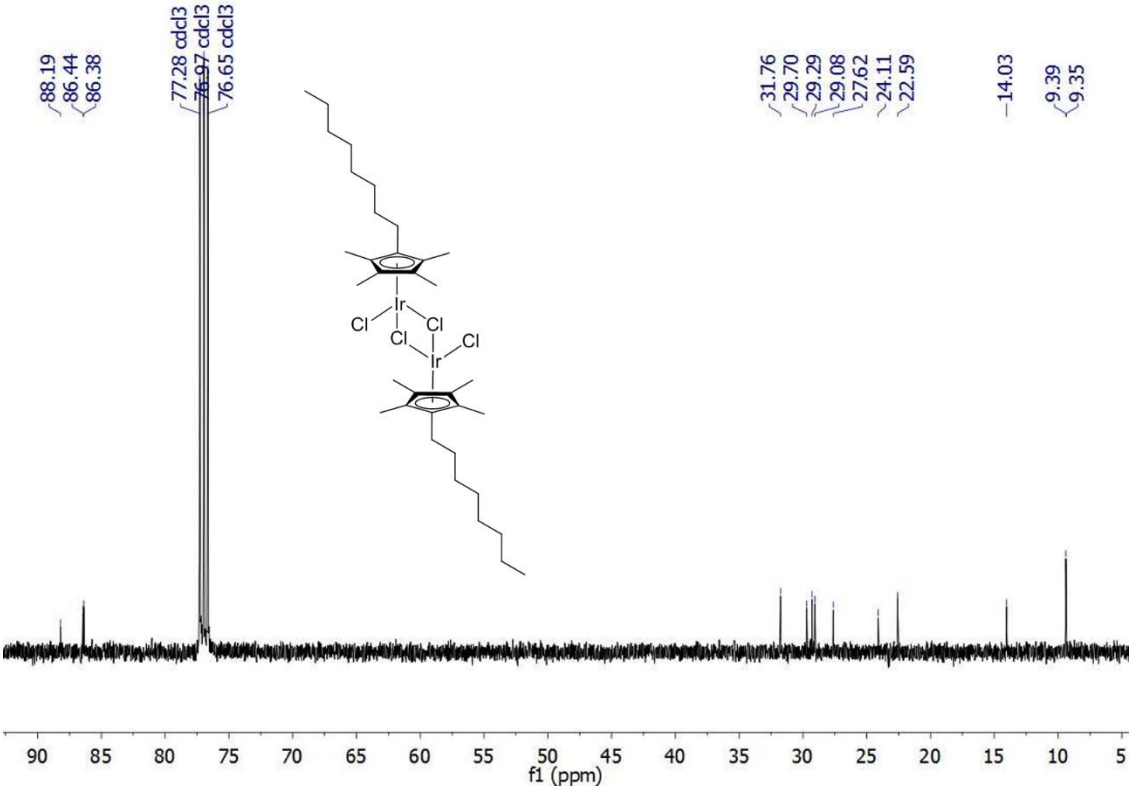

Figure A55: ^{13}C Spectra of [(η^5-C_5Me_4-n-octyl)$IrCl_2$]$_2$

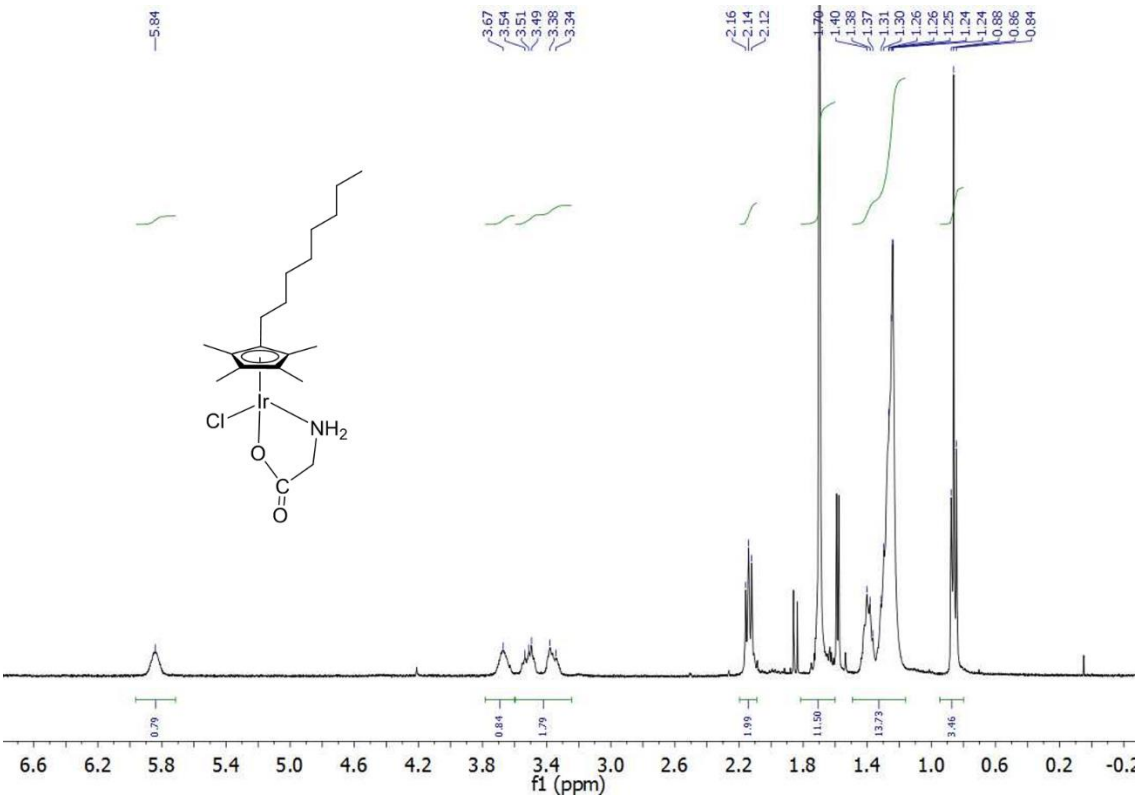

Figure A56: ^{1}H Spectra of (η^5-C_5Me_4-n-octyl)Ir(Glycine)Cl Complex

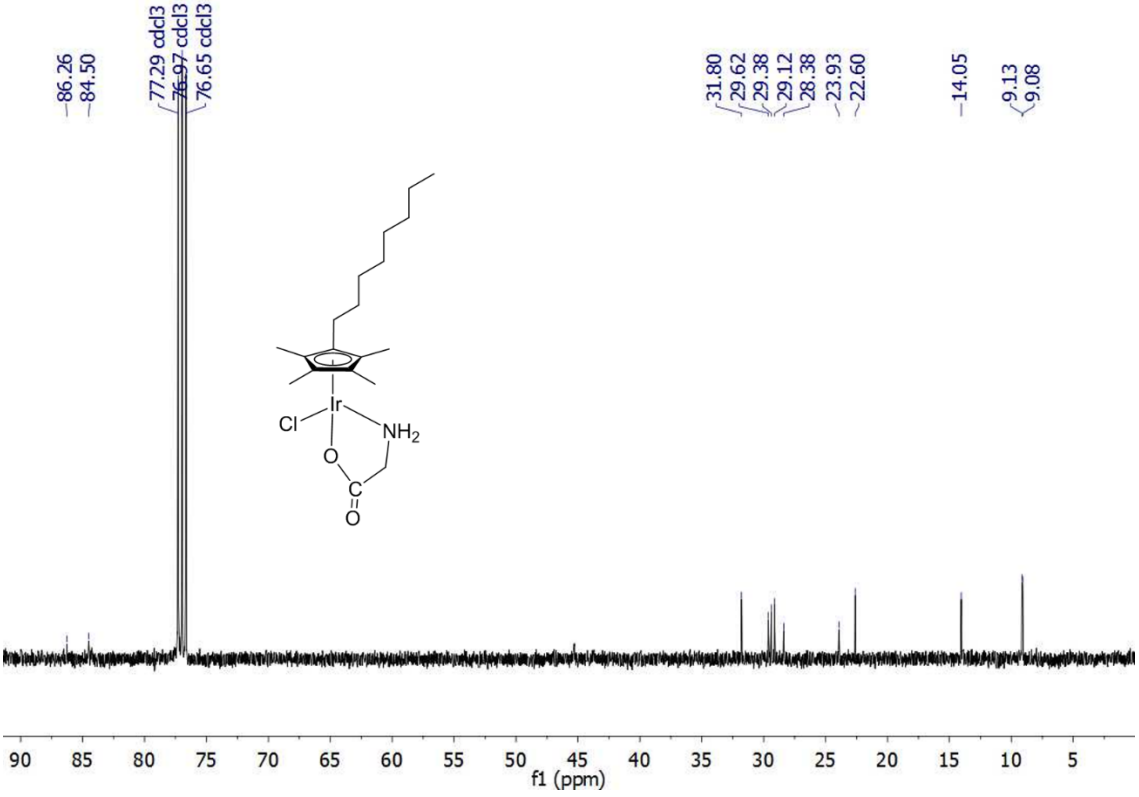

Figure A57: ^{13}C Spectra of (η^5-C_5Me_4-n-octyl)Ir(Glycine)Cl Complex

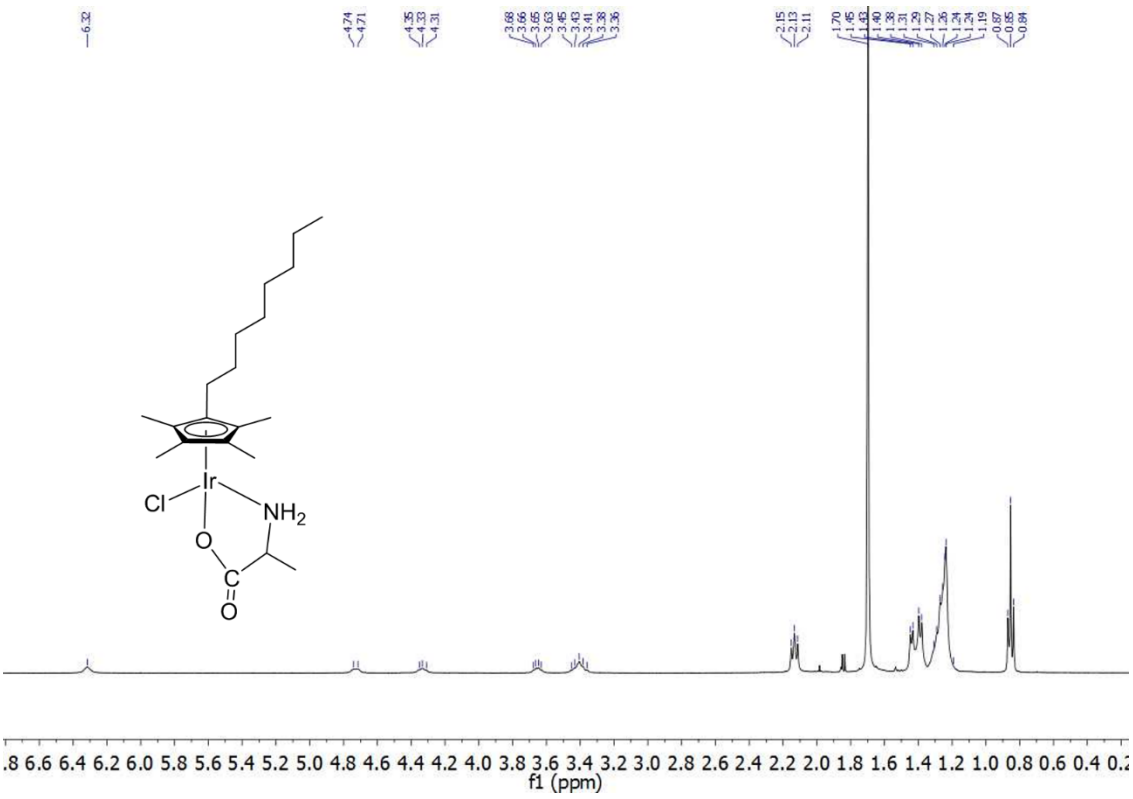

Figure A58: ^{1}H Spectra of (η^5-C_5Me_4-n-octyl)Ir(L-alanine)Cl Complex

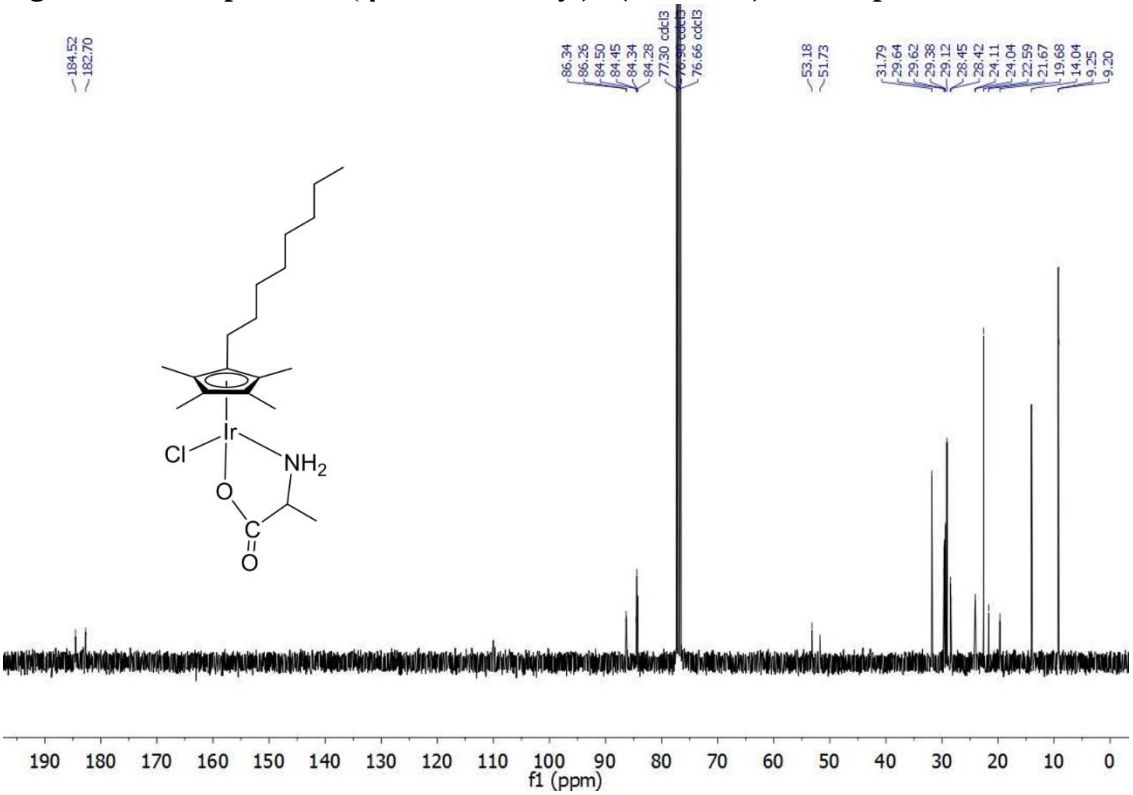

Figure A59: ^{13}C Spectra of (η^5-C_5Me_4-n-octyl)Ir(L-alanine)Cl Complex

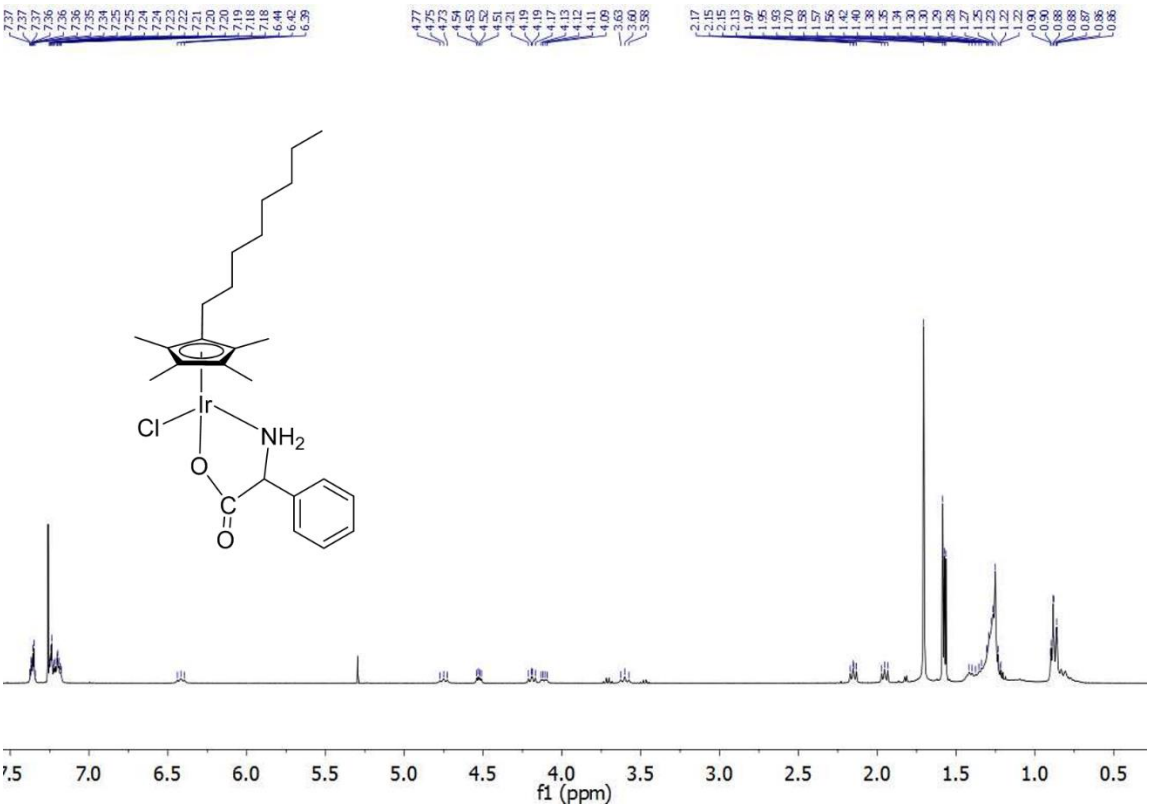

Figure A60: ^{1}H Spectra of (η^5-C_5Me_4-n-octyl)Ir(L-phenylglycine)Cl

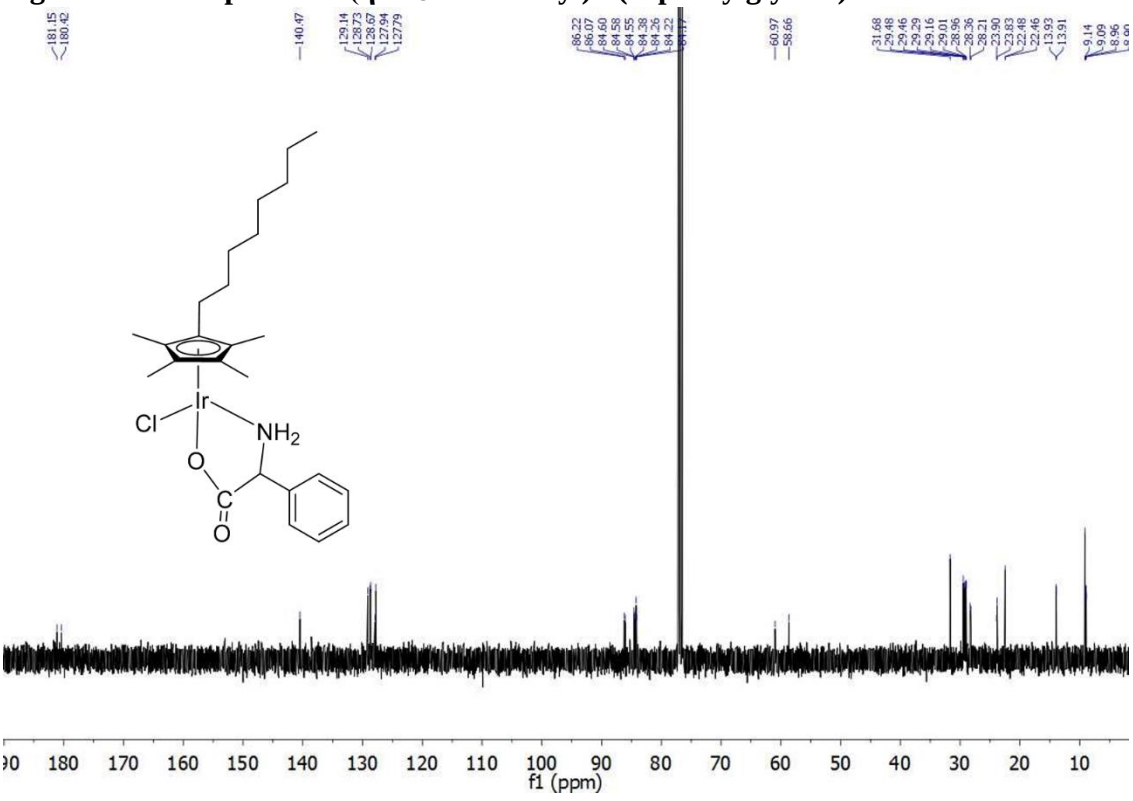

Figure A61: ^{13}C Spectra of (η^5-C_5Me_4-n-octyl)Ir(L-phenylglycine)Cl

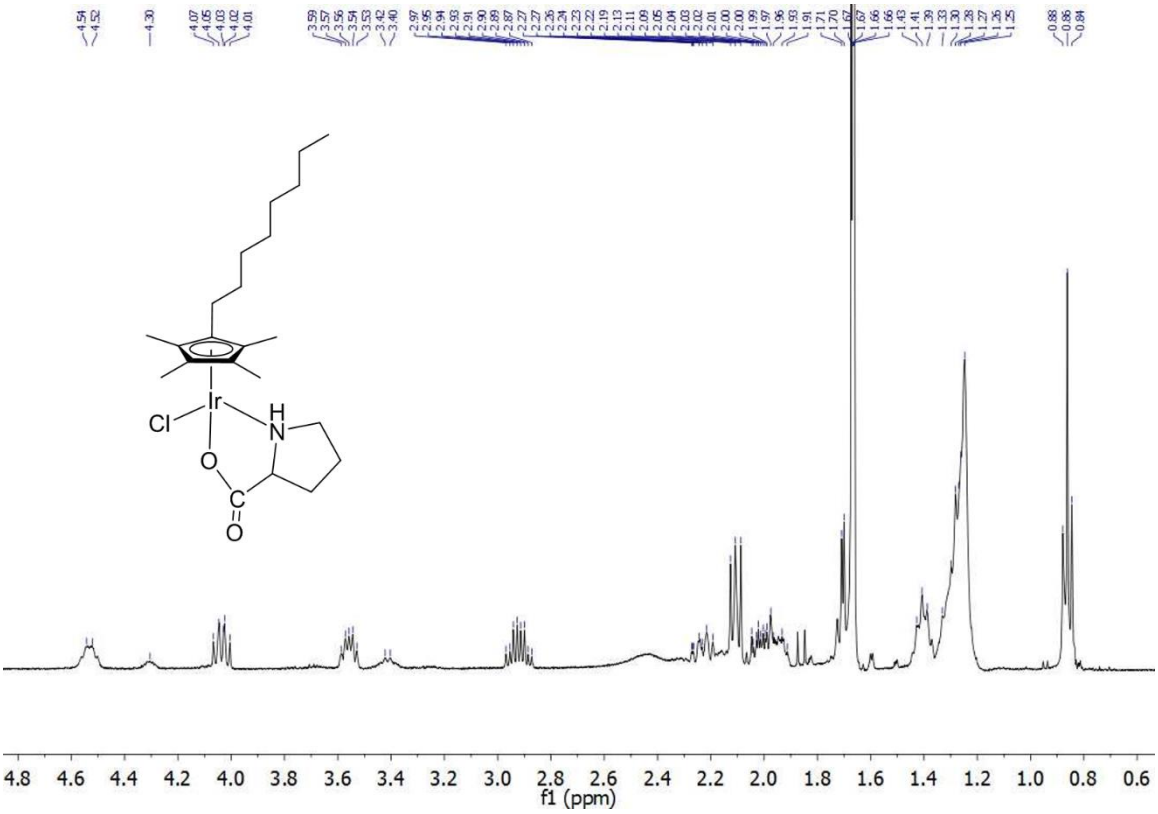

Figure A62: ^{1}H Spectra of (η^5-C_5Me_4-n-octyl)Ir(L-proline)Cl Complex

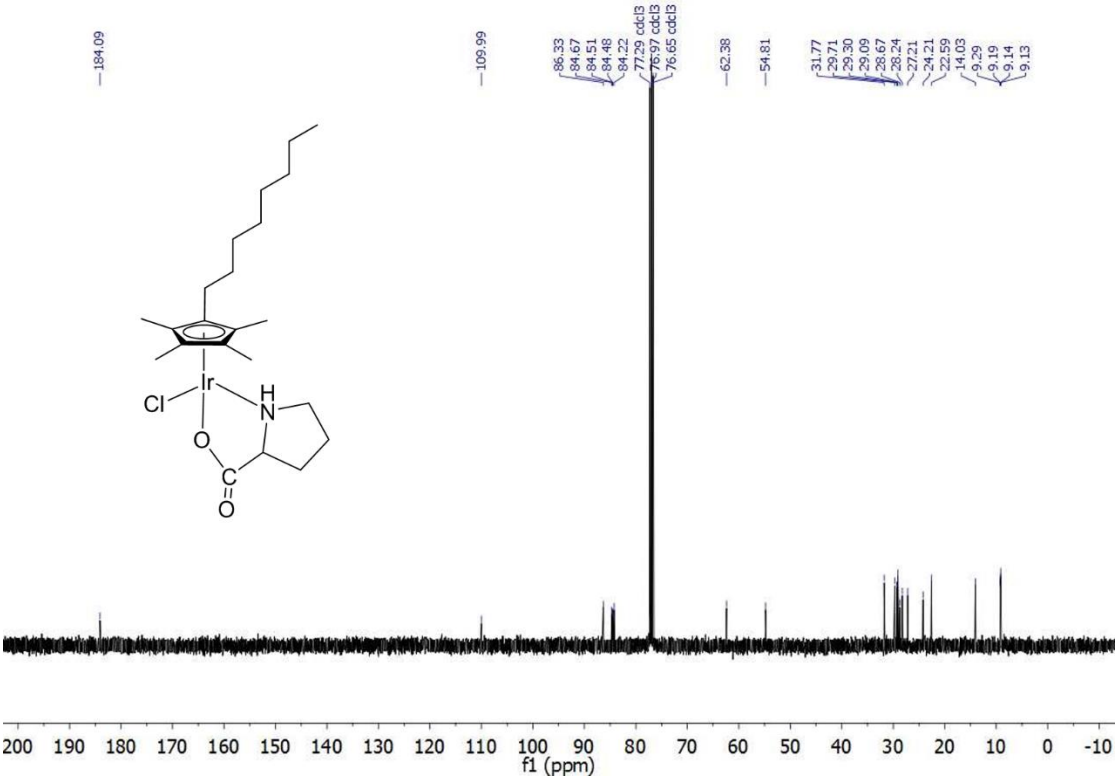

Figure A63: ^{13}C Spectra of (η^5-C_5Me_4-n-octyl)Ir(L-proline)Cl Complex

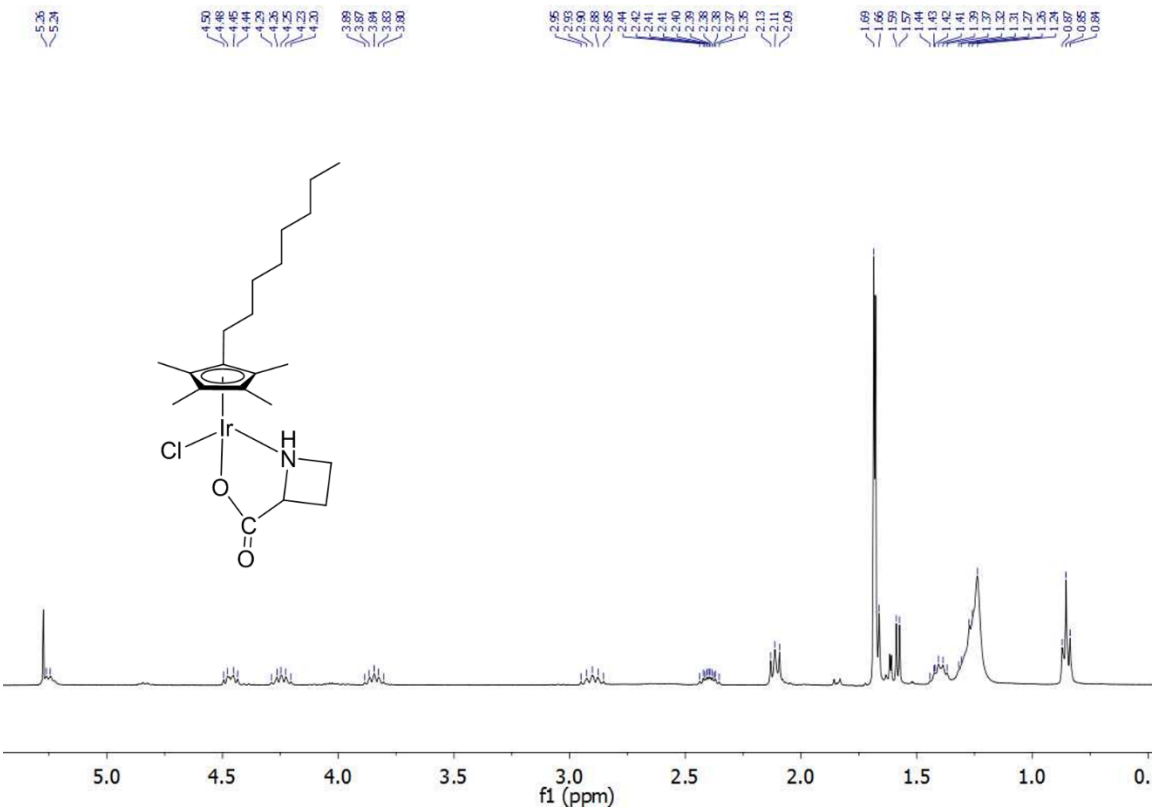

Figure A64: ^{1}H Spectra of (η^5-C_5Me_4-n-octyl)Ir(L-Aze)Cl Complex

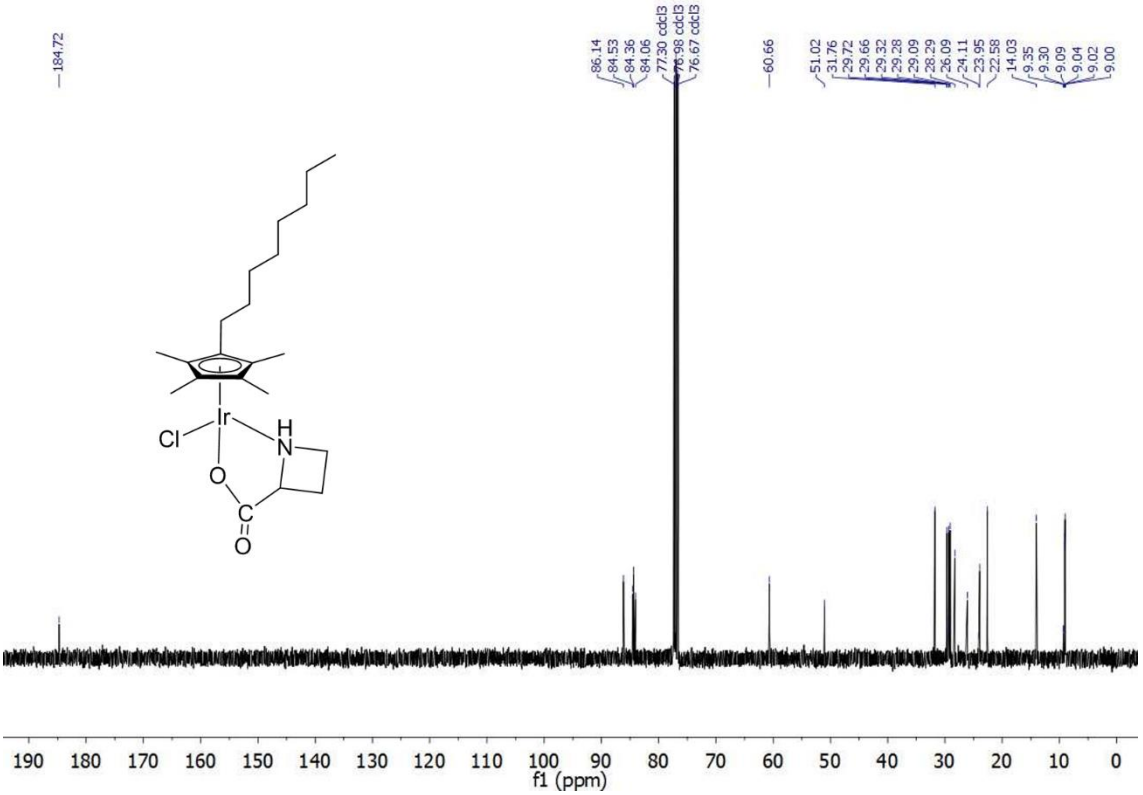

Figure A65: ^{13}C Spectra of (η^5-C_5Me_4-n-octyl)Ir(L-Aze)Cl Complex

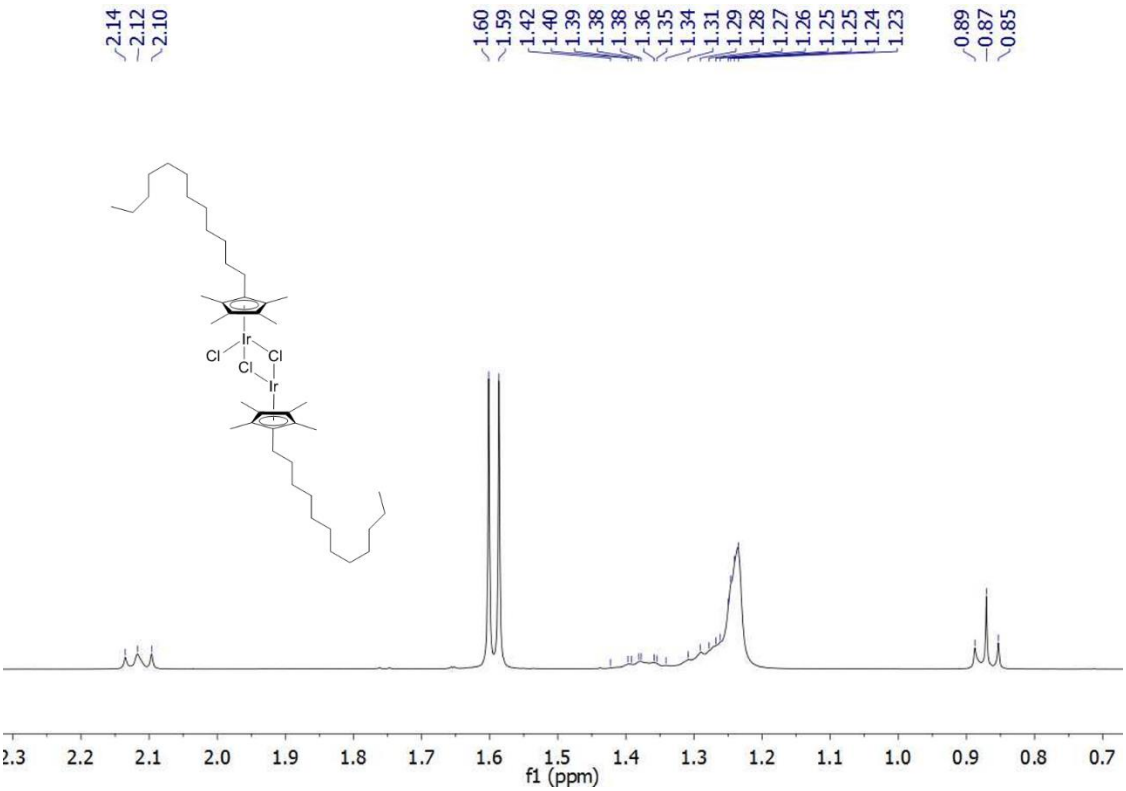

Figure A66: ^{1}H Spectra of [(η^5-C_5Me_4-n-dodecyl)$IrCl_2$]$_2$

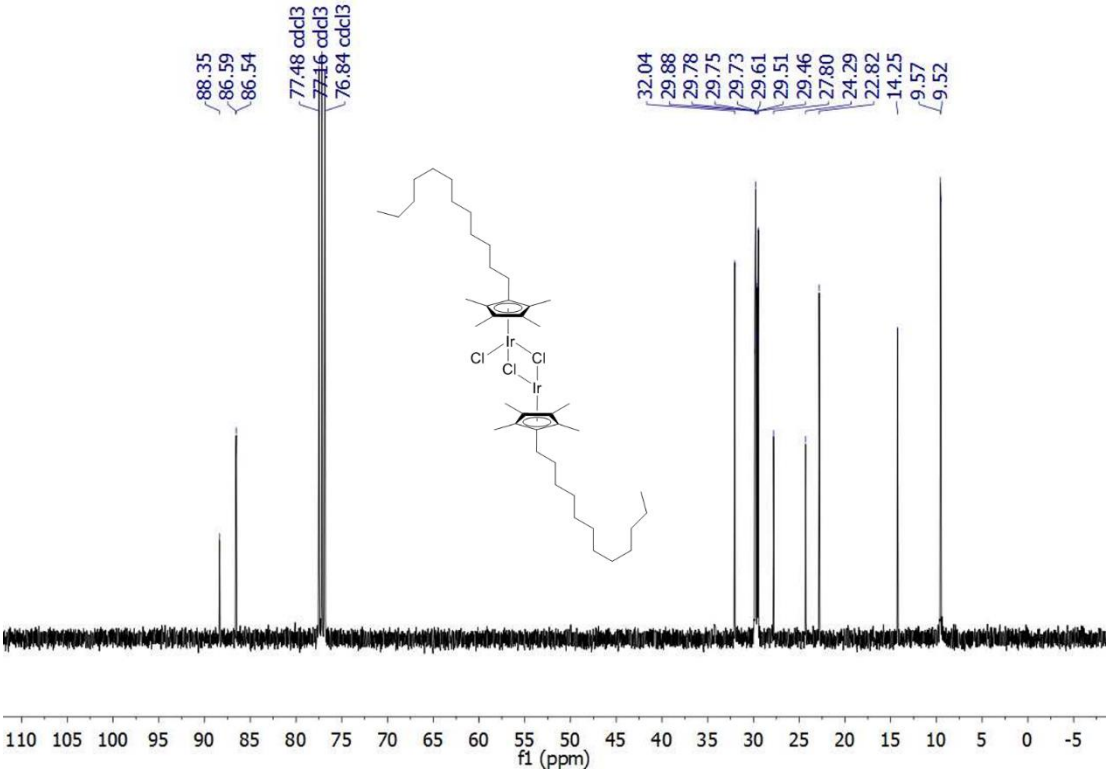

Figure A67: ^{13}C Spectra of [(η^5-C_5Me_4-n-dodecyl)$IrCl_2$]$_2$

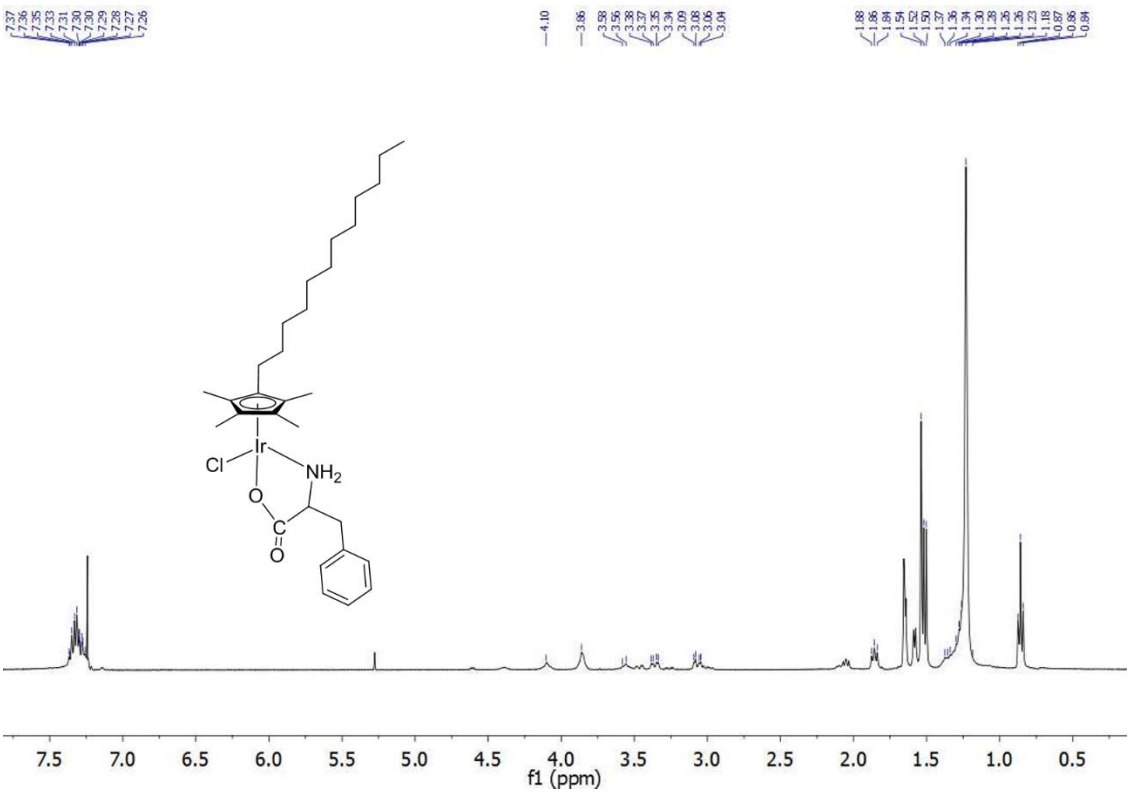

Figure A68: ^{1}H Spectra of (η^5-C_5Me_4-n-dodecyl)Ir(L-Phe)Cl Complex

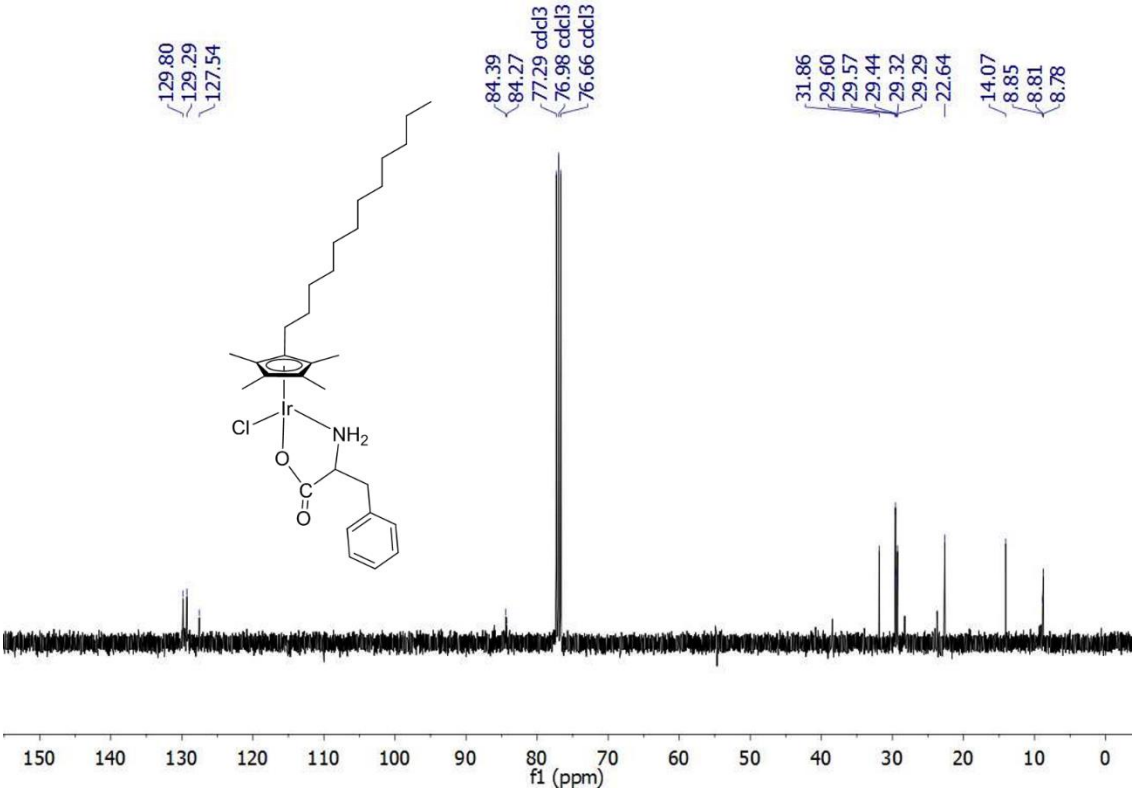

Figure A70: ^{13}C Spectra of (η^5-C_5Me_4-n-dodecyl)Ir(L-Phe)Cl Complex

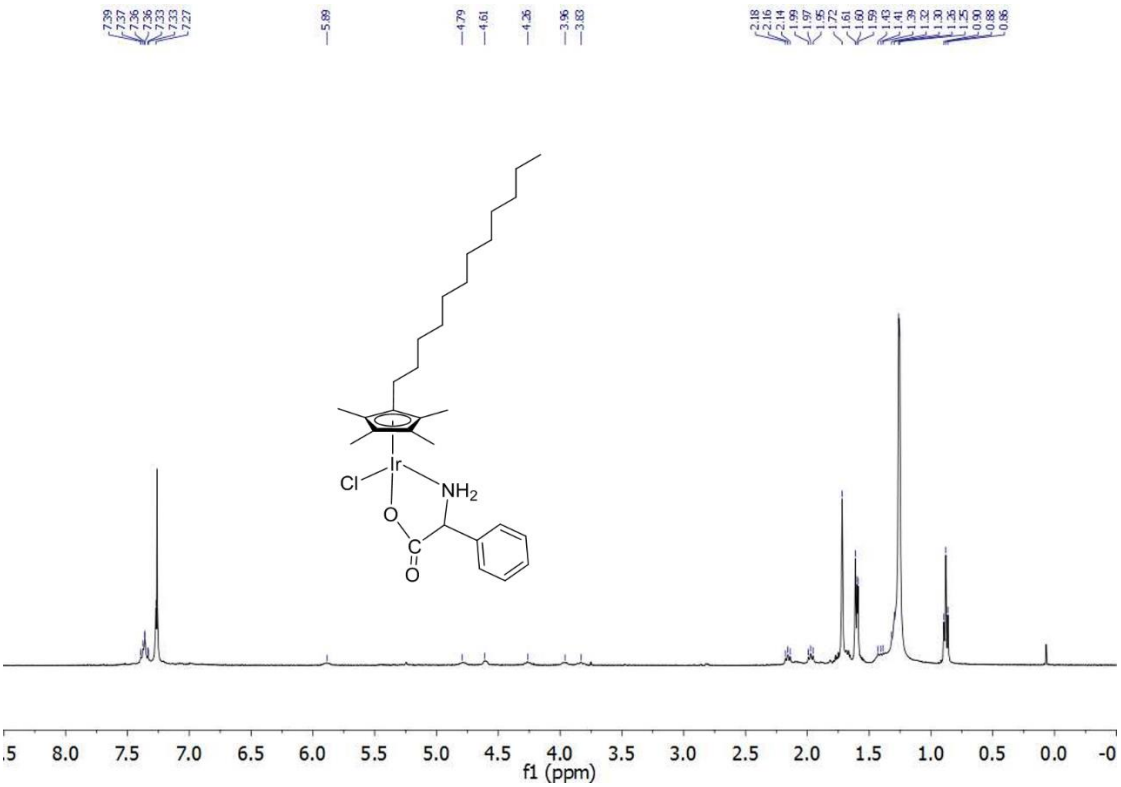

Figure A72: ^{1}H Spectra of (η^5-C_5Me_4-n-dodecyl)Ir(L-Phengly)Cl Complex

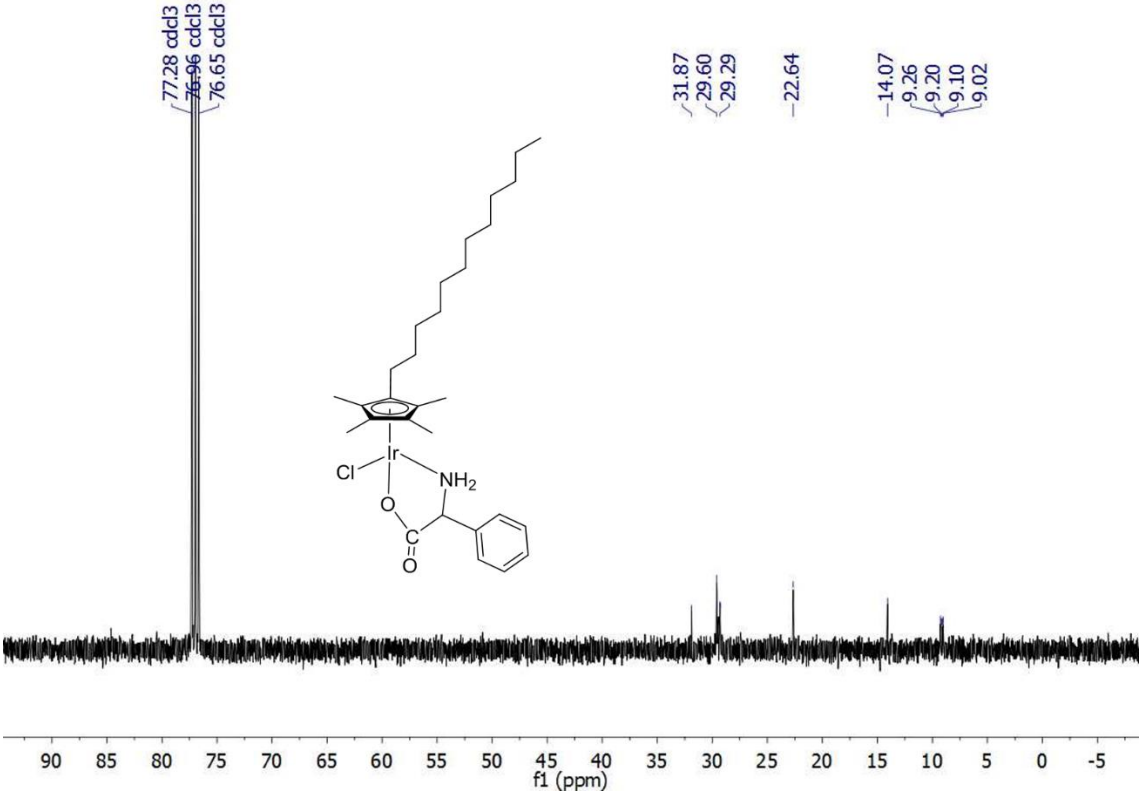

Figure A73: ^{13}C Spectra of (η^5-C_5Me_4-n-dodecyl)Ir(L-Phengly)Cl Complex

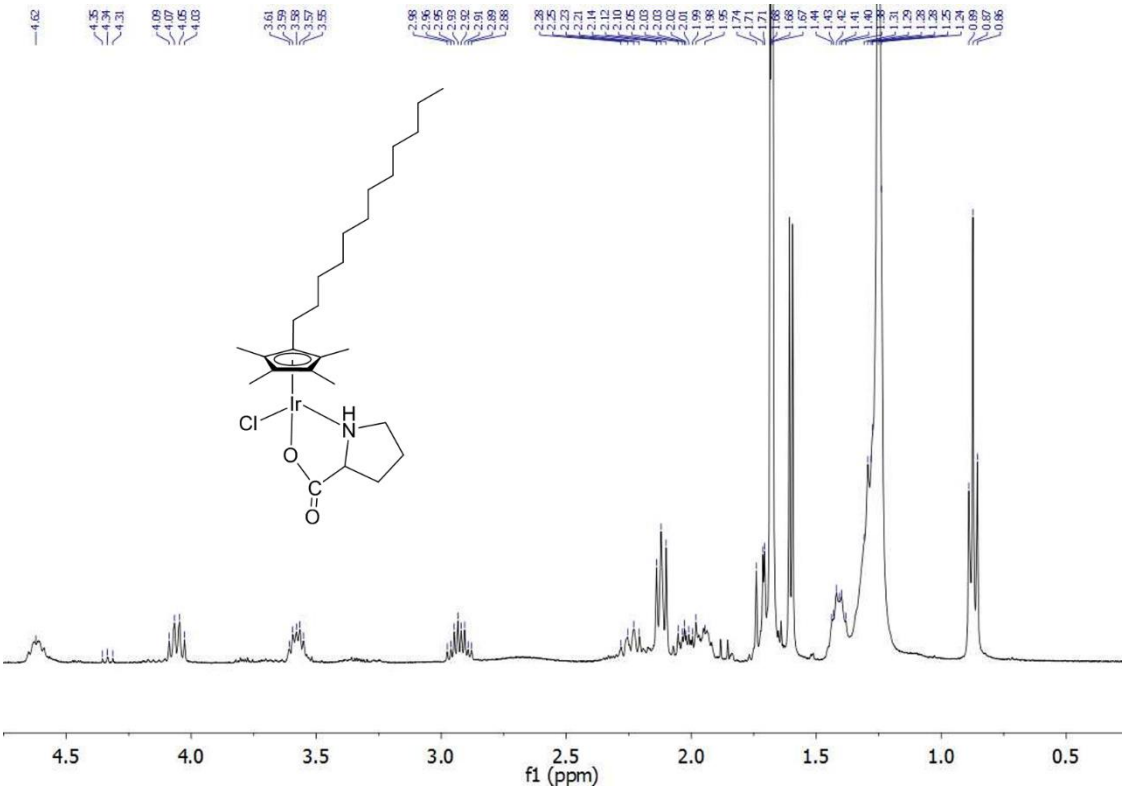

Figure A74: ^{1}H Spectra of (η^5-C_5Me_4-n-dodecyl)Ir(L-pro)Cl Complex

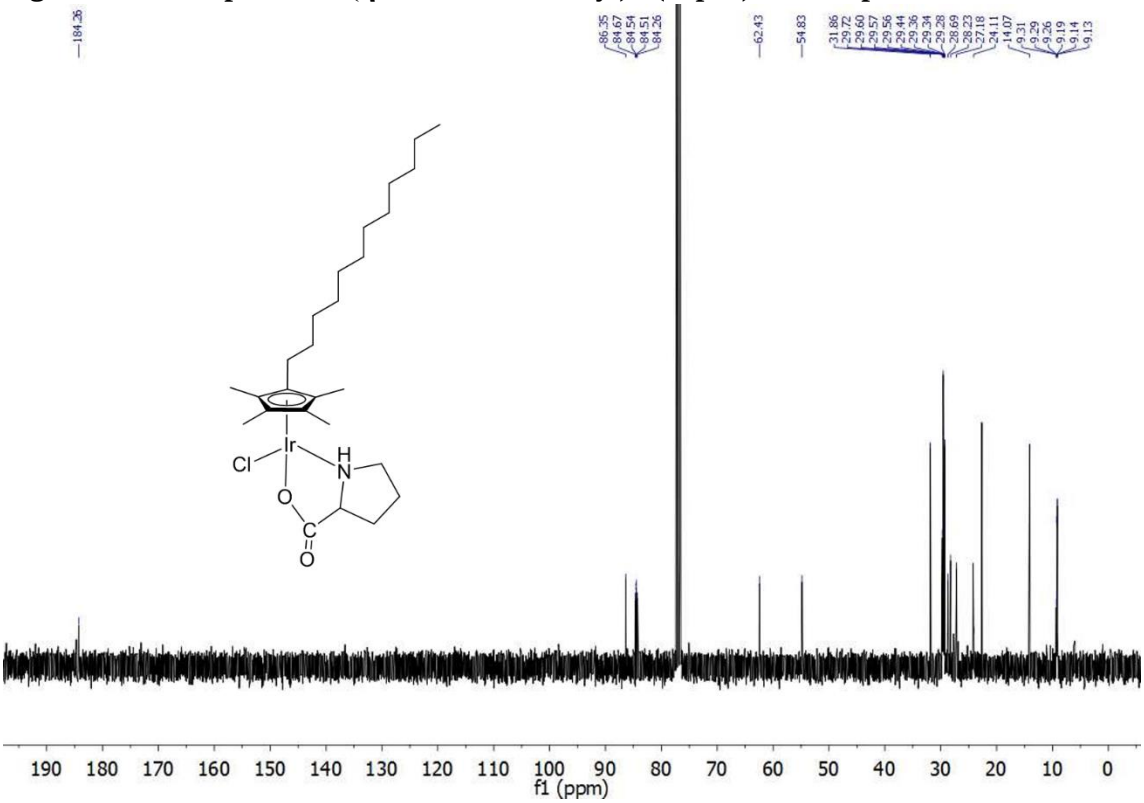

Figure A75: ^{13}C Spectra of (η^5-C_5Me_4-n-dodecyl)Ir(L-pro)Cl Complex

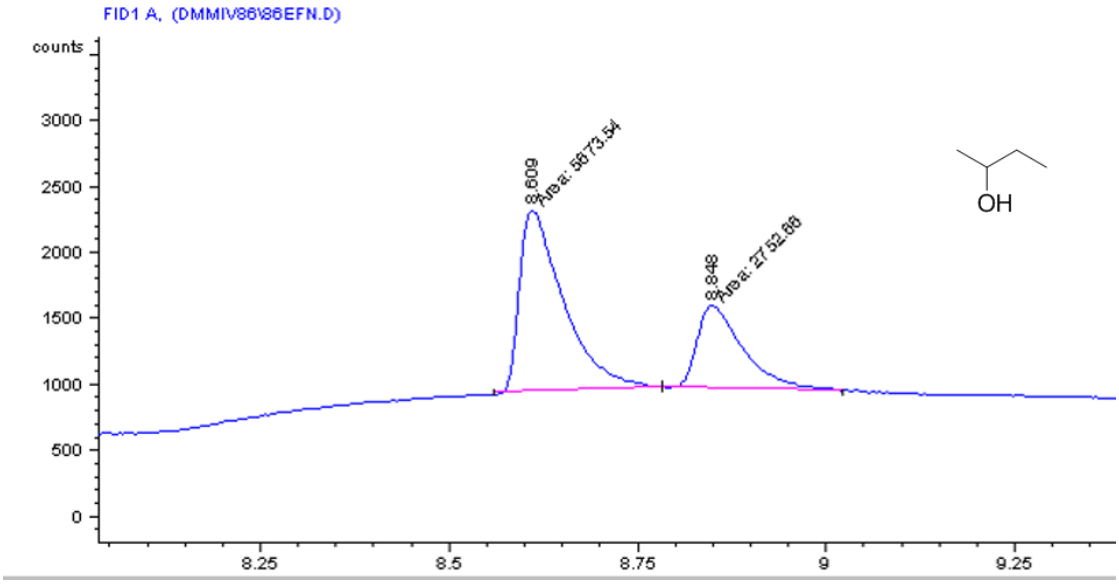

Figure A76: GC chromatogram of butan-2-ol

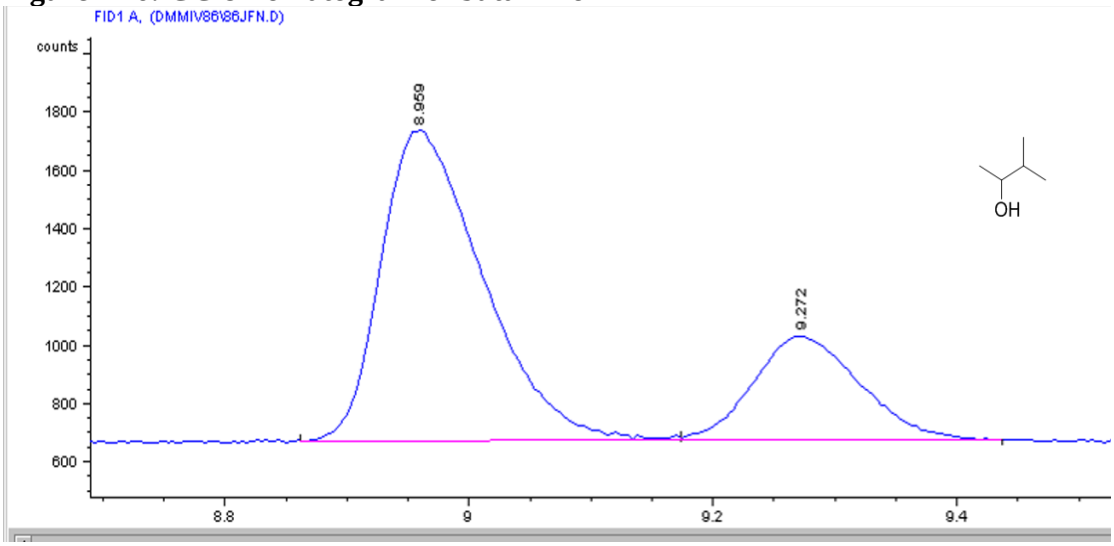

Figure A77: GC chromatogram of 3-methylbutan-2-ol

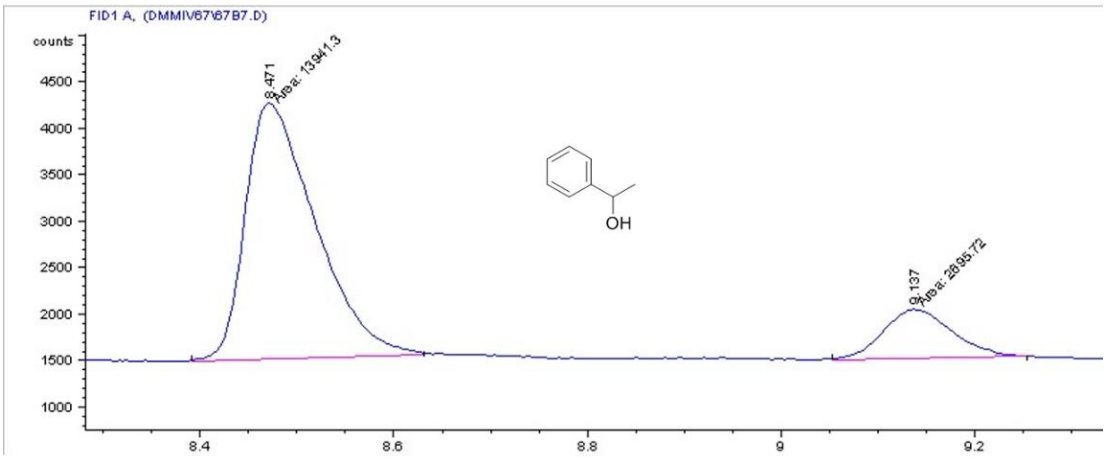

Figure A78: GC chromatogram of 1-phenylethan-1-ol

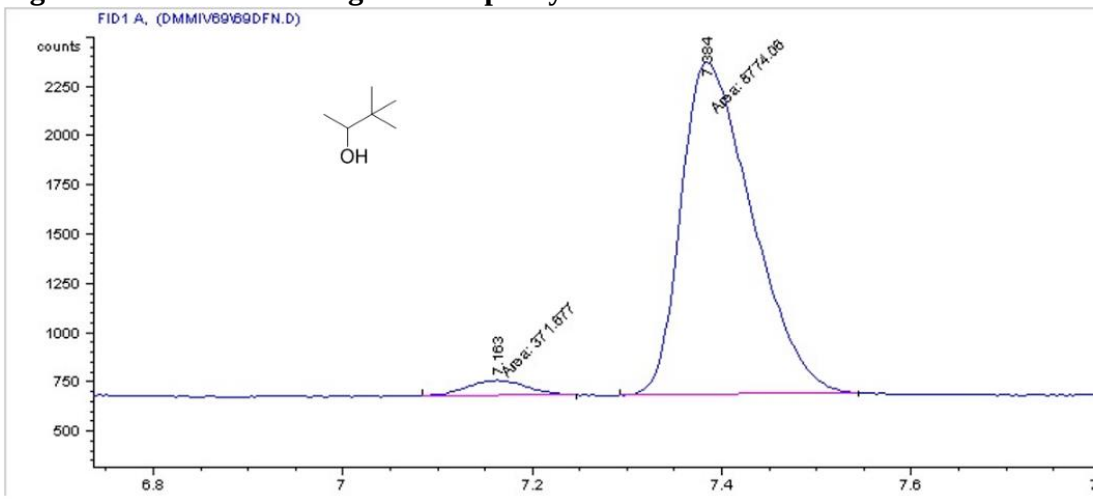

Figure A79: GC chromatogram of 3,3-dimethylbutan-2-ol

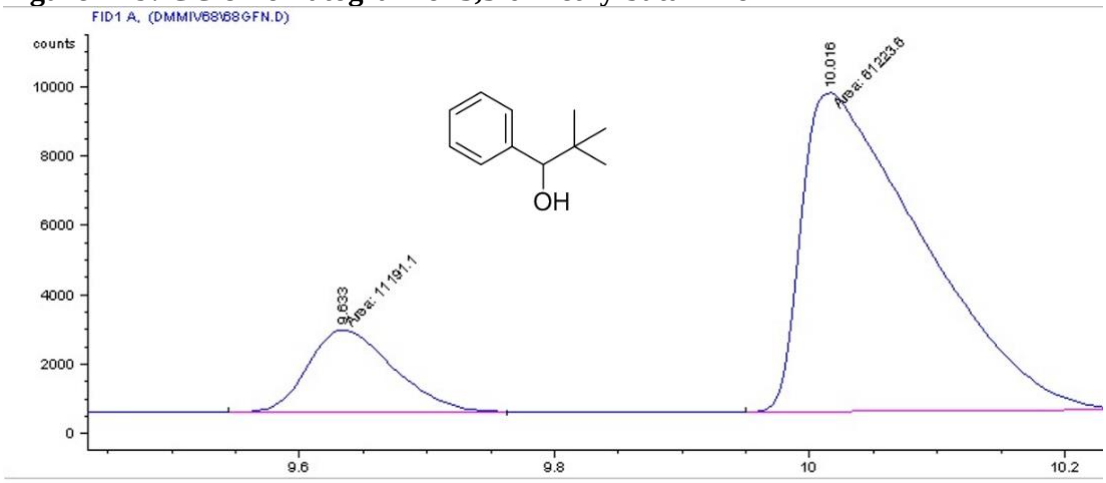

Figure A80: GC chromatogram of 2,2-dimethyl-1-phenylpropan-1-ol